Beam-Column Element Model Calibrated for Predicting Flexural Response Leading to Global Collapse of RC Frame Buildings

Curt B. Haselton
Assistant Professor
Department of Civil Engineering
California State University, Chico

Abbie. B. Liel
Ph.D. Candidate
Department of Civil and Environmental Engineering
Stanford University

Sarah Taylor Lange
Graduate Student Researcher
Department of Civil and Environmental Engineering
University of California, Los Angeles

Gregory G. Deierlein
Professor and Director of Blume Earthquake Engineering Research Center
Department of Civil and Environmental Engineering
Stanford University

PEER Report 2007/##
Pacific Earthquake Engineering Research Center
College of Engineering
University of California, Berkeley

December 2007

ABSTRACT

Performance-based earthquake engineering relies on the availability of analysis models that can be used to predict structural performance, including collapse. In this report, a lumped plasticity element model developed by Ibarra et al. (2005) is used to model the behavior of reinforced concrete beam-columns. The backbone and its associated hysteretic rules provide for versatile modeling of cyclic behavior and, importantly, the model captures the negative stiffness of post-peak response, enabling modeling of the strain softening behavior that is critical for simulating collapse of RC frame structures.

The Ibarra element model has been calibrated to data from 255 reinforced concrete column tests. For each column test, the element model parameters (eg. plastic rotation capacity, cyclic deterioration parameters, etc.) were systematically calibrated such that the analysis results closely matched the experimental results. Column design parameters (eg. axial load ratio, spacing of transverse reinforcement, etc.) are then related to the column element model parameters through regression analysis.

The outcome of this work is a set of predictive equations that can be used to predict a column's element model parameters for input into analysis models, given the various design parameters of a reinforced concrete column. Moreover, by demonstrating which column design factors are most important predictors of key aspects of structural collapse behavior, they can provide an important tool for improving design and design provisions.

ACKNOWLEDGMENTS

This work was supported in part by the Earthquake Engineering Research Centers Program of the National Science Foundation under award number EEC-9701568 through the Pacific Earthquake Engineering Research Center (PEER). Any opinions, findings, and conclusions expressed in this document are those of the authors and do not necessarily reflect those of the National Science Foundation.

Additional funding was provided by FEMA, through the Applied Technology Council (ATC-63). Abbie Liel is supported by a Stanford Graduate Fellowship and a National Science Foundation Fellowship. Work by Sarah Taylor Lange was supported by PEER's Research Center's Research Experience for Undergraduates summer internship program.

The authors would also like to acknowledge the valuable input from Professors Helmut Krawinkler, Eduardo Miranda, Jack Baker and Ken Elwood, post-doctoral fellow Paul Cordova, and graduate students Polsak Tothong and Farzin Zareian.

CONTENTS

LIST OF FIGURES

LIST OF TABLES

NOTATION LIST

A_g - gross cross-sectional area of column (bh) (mm^2)

A_s – total cross-sectional area of longitudinal reinforcement, including any intermediate (web) reinforcement ($A_{st} + A_s'$) (mm^2)

A_s' – total cross-sectional area of longitudinal *compression* reinforcement, including any intermediate (web) reinforcement (mm^2)

A_{sh} - total cross-sectional area of transverse reinforcement (including cross-ties) within spacing, **s,** and parallel to loading direction (ACI 318-02 definition, chapter 21) (mm^2)

A_{st} – total cross-sectional area of longitudinal *tension* reinforcement, including any intermediate (web) reinforcement (mm^2)

a_{sl} – indicator variable (0 or 1) to signify possibility of longitudinal rebar slip past the column end ; a_{sl} = 1 if slip is possible (defined by Fardis and Biskinis, 2003; Panagiotakos, 2001)

A_{sw} – total cross-sectional area of longitudinal intermediate (web) reinforcement (mm^2)

b – width of column, measured perpendicular to transverse load (mm)

c – cyclic deterioration calibration term (exponent); describes the change in the *rate* of cyclic deterioration as the energy dissipation capacity is exhausted (c = 1.0 causes constant rate of deterioration, c > 1.0 causes rate to be slower to start and faster as energy dissipation progresses)

c_{units} - a units conversion variable that equals 1.0 when f'_c and f_y are in MPa units and 6.9 for ksi units.

d – effective depth of column (h – d′) (mm)

d′ – distance from center of compression reinforcement to extreme compression fiber (mm)

d_b – diameter of longitudinal rebar (mm)

$d_{b,sh}$ – diameter of transverse reinforcement, region of close spacing (mm)

$d_{b,sh,wide}$ – diameter of transverse reinforcement, region of wide spacing (mm)

dr – data removed due to questionable reliability; notation used in Table 13

EI_g – gross cross-sectional moment of inertia (kN/mm/mm)

EI_{stf_40} – effective cross-sectional moment of inertia such that the stiffness is defined through the point at 40% of the yield moment (kN/mm/mm) (Figure 13)

E_t – cyclic energy dissipation capacity (= $\lambda M_y \theta_y$)

EI_y – effective cross-sectional moment of inertia that provides a secant stiffness through the yield point (kN/mm/mm) (Figure 13)

$EI_{y\_noFlexure}$ – effective cross-sectional moment of inertia that provides a secant stiffness through the yield point after the flexure component of deformation has been removed from the data (kN/mm/mm); this stiffness is consistent with using an effective yield deformation of $\theta_y - \theta_{y,f}$; the purpose of this variable is to define a flexibility that one could use to account for bond-slip and shear deformations while using fiber element model that accounts for only flexural deformations

f'_c – compressive strength of unconfined concrete, based on standard cylinder test (MPa)

Failure classification - 0 for flexural failure, 1 for flexure-shear failure (as defined by Berry et al. 2004)

f_y – yield stress of longitudinal reinforcement (MPa)

$f_{y,sh}$ – yield stress of transverse reinforcement (MPa)

h – height of column, measured parallel to transverse load (mm)

K_c – post-capping stiffness, ie. stiffness beyond $\theta_{cap,pl}$ ($K_c = \alpha_c K_e$)

K_e – initial "elastic" secant stiffness to the yield point (Figure 13)

K_s – hardening stiffness, ie. stiffness between θ_y and $\theta_{cap,pl}$ ($K_s = \alpha_s K_e$)

LB – indicator variable showing if the data had a observed capping point (LB=0) or a lower bound plastic rotation capacity was calibrated to the data (LB=1); also sometimes called isLB (see Section 2.1.2)

L_s – shear span, distance between column end and point of inflection (= L for all columns in Berry and Eberhard database) (mm)

M_n – nominal moment, expected flexural strength (kN-m)

$M_{n(ACI)}$ – nominal moment, expected flexural strength, as computed by the ACI 318-02 recommendations (kN-m)

M_y – "yield" moment from calibration (this is closer to M_n based on how calibration was performed); note that this is the average of the calibrated yield moments in the positive and negative directions (kN-m)

$M_{y(Fardis)}$ – "yield" moment as calculated based on Fardis' predictive equations (Fardis and Biskinis, 2003; Panagiotakos, 2001) (kN-m)

nd – no data available for this value, commonly referring to the lack of an observed post-capping slope in the experimental data; notation used in Table 13

P – axial load (kN)

P_b – axial load at the balanced condition (kN)

P_o – nominal axial load capacity of a column (kN)

s – spacing of transverse reinforcement, measured along height of column; region of close spacing (mm)

s_n – rebar buckling coefficient, $(s/d_{b.})(f_y/100)^{0.5}$, (where f_y is in MPa); similar to a term used by Dhakal and Maekawa (2002) which was used to predict the ductility and post-buckling stiffness of bare rebar

s_{wide} – spacing of transverse reinforcement, measured along height of column; region of wide spacing (mm)

V_c – shear capacity of concrete, as per ACI 318-02 (kN)

$V_{n,close}$ – nominal shear capacity ($V_c + V_{s,close}$), as per the ACI 318-02 (ACI, 2002), region of close stirrup spacing (kN)

$V_{n,wide}$ – nominal shear capacity ($V_c + V_{s,wide}$), as per the ACI 318-02 (ACI, 2002), region of wide stirrup spacing (kN)

V_p – shear demand at point of flexural yielding (M_y / L_s) (kN)

$V_{s,close}$ – shear capacity of steel, as per ACI, region of close stirrup spacing (kN)

$V_{s,wide}$ – shear capacity of steel, as per ACI, region of wide stirrup spacing (kN)

α_c – post-capping stiffness ratio ($K_c = \alpha_c K_e$)

α_{eff} – confinement effectiveness factor, proposed by Sheikh et al. and used by Fardis et al. (Sheikh and Uzumeri, 1982; Fardis and Biskinis, 2003; Panagiotakos, 2001)

α_s - hardening stiffness ratio ($K_s = \alpha_s K_e$)

α_{st}^{pl} – coefficient for the type of steel (Fardis and Biskinis, 2003; Panagiotakos, 2001)

ε_y – yield strain of longitudinal reinforcement

$\theta_{cap,tot}$ – total (sum of elastic and plastic) chord rotation at capping (rad)

$\theta_{cap,pl}$ - plastic chord rotation from yield to cap (rad)

θ_{pc} – post-capping plastic rotation capacity, from the cap to point of zero strength (rad)

θ_{stf_40} - chord rotation demand at 40% of the yield moment, associated with EI_{stf} (rad)

$\theta_{u,mono}$ - total (elastic + plastic)chord rotation at "ultimate"(defined as 20% strength loss); as predicted by Fardis and Biskinis (2003) (rad)

$\theta_{u,mono}^{pl}$ - plastic chord rotation from yield to "ultimate" (defined as 20% strength loss) ; as predicted by Fardis and Biskinis (2003) (rad)

θ_y - chord rotation at "yielding", considered as the sum of flexural, shear and bond-slip components ($\theta_{y,f} + \theta_{y,s} + \theta_{y,b}$); yielding is defined as the point of significant stiffness change, ie. steel yielding or concrete crushing (rad)

$\theta_{y,b}$ – bond-slip component of chord rotation at "yielding" (rad)

$\theta_{y,f}$ – flexural component of chord rotation at "yielding" (rad)

$\theta_{y,f\ (PF2001)}$ – flexural component of chord rotation at "yielding"; computed with method proposed by Panagiotakos and Fardis (2001) (rad)

$\theta_{y,s}$ – shear component of chord rotation at "yielding" (rad)

$\theta_{y(Fardis)}$ - chord rotation at "yielding," as predicted by Fardis and Biskinis (2003); Panagiotakos and Fardis (2001) also propose similar formula (rad)

λ – normalized energy dissipation capacity; it is important to note that this is a normalized value defined by the total energy dissipation capacity of $E_t = \lambda M_y \theta_y$. When creating an element model, the input value must be adjusted if an initial stiffness other then EI_y/EI_g is used.

ν – axial load ratio ($P/A_g f'_c$) (kN)

ρ – ratio of total area of longitudinal reinforcement (A_s'/bd; $\rho_t + \rho'$)

ρ' – ratio of longitudinal reinforcement in *compression,* including web steel (A_s'/bd)

ρ'_{eff} – effective ratio of longitudinal compression reinforcement ($\rho' f_y / f'_c$)

ρ_{eff} – effective ratio of longitudinal tension reinforcement ($\rho f_y / f'_c$)

ρ_{sh} – area ratio of transverse reinforcement, in region of close spacing at column end (A_{sh}/sb)

$\rho_{sh,eff}$ – effective ratio of transverse reinforcement, in region of close spacing at column end ($\rho_{sh} f_{y,w} / f'_c$)

$\rho_{sh,wide}$ – area ratio of transverse reinforcement, near center of column in region of wide spacing

ρ_t – ratio of longitudinal reinforcement in *tension,* including web steel (A_{st}/bd)

ρ_w – ratio of longitudinal intermediate (web) reinforcement (A_{sw}/bd)

τ_e – bond strength between concrete and elastic rebar in tension; taken as $0.5*f'^{0.5}_c$ (Sozen 1992), where f'_c is in MPa (MPa)

φ_{stf_40} – curvature at 40% of the yield moment (based on φ_y and φ_{cr}) (rad/m)

φ_y – "yield" curvature; curvature at the onset of either steel yielding (for tension controlled) or significant concrete nonlinearity (for compression controlled) (rad/m)

$\varphi_{y(PF2001)}$ – "yield" curvature; curvature at the onset of either steel yielding (for tension controlled) or significant concrete nonlinearity (for compression controlled); computed with method proposed by Panagiotakos and Fardis (2001) (rad/m)

1. Introduction and Methodology

1.1 PURPOSE AND SCOPE

Emerging performance-based earthquake engineering design approaches seek to enable more accurate and transparent assessment of both life-safety risks and damage, through the use of advanced analysis models and design criteria. The first generation of performance-based assessment provisions, such as FEMA 273 and 356 (ASCE, 1997; ASCE 2000b) and ATC 40 (ATC, 1996), provided an excellent first step towards codifying approaches that embrace nonlinear analysis to simulate system performance and articulate performance metrics for the onset of damage up to structural collapse. As such, these documents marked the first major effort to develop consensus-based provisions that went beyond the traditional emphasis on linear analysis and specification of component strengths, which have long been the mainstay of engineering design practice and building code provisions.

The FEMA 273/356 project (FEMA, 1997; ASCE, 2000) was an important milestone in codifying degrading nonlinear models and procedures in order to explicitly evaluate structural collapse. A key component of these procedures is the specification of nonlinear structural component models in the form of monotonic backbone curves that define characteristic force-deformation behavior of the components as a function of seismic detailing parameters. For example, FEMA 356 specifies backbone curve parameters that define the nonlinear moment-rotation response of reinforced concrete beam-columns as a function of longitudinal and horizontal reinforcement, and axial and shear demands. While these models have limitations in that they are highly idealized and generally conservative in deterministic evaluations of response, they are noteworthy in terms of their breadth, and are capable of modeling the full range of behavior for a wide variety of structural components for all major forms of building construction.

Equally important is the integration of the element modeling guidelines within formal nonlinear assessment methods.

Building upon these efforts, the goal of this research project is to develop reliable and accurate element models that can be used to evaluate the collapse performance of reinforced concrete frame buildings, focusing particularly on reinforced concrete beam-columns. With the availability of an accurate and well-calibrated beam-column element model, nonlinear dynamic simulation may be used to predict building behavior up to the point of collapse. This project is part of a larger research effort coordinated by the Pacific Earthquake Engineering Research (PEER) Center to further the development of performance-based earthquake engineering, improving and refining the PBEE tools developed by the earlier FEMA and ATC documents.

The calibrations of reinforced concrete columns presented here are based on an element model developed by Ibarra, Medina, and Krawinkler (2005, 2003), as implemented in PEER's open-source structural analysis and simulation software tool, OpenSees. The model parameters, hysteretic rules and implementation are discussed in more detail in the following section. The outcome of the calibration work is empirical functions relating the seven calibrated model parameters to the physical properties of a beam-column (i.e. axial load, concrete strength, confinement, etc.). The uncertainty associated with each prediction is also investigated. Ideally, the full set of empirical equations developed can be used to begin a dialogue in order to develop consensus in the engineering community regarding modeling parameters, so that equations of this type can be implemented into future performance-based guidelines.

1.2 HYSTERETIC MODEL

The beam-column element model was developed by Ibarra, Medina, and Krawinkler (2005, 2003) and is composed of a tri-linear monotonic backbone. This backbone and its associated hysteretic rules provide for versatile modeling of cyclic behavior as shown in Figure 1. An important aspect of this model is the negative stiffness branch of post-peak response, which enables modeling of strain softening behavior associated with physical phenomena such as concrete crushing, rebar buckling and fracture, and bond failure. The model also captures four basic modes of cyclic deterioration: strength deterioration of the inelastic strain hardening branch, strength deterioration of the post-peak strain softening branch, accelerated reloading

stiffness deterioration, and unloading stiffness deterioration. Additional reloading stiffness deterioration is automatically incorporated through the peak-oriented cyclic response rules. Cyclic deterioration is based on an energy index that has two parameters: normalized energy dissipation capacity and an exponent term to describe how the rate of cyclic deterioration changes with accumulation of damage. The element model was implemented in OpenSees by Altoontash (2004).[1]

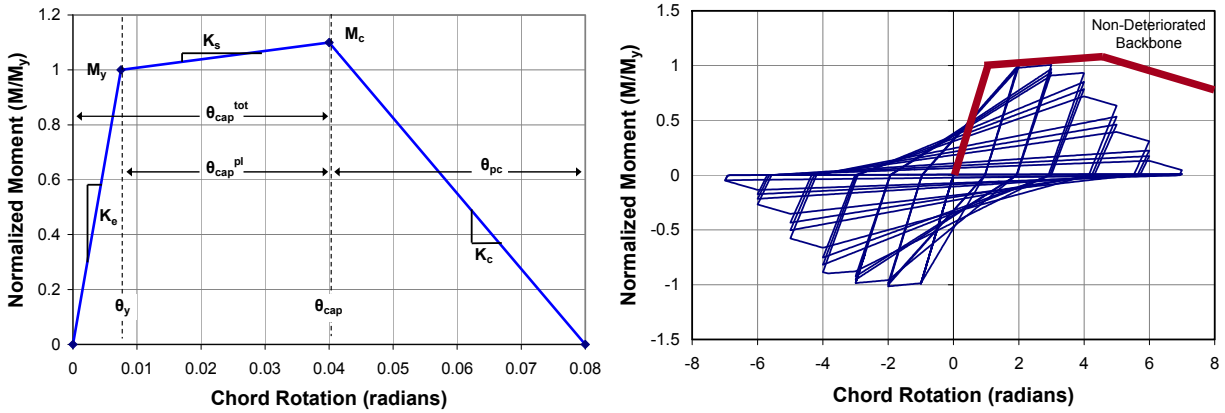

Figure 1. Monotonic and cyclic behavior of component model used in this study. Model developed by Ibarra, Medina, and Krawinkler.

Table 1. Description of model parameters and associated physical behavior and properties

Model Parameter	Description	Physical Behavior Contributing to Parameter	Physical Properties / Possible Predictors	References
M_y	"Yield" moment	Longitudinal rebar yielding, concrete cracking (flexure and shear), concrete crushing (for over-reinforced)	Whitney stress block approach or fiber analysis (section geometry, axial load (ratio), material strengths and stiffnesses)	Basic beam theory; Fiber moment-curvature; Fardis, 2003; Panagiotakos, 2001
θ_y	Chord rotation at "yield"	(same as above)	Section geometry (d-d', rebar diameter), level of shear cracking (shear span, shear demand/capacity), axial load (ratio), material stiffnesses/strengths	Fardis, 2003; Panagiotakos, 2001; Fiber moment-curvature
θ_{cap}	Chord rotation (mono.) at onset of strength loss (capping)	Longitudinal rebar buckling/fracture, concrete core failure for high axial loads and/or minimal lateral confinement (stirrup fracture)	Confinement (amount, spacing, type and layout, effectiveness index), axial load (ratio), end conditions (possibility of bond-slip), geometry (shear span, etc.), reinforcement ratio	Fardis, 2003; Panagiotakos, 2001; Berry 2003
M_c/M_y (or K_s)	Hardening stiffness	Steel strain hardening, nonlinearity of concrete, bond-slip flexibility	Steel hardening modulus, section/element geometry, presence of intermediate longitudinal steel layers	Fiber moment-curvature and plastic hinge length approach; Zareian 2006
θ_{pc} (or K_c)	Post-capping stiffness	Research still needed - Post- rebar buckling behavior, behavior after loss of core concrete confinement	To be determined - Rebar slenderness between stirrups (large stirrup spacing), and over several stirrups (small stirrup spacing)	Ibarra, 2005/2003; Zareian, 2006
λ	Normalized hysteretic energy dissipation capacity (cyclic)	Research still needed - Progression over cycles of concrete crushing, stirrup fracture, rebar buckling, longitudinal steel fracture	To be determined - Confinement (amount, spacing, effectiveness index), stirrup spacing, axial load (ratio)	Ibarra, 2005/2003; Zareian, 2006
c	Exponent term to model rate of deterioration (cyclic)	(same as above)	(same as above)	Ibarra, 2005/2003

[1] http://opensees.berkeley.edu

This element model requires the specification of seven parameters to control both the monotonic and cyclic behavior of the model: M_y, θ_y, K_s, θ_{cap}, and K_c, λ, and c.[2] The goal of the calibration studies is to empirically determine stiffness, capping (peak) point, post-peak unloading stiffness, and hysteretic stiffness/strength deterioration for reinforced concrete beam-column elements to be used in collapse simulation of RC frames. The connection between these model parameters and the physical behavior of beam-column elements is explored in Table 1.

1.3 EXPERIMENTAL DATABASE

The database used in this study is the Pacific Earthquake Engineering Research Center's Structural Performance Database (PEER 2005) that was developed at the University of Washington by Berry, Parrish, and Eberhard (Berry et al. 2004). This database includes the results of cyclic and monotonic tests of 306 rectangular columns and 177 circular columns. Where the test set-up is not a simple cantilever (e.g. hammerhead tests, etc.), Berry et al. transformed the data into that of an equivalent cantilever for ease of comparison (Berry et al. 2004). For each column test, the database reports the force displacement history, the available column geometry and reinforcement information, the failure mode, and often other relevant information.

From this database, we selected rectangular columns failing in a flexural mode (220 tests) or in a combined flexure-shear mode (35 tests), for total of 255 tests. Figure 2 shows the range of selected important column design parameters for these 255 tests.

Depending on the experimental test setup, a variety of methods are used to apply the axial load to the column. To address this, the force-displacement data for each column was transformed to be consistent with a vertical axial load applied at the column top (section 2.1.2.1; item #1). In the OpenSees column model used for calibration, the vertical load is also applied at the top of the column.

[2] Please that there is a difference in notation between this work and Ibarra's: what we call λ is identical to his cyclic deterioration parameter γ.

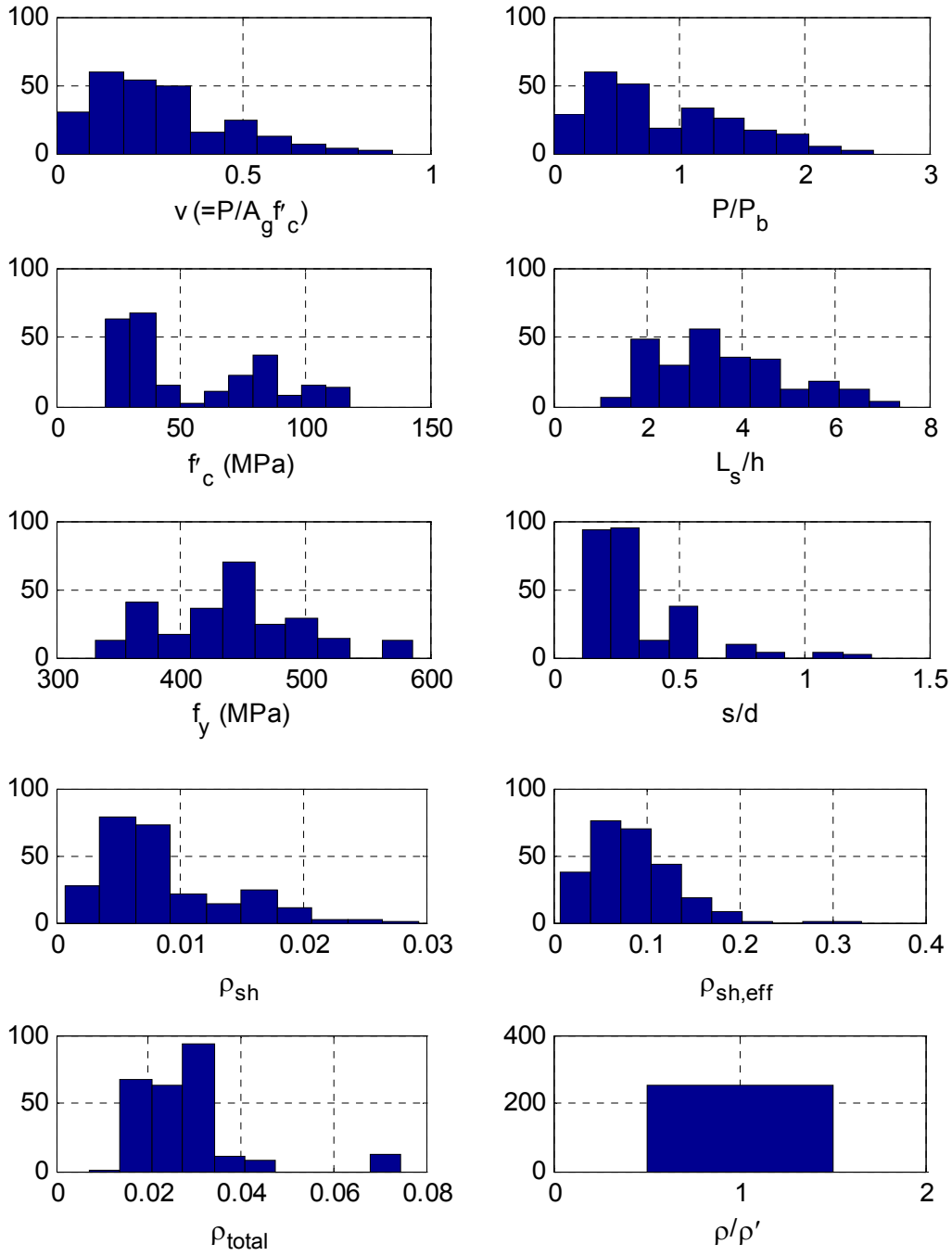

Figure 2. Histograms showing the range of column design parameters for the 255 experimental tests included in this calibration study.

2. Calibration Procedure and Results

2.1 CALIBRATION OVERVIEW

2.1.1 Idealization of Columns

In the OpenSees model, each cantilever column is idealized using an elastic element and a zero-length plastic hinge at the base of the column. The plastic hinge has a relatively high pre-yield stiffness, and the stiffness of the elastic element is increased accordingly such that the full column assembly has the correct lateral stiffness. The properties of the plastic hinge are the subject of this calibration effort.

2.1.2 Calibration Procedure

2.1.2.1 Calibration Steps

The calibration of the beam-column element model to each experimental test was conducted in a systematic manner. Every effort was made to standardize the process in order to reduce possible errors and inconsistencies associated with the judgment present in the calibration process.

It is important to note that the Ibarra element model is based on the definition of a monotonic backbone and cyclic deterioration rules. In this calibration work we use cyclic tests with many cycles to calibrate both the monotonic backbone (eg. capping point) and the cyclic deterioration rules. As a result, the monotonic backbone and the cyclic deterioration rules are

interdependent, and the approximation of the monotonic backbone depends on cyclic deterioration rules assumed, which are discussed below. This approximation of the monotonic backbone from cyclic data is non-ideal; to facilitate more accurate and transparent calibration of element models in the future, Section 4.3 contains recommendations for future experimental testing.

Each test was calibrated according to the following standardized procedure. These steps are shown on Figure 4.

1. The test data is processed to have a consistent treatment of P-delta effects such that the element calibrations are not affected by differences in the experimental set-ups that are used by various researchers.[3]
2. The yield shear force is estimated visually from the experimental results. In order to accurately calibrate the cyclic deterioration in step #6, it was necessary to calibrate the yield force separately for the positive and negative loading directions. Note that in cases where the test data exhibited cyclic hardening the yield shear force was slightly overestimated, as cyclic hardening is not accounted for in the element model.
3. The third step in the calibration process is to estimate the "yield" displacement, defined is the point at which the rebar yields or the concrete begins to significantly crush, depending on the level of axial load. In either case, this displacement was calibrated to be the point at which there was a significant observed change in the lateral stiffness of the column. This calibration of this point often required some judgment, as the concrete becomes nonlinear well before rebar yielding, and some tests with many pre-yield cycles had significant stiffness changes in the pre-yield region.
4. In the fourth step we looked more closely at the changes in stiffness in the pre-yield region. From the results of many experiments we observed that the stiffness often changes significantly near 40% of the yield load. Therefore, we also calibrate the displacement at 40% of the yield force. As in step #3, this was difficult for those tests that had many cycles before this level of loading.
5. In the fifth step, we calibrated the strength increase from the yield point to the capping point by visually calibrating the post-yield stiffness to the test data.

[3] We transformed all the force-displacement data to be consistent with P-Delta case #2 in Eberhard's database (Berry et al. 2004).

6. The sixth step is to calibrate the normalized cyclic energy dissipation capacity, λ. The element model allows cyclic deterioration coefficients λ and c to be calibrated independently for each cyclic deterioration mode. However, based on a short study of 20 columns, we found that c = 1.0 was acceptable for columns failing in flexure and flexure-shear modes.[4] We assumed the deterioration rates (λ) to be equal for the basic strength and post-capping strength deterioration modes (Ibarra 2003, chapter 3). Based on observations of the hysteretic response of the RC columns, we set the accelerated stiffness deterioration mode to have zero deterioration. We also set the unloading stiffness deterioration mode to have zero deterioration.[5] These simplifications reduce the calibration of cyclic energy dissipation capacity to one value (λ).

   When calibrating λ, we aimed to match the average deterioration for the full displacement history, but with a slightly higher emphasis on matching the deterioration rate of the later, more damaging, cycles. Calibration of λ is based only on the cyclic deterioration before capping occurs, so the assumption of an equal post-capping strength deterioration rate has not been verified.

7. The next step of the calibration process involved quantification of the capping point (and associated plastic rotation capacity) and the post-capping deformation capacity.

   The calibration of the capping point is a critical component of the element model calibration procedure. The capping point and post-capping stiffness are only included when a clear negative post-failure stiffness is seen in the data, causing strength loss to occur *within a single* cycle (often called "in-cycle deterioration"). A negative slope is never used to represent strength deterioration that occurs *between two cycles* (often called "cyclic deterioration"). The distinction between these two types of deterioration is illustrated in Sections 2.1.2.4.

   Often the test specimen did not undergo sufficient deformations for a capping point to be observed (i.e. no negative stiffness post-capping behavior was observed). In this case, we can not quantify the capping point from the test, but the data does tell us that the capping

[4] For the columns failing in flexure, c = 1.2 is the ideal value. For those failing in flexure-shear, c = 1.0 is more appropriate. For simplicity and consistency, we used c = 1.0 for all columns.

[5] We excluded unloading stiffness deterioration when performing these calibrations because there is currently an error in the Opensees implementation of the model; this error causes incorrect cyclic responses when the unloading stiffness deterioration mode is employed. Even so, unloading stiffness deterioration is appropriate and should be used when modeling RC elements. The Drain-2D implementation of the element model does not have this error.

point is at a displacement larger than those seen in the test. To incorporate this information for these types of tests, we calibrate a "lower bound value" of the capping point; to indicate that the value is a lower bound, LB=1 is added to the legend on the calibration plot.

In addition, when tests have many cycles and have a failure on the second (or later) cycle at the same level of displacement, the tests are treated in the same manner. Again, in this case, we calibrate a lower bound value for the capping point. This decision is motivated by the observation that earthquakes that can cause collapse of buildings typically do not have many large cycles before failure; instead, a few strong pulses and ratcheting of displacements will likely cause collapse. As a result, for tests with many cycles, the failure mode observed in the test (from fatigue, etc.) may not be representative of the failure mode expected for real seismic building behavior, and we chose to use the lower bound approximation for capping points in these tests as shown in Figure 3.

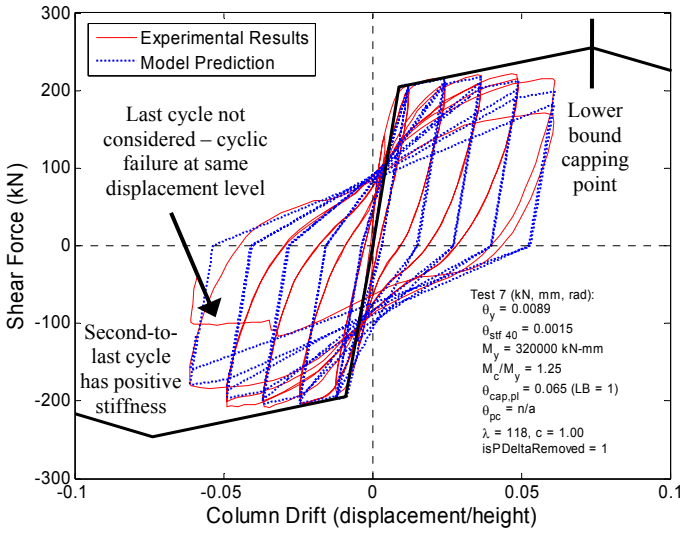

Figure 3. Illustration of lower bound in calibration of capping point. Calibration of RC beam-column model to experimental test by Soesianawati et al. [6], specimen 1.

[6] Soesianawati et al., 1986; PEER, 2005

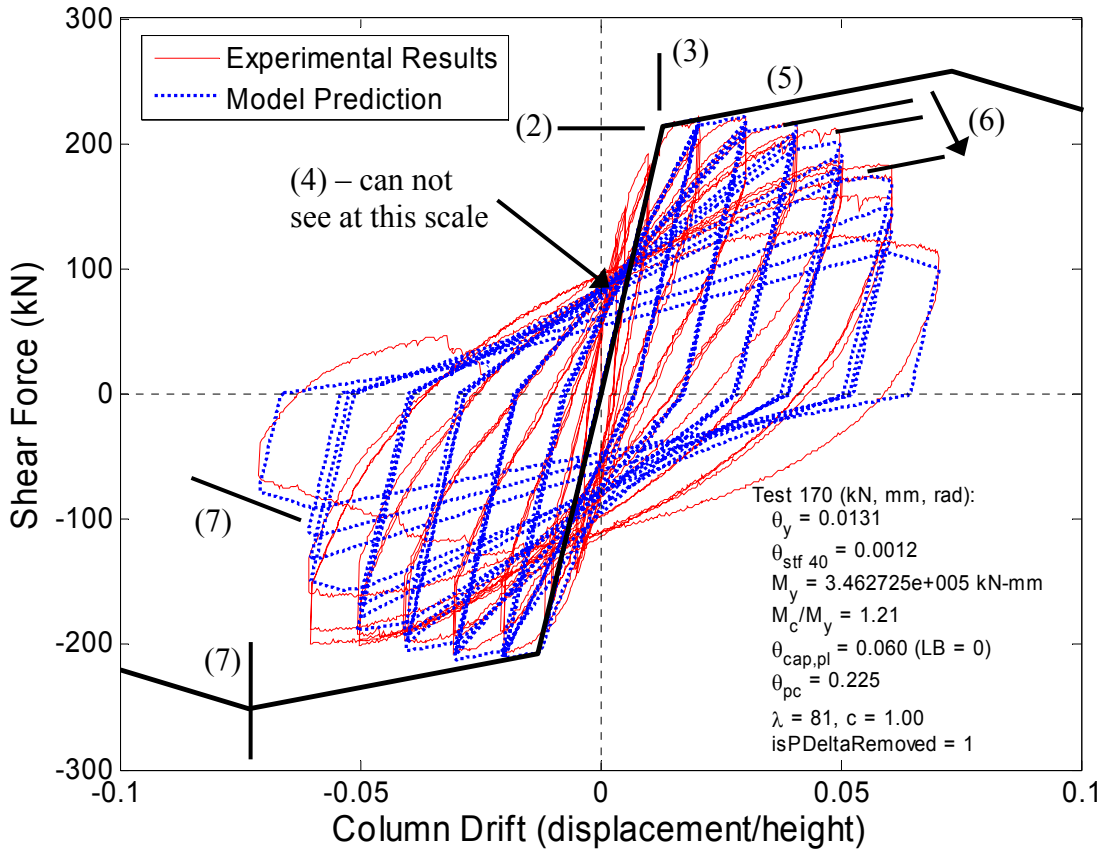

Figure 4. Example of calibration procedure; calibration of RC beam-column model to experimental test by Saatcioglu and Grira[7], specimen BG-6.

2.1.2.3 Treatment of Pinching

Typically, pinching was not a dominant factor in the 220 tests with flexural failure. In the 35 flexure-shear tests, nine tests exhibited significant pinching behavior. Contrary to common expectation, Medina (2002; chapter 7) shows that while element pinching behavior does increase the displacements of a building, it has nearly no impact on the collapse behavior. We also completed some simple sensitivity studies that validated these results. As a result, pinching effects are not calibrated in this study. The Ibarra element model does have the capability to represent pinching, however, so this could be easily incorporated in other calibration efforts where the phenomenon has more importance.

2.1.2.4 Common Calibration Pitfalls: Incorrect Calibration of Strength Deterioration

Incorrect calibration of strength deterioration can have a huge impact on structural response prediction. To obtain meaningful structural analysis predictions, it is critical to clearly distinguish between in-cycle and cyclic strength deterioration and to correctly account for them in the way the structural model is created and calibrated. Often these two modes of strength deterioration are mixed together, creating significant modeling errors.

The two types of strength deterioration are explained in several references (Ibarra et al. 2005, 2003, etc.), but the simplest explanation is given in chapter 4 of FEMA 440 (2005). The two types of strength deterioration are as follows:

- In-cycle strength deterioration: In this mode, strength is lost in a single cycle, which means that the element exhibits a negative stiffness. This is the type of strength deterioration that is critical for modeling structural collapse (Ibarra et al. 2005, 2003).
- Cyclic strength deterioration: In this mode, strength is lost between two subsequent cycles of deformation, but the stiffness remains positive. This is the type of strength deterioration is less important for modeling structural collapse (Ibarra et al. 2005, 2003; chapter 5 of Haselton et al. 2006).

Figure 5a shows Saatcioglu and Grira (1999) test specimen BG-6[8] calibrated with the two modes of strength deterioration properly separated. In this test, we see cyclic strength deterioration in the cycles before 5% drift and in-cycle strength deterioration in the two cycles that exceed 5% drift.

To investigate the significance of improperly modeling the strength deterioration, we also calibrated the model to specimen BG-6 in two incorrect ways and then completed collapse predictions for calibrated single degree-of-freedom systems. Figure 5b shows specimen BG-6 calibrated incorrectly with all strength loss caused by in-cycle strength deterioration. Notice that this method of calibration causes the negative failure slope to be reached a lower drift level and leads to a steeper post-failure slope than in Figure 5a. In Figure 5c, the same test is calibrated incorrectly with all strength loss caused by cyclic strength deterioration. In this case, the element

[7] Saatcioglu, 1999; PEER, 2005.
[8] Saatcioglu and Grira, 1999, specimen BG-6 (PEER 2005). This corresponds to test # 170 (for tables in the appendices).

never reaches a capping point and negative stiffness; therefore, when calibrated this way, dynamic instability can only occur with a combination of P-Delta and severe cyclic strength loss.

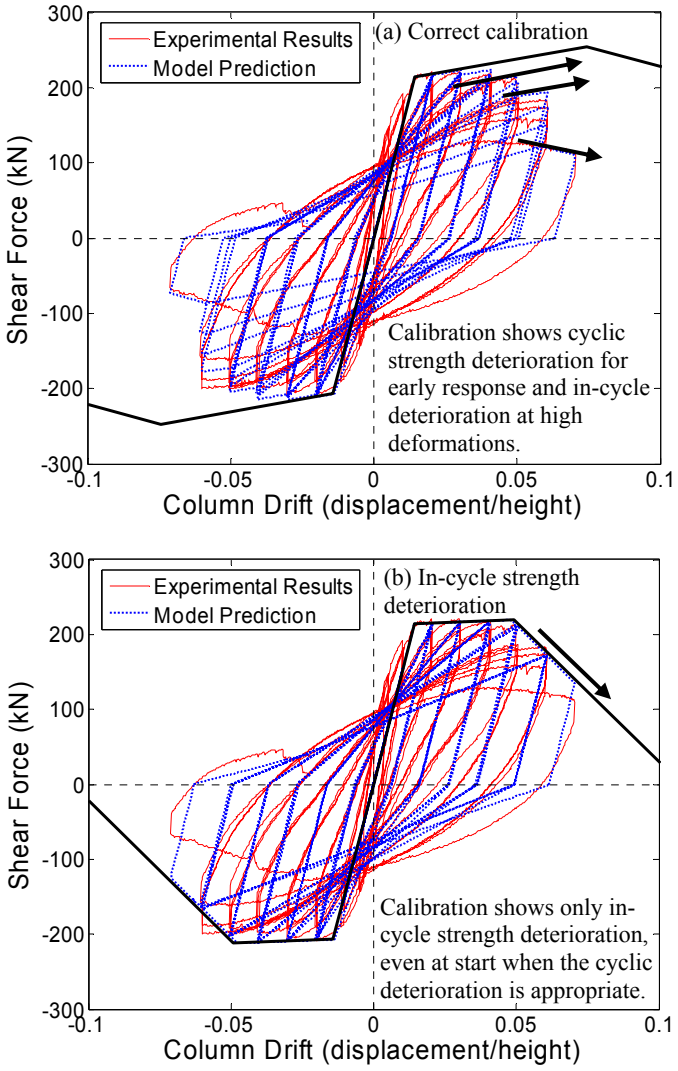

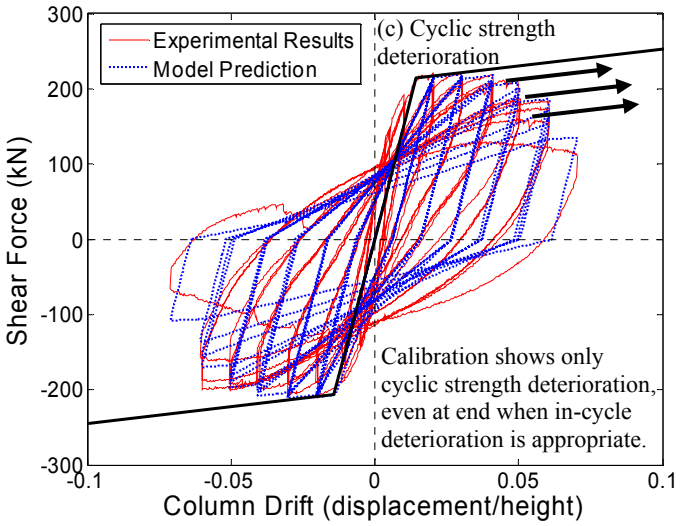

Figure 5. Illustration of a) correct calibration, b) incorrect calibration using only in-cycle strength deterioration, and c) incorrect calibration using only cyclic strength deterioration. Calibrated to Saatciolgu and Grira, specimen BG-6.

Using the three calibrations from Figure 5, we created three single degree-of-freedom (SDOF) models, each with an initial period of 1.0 second, a yield spectral acceleration (at 1 sec) of 0.25g, a damping ratio of 5%, and an axial load resulting in a relatively low amount of P-Delta (stability coefficient of 0.02). We used a set of 20 ground motions developed for a 1.0 second structure (Haselton and Baker, 2006) and performed Incremental Dynamic Analysis (IDA) (Vamvatsikos and Cornell, 2002) to collapse.

The results of the time-history of drift response for one ground motion, scaled to two different intensity levels, are shown in Figure 6, where S_a(1sec) = 1.0g in Figure 6a and S_a(1sec) = 2.6g in Figure 6b. At 1.0g, the model calibrated with Method B (all in-cycle) collapses while the other two models do not collapse and have similar drift responses. At 2.6g, the models calibrated with Methods A and B (correct, all in-cycle) collapse, while the model calibrated with Method C (all cyclic) does not collapse because it is calibrated without the negative post-failure stiffness.

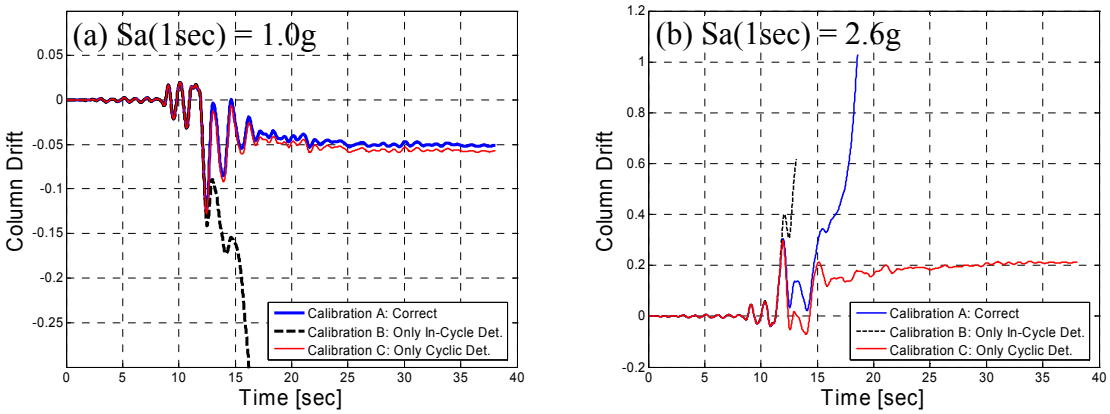

Figure 6. Time-history drift responses for the three SDOF systems calibrated in Figure 5 (a) showing drift response for Sa(1sec) = 1.0g and (b) showing response for Sa(1sec) = 2.6g.

When the incremental dynamic analysis results from all 20 ground motions are considered, the collapse capacities computed are shown in Figure 7. The median collapse capacity for the correct calibration method (method A) is 2.9g. If strength deterioration is incorrectly assumed to be all in-cycle (method B), then the median collapse capacity drops by 65% to 1.6g. If strength deterioration is incorrectly assumed to be all cyclic (method C) the median collapse capacity increases by 97% to 5.7g.

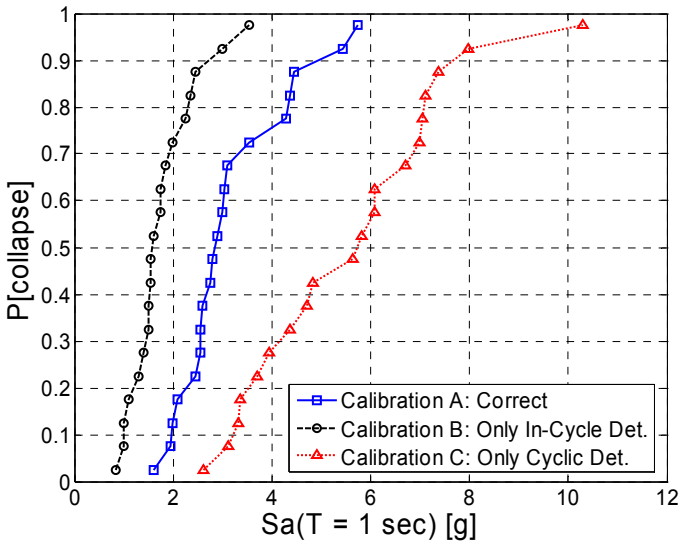

Figure 7. Cumulative distribution of collapse capacity for the three SDOF systems calibrated in Figure 5.

This example demonstrates that properly modeling and calibrating the two types of strength deterioration is critical.[9] Nonlinear dynamic analyses based on incorrect modeling/calibration methods will provide unrealistic results; this is especially true when modeling sidesway collapse (as is shown in Figure 7).

2.2 INTERPRETATION OF CALIBRATION RESULTS AND CREATION OF EMPIRICAL EQUATIONS

After the calibrations of the 255 columns were completed as outlined in Section 2.1.2.1 this information was used to create empirical equations that predict the element model parameters based on the column design parameters. A variety of analytical and graphical tools were used to interpret the calibration data and to assist in creation of these equations. Histograms illustrating the range of the calibrated parameters for the 255 columns are shown in Figure 8.

[9] Please note also that the monotonic backbone defined for the Ibarra element model (as shown in Figure 1) cannot be directly compared with backbones reported by other researchers, which are often created by connecting the peak point of every cycle. The latter mixes cyclic and in-cycle deterioration, and the negative slope shown has a different meaning.

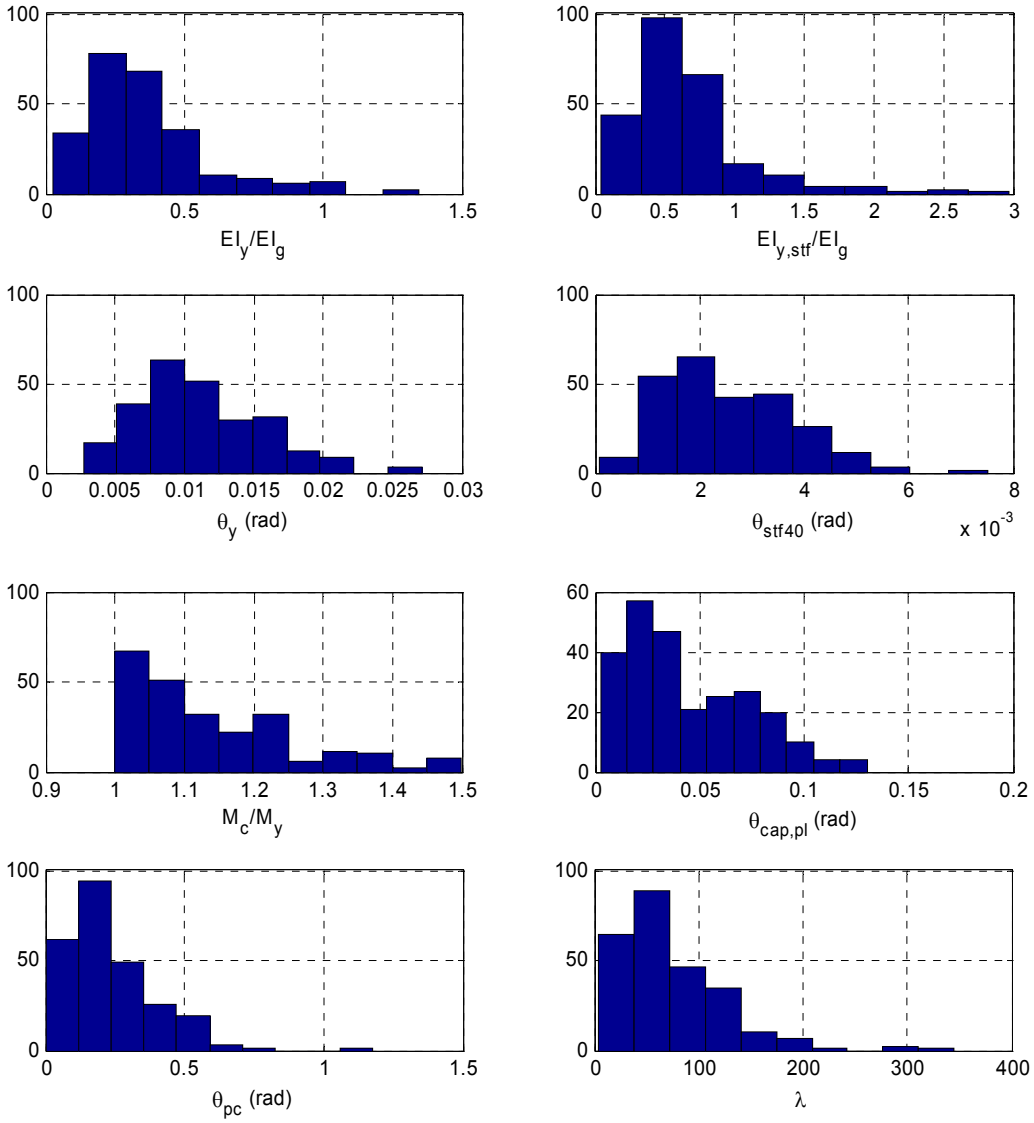

Figure 8. Histograms showing the range of calibrated model parameters for the 255 experimental tests included in this calibration study.

The simplest method of visually searching for relationships between the calibrated parameters (e.g. initial stiffness, plastic rotation capacity, etc.) and the column design variables (e.g. axial load ratio, confinement ratio, etc.) is by plotting the parameters versus the design variables and looking for trends. The major limitation of this approach is that these plots, or "scatterplots", may obscure trends when multiple variables are changing between the different tests. As a result, the scatterplots only show clear trends when there are only a few dominant column design variables that affect the modeling parameter of interest. For example, we will see that the

scatterplot approach does not work well for finding trends in plastic rotation capacity and we will need to progress to a better approach.

Figure 9 shows these scatterplots with EI_y/EI_g plotted against a small subset of possible predictor/design variables.[10] These scatterplots show obvious trends between EI_y/EI_g and both axial load ratio (ν) and the aspect ratio of the column (L_s/H). A weaker positive trend seems to exist between EI_y/EI_g and f'_c, while there is no clear trend between EI_y/EI_g and longitudinal reinforcement ratio (ρ_{total}).

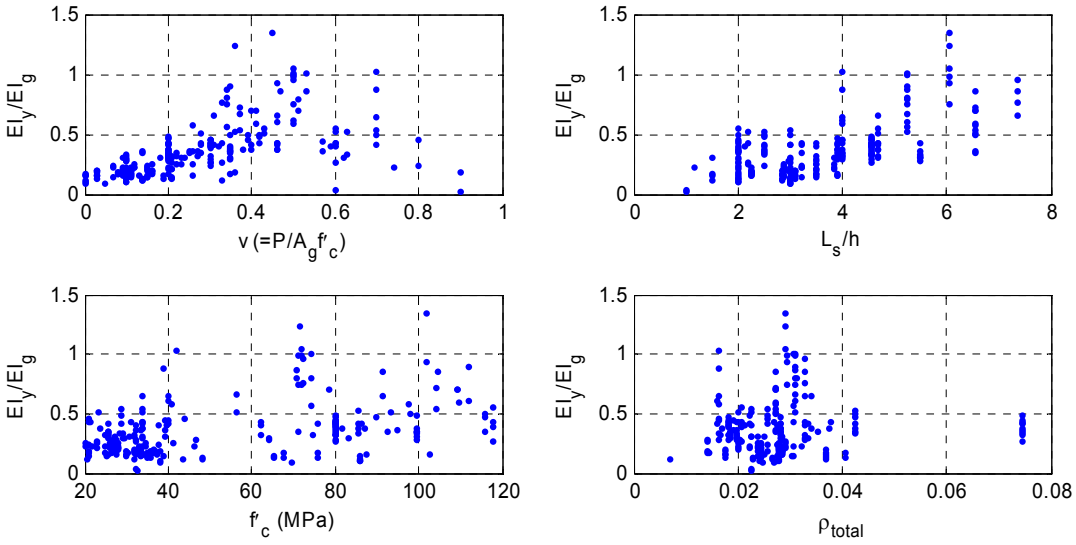

Figure 9. Selected scatterplots showing the trends between EI_y/EI_g and four column design variables.

Figure 10 is similar to Figure 9 but shows $\theta_{cap,\ pl}$ plotted against four possible predictor variables. The plastic rotation capacity of an element is much more difficult to predict as compared to the initial stiffness, and Figure 10 emphasizes this point. The scatterplots show a slight trend with axial load ratio, but the other design variables seem to have little impact on the plastic rotation capacity. However, we will later show that all of these predictor variables are statistically significant. In this case many column design variables are being varied between each point on the scatterplot and, consequently, important trends are hidden.

[10] Similar plots are shown in later sections with a larger number of column design variables. In Figure 9 we include a small number of plots to illustrate the general process of interpretation and use of the calibrated data.

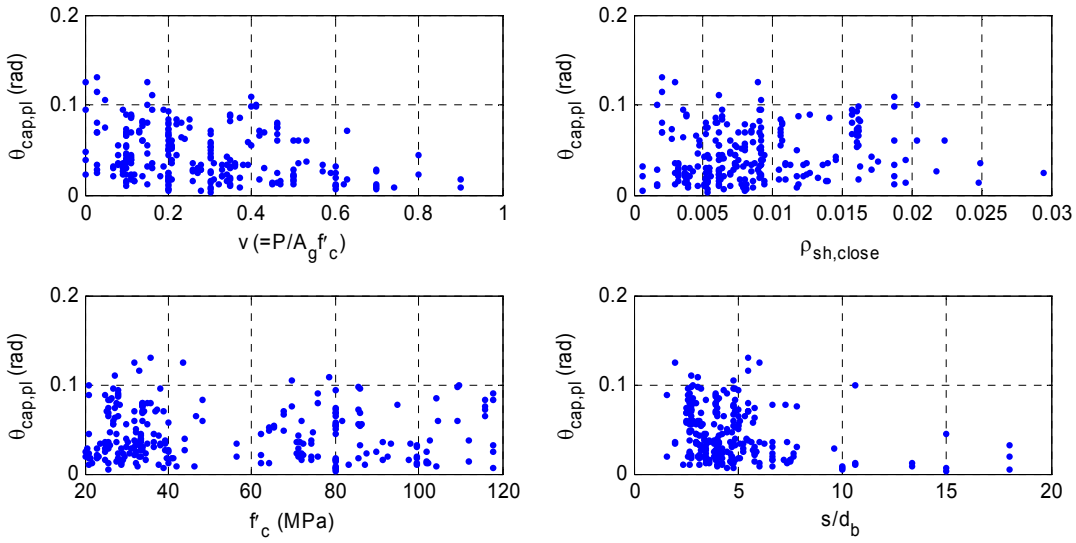

Figure 10. Scatterplots showing the trends between $\theta_{cap,\,pl}$ and four column design variables.

To more clearly see how each column design variable affects the model parameters, we separated the data into test series in which only one design variable is changed between the various column tests. For example, tests #215-217 by Legeron and Paultre (2000) are identical columns, with the exception that the axial load ratio applied varies. A complete list of test series of this type is available in Appendix A; in each of these 96 test series only one column design parameter was varied.[11] We use these series to see the effects of each design variable on the calibration results more clearly.

To illustrate the usefulness of this separation, Figure 11 shows a series of tests in which the only parameter varied was the confinement ratio (ρ_{sh}). This figure shows the impact that a change in the value of ρ_{sh} has on the plastic rotation capacity of an element, with all other design parameters held constant. Whereas the relationship between plastic rotation capacity and confinement ratio was murky in Figure 10, Figure 11 shows a clearer trend.

[11] Appendix B also includes tests that varied both stirrup spacing and lateral confinement ratio. Since these two parameters are correlated and often varied together, it is difficult to separate the effects of these two design variables.

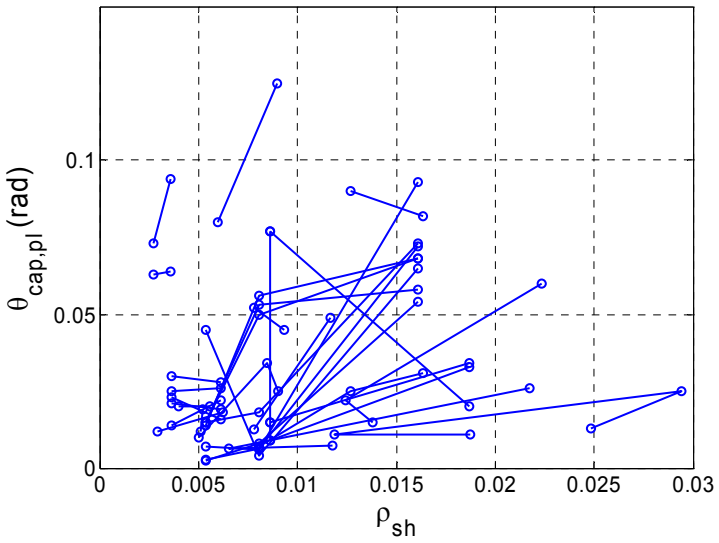

Figure 11. Plot showing the effects of ρ_{sh} on $\theta_{cap,\,pl}$.
Each line connects the dots corresponding to a single test series in which ρ_{sh} was the only variable changed.

More detailed information about the relationship between plastic rotation capacity and confinement ratio can be obtained by looking at the rate of change of $\theta_{cap,pl}$ with ρ_{sh} for each test series, ie. the slope of each line in Figure 11. Figure 12 shows these slopes plotted against ρ_{sh}. The p-values at the top of the figure show the results of simple statistical tests to see if the mean slope is nonzero and if the "slope of the slope" is non-zero (i.e. if the effect of ρ_{sh} on $\theta_{cap,\,pl}$ differs for different values of ρ_{sh}); $p < 0.05$ indicates statistical significance at 95%. Figures like Figure 12 are important because they show how much changes in ρ_{sh} should affect the predicted value of $\theta_{cap,\,pl}$. In addition, this figure provides useful information about the proper functional form of the equation. In the case of $\theta_{cap,\,pl}$ and ρ_{sh}, we see that $\theta_{cap,\,pl}$ should be more sensitive to ρ_{sh} for smaller values of ρ_{sh}. This information is used to check the results of regression analyses and ensure that the empirical equations (Chapter 3) are consistent with a close examination of the data.

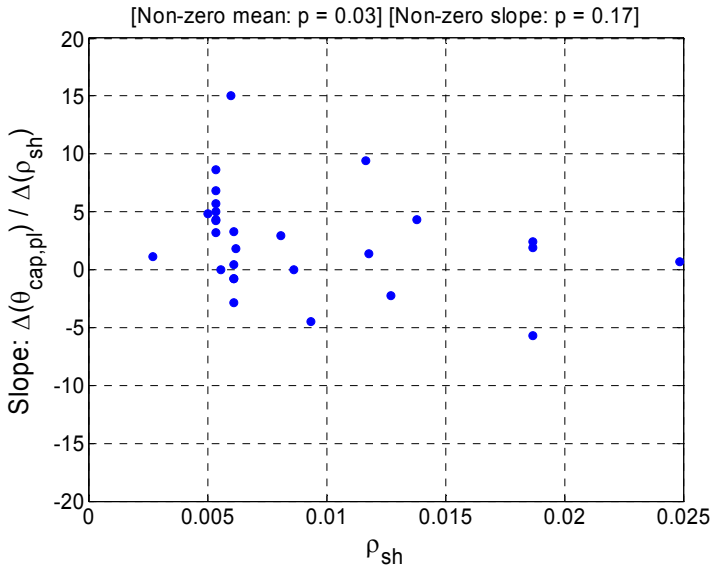

Figure 12. Plot showing the slopes from the data in Figure 11. Each point corresponds to one line in Figure 11. This type of plot is used to see the relationship (slope) between a model parameter and a design variable, and to investigate the appropriate functional form of an empirical equation relating the two variables.

We also use figures similar to Figure 12 to look for interactions between the effects of different variables. For example, we could plot axial load ratio on the x-axis instead of ρ_{sh}; this would help us learn if the level of axial load changes the relationship between $\theta_{cap,\ pl}$ and ρ_{sh}. This information can shed light on the appropriate functional form of the equation. However, it often becomes difficult to judge interactions because there is little data where two variables are both changed without other variables also being changed.

This section broadly outlined the approach used to identify trends in calibrated model parameters and the design variables, and to determine the proper form for empirical predictive equations. Chapter 3 explains this process in more detail for each empirical equation created.

3. Predictive Equations

3.1 OVERVIEW OF EQUATION FITTING METHOD

3.1.1 Regression Analysis Approach

3.1.1.1 Functional Form and Transformation of Data

One of the most important and difficult parts of creating an empirical equation is determining the appropriate functional form. The functional form must accurately represent the way in which the individual predictors affect the calibrated parameters and, additionally, how the various predictors interact with each other. To determine functional form, we (a) look closely at the data and isolate individual variables, as discussed in section 2.2 (eg. Figure 10, Figure 11, and Figure 12), (b) use previous research when available, and (c) use judgment based on an understanding of mechanics and expected behavior. The choice of functional form was often iterative, based on a process of developing an equation and then improving the equation based on the trends between the residuals (prediction errors) and the design parameters (predictors).

After establishing the functional form, we transformed the data to fit the functional form (typically using various natural logarithmic transformations), and then use standard linear regression analysis to determine the coefficients in the equation. We assume that the model parameters (e.g. plastic rotation capacity, etc.) follow a lognormal distribution, so we always perform the regression on the natural log of the model parameter or (or the natural log of some

transformed model parameter).[12] The logarithmic standard deviation is used to quantify the error.

We use the stepwise regression approach and include only variables that were statistically significant at the 95% level using a standard F-test. When creating the equations, we include all variables that are statistically significant. (For more details on regression analysis, see Chatterjee et al. 2000.)

After this full equation is completed, we often simplify the equation by removing some of the less influential variables; this can often be achieved without sacrificing a great deal of prediction accuracy. In the cases where this simplification is appropriate, we propose two equations: one *full* equation that includes all statistically significant variables, and a *simplified* equation with fewer variables. This leaves the reader with the decision regarding which equation they prefer to use.

3.1.1.2 Criteria for Removal of Data and Outliers

In the process of creating each predictive equation some data points were removed from the statistical analysis. In each case, a few tests were removed because either the experimental data or the calibration results indicated that the possibility of some problems or unusual conditions related to the calibrated parameter from that particular test. The removal of these tests was based on our judgment. Data points were removed from the equation for initial stiffness, for example, because of possible errors in the transformation to account for P-Δ effects or when the baseline displacement at the beginning of the test was negative. Data for post-yield (hardening) stiffness was also eliminated where there were possible problems with the P-Δ transformation. When creating the plastic rotation capacity equation, tests were removed when there were an unreasonable number of cycles causing a failure mode governed by cyclic damage, unlike the damage likely to occur in a real earthquake. Similarly, experimental tests lacking enough strength deterioration to judge an appropriate value for the cyclic deterioration parameter, λ, were not considered in the creation of the predictive equation for λ. A complete list of the tests removed is shown in Appendix B, Table 13.

[12] Exception: when creating equations for EI_y and EI_{stf40}, we do not use a natural log transformation because the form of the equation does not allow this transformation. Even so, we still report the errors using a lognormal

In addition, in the creation of each equation some data was removed based on a statistical test to identify which points were outliers, as based on their residuals. To identify the outliers we used a t-test to statistically determine whether each residual had the same variance as the other residuals; outliers were removed when the t-test showed a 5% or lower significance level (Mathworks 2005). In most cases the number of outliers removed was fewer than 10, or approximately 4% of the total number of data points. For each equation, we report prediction errors twice, in the first case including all data, and, in the second, excluding outliers removed by the t-test described above.

3.2 EFFECTIVE STIFFNESS

3.2.1 Literature Review

A great deal of previous research has been completed to determine the effective stiffness of reinforced concrete elements. This section outlines only four of the many studies and guidelines that exist.

The FEMA 356 guidelines (ASCE 2000; chapter 6) state that the "component stiffness shall be calculated considering shear, flexure, axial behavior and reinforcement slip deformations," and that generally the "component effective stiffness shall correspond to the secant value to the yield point of the component." Alternatively, for linear procedures, FEMA 356 permits the use of standard simplified values: $0.5E_cI_g$ when $P/(A_g f'_c) < 0.3$, and $0.7E_cI_g$ when $P/(A_g f'_c) > 0.5$. It is important to note than when the more rigorous FEMA 356 guidelines are followed the resulting element stiffnesses can as much as to 2.5 times lower than the simplified FEMA 356 values.

Mehanny (1999) utilized test results from twenty concrete columns and one reinforced concrete beam. From these data and a comprehensive review of previous research and design guidelines, he proposed an equation for the effective flexural stiffness and the effective shear stiffness of a column. Flexural stiffness is given by $EI_{eff} / EI_{g,tr} = \left(0.4 + 2.4\left(P / P_b\right)\right) \le 0.9$, where $I_{g,tr}$ is the gross transformed stiffness of the concrete section.

---

distribution (i.e. we use σ_{LN} to quantify the error).

More recently, Elwood and Eberhard (2006) proposed an equation for effective stiffness that includes all components of deformation (flexure, shear, and bond-slip), where the effective stiffness is defined as the secant stiffness to the yield point of the component. Their equation proposes $0.2E_cI_g$ when $P/(A_g f'_c) < 0.2$, $0.7E_cI_g$ when $P/(A_g f'_c) > 0.5$, and a linear transition between these two extremes.

Panagiotakos and Fardis (2001) took a slightly different approach and quantified the deformation (chord rotation) at yielding instead of quantifying the stiffness. The Panagiotakos et al. equations are based on a database of more than 1000 experimental tests (mainly cyclic). The empirical equation developed contains three terms: (a) a flexural term based on the yield curvature of the member, (b) a constant shear term, and (c) a bond-slip term that is derived from integrating rebar strains into the support of the column. When their predictions of yield deformation are used to predict stiffness, a typical value is approximately $0.2E_cI_g$.

3.2.2 Equation Development

The initial stiffness of a reinforced concrete element is not well defined. Figure 13 shows a monotonic test of a reinforced concrete column (Ingham et al., 2001) with the yield force and displacement labeled. It is clear that the "effective stiffness" depends highly on the force level. In this work, we attempt to bound the possible values of effective stiffness and quantify the effective stiffness in two ways: (a) secant value of effective stiffness to the yield point of the component (i.e. K_y or EI_y), and (b) secant value of effective stiffness to 40% of the yield force of the component (i.e. K_{stf_40} or EI_{stf_40}). Typically, the ratio between these two definitions of stiffness is approximately two.

Quantifying effective stiffness also requires that we be clear about which modes of deformation are included. In these simplified equations for initial stiffness, we include all modes of deformation (flexure, shear, and bond-slip). For those interested in separating the modes of deformation, we also propose an equation in Section 3.2.6 that includes only the shear and bond-slip components of deformation.[13]

[13] This method is proposed for use with a fiber element model, where the flexural component of deformation is modeled by the fiber element, but the additional flexibilities from shear and bond-slip need to be accounted by an additional spring in series.

With respect to functional form, we are attempting to keep the equations for initial stiffness simple, so an additive functional form is used. Using this additive functional form implicitly assumes the value of one column design variable does not change the impact of another design variable on the effective stiffness, i.e. there are not interactions between effects of each design variable.[14]

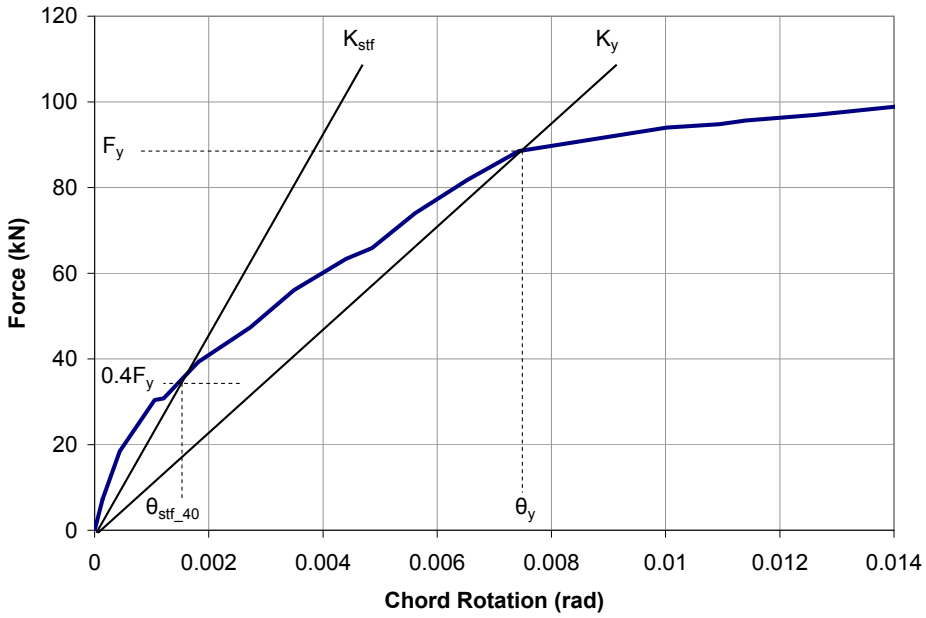

Figure 13. Monotonic test of a reinforced concrete element, and illustration of the definitions of effective stiffness.[15]

3.2.3 Trends in Calibration Results

Figure 14 shows the scatterplots relating the secant stiffness to the yield point of the component (EI_y/EI_g) to various column design parameters. (Note that the scatterplots show similar trends for the stiffer effective stiffness ($EI_{stf,40}/EI_g$), and are not included here.) There are clear trends between effective stiffness and both axial load ratio (v) and column aspect ratio (L_s/H), and a weaker trend with concrete compressive strength (f'_c). There are also clear trends with the level of shear force at flexural yielding (V_p/V_n and V_p/V_c), but these parameters are highly correlated with L_s/H.

[14] This assumption is not required and there are, of course, many possible other function forms. Our choice of the additive form was motivated by a desire for simplicity.

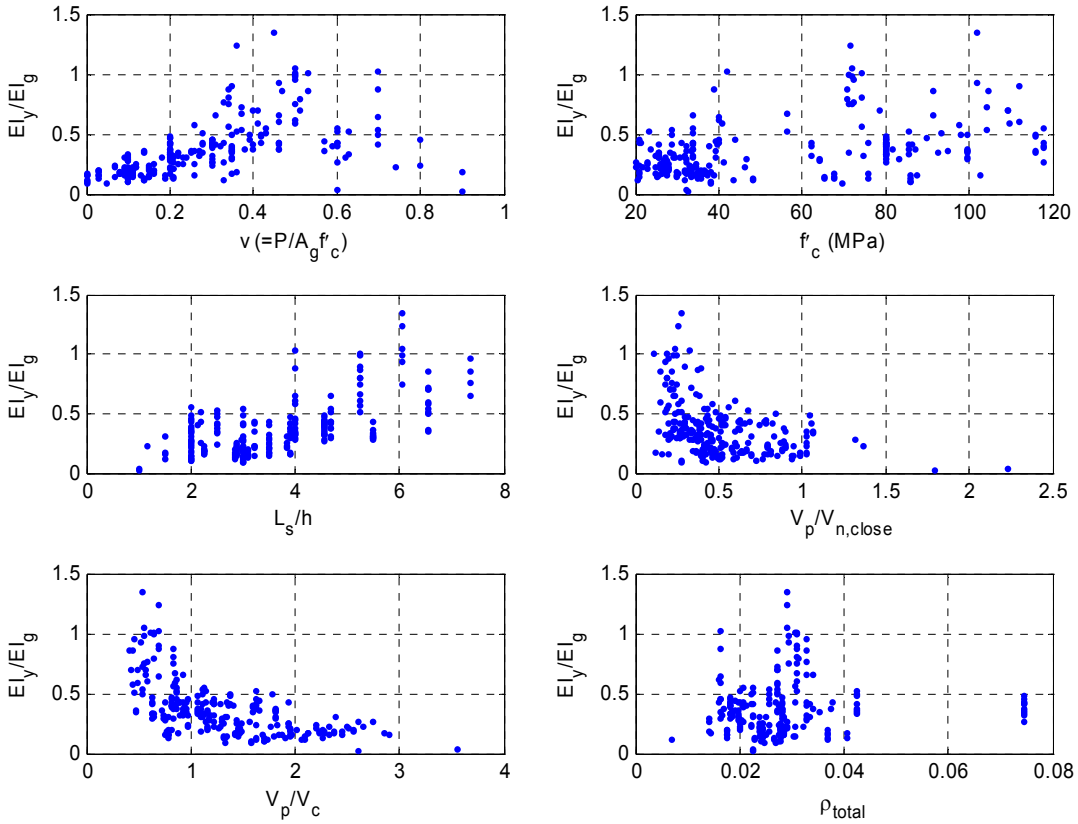

Figure 14. Scatterplots showing the trends between EI_y/EI_g and six column design variables.

3.2.4 Proposed Equations

For most equations in this report, we present a full equation which includes all statistically significant variables, and a simplified equation that is easier to use. For the following stiffness equations, concrete compressive strength (f'_c) is a statistically significant predictor. However the axial load ratio (ν) and the shear span ratio (L_s/H) have much stronger statistical significance, so f'_c is excluded for simplicity.

[15] data from Ingham et al, 2001

3.2.4.1 Secant Stiffness to Yield

Equation 1 presents the full equation for secant stiffness to yield, including axial load ratio and shear span ratio. Note that prediction errors are reported in terms of the logarithmic standard deviation, following the standard assumption that modeling parameter is lognormally distributed.[12]

$$\frac{EI_y}{EI_g} = -0.07 + 0.59\left[\frac{P}{A_g f'_c}\right] + 0.07\left[\frac{L_s}{H}\right], \text{ where } 0.2 \le \frac{EI_y}{EI_g} \le 0.6 \qquad (1)$$

$\sigma_{LN} = 0.28$ (with 2 outliers removed)
$\sigma_{LN} = 0.37$ (with no outliers removed)

This equation shows that the axial load ratio (ν) is very important to stiffness prediction; this is well known. The regression analysis also shows the significance of column aspect ratio (L_s/H) for predicting stiffness, with more slender columns having a higher stiffness ratio; this may seem counter-intuitive, but the stiffness is already normalized by I_g which is related to H.

We imposed the lower limit because there is limited data for columns with very low axial load. The lower limit of 0.2 is based on an (approximate) median stiffness for the tests in the database with ν < 0.10. We imposed an upper limit on the stiffness because for high levels of axial load, the positive trend diminishes and the scatter in the data is large. We chose the upper limit of 0.6 based on a visual inspection of the data.

Table 2 illustrates the impact that each variable has on the prediction of initial stiffness. The first row of this table includes the stiffness prediction for a baseline column design, while the following rows show how changes in each design parameter impact the stiffness prediction.

Table 2. Effects of column design parameters on predicted values of EI_y/EI_g.

EI_y/EI_g		
parameter	**value**	**EI_y/EI_g**
Baseline	v = 0.10, L_s/h = 3.5	0.23
v	0	0.20
	0.3	0.35
	0.8	0.60
L_s/h	2	0.20
	6	0.41

3.2.4.2 Secant Stiffness to Yield: Simplified Equation

Where a further simplified equation is desired, Equation 2 predicts effective stiffness, including only the effects of axial load ratio, and therefore has larger prediction error.

$$\frac{EI_y}{EI_g} = 0.065 + 1.05\left[\frac{P}{A_g f'_c}\right], \text{ where } 0.2 \le \frac{EI_y}{EI_g} \le 0.6 \quad (2)$$

$\sigma_{LN} = 0.36$ (with 2 outliers removed)

$\sigma_{LN} = 0.45$ (with no outliers removed)

3.2.4.3 Initial Stiffness

In order to better quantity initial stiffness, as compared to secant stiffness to the point of yielding, this section presents an equation for the secant value of effective stiffness to 40% of the yield force of the component. (See Figure 13 for illustration of these definitions of stiffness for RC elements.) In developing Equation 3 we followed the same procedure as detailed for Equation 1.

$$\frac{EI_{stf\,40}}{EI_g} = -0.02 + 0.98\left[\frac{P}{A_g f'_c}\right] + 0.09\left[\frac{L_s}{H}\right], \text{ where } 0.35 \le \frac{EI_{stf}}{EI_g} \le 0.8 \quad (3)$$

$\sigma_{LN} = 0.33$ (with 2 outliers removed)

$\sigma_{LN} = 0.42$ (with no outliers removed)

Table 3 illustrates the impact that each variable has on the stiffness prediction. Both axial and column slenderness ratio may have a significant overall impact on the predicted initial

stiffness. For a typical column Equation 3 predicts the initial stiffness (as defined to 40% of yield) will be approximately 1.7 times stiffer than the secant stiffness (Equation 1).

Table 3. Effects of column design parameters on predicted values of EI_{stf}/EI_g.

EI_{stf}/EI_g		
parameter	**value**	**EI_{stf}/EI_g**
Baseline	v = 0.10, L_s/h = 3.5	0.39
v	0	0.30
	0.3	0.59
	0.8	0.80
L_s/h	2	0.35
	6	0.62

3.2.4.4 Initial Stiffness: Simplified Equation

Equation 4 is a simplified equation for stiffness that only includes the effects of axial load ratio, and therefore has larger prediction error.

$$\frac{EI_{stf\,40}}{EI_g} = 0.17 + 1.61\left[\frac{P}{A_g f'_c}\right], \text{ where } 0.35 \le \frac{EI_{stf}}{EI_g} \le 0.8 \qquad (4)$$

$\sigma_{LN} = 0.38$ (with 2 outliers removed)

$\sigma_{LN} = 0.46$ (with no outliers removed)

3.2.5 Validation of Proposed Equations

3.2.5.1 Comparisons of Predicted and Observed Stiffness

Figure 15 shows the observed and predicted element stiffnesses for the secant stiffness to yielding (EI_y/EI_g). Below the figure, we also show the median and mean values of the ratio of

predicted to observed values.[16] These figures and the ratio of predicted/observed values show that the proposed equations provide dependable predictions of element stiffness.

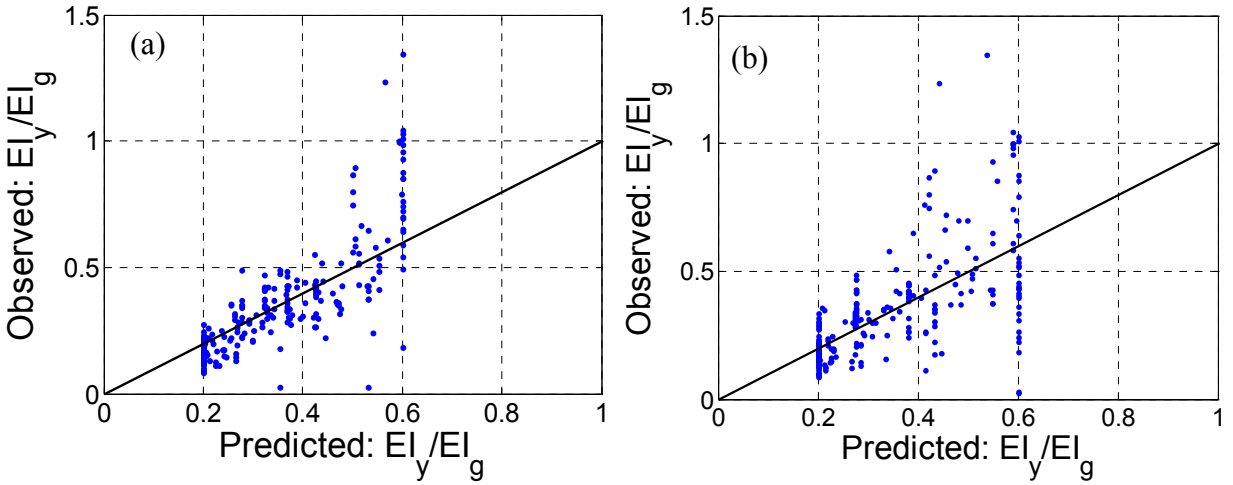

Median(predicted/observed) = 1.05
Mean(predicted/observed) = 1.23

Median(predicted/observed) = 1.02
Mean(predicted/observed) = 1.29

Figure 15. Comparison of observed values and predictions for secant stiffness (a) using Equation 1 and (b) using Equation 2.

Figure 16 shows the observed and predicted element stiffnesses for the initial stiffness through 40% of the yield force level (EI_{stf40}/EI_g) and reports the median and mean values of the ratio of predicted to observed values.[16] These figures and ratio of predicted and observed values show that the proposed equations provide good predictions of element stiffness.

[16] If the data are lognormally distributed, regression analysis shows that the median should be close to 1.0 and the mean should be larger than 1.0 for a good predictive equation. (Chatterjee et al. 2000)

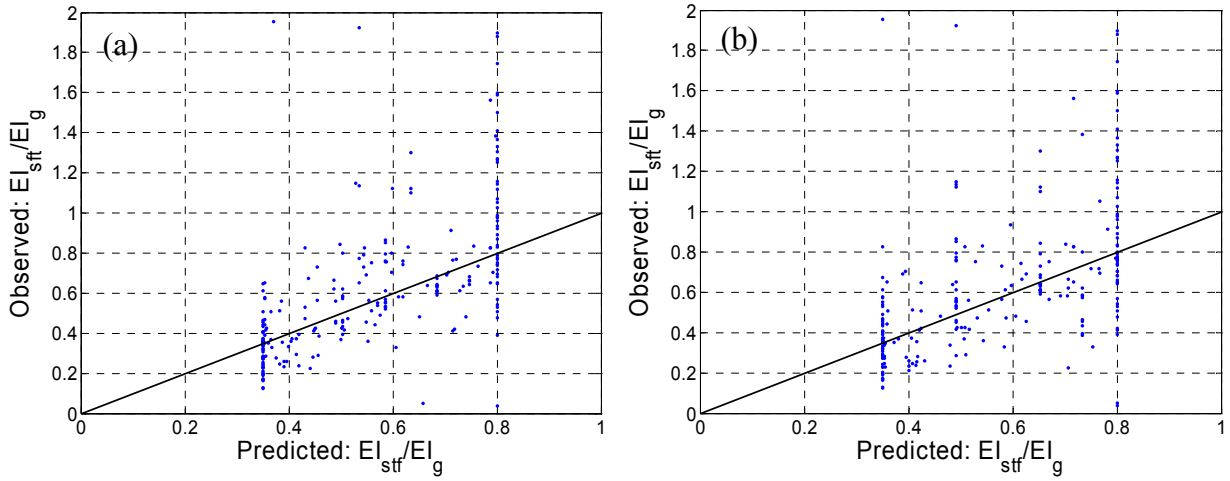

Median(observed/predicted) = 0.98
Mean(observed/predicted) = 1.52

Median(observed/predicted) = 1.00
Mean(observed/predicted) = 1.56

Figure 16. Comparison of observed values and predictions for initial stiffness (a) using Equation 3, and (b) using Equation 4.

3.2.5.2 Comparison of Proposed Equations with Previous Research

The equations proposed for secant stiffness to yielding of the component (Equations 2 and 4) are very similar to those recently proposed by Elwood and Eberhard (2006); the primary difference is that the proposed equation predicts slightly lower stiffness for stiff elements. Elwood and Eberhard (2006) report a coefficient of variation of 0.35 for his equation; our simplified equation is similar with a $\sigma_{LN} = 0.36$, but our full equation has a lower prediction error of $\sigma_{LN} = 0.28$.

The equation proposed for deformation at yield by Panagiotakos and Fardis (2001) provide an average prediction of $0.2E_cI_g$, and their equation is less sensitive to axial load than the proposed equations. For high levels of axial load, the effective stiffness predicted by Pangiotakos and Fardis increases to approximately $0.4E_cI_g$ on average. Our equations predict $0.2E_cI_g$ for low levels of axial load transitioning to $0.6E_cI_g$ for high levels of axial load.

The stiffness predictions in FEMA 356 (ASCE 2000) are much higher than our predictions. Elwood and Eberhard (2006) shows that most of this difference can be explained if it is assumed that the FEMA 356 values only include flexural deformation, and do not account for significant bond-slip deformations.

It is more difficult to compare the equations proposed for secant stiffness to 40% of the yield force of the component (Equations 3 and 4) to previous research. Although there has been significant work on initial stiffness of reinforced concrete elements, in many cases the definition of stiffness was unclear, and we did not find other researchers' results that were directly comparable to our proposed equations.

3.2.6 Effective Stiffness: Modeling the Shear and Bond-slip Components of Deformation When Using a Fiber Element Model

Commonly available fiber element models do not automatically account for bond-slip and shear deformations, so the analyst must determine the best way in account for these additional flexibilities. The purpose of this section is to provide recommendations on how to account for the additional flexibility due to bond-slip and shear when using a fiber element model.

3.2.6.1 Deformation at Yielding

At the yield point of the element, the deformation is composed of three components: flexure, bond-slip, and shear, as shown in Equation 5. To provide guidance on what proportion of the deformation is flexural, we computed the flexural component of deformation at yield using the equations proposed by Panagiotakos and Fardis (2001), as shown in Equation 6. We then computed the ratio of the observed yield deformation to the predicted flexural component of deformation, as show in Equation 7.

$$\theta_y = \theta_{y,f} + \theta_{y,b} + \theta_{y,s} \tag{5}$$

$$\theta_{y,f(PF2001)} = \phi_{y(PF2001)} \left[\frac{L_s}{3} \right] \tag{6}$$

$$\left[\frac{\theta_y}{\theta_{y,f(PF2001)}} \right]: \text{ Median} = 1.96, \text{ Mean} = 2.14, \ \mu_{LN} = 0.59 \ , \ \sigma_{LN} = 0.62 \tag{7}$$

From the results shown in Equation 7, we see that the flexural deformation is approximately half of the total deformation at yield.

A common modeling approach is to add a rotational spring at the ends of each fiber element to account for this additional flexibility. Equation 1, modified to incorporate the

information that the flexural deformation is approximately half of the total deformation, can be used to determine the effective stiffness properties of the additional spring.

3.2.6.2 Deformation at 40% of Yielding

With the goal of accurately capturing the nonlinearity in stiffness from zero load to the yield load, this section looks at the deformation at 40% of yield. To approximate the relative contributions of flexure, bond-slip, and shear deformation at this load level, we must first make an assumption about how flexural stiffness changes as the load increases.

At 40% of the yield load, the flexural stiffness will likely be higher than at yield, due to incomplete cracking and tension stiffening behavior. Even so, to keep these recommendations simple, we assume that the flexural stiffness is constant for all levels of loading. To be consistent with this assumption, when using the recommendations of this subsection for creating a fiber model, one should try to make the flexural stiffness of the fiber element constant over all load levels; this can be approximately done by excluding any additional stiffness from cracking or tension stiffness effects.

Using this assumption, we compute the ratio of total deformation to flexural deformation, at 40% of the yield force; this is shown in Equation 8. This shows that the contributions of bond-slip and shear deformations are relatively unimportant at 40% of the yield load, such that assuming pre-cracked concrete accounts for virtually all of the deformation at this load level. This conclusion that bond-slip and shear deformations are small at 40% of yield load is consistent with common understanding of element behavior and theoretical estimates of bond-slip deformation (Lowes et al., 2004). Therefore, at this load level the fiber model can be used without modifications for flexibility due to bond-slip and shear.

$$\left[\frac{\theta_{stf\_40}}{0.4*\theta_{y,f(PF2001)}}\right]: \text{ Median} = 0.99, \text{ Mean} = 1.18, \ \mu_{LN} = -0.032 \ , \ \sigma_{LN} = 0.71 \qquad (8)$$

3.3 CHORD ROTATION AT YIELD

This study focuses on the initial stiffness rather than chord rotation at yielding. We, therefore, do not present equations here to directly predict the chord rotation at yielding, but refer interested readers to Panagiotakos and Fardis (2001) and Fardis and Biskinis (2003).

When comparing our calibrated values to predictions from Fardis and Biskinis (2003), the mean ratio of θ_y / $\theta_{y,Fardis}$ is 1.12, the median ratio is 1.07, and the coefficient of variation is 0.50. Fardis et al. reports a coefficient of variation of 0.39 for their data.

In some preliminary studies looking for ways to improve the equation for chord rotation at yielding, we found that our data had a much stronger trend with axial load than would be expected from Fardis et al.'s equation. This is a topic of continued research.

3.4 FLEXURAL STRENGTH

Panagiotakos and Fardis (2001) have published equations to predict flexural strength; therefore, we use their proposed method to determine model parameter M_y. Their method works well, so we made no attempt to improve upon it.

When comparing our calibrated values to flexural strength predictions by Panagiotakos and Fardis (2001), the mean ratio of M_y / $M_{y,Fardis}$ is 1.00, the median ratio is 1.03, and the coefficient of variation is 0.30. Panagiotakos reports a coefficient of variation of 0.20 for their data, so their equation does not match our data as well as it matches the data that they used when creating the equation; this is to be expected for empirically calibrated equations.

Alternatively, a standard Whitney stress block approach, assuming plane sections remain plane, and expected material strengths may also be used to predict the flexural strength (M_y).

3.5 PLASTIC ROTATION CAPACITY

3.5.1 Literature Review

3.5.1.1 Theoretical Approach Based on Curvature and Plastic Hinge Length

Element rotation capacity is typically predicted based on a theoretical curvature capacity and an empirically derived plastic hinge length, and expressed in terms of a ductility capacity (i.e. normalized by the yield point).

A summary of this approach to predict element rotation capacity can be found in many references (Panagiotakos and Fardis, 2001; Lehman and Moehle, 1998, chapter 4; Paulay and Priestley, 1992; and Park and Paulay, 1975). Because the procedure is well-documented elsewhere, only a brief summary is provided here.

This approach uses a concrete (or rebar) strain capacity to predict a curvature capacity, and then uses the plastic hinge length to obtain a rotation capacity. The material strain capacity must be estimated, typically associated with a limit state of core concrete crushing, stirrup fracture, rebar buckling, or low cycle fatigue of the rebar. Concrete strain capacity before stirrup fracture can be estimated using a relationship such as that proposed by Mander et al. (1988); such predictions of concrete strain capacity are primarily based on the level of confinement of the concrete core. After the material strain capacity is determined, this strain capacity is related to a curvature capacity through using a section fiber analysis. The curvature capacity can then be converted to a rotation capacity using an empirical expression for plastic hinge length. Lehman and Moehle (1998, chapter 2) provide a review of expressions derived for predicting plastic hinge length.

Many researchers have concluded that this approach leads to an inaccurate, and often overly conservative, prediction of deformation capacity (Panagiotakos and Fardis, 2001; Paulay and Priestley, 1992). Paulay et al. (1992, page 141) explains that the most significant limitation of this method is that the theoretical curvature ends abruptly at the end of the element, while in reality the steel tensile strains (bond-slip) continue to a significant depth into the footing. Provided that the rebar are well anchored and do not pull out, this bond-slip becomes a

significant component of the deformation and increases the deformation capacity. Panagiotakos and Fardis (2001) show that bond-slip accounts for over one-third of the plastic rotation capacity of an element. In this study, we also found that this approach does not agree well with test data, and specifically that the concept of ductility does poorly at explaining element deformation capacity (Section 3.5.4.1).

Based on the preceding observations, we do not use the theoretical approach; we instead take the approach of predicting plastic rotation capacity empirically from the test data.

3.5.1.2 Empirical Relationships for Rotation Capacity

A small number of researchers have developed empirical equations directly predicting rotation capacity based on review of experimental data. Berry and Eberhard (Eberhard, 2005; PEER, 2005; Berry and Eberhard, 2003) assembled the PEER Structural Performance Database, consisting of cyclic test results for rectangular and circular RC columns. From this data, they created empirical equations that predict plastic rotation at the onset of two distinct damage states: spalling and rebar buckling. For columns controlled by rebar buckling, the rebar buckling damage state should be closely related to the plastic rotation capacity ($\theta_{cap,pl}$) as defined in this study.

Fardis et al. (Fardis and Biskinis 2003; Panagiotakos and Fardis 2001) developed empirical relationships for ultimate rotation capacity based on a comprehensive database of experimental results of RC element tests. The database includes a total of 1802 tests, 727 of which are cyclic tests of rectangular columns with conforming detailing and failing in a flexural mode. Fardis et al. developed an equation to predict the chord rotation at "ultimate," where "ultimate" is defined as a reduction in load resistance of at least 20%. Equations are provided for both monotonic and cyclic loading. The equations proposed by Fardis for monotonic plastic rotation from yield to point of 20% strength loss ($\theta_{u,mono,pl}$) is given below:

$$\theta_{u,mono}{}^{pl} = \alpha_{st}{}^{pl}(1+0.55a_{sl})(1-0.4a_{wall})(0.2)^{v}\left(\frac{\max(0.01,\omega')}{\max(0.01,\omega)}f'_{c}\right)^{0.225}\left(\frac{L_s}{h}\right)^{0.375}25^{\left(\alpha\rho_{sh}\frac{f_{y,sh}}{f'_{c}}\right)}1.3^{100\rho_d} \quad (9)$$

where L_s is distance between maximum and zero moment, a_{sl} is a bond-slip indicator, $f_{y,sh}$ is the stirrup yield strength), f'_c is concrete strength, α_{st} is a coefficient for type of steel, a_{wall} is a coefficient to indicate if the member is a wall, v is the axial load ratio, ω and ω‘ are reinforcement ratios, h is the height of the section, α is a confinement effectiveness factor, ρ_{sh} is the area ratio of transverse steel parallel to direction of loading, and ρ_d is ratio of diagonal reinforcement.

Berry et al. and Fardis et al. provide an important point of comparison for the empirical plastic rotation capacity equation proposed in this work. The primary advantage of the $\theta_{cap,pl}$ proposed in this research is that the predicted rotation capacity can be directly linked to the beam-column element model. In particular, while Berry et al. quantify the onset of the rebar buckling, their model does not provide a quantitative link to the associated degradation parameters ($\theta_{cap,pl}$ and θ_{pc}) needed in the model. Likewise, Fardis et al. provides explicit equations of the degraded plastic rotations (e.g., $\theta_{u,mono,pl}$), but $\theta_{cap,pl}$ must be inferred based on the ultimate rotation ($\theta_{u,mono,pl}$) and an assumed negative post-capping stiffness.

3.5.1.3 Potential Predictors

Previous work (especially by Fardis et al.) in development of empirical equations and observations from experimental tests were used to identify the most important column design parameters in prediction of plastic rotation capacity. These parameters are listed below:

- Axial load ratio (ν), lateral confinement ratio (ρ_{sh}): These are particularly important variables that are incorporated by Fardis et al. and also in the proposed equations. We considered using the ratio of axial load to the balanced axial load (P/P_b) in place of the axial load ratio. However, we concluded that the prediction improvement associated with using P/P_b did not warrant the additional complexity, so axial load ratio is used.
- Bond-slip indicator variable (a_{sl}): Fardis et al. showed that bond-slip is responsible for approximately one-third of the ultimate deformation; he uses an indicator variable to distinguish between tests where slip is ($a_{sl} = 1$) or is not ($a_{sl} = 0$) possible. We use the same variable in our proposed equation.

- Concrete strength (f'_c): Fardis et al. uses a concrete strength term that causes the predicted deformation capacity to increase with increases in concrete strength (Panagiotakos and Fardis, 2001). Our regression analysis revealed the opposite trend, so our proposed equation predicts a decrease in deformation capacity with an increase in concrete strength.
- Column aspect ratio (L_s/H): Fardis et al. found this term to be a statistically significant predictor. In our regression analyses, we consistently found this term to be statistically insignificant.
- Confinement effectiveness factor: Fardis et al. use a term for confinement effectiveness based on Paultre et al. (2001), $\rho_{sh,eff} = \rho_{sh} f_{y,sh} / f'_c$. In the regression analysis, we found this to be a slightly more statistically significant predictor than the transverse reinforcement ratio, but we decided to use ρ_{sh} for lateral confinement in the interest of simplicity.
- Rebar buckling terms: Dhakal and Maekawa (2002) investigated the post-yield buckling behavior of bare reinforcing bars. In this work, they developed a we refer to as the rebar buckling coefficient: $s_n = \left(s / d_{b,l}\right)\sqrt{\left(f_y / 100\right)}$ where f_y is in MPa units. We found that this coefficient is a better predictor of element plastic rotation capacity than simple stirrup spacing and we use it in our proposed equation. In another study, Xiao et al. (1998) found that columns with large diameter rebar have larger deformation capacity because the rebar buckling is delayed. In their test series, they kept the stirrup spacing constant, so their statement could be interpreted to mean that a larger deformation capacity can be obtained by either increasing $d_{b,l}$ or decreasing $s/d_{b,l}$. When creating the equation, we tried using both $s/d_{b,l}$ and s_n, and found that s_n is a performs slightly better predictor, but $s/d_{b,l}$ could have been without a significant change in the prediction accuracy.

3.5.2 Trends in Calibration Results

Figure 17 shows the scatterplots for the plastic rotation capacity of an element ($\theta_{cap,pl}$). Some trends are evident, but the significant scatter makes other trends unrecognizable (Section 2.2).

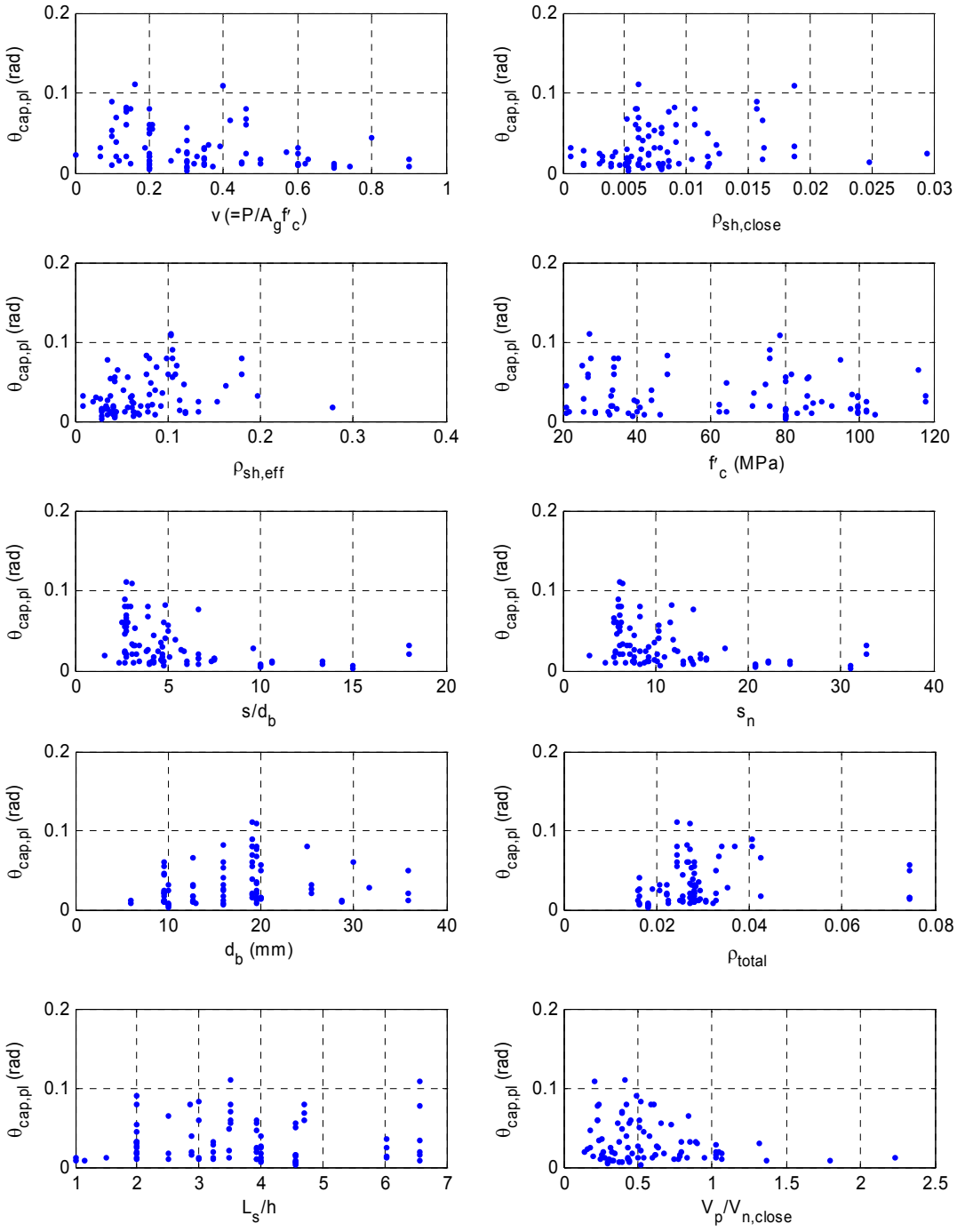

Figure 17. Scatterplots showing the trends between $\theta_{cap,pl}$ and ten column design variables. In order to see trends clearly, this only includes data that has an observed cap and negative stiffness (i.e. LB = 0).

To help see trends more clearly, Figure 18 shows the effects that a variation of a single design parameter has on the observed plastic rotation capacity. (Section 2.2 discusses this approach in detail.)

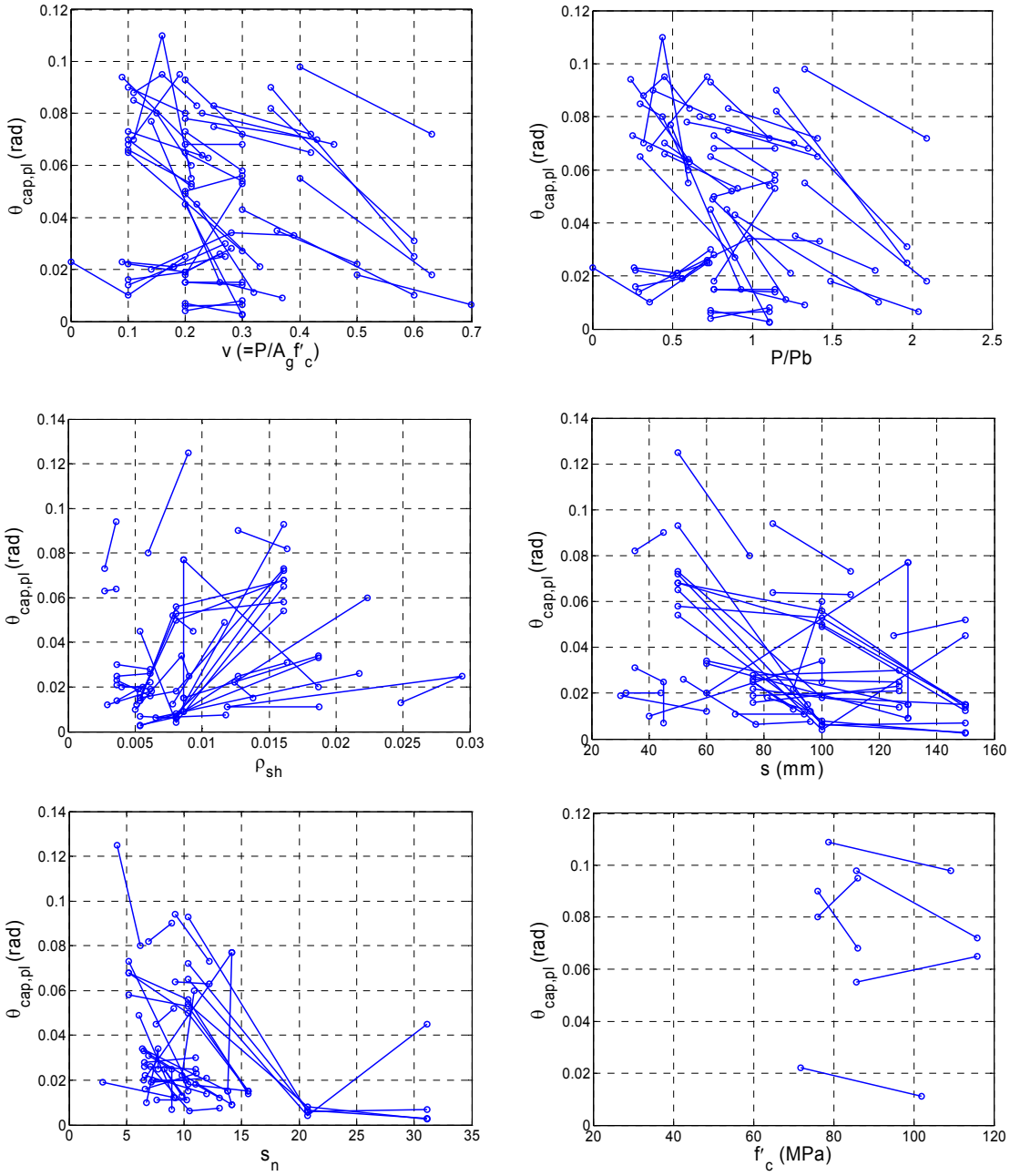

Figure 18. Plot showing the effects of individual variables on the observed value of $\theta_{cap,\,pl}$. Each line connects the dots of a single test series where the x-axis variable was the only variable changed. This figure is based on data where a capping point was observed.[17]

[17] See Appendix A for more detail on these test series.

3.5.3 Equation Development

The prediction for plastic rotation capacity was created using standard linear regression analysis by transforming the data with log-transformations. We used a multiplicative form of the equation, which introduces interaction between the effects of the predictors; this equation form is similar to that used by Fardis et al. (Fardis and Biskinis, 2003; Panagiotakos and Fardis, 2001).

As discussed previously, many of the column tests in the calibration study were not tested at large enough deformations to observe a capping point, providing an additional complexity in the development of this equation. During the calibration process we labeled tests as lower bound LB = 0 or 1. LB = 0 refers to tests where a cap and negative stiffness was observed. When a cap was not observed in the data, we set LB = 1 and calibrated a lower bound plastic rotation capacity. (See Section 2.1)

The equation developed is based on both sets of data (LB = 0 and LB =1). We found it necessary to use all the data because the LB = 0 data tended to include mostly columns with small rotation capacities. As a result, LB = 0 excludes most of the ductile column data from the regression and the resulting equation underestimates the rotation capacity for ductile columns. Including all the data (LB = 0 and LB = 1) provides more accurate predictions for conforming elements and is still conservative for columns of high ductility (because of the use of lower bound data for the most ductile columns).

3.5.4 Proposed Equations

3.5.4.1 Full Equation

Equation 10 presents the full equation, including all variables that are statistically significant. As usual, the prediction error associated with this equation is quantified in terms of the logarithmic standard deviation. We checked the possibility of high correlation between ρ_{sh} and stirrup spacing, but we found that the correlation coefficient between ρ_{sh} and s_n is only -0.36 for the data set, which shows that collinearity should not be a problem in this equation.

$$\theta_{cap,pl} = 0.12\left(1+0.55a_{sl}\right)\left(0.16\right)^{v}\left(0.02+40\rho_{sh}\right)^{0.43}\left(0.54\right)^{0.01c_{units}f'_c}\left(0.66\right)^{0.1s_n}\left(2.27\right)^{10.0\rho} \quad (10)$$

$\sigma_{LN} = 0.54$ (when 7 outliers removed)

$\sigma_{LN} = 0.63$ (with no outliers removed)

where a_{sl} is a bond-slip indicator (a_{sl} = 1 where bond-slip is possible), ν is the axial load ratio, ρ_{sh} is the area ratio of transverse reinforcement in the plastic hinge region spacing, s_n is a rebar buckling coefficient ($\left(s/d_b\right)\left(c_{units}\, f_y/100\right)^{0.5}$), s is stirrup spacing, d_b is the longitudinal rebar diameter, f_y is the yield strength of the longitudinal rebar, and c_{units} is a units conversion variable that equals 1.0 when f'_c and f_y are in MPa units and 6.9 for ksi units.

The impact of each of these parameters on the predicted plastic rotation capacity is shown in Table 4. Within the range of column parameters considered in Table 4 the plastic rotation capacity can vary from 0.015 to 0.082. The table shows that the axial load ratio (ν) and confinement ratio (ρ_{sh}) have the largest effect on the predicted value of $\theta_{cap,pl}$. The concrete strength (f'_c), rebar buckling coefficient (s_n), and longitudinal reinforcement ratio (ρ) have less dominant effects, but are still statistically significant.

Table 4. Effects of column design parameters on predicted values of $\theta_{cap,pl}$, using the full equation.

$\theta_{cap,pl}$		
parameter	**value**	**$\theta_{cap,pl}$**
Baseline	ρ_{sh} = 0.0075, f'_c = 30 MPa, v = 0.10, α_{sl} = 1, s_n = 12.7, ρ = 0.02	0.055
α_{sl}	0	0.035
v	0 0.3 0.8	0.066 0.038 0.015
ρ_{sh}	0.002 0.01 0.02	0.033 0.062 0.082
f'_c (MPa)	20 40 80	0.058 0.052 0.040
s_n	8 16 20	0.067 0.048 0.040
ρ	0.01 0.03	0.050 0.059

The shear span ratio (L_s/H) is notably absent from the equations developed. The stepwise regression process consistently showed L_s/H to be statistically insignificant. The relative unimportance of this predictor implies that the ductility capacity concept is not well-supported by this data. The flexural component of the yield chord rotation was also consistently shown to be statistically insignificant in prediction of plastic rotation capacity. These findings differ from the results from Panagiotakos and Fardis (2001), which was not expected.

3.5.4.2 Simplified Equation

The previous equation included all statistically significant variables, but in many cases a simpler equation is desirable. Therefore, Equation 11 is a simplified equation that has only a slightly larger prediction error. Table 5 shows the impact of each of the parameters on the predicted

plastic rotation capacity; this shows that the simplified equation often predicts 20% larger deformation capacity as compared to the full equation.

$$\theta_{cap,pl} = 0.13\left(1+0.55a_{sl}\right)\left(0.13\right)^{v}\left(0.02+40\rho_{sh}\right)^{0.65}\left(0.57\right)^{0.01c_{units}f'_c} \qquad (11)$$

where a_{sl}, ν, ρ_{sh}, f'c, and c_{units} are defined as above.

$\sigma_{LN} = 0.61$ (when 4 outliers removed); compared to $\sigma_{LN} = 0.59$ for Equation 10

$\sigma_{LN} = 0.69$ (with no outliers removed)

Table 5. Effects of column design parameters on predicted values of $\theta_{cap,pl}$, using the simplified equation.

$\theta_{cap,pl}$		
parameter	**value**	**$\theta_{cap,pl}$**
Baseline	ρ_{sh} = 0.0075, f'c = 30 MPa, ν = 0.10, α_{sl} = 1	0.071
α_{sl}	0	0.046
v	0	0.087
	0.3	0.047
	0.8	0.017
ρ_{sh}	0.002	0.033
	0.01	0.085
	0.02	0.131
f'_c *(MPa)*	20	0.075
	40	0.067
	80	0.054

3.5.4.3 Equation Including the Effects of Unbalanced Reinforcement

The experimental data used in this study does not include any tests with unbalanced longitudinal reinforcement; all tests are columns with symmetrical arrangements of reinforcement. Therefore, Equations 10 and 11 can only be used for cases where the reinforcement is balanced. This is a significant limitation, as virtually all beams have unbalanced reinforcement which will affect the plastic rotation capacity, causing the rotation capacity to be smaller when the element is loaded with more steel in tension and larger when more steel is in compression.

Fardis et al.'s data set did not have this limitation, so they developed a term that accounts for the effects of unbalanced reinforcement (Fardis and Biskinis 2003). To remove the balanced reinforcement limitation from Equations 10 and 11, we propose incorporating the term from Fardis et al. into Equations 10 and 11 and they become Equations 12 and 13.

$$\theta_{cap,pl} = 0.12\left(\frac{\max\left(0.01, \frac{\rho' f_y}{f_c'}\right)}{\max\left(0.01, \frac{\rho f_y}{f_c'}\right)}\right)^{0.225} \left(1+0.55a_{sl}\right)\left(0.16\right)^{v}\left(0.02+40\rho_{sh}\right)^{0.43} (continued...)$$

$$\left(0.54\right)^{0.01c_{units}f'_c}\left(0.66\right)^{0.1s_n}\left(2.27\right)^{10.0\rho} \quad (12)$$

$$\theta_{cap,pl} = 0.13\left(\frac{\max\left(0.01, \frac{\rho' f_y}{f_c'}\right)}{\max\left(0.01, \frac{\rho f_y}{f_c'}\right)}\right)^{0.225} \left(1+0.55a_{sl}\right)\left(0.13\right)^{v}\left(0.02+40\rho_{sh}\right)^{0.65}\left(0.57\right)^{0.01c_{units}f'_c} \quad (13)$$

where variables are defined as above, and ρ is the ratio of tension reinforcement (A_s/bd) and ρ' is the ratio of tension reinforcement (A_s'/bd).

3.5.5 Validation of Proposed Equation

3.5.5.1 Predictions and Observations

Figure 19 compares the observed and predicted values of plastic rotation capacity (Equation 10), including both test data where capping was observed (LB = 0), and those where a lower bound was inferred (LB =1). The figure shows the mean and median ratios of observed and predicted values for the full data set, and for the subset of data where a capping point was observed. These results imply that when a cap is observed (ie. subset including only LB = 0), Equation 10 overpredicts the plastic rotation capacity by 15% on average. This does not necessarily mean that the Equation 10 is non-conservatively biased for less-ductile specimens. In fact, this is the expected result when we choose to look only at the subset of columns that exhibited capping during the experimental test. When looking at only this subset of tests, it is likely that a higher

number of specimens will have plastic rotation capacities below the mean predicted for each specimen. Despite the large scatter, we see that when the full data set is considered (as in Figure 19) Equation 10 accurately captures the median tendency of the data.

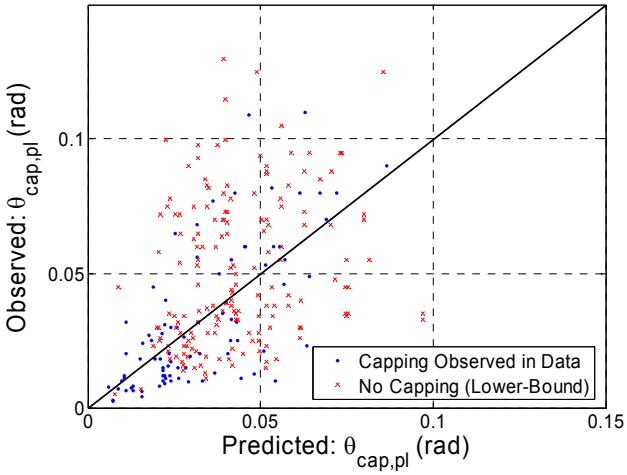

All data (cap observed and lower bound):
Median(observed/predicted) = 0.99
Mean(observed/predicted) = 1.18

Only data with observed capping point:
Median(observed/predicted) = 0.85
Mean(observed/predicted) = 0.96

Figure 19. Comparison of observed values and predictions for $\theta_{cap,pl}$ using Equation 10 and including all test data.

3.5.5.2 Verification of Accuracy for Column Subsets

We further verified the predictive accuracy of the equation by examining subsets of the data and checking for systematic over or under-predictions. The purpose of Table 6 is to specifically verify that Equation 10 does not create systematic errors for particular types of columns we would like to model.

Table 6 shows the ratio of predicted to observed plastic rotation capacity values for three subsets of the columns. Subset A has "conforming" levels of confinement ($\rho_{sh} > 0.006$), low axial load levels ($\nu < 0.3$), and lower concrete strengths ($f'_c < 40$ MPa). Subset B has "non-conforming" levels of confinement ($\rho_{sh} < 0.003$), and the same ranges of axial load and f'_c as Subset A. Subset C has high axial loads with $\nu > 0.65$.

Table 6. Ratio of predicted $\theta_{cap,pl}$ (Equation 10) to observations for subsets of the data.

		Observed/Predicted		
Subset	**NumTests**	**Mean**	**Median**	**Coeff. Of Var.**
(A) Conforming Confinement	30	1.23	1.14	0.46
(B) Non-Conforming Confinement	9	1.16	0.99	0.63
(C) High Axial Load	11	0.97	0.92	0.59

Table 6 shows that the predicted plastic rotation capacities ($\theta_{cap,pl}$) are 14% too low for the conforming confinement subset (Subset A). A close examination of the data showed that this is due to experimental tests where bond-slip is possible beyond the section of maximum moment[18]; when only tests without bond-slip are included the median ratio of observed to predicted becomes 1.05. This discrepancy suggests that the bond-slip component of deformation is a larger ratio of the total deformation for elements that have higher deformation capacity; from physical behavior this makes sense, as we expect more bond-slip deformation when there are higher rebar strains and more cyclic damage. We considered altering the Equations 10 and 11 to reflect this behavior, but decided that the added complexity was not warranted. As a result, Equation 10 is slightly conservative for very ductile columns.

Table 6 shows that the equation gives good predictions for the subset of non-conforming confinement (Subset B), although this is only based on nine tests and has a high coefficient of variation. Table 6 shows that the equation over-predicts deformation capacity by 8% for columns with very high axial loads; however, this observation is only based on the 11 tests available with such high axial loads. These comparisons should be reconsidered when more test data is available.

In summary, considering the large prediction uncertainty associated with Equation 10, Table 6 shows that mean and median predictions are relatively accurate for the subsets of the data considered. In addition, the coefficient of variation is relatively consistent across subsets of columns with very different characteristics.

3.5.5.3 Comparisons to Predictions by Fardis et al.

It is also useful as verification to compare the predicted rotation capacity (Equation 10) to the ultimate rotation capacity predicted by Fardis et al. as shown in Equation 9 (Fardis and Biskinis

2003, Panagiotakos and 2001). Figure 20 compares these predictions and includes only the data that have an observed capping point.

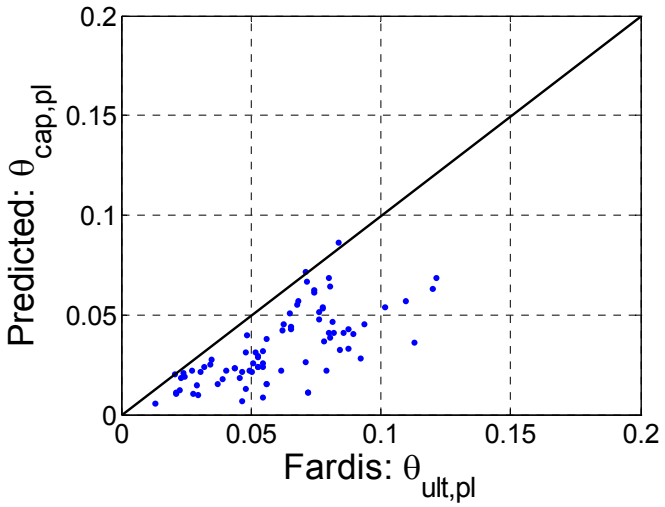

Figure 20. Our prediction for plastic rotation capacity at the capping point (Equation 10), as compared to Fardis' prediction of ultimate rotation capacity (at 20% strength loss). Note that this is not a direct comparison; see also Figure 21.

As expected, the Fardis et al. equation consistently predicts higher values, accounting for the fact that we are predicting the capping point and he is predicting the ultimate point (where the ultimate point is defined as the point of 20% strength loss[19]). The mean ratio of the our prediction to the Fardis et al. prediction is 0.56, while the median ratio is 0.53. These results are not directly comparable, so the ratio is expected to be less than 1.0.

To make a clearer comparisons between the predictions from Equation 10 and the equation from Fardis et al., we used their prediction of the ultimate rotation (at 20% strength loss) and use our calibrated value of post-capping slope (θ_{pc}) to back-calculate a prediction of $\theta_{cap,pl}$ from Equation 9. These results are shown in Figure 21 which shows that the two predictions are closer, but Fardis et al. prediction is still higher than our prediction on average. The mean ratio of our prediction to Fardis et al.'s prediction is 0.94, while the median ratio is 0.69. If the two equations were completely consistent we would expect these ratios to be near 1.0, but our equation predicts slightly lower deformation capacities on average. There are several differences between these two equations that may cause this difference in prediction; a primary difference is that our equation does not include an L_s/H term.

---

[18] These tests are denoted as $a_{sl} = 1$ tests. See notation list for more details.
[19] For reference see Figure 1.

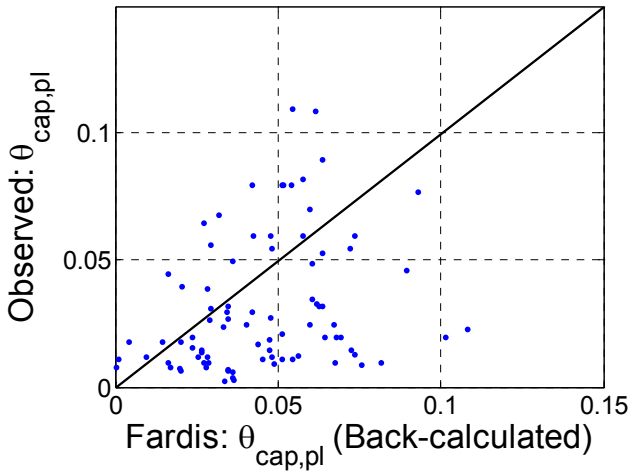

Figure 21. Our prediction for plastic rotation capacity at the capping point (Equation 10), as compared to a back-calculated prediction of the capping point using Fardis' equation for ultimate rotation capacity and our calibrated post-capping stiffness (θ_{pc}).

It is also possible to compare the prediction error obtained from our equation (Equation 10), and the one developed by Fardis et al. (Equation 9). Fardis et al. reports their prediction error in terms of coefficient of variation and the value ranges from 0.29-0.54 for various subsets of the data. The primary difference in Fardis et al.'s level of prediction error is whether the element was subjected to monotonic or cyclic loading. Since our equation predicts a capping plastic rotation for monotonic loading, the fair comparison would be to use Fardis et al.'s reported error for monotonic loading, which is a coefficient of variation of 0.54. Our equation resulted in a prediction error of $\sigma_{LN} = 0.59$, producing surprisingly similar results in terns of the overall errors associated with the empirical equations.

3.6 TOTAL ROTATION CAPACITY

3.6.1 Proposed Equation

This section presents an equation to predict the total rotation capacity to the capping point, including both elastic and plastic components of deformation. The method used to develop this equation is identical to that discussed previously for plastic rotation capacity.

Equation 14 presents the proposed equation, including all variables that are statistically significant. As usual, the prediction error associated with this equation is quantified in terms of the logarithmic standard deviation.

$$\theta_{cap,tot} = 0.14\left(1+0.4a_{sl}\right)\left(0.19\right)^{\nu}\left(0.02+40\rho_{sh}\right)^{0.54}\left(0.62\right)^{0.01c_{units}f'_c} \quad (14)$$

$\sigma_{LN} = 0.45$ (when 8 outliers removed)

$\sigma_{LN} = 0.52$ (with no outliers removed)

where a_{sl} is a bond-slip indicator (a_{sl} = 1 where bond-slip is possible), ν is the axial load ratio, ρ_{sh} is the area ratio of transverse reinforcement in the plastic hinge region spacing, f'$_c$ is the standard concrete compressive strength, and c_{units} is a units conversion variable that equals 1.0 when f'$_c$ in MPa units and 6.9 for ksi units.

The impact of each of these parameters on the predicted total rotation capacity is shown in Table 4. Within the range of column parameters considered in Table 4 the total rotation capacity can vary from 0.024 to 0.129. The table shows that the axial load ratio (ν) and confinement ratio (ρ_{sh}) have the largest effect on the predicted value of $\theta_{cap,tot}$. The concrete strength (f'$_c$) has a less dominant effects, but is still statistically significant.

We do not propose a further simplified equation for the total rotation capacity, instead equation 14 is already simplified. We could have included a longitudinal reinforcement ratio term in equation 14, but this was not done because it did not increase the prediction accuracy (i.e. $\sigma_{LN} = 0.45$ with the expanded equation as well).

Table 7. Effects of column design parameters on predicted values of $\theta_{cap,tot}$.

$\theta_{cap,tot}$		
parameter	**value**	**$\theta_{cap,tot}$**
Baseline	ρ_{sh} = 0.0075, f'$_c$ = 30 MPa, v = 0.10, α_{sl} = 1	0.078
α_{sl}	0	0.056
v	0	0.092
	0.3	0.056
	0.8	0.024
ρ_{sh}	0.002	0.041
	0.01	0.090
	0.02	0.129
f'_c *(MPa)*	20	0.082
	40	0.074
	80	0.061

3.6.2 Equation Including the Effects of Unbalanced Reinforcement

Equation 15 is proposed for use when the element has unbalanced reinforcement. An explanation of the rationale behind this equation can be found in the previous discussion associated with the plastic rotation capacity equations. This utilizes a correction factor from (Fardis and Biskinis 2003); note that the exponent in the correction term is different in the equations for plastic versus total rotation capacity.

$$\theta_{cap,tot} = 0.14\left(\frac{\max\left(0.01, \frac{\rho' f_y}{f_c'}\right)}{\max\left(0.01, \frac{\rho f_y}{f_c'}\right)}\right)^{0.175} \left(1+0.4a_{sl}\right)\left(0.19\right)^{v}\left(0.02+40\rho_{sh}\right)^{0.54}\left(0.62\right)^{0.01c_{units}f'_c} \quad (15)$$

where variables are defined as above, and ρ is the ratio of tension reinforcement (A_s/bd) and ρ' is the ratio of tension reinforcement (A_s'/bd).

3.7 POST-CAPPING ROTATION CAPACITY

3.7.1 Background (Literature and Equation Development)

The research on predicting post-capping rotation capacity has been limited despite its important impact on predicted collapse capacity. The key parameters considered in the development of this equation are those that are known to most affect ductility: axial load ratio (v), transverse steel ratio (ρ_{sh}), rebar buckling coefficient (s_n), stirrup spacing, and longitudinal steel ratio. The equation is based on only those tests where a post-capping slope was observed, denoted LB = 0.

3.7.2 Trends in Calibration Results

Figure 22 shows the scatterplots for the post-capping rotation capacity (θ_{pc}) for each test with an observed capping point. As we found in predicting plastic rotation capacity, there is significant scatter in the data, and other tools are needed in the development of predictive equations for θ_{pc}.

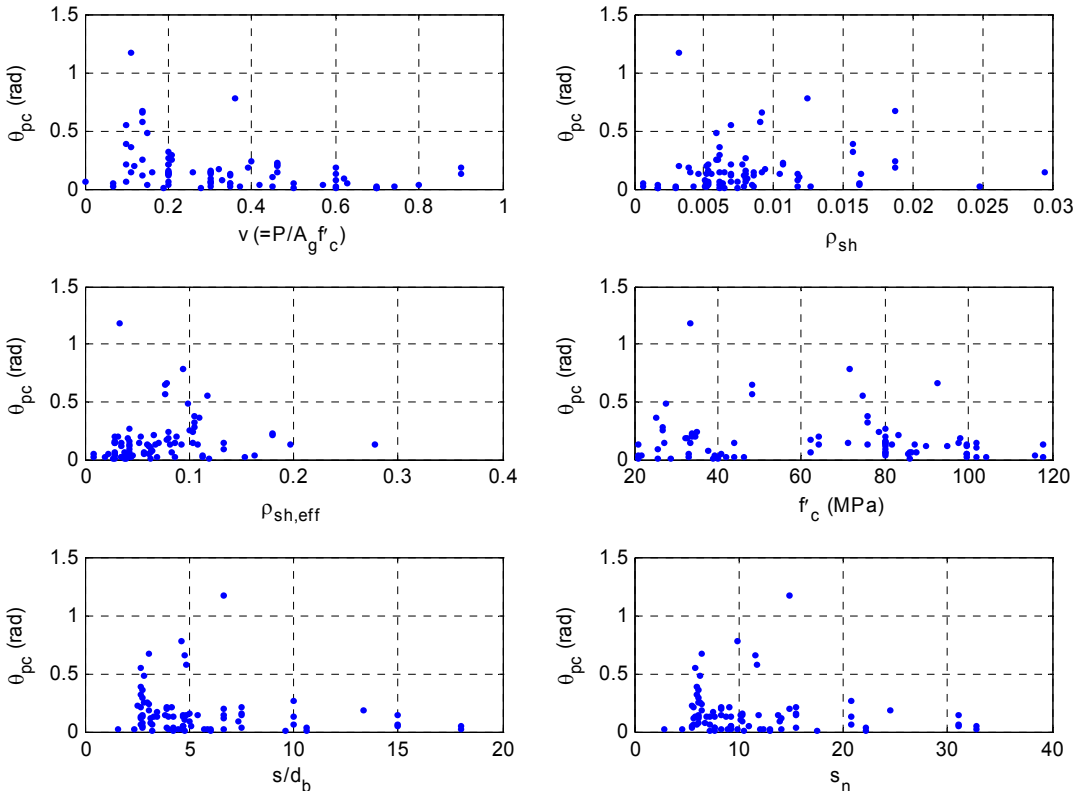

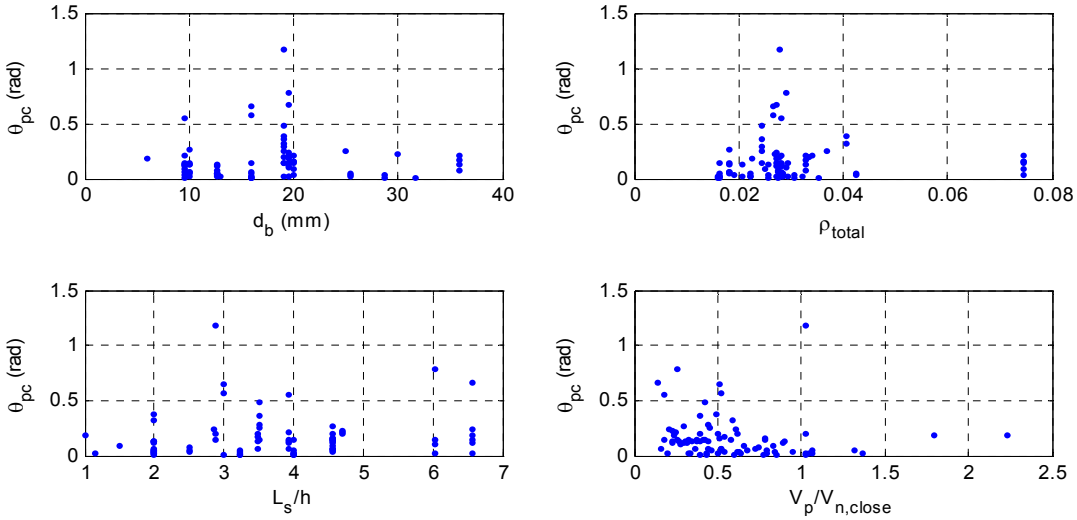

Figure 22. Scatterplots showing potential trends between θ_{pc} and ten column design variables.[20]

To help see trends more clearly, Figure 23 shows the effects that a single parameter variation has on the observed post-capping rotation capacity (section 2.2 discusses this approach in detail).

[20] Of course, this only includes data that has an observed cap and negative stiffness (i.e. LB = 0).

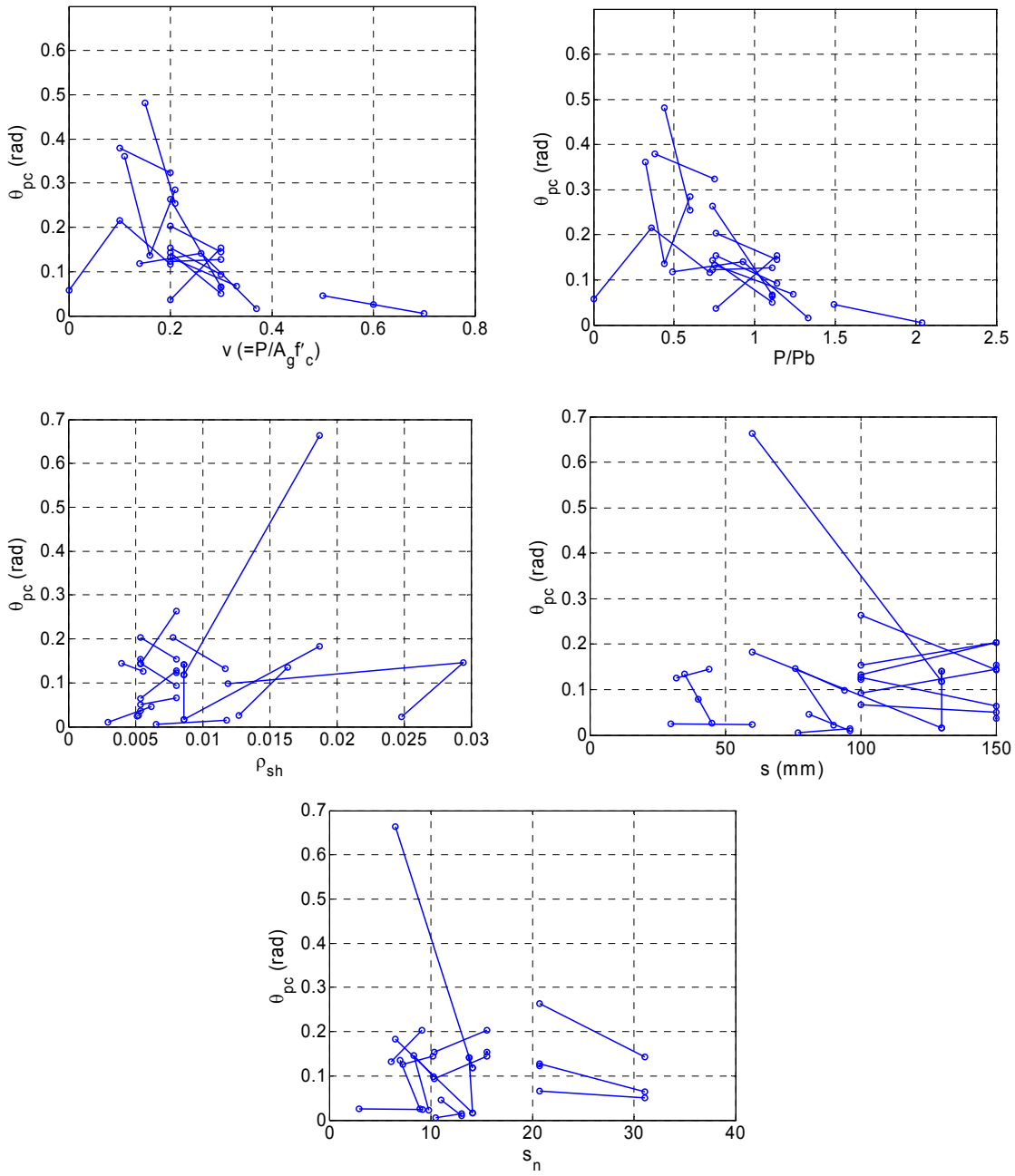

Figure 23. Plot showing the effects of individual variables on the observed value of θ_{pc}.

3.7.3 Proposed Equations

We propose 16 to predict post-capping rotation capacity. The stepwise regression analysis identified axial load ratio and transverse steel ratio as statistically significant parameters.

$$\theta_{pc} = (0.76)(0.031)^{\nu}(0.02 + 40\rho_{sh})^{1.02} \leq 0.10 \qquad (16)$$

where $\nu = \frac{P}{A_g f'_c}$, and ρ_{sh} is the transverse steel ratio.

$\sigma_{LN} = 0.72$ (when 4 are outliers removed)

$\sigma_{LN} = 0.86$ (with no outliers removed)

The upper bound imposed on Equation 16 is judgmentally imposed due to lack of reliable data for elements with shallow post-capping slopes. We found that test specimens with calibrated $\theta_{pc} > 0.10$ (i.e. very shallow post-capping slopes) typically were not tested deformation levels high enough to exhibit significant in-cycle degradation; this makes the accuracy of the calibrated value of θ_{pc} suspect, because the post-capping slope may become increasingly negative as the column strength degrades toward zero resistance. To determine the appropriate limit, we looked at all data that had well-defined post-capping slopes that ended near zero resistance (approximately 15 tests); the limit of 0.10 is based on an approximate upper bound from these data. Using this approach, this 0.10 limit may be conservative for well-confined, "conforming" elements with low axial load. However, the test data are simply not available to justify using a larger value.

The range of θ_{pc} expected for columns with different parameters is demonstrated in Table 8. Both ν and ρ_{sh} will significantly affect the predicted value of θ_{pc}; for the range of axial load and transverse steel ratio considered, θ_{pc} varies between 0.015 and 0.10.

Table 8. Effects of column design parameters on predicted values of θ_{pc}.

θ_{pc}		
parameter	**value**	**θ_{pc}**
Baseline	ρ_{sh} = 0.0075, v = 0.10	0.100
v	0	0.100
	0.3	0.084
	0.8	0.015
ρ_{sh}	0.002	0.051
	0.01	0.100
	0.02	0.100

3.7.4 Validation of Proposed Equations

Figure 24 compares the calibrated values of θ_{pc} to predictions from Equation 16. Figure 24a shows the calibrated and predicted values without any imposed cap; without the cap imposed, the mean and median ratios of observed to predicted values are 1.05 and 0.53, respectively. As discussed earlier in this section, a review of the calibrated data showed that calibrated values of $\theta_{pc} > 0.10$ are typically based on tests that were not pushed to deformation levels high enough to provide a reliable θ_{pc} estimate. Figure 24b shows the data with this upper bound value imposed for both the calibrated and predicted values; the mean and median ratios of observed to predicted values are 1.20 and 1.00.

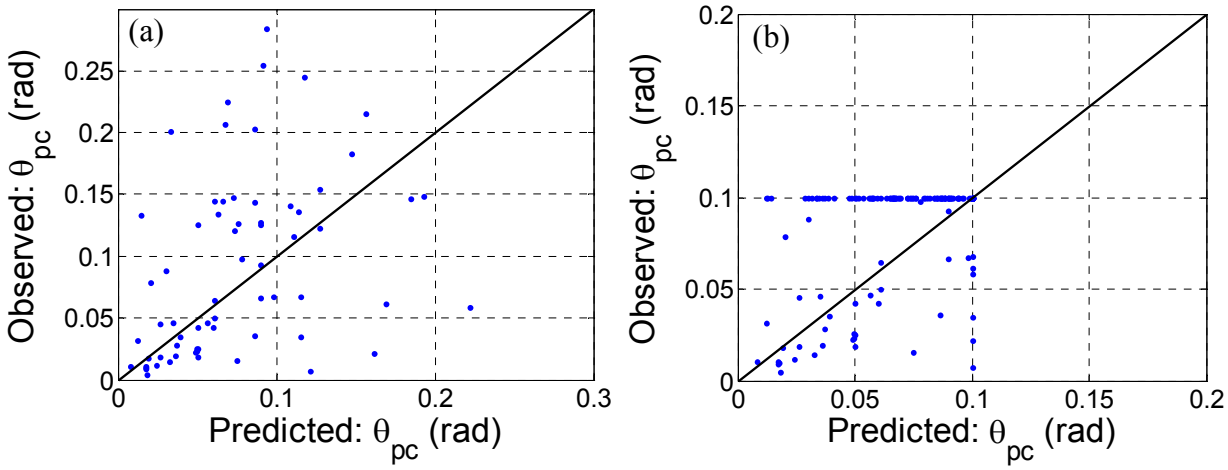

Median(observed/predicted) = 0.53
Mean(observed/predicted) = 1.05

Median(observed/predicted) = 1.00
Mean(observed/predicted) = 1.20

Figure 24. Comparison of observed values and predictions for θ_{pc} using Equation 14.

3.8 POST-YIELD HARDENING STIFFNESS

3.8.1 Background (Literature and Equation Development)

Post-yield hardening stiffness is described by the ratio of the maximum moment capacity and the yield moment capacity (M_c/M_y). There is limited literature on this topic, though Park et al. (1972) found that hardening ratio depended on axial load ratio and tensile reinforcement ratio. In developing an equation for post-yield hardening stiffness we investigated the same key predictors as in the previous equations.

3.8.2 Trends in Calibration Results

Figure 25 shows the scatterplots for the hardening stiffness of an element (M_c/M_y). The primary trends are with axial load ratio and concrete compressive strength, but there is significant scatter in the data that makes other trends difficult to distinguish.

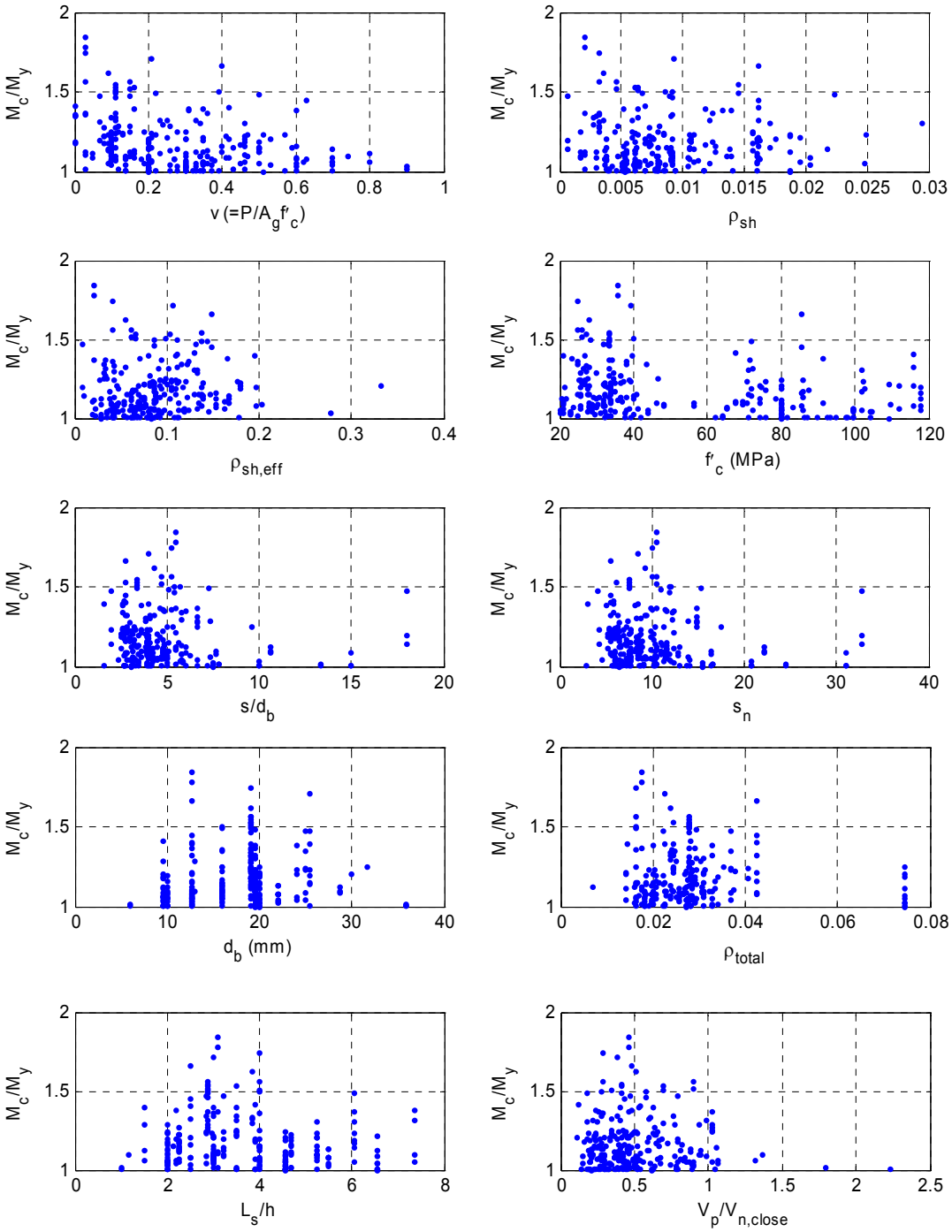

Figure 25. Scatterplots showing potential trends between hardening stiffness (M_c/M_y) and ten column design variables.[21]

Figure 26 shows the effects that a single parameter variation has on the observed hardening stiffness (M_c/M_y) (see Section 2.2 discusses this approach in detail). This clarifies the trends

[21] Again, this only includes data that has an observed cap and negative stiffness (i.e. LB = 0)

with axial load, but the data are limited to more closely look at trends with concrete compressive strength.

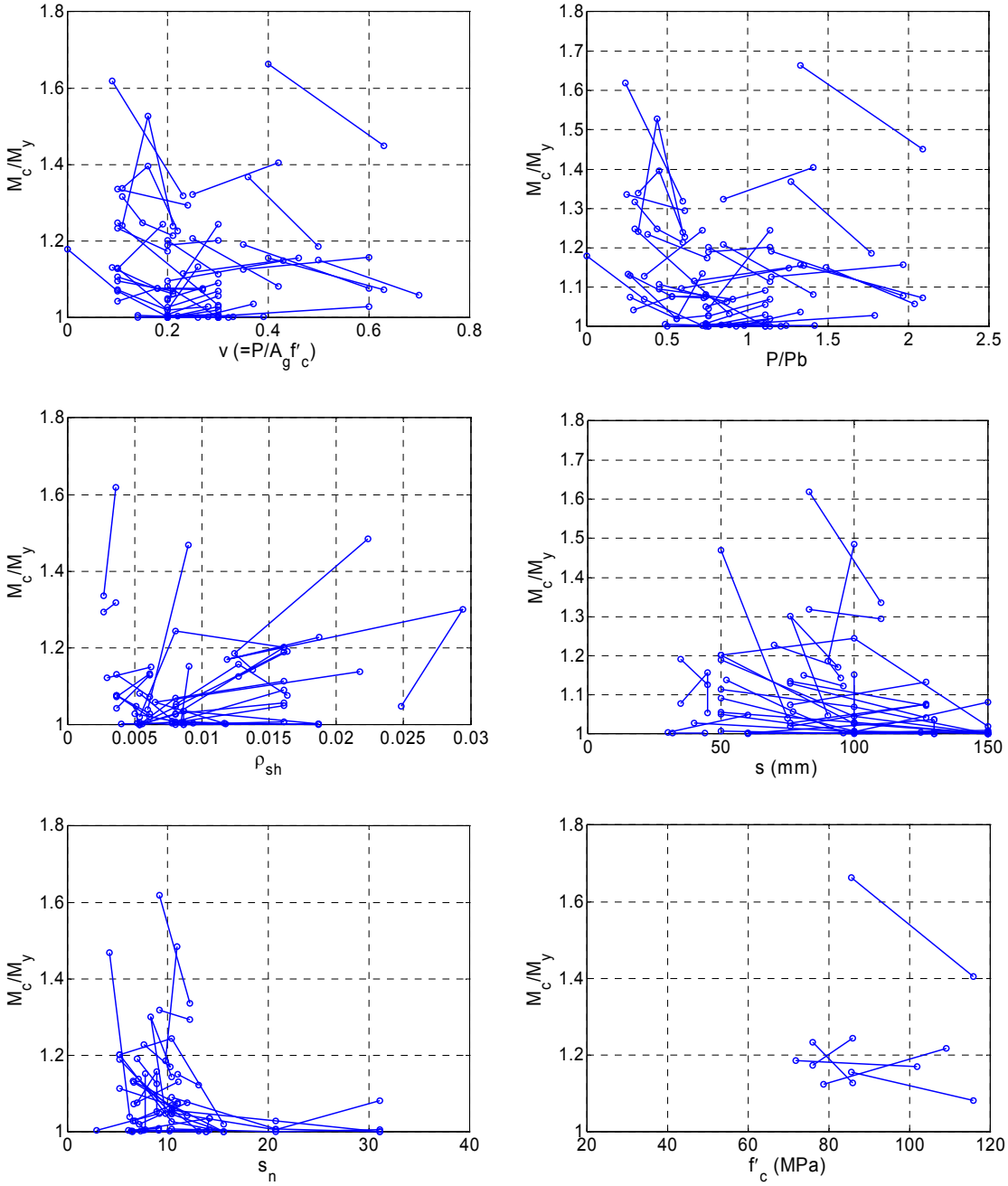

Figure 26. Plot showing the effects of individual variables on the observed hardening stiffness (M_c/M_y).

3.8.3 Proposed Equations

3.8.3.1 Full Equation

Regression analysis shows that axial load ratio and concrete strength are the key factors in determining hardening stiffness (M_c/M_y). Using these predictors M_c/M_y may be given by Equation 17.

$$M_c / M_y = (1.25)(0.89)^{v}(0.91)^{0.01 c_{units} f'_c} \quad (17)$$

where $v = P/A_g f'_c$ and f'_c is the compressive strength of the concrete, and c_{units} is a units conversion variable that equals 1.0 when f'_c is in MPa units and 6.9 for ksi units.

$\sigma_{LN} = 0.10$ (when 12 outliers are removed)

$\sigma_{LN} = 0.12$ (no outliers removed)

Table 9 shows the effect of concrete strength and axial load ratio on the predicted value of M_c/M_y. For a typical column with concrete strength of 30 MPa and an axial load ratio of 0.10 M_c/M_y is predicted to be 1.20. For columns within a typical range of f'_c and v, M_c/M_y varies between 1.11 and 1.22.

Table 9. Effects of column design parameters on predicted values of M_c/M_y.

M_c/M_y		
parameter	**value**	**M_c / M_y**
Baseline	f'_c = 30 MPa, v = 0.10	1.20
f'_c (MPa)	20	1.21
	40	1.19
	80	1.15
v	0	1.22
	0.3	1.17
	0.8	1.11

3.8.3.2 Simplified Equation

Due to the small scatter in the original data, a simplified constant equation for M_c/M_y also provides relatively good agreement with the test data, as shown in Equation 18. The logarithmic standard deviation of Equation 18 is not significantly larger than that from Equation 17:

$$M_c / M_y = 1.13 \quad (18)$$

$\sigma_{LN} = 0.10$ (when 17 outliers are removed)

$\sigma_{LN} = 0.13$ (with no outliers removed)

3.8.5 Verification of Proposed Equations

Figure 27 shows compared the calibrated and predicted values associated with Equation 17. Previous work and sensitivity studies have shown that this parameter does not have a large overall impact on the collapse capacity of low-rise reinforced concrete frame buildings (Haselton et al. 2006), but findings by Ibarra (2003; chapter 4) indicate that this parameter will be more important for taller buildings that are more susceptible to P-Δ effects.

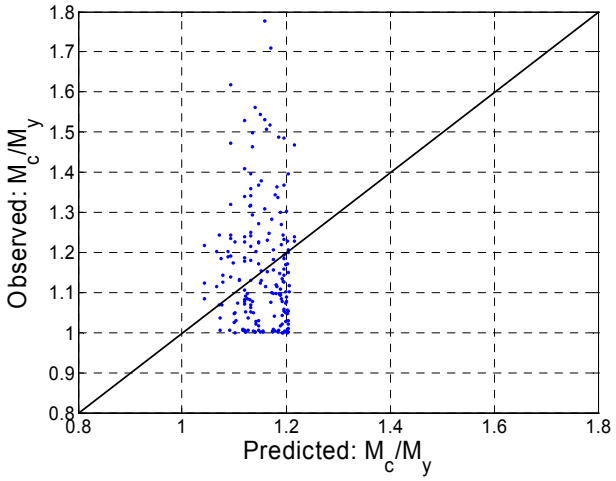

Median(observed/predicted) = 0.97
Mean(observed/predicted) = 1.01

Figure 27. Comparison of observed values and predictions for M_c/M_y using Equation 15.

3.9 CYCLIC STRENGTH AND STIFFNESS DETERIORATION

3.9.1 Literature Review

Cyclic energy dissipation capacity has been a topic of past research, but most of the past researcher was primarily focused on the use of damage indices for predicting damage states and accumulation of damage in a post-processing mode. This is similar to, but not the same as, the goal of this study, which is to determine an energy dissipation capacity that can be directly used in an element model to deteriorate the strength and stiffness of the element during nonlinear analysis. Therefore, past work on damage indices is not reviewed here.

In a state-of-the-art review focused on reinforced concrete frames under earthquake loading, the Comité Euro-International du Béton (1996) noted that cyclic degradation was closely related to both the axial load level and the degree of confinement of the concrete core. They notes that the axial load and degree of confinement have competing effects on the cyclic energy dissipation capacity.

As described previously, Ibarra's hysteretic model captures four modes of cyclic deterioration: basic strength deterioration, post-cap strength deterioration, unloading stiffness deterioration, and accelerated reloading stiffness deterioration. Each mode of cyclic deterioration is defined by two parameters, normalized energy dissipation capacity (λ), and an exponent term (c) to describe the rate of cyclic deterioration changes with accumulation of damage. To reduce complexity, we use simplifying assumptions to consolidate the cyclic deterioration parameters from eight to two (as per Ibarra, 2003): λ and c. Calibration of λ is the topic of this section and c, the exponent, is set to 1.0 in all cases.

3.9.2 Trends in Calibration Results

Figure 28 shows the scatterplots for the energy dissipation capacity (λ). It is difficult to see trends in these plots.

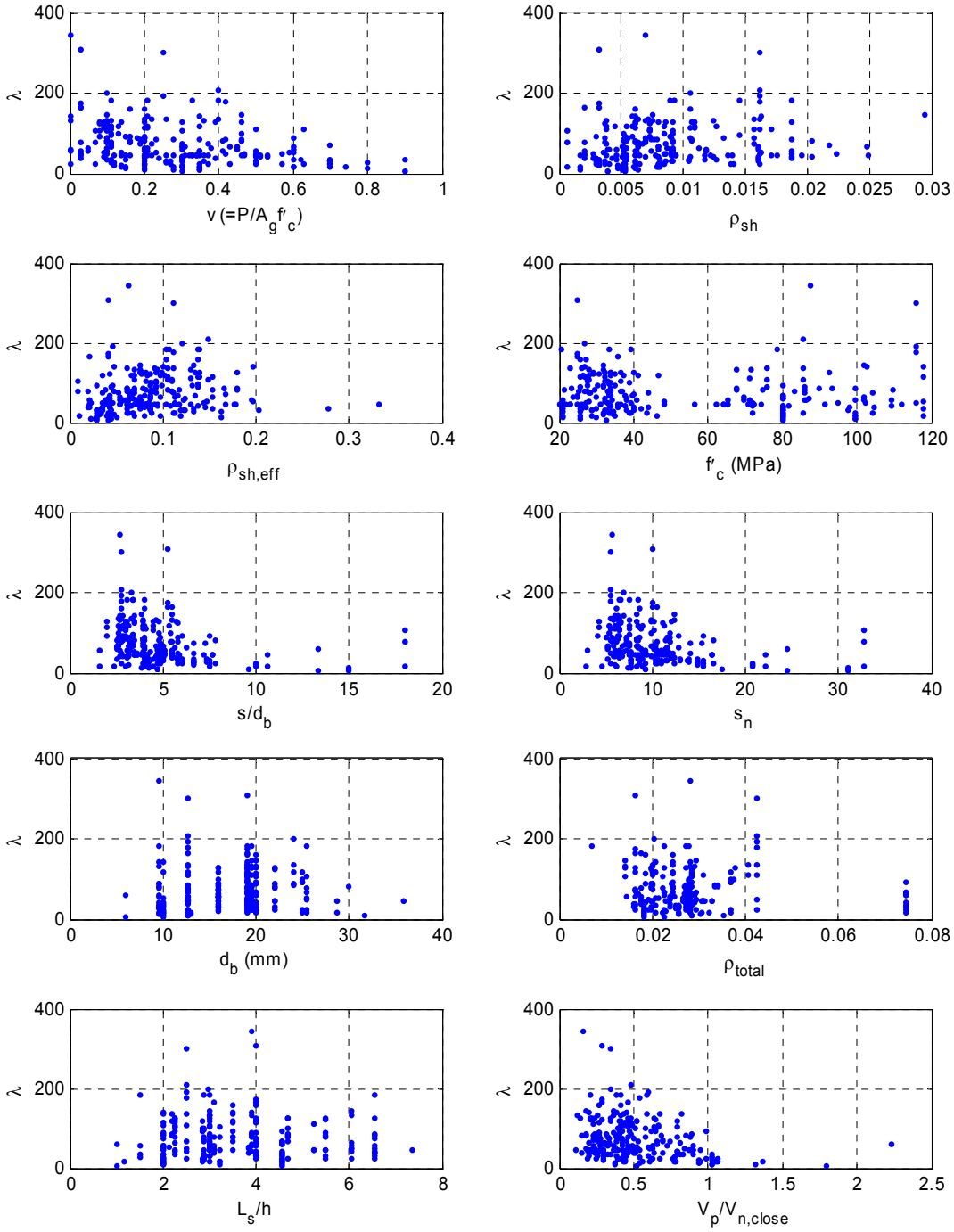

Figure 28. Scatterplots showing potential trends between energy dissipation capacity (λ) and ten column design variables.

Figure 29 shows the effects that a single parameter variation has on the observed normalized energy dissipation capacity (λ) (see Section 2.2). As compared to the simple scatterplots shown

in the last figure, these figures show the trends with remarkable clarity. Trends are evident for axial load, confinement ratio, stirrup spacing, and concrete compressive strength.

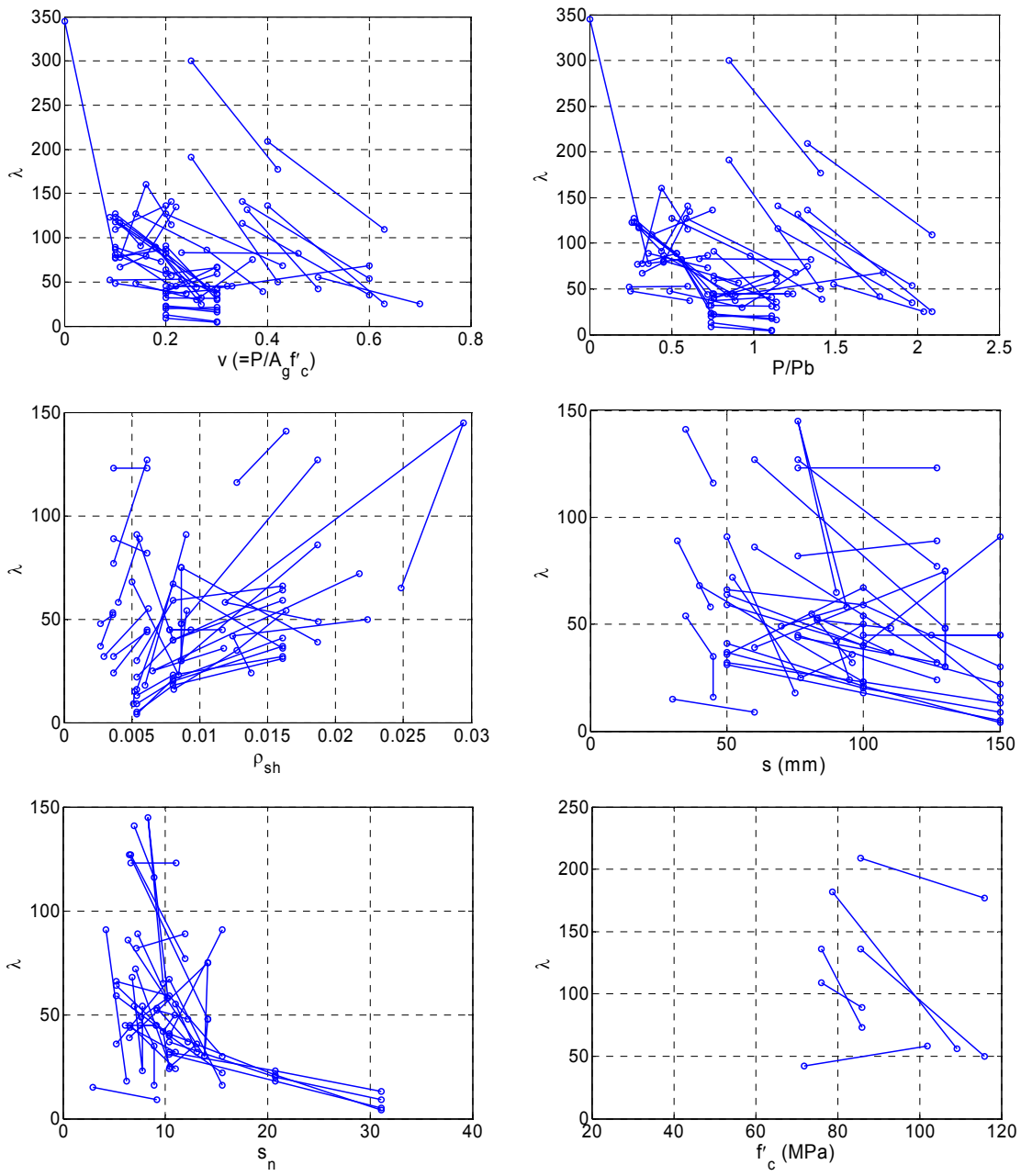

Figure 29. Plot showing the effects of individual variables on the observed energy dissipation capacity (λ).

3.9.3 Equation Development

As usual, we used regression analysis to determine which parameters were the best predictors for cyclic energy dissipation capacity. For quantifying confinement effects, the ratio of stirrup spacing to column depth (s/d) was found to be a better predictor of deterioration than transverse steel ratio (ρ_{sh}).

We found that the concrete compressive strength (f'_c) was important but the effective confinement ratio ($\rho_{sh,eff}$), which relates to both confinement and f'_c, showed to be more statistically significant; this indicates that the s/d term did not fully capture the effects of stirrups and confinement. Since both these variables are related to the spacing and density of stirrups, we checked the possible correlation between the variables, computing a linear correlation coefficient of -0.4. This correlation is low enough so collinearity will not be a problem in the regression analysis.

The form of Equation 19 was chosen based on the observed trends in the data, and is similar to the functional form used in predicting plastic rotation capacity.

3.9.4 Proposed Equations

3.9.4.1 Full Equation

Equation 19 was developed using stepwise regression analysis and includes all statistically significant predictors.

$$\lambda = (127.2)(0.19)^{v}(0.24)^{s/d}(0.595)^{V_p/V_n}(4.25)^{\rho_{sh,eff}} \qquad (19)$$

where $v = P/A_g f'_c$, and s/d is the ratio of stirrup spacing and the depth of the column[22], V_p/V_n is the ratio of shear demand at flexural yielding and the shear strength of the column, and $\rho_{sh,eff}$ is a measure of confinement.

$\sigma_{LN} = 0.49$ (with 12 outliers removed)

$\sigma_{LN} = 0.62$ (with no outliers removed)

Table 10 shows the range of λ predicted by Equation 19 for typical columns. There is a large variation in λ depending on the axial load ratio and tie spacing. As expected, increasing axial load ratio can significantly decrease the cyclic energy dissipation capacity. Likewise, increasing tie spacing also decreases the cyclic energy dissipation capacity.

Table 10. Effects of column design parameters on predicted values of λ.

λ		
parameter	**value**	**λ**
Baseline	v = 0.1, s/d = 0.2, V_p/V_n = 0.5, and $\rho_{sh,eff}$ = 0.1	72
v	0	85
	0.3	52
	0.8	23
s/d	0.1	83
	0.4	54
	0.6	41
V_p/V_n	0.2	84
	0.8	62
	1.5	43
$\rho_{sh,eff}$	0.01	63
	0.10	72
	0.20	83

3.9.4.2 Simplified Equation

The full equation can be significantly simplified without greatly reducing the prediction accuracy. Equation 20 presents a much simpler equation with virtually the same prediction error as with the first equation.

$$\lambda = (170.7)(0.27)^{v}(0.10)^{s/d} \quad (20)$$

where $v = P/A_g f'_c$, and s/d is the ratio of tie spacing to the depth of the column.

$\sigma_{LN} = 0.50$ (when 15 outliers removed)

$\sigma_{LN} = 0.64$ (without removing any outliers)

[22] If s/d varies over the height of the column, the value in the hinge region should be used.

3.9.5 Verification of Proposed Equations

Figure 30 compares the calibrated and predicted values of λ. Despite the significant scatter in the data, the predictive Equation 20 captures well the overall trends.

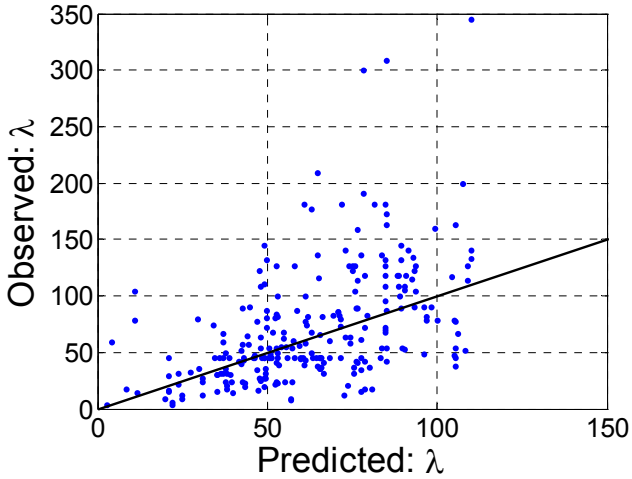

Figure 30. Comparison of observed values and predictions for λ using Equation 18.

3.10 RESIDUAL STRENGTH

The residual strength was not quantified in this study, simply due to a lack of experimental data that showed the residual. Some of the non-conforming columns that were tested to large deformations showed little or no residual strength, while most conforming columns did not experience enough strength deterioration to provide a good estimate of a residual strength.

4. Summary and Future Research Directions

4.1 SUMMARY OF EQUATIONS DEVELOPED

The purpose of this research is to create a comprehensive set of equations which can be used to predict the model parameters of a lumped plasticity element model for a reinforced concrete beam-column, based on the properties of the column. The equations were developed for use with the element model developed by Ibarra et al. (2003, 2005), and can be used to model cyclic and in-cycle strength and stiffness degradation to track element behavior to the point of structural collapse. Even though we use the Ibarra et al. model in this study, the equations presented in this report are general (with the exception that cyclic deterioration must be based on an energy index) and can be used with most lumped plasticity models that are used in research.

Empirical predictive equations are presented for element secant stiffness to yield (Equations 1, 2, and 7), initial stiffness (Equations 3, 4, and 8), plastic rotation capacity (Equations 10 – 13), post-capping rotation capacity (Equation 14), hardening stiffness ratio (Equations 15 – 16) and cyclic deterioration capacity (Equations 17 – 18). These quantities provide the key parameters for input into the Ibarra et al. element model, but are also general for use with most other models. The predictive equations are based on a variety of parameters representing the important characteristics of the column to be modeled. These include the axial load ratio (ν), shear span ratio (L_s/H), lateral confinement ratio (ρ_{sh}), concrete strength (f'_c), rebar buckling coefficient (s_n), longitudinal reinforcement ratio (ρ), ratio of transverse tie spacing to column depth (s/d), and ratio of shear at flexural yielding to shear strength (V_p/V_n). Given a column design, these parameters can be quickly determined for input into the predictive equations. In some cases more than one equation is given to predict a model parameter, usually a

full equation that includes all statistically significant paramaters, and a simpler equation based on a smaller number of column parameters. The choice of which equation to use is left to the reader.

The prediction error associated with each equation is also quantified and reported. These provide an indication of the uncertainty in prediction of model paramaters, and can be used in sensitivity analyses or propagation of structural modeling uncertainties.

4.2 LIMITATIONS

The predictive empirical equations developed here provide a critical linkage between column design parameters and element modeling parameters, facilitating the creation of nonlinear analysis models for RC structures needed for performance-based earthquake engineering. The limitations of these equations, in terms of scope and applicability, are discussed in this section.

4.2.1 Availability of Experimental Data

The equations developed here are based on a comprehensive database assembled by Berry et al. (2004). Even so, the range of column parameters included in the column database provides an important indication of the applicability of the calibration equations developed. Figure 2 shows the ranges of column parameters included in this calibration study. The equations developed may not be applicable for columns with characteristics outside the range shown. For example, the data set includes only columns with balanced reinforcement.

The equations are also limited more generally by the number of test specimens available. In some cases the prediction errors could be reduced if more test data were available. This is particularly true for the equations for plastic rotation capacity and post-capping rotation capacity, which require columns be tested up to significant deformations for the negative post-capping stiffness to be observed. Data with observed negative post-capping stiffnesses are severely limited. For model calibration and understanding of element behavior, it is important that future testing continue to deformation levels large enough to clearly show the negative post-capping stiffnesses. Section 4.3 also discusses the need for this further test data.

We are further limited by the fact that virtually all of the available test data has a cyclic loading protocol with many cycles and 2-3 cycles per deformation level. This type of loading is

not representative of earthquake induced loading, which would generally contain far fewer cycles. This is problematic because we use the cyclic data to calibrate both the monotonic backbone and cyclic deterioration behavior of the element (see Section 2.1.2.1). More test series' are needed that subject identical columns to multiple types of loading protocols. This will allow independent calibration of the monotonic backbone and cyclic deterioration behavior, and will also help verify that the element model cyclic behavior is appropriate. For example, data from a monotonic push can be used to calibrate the monotonic backbone of the element. Cyclic tests, using multiple loading protocols, can then both (a) illustrate cyclic deterioration behavior and show how it various with loading protocol, and (b) show how the backbone should migrate as damage progresses.

Ingham et al. (2001) completed such as test series as describe above. This series provides useful data on the monotonic backbone curve and shows how cyclic behavior varies with loading protocol. The important limitation of the Ingham test series is that the tests were not continued to deformations levels large enough to show negative post-capping stiffness of the element. For future testing with the purpose of calibrating element models, we suggests a test series similar to that used by Ingham (but possibly with fewer cycles in the loading protocols to better represent expected seismic loading), but suggest that the tests be continued to deformations large enough to clearly show negative post-capping stiffness.

4.2.2 Improvements to Hysteretic Model

There are additional limitations in the implementaiton of this work due to deficiencies in the element material model which come from errors in the OpenSees implementation. Although these bugs did not cause significant problems in the calibration process we include them here for completeness, and as reference for other users. These errors are likely to be fixed in future versions of OpenSees. Note that these bugs can generally be avoided by using the recomendations of this section.

One problem sometimes occurs when no residual strength, the element has completely lost strength, and is being loaded with zero strength and zero stiffness. At this point, a bug may cause the element to begin to elastically reload and unload with approximately the initial stiffness. This problem is illustrated in Figure 31, where the same test is calibrated with the

correct value of λ, and a smaller value of λ which causes the element to deteriorate too quickly.[23] Figure 31 is based on Soesianawati et al. 1986, specimen No. 4. To avoid this bug, one can simply use a non-zero residual strength (0.01 is enough) and use c = 1.0; this solves the problem in most cases, but not all.

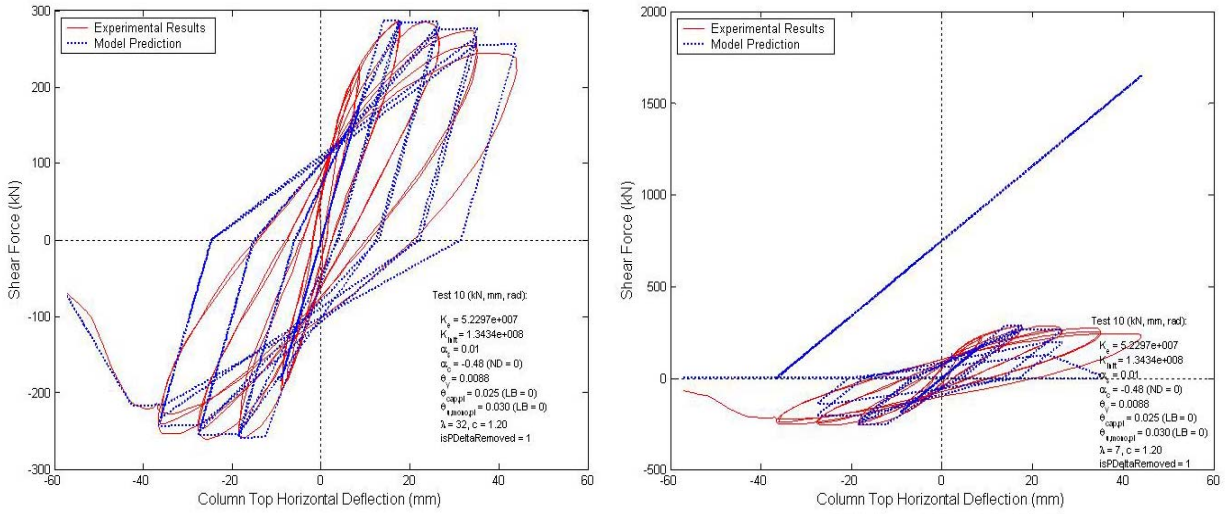

Figure 31. Hysteretic model with (a) accurately calibrated λ parameter and (b) inaccurately calibrated λ parameter, illustrating error in element material model implementation.

A less common model error occurred when the element was cycled in one direction instead of being cycled to both positive and negative displacements. We are not sure of the precise reason for this error, as shown in

Figure **32**, but it seems to be associated with improper deterioration in the reloading stiffness when being consistently cycled in one direction.

[23] The same problem can occur if c> 1.0 is used in an MDOF system; therefore c = 1.0 should always be used when using the OpenSees implementation.

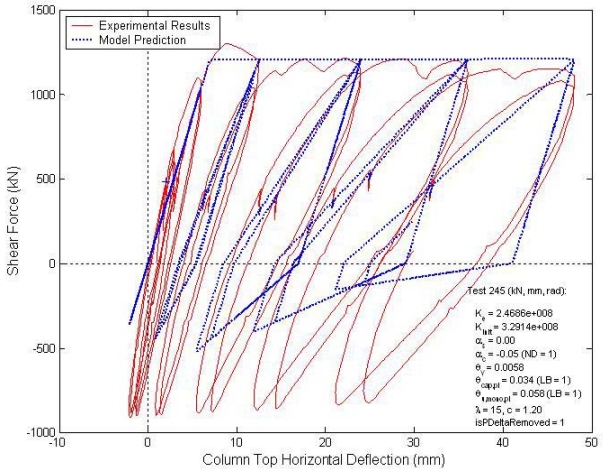

Figure 32. Illustration of implementation error in hysteretic model.[24]

As was briefly noted earlier, there is also an error in the unloading stiffness deterioration in the OpenSees implementation in the model. Unloading stiffness deterioration should not be used in the OpenSees implementation of the model; this can cause problems with the cyclic behavior of the element. Unloading stiffness deterioration is an important aspect of modeling the cyclic response of RC elements, so the OpenSees implementation of this model needs to be corrected as soon as possible to remove this error.

4.3 FUTURE RESEARCH

4.3.1 Suggestions for Future Experimental Tests

From our experiences calibrating the element model to 255 column tests, our wish list for future experimental tests includes both more tests and different types of tests. The following general suggestions can be made:

- Monotonic tests are needed in addition to cyclic tests, both for identical test specimens when possible. In this study we used cyclic tests with many cycles to calibrate both the monotonic backbone and the cyclic deterioration rules. As a result,

[24] Test by Bechtoula et al. (2002) , specimen L1D60.

the monotonic backbone and the cyclic deterioration rules are interdependent, and the approximation of the monotonic backbone depends on cyclic deterioration rules assumed. Ideally, we would have enough test data to separate these effects.

- Tests should be conducted with a variety of cyclic loading histories. This will lead to a better understanding of how load history affects cyclic behavior, and provide a basis for better development/calibration of the element model cyclic rules. Section 4.2.1 discusses this point in more detail. Ideally, loading histories should be more representative of the type of earthquake loading that causes structural collapse. Tests with loading histories including too many cycles cause failure modes which are unlikely to occur in a seismic event.
- For predicting collapse, tests should be conducted at large enough deformations for capping and post-capping behavior to be clearly observed. Most current test data do not continue to large enough deformations; this is a serious limitation in the available data and makes it difficult to accurately predict the capping point. Due to this limitation in test data, we were forced to make conservative assumptions when predicting the capping point in this work; better data would allow this conservatism to be removed from our predictions. Accurate data on the capping point is imperative for predicting structural collapse, so it is important that better test data is developed. In addition, there is virtually no data that shows post-peak cyclic deterioration behavior.

The proposal of a loading protocol suitable for calibrating element material model for collapse is outside the scope of this research. Interested readers should investigate the loading protocols developed for testing of steel components (eg. ATC, 1992).

4.3.2 Consensus and Codification[25]

The outcome of this study, empirical equations to predict element model parameters for RC beam-columns based on column design parameters, is an important contribution to wider

[25] Readers are referred to Haselton and Deierlein, 2006, *Toward the Codification of Modeling Provisions for Simulating Structural Collapse*, which provides the basis for the remarks in this section.

research efforts aiming to provide systematic collapse assessment of structures. Research by the PEER Center and others is progressing close to the goal of directly modeling sidesway structural collapse of some types of structural systems, though use of nonlinear dynamic simulation. However, the collapse assessment process sometimes requires considerable interpretation and engineering judgment. As a result, it is critical for the required models and methods to be put through a consensus and codification process – as has long been the tradition in building code development. This consensus process will allow a larger group of researchers and engineering professionals to review the research development, assumptions, and judgment that provide the basis for the newly proposed collapse assessment methods.

We propose that such a consensus and codification process be started to develop consensus guidelines that explain proper procedures for directly simulating sidesway collapse. These procedures would include guidance on all important aspects of the collapse assessment process, including treatment of failure modes, element-level modeling, system-level modeling, numerical issues for nonlinear dynamic analyses, treatment of structural modeling uncertainties, etc.

We propose that the equations presented in this report be included in such a consensus and codification process. In concept, this consensus process is no different than for other code provisions, such as those for predicting the strengths of reinforced concrete elements. The primary difference is that additional information will need to be specified, such as the element cyclic deterioration characteristics and element plastic rotation capacity.

These codified models and guidelines for collapse assessment will give engineers the basis for directly predicting structural collapse based on realistic element models. In addition, the existence of such models will provide a foundation for advancing simplified performance-based design provisions (e.g. a codified equation predicting plastic rotation capacity from element properties could be used to make detailing requirements more flexible, allowing the engineer to design the element based on a target plastic rotation capacity).

REFERENCES

Altoontash, A. (2004). *Simulation and Damage Models for Performance Assessment of Reinforced Concrete Beam-Column Joints*, Dissertation, Department of Civil and Environmental Engineering, Stanford University.

ATC-24, Applied Technology Council (1992). "Guidelines for Cyclic Seismic Testing of Components of Steel Structures", Redwood City, California.

ATC-40, Applied Technology Council (1996). " Seismic Evaluation and Retrofit of Concrete Buildings," Report No. SSC 96-01, *Seismic Safety Commission*, Redwood City, California.

Berry, M., Eberhard, M. (2005). "Practical Performance Model for Bar Buckling," *Journal of Structural Engineering*, Vol. 131, No. 7, July 2005, pp. 1060-1070.

Berry, M., Parrish, M., and Eberhard, M. (2004). *PEER Structural Performance Database User's Manual*, Pacific Engineering Research Center, University of California, Berkeley, California, 38 pp. Available at http://nisee.berkeley.edu/spd/ and http://maximus.ce.washington.edu/~peera1/ (March 10, 2005).

Berry, M., Eberhard, M. (2003). *Performance Models for Flexural Damage in Reinforced Concrete Columns*, PEER Report 2003/18, Pacific Engineering Research Center, University of California, Berkeley, California, 158 pp.

Chatterjee, S., Hadi, A.S., and Price, B. (2000). *Regression Analysis by Example*, 3rd Edition, John Wiley and Sons Inc., New York.

Comité Euro-International du Béton (CEB) (1996). "RC Frames Under Earthquake Loading – State of the Art Report," Comité Euro-International du Bénton, Convenor Michael N. Fardis, Published by Thomas Telford, London.

Dhakal, R.P. and Maekawa, K. (2002). "Modeling of Post-yielding Buckling of Reinforcement," *Journal of Structural Engineering*, Vol. 128, No. 9, September 2002, pp. 1139-1147.

Elwood, K.J., Eberhard, M.O. (2006). "Effective Stiffness of Reinforced Concrete Columns," *Research Digest of the Pacific Earthquake Engineering Research Center*, 2006-01, March 2006.

Fardis, M. N. and Biskinis, D. E. (2003). "Deformation Capacity of RC Members, as Controlled by Flexure or Shear," *Otani Symposium*, 2003, pp. 511-530.

Federal Emergency Management Agency (2005). "FEMA 440: Improvement of Nonlinear Static Analysis Procedures", Report No. FEMA 440, Prepared by Applied Technology Council, Prepared for Federal Emergency Management Agency, Washington, DC.

Federal Emergency Management Agency (2000). “FEMA 356: Prestandard and Commentary for the Seismic Rehabilitation of Buildings”, Report No. FEMA 356, Prepared by Applied Technology Council, Prepared for Federal Emergency Management Agency, Washington, DC.

Federal Emergency Management Agency (1997). “FEMA 273: NEHRP Commentary on the Guidelines for the Seismic Rehabilitation of Buildings”, Report No. FEMA 273, Prepared by Applied Technology Council, Prepared for Federal Emergency Management Agency, Washington, DC.

Haselton, C.B. and J.W. Baker (2006). “Ground motion intensity measures for collapse capacity prediction: Choice of optimal spectral period and effect of spectral shape”, *8th National Conference on Earthquake Engineering*, San Francisco, California, April 18-22, 2006.

Haselton, C.B. and G.G. Deierlein (2006). “Toward the Codification of Modeling Provisions for Simulating Structural Collapse,” *8th National Conference on Earthquake Engineering (100th Anniversary Earthquake Conference)*, San Francisco, California, April 18-22, 2006, 10 pp.

Haselton, C. B., C. Goulet, J. Mitrani-Reiser, J. Beck, G.G. Deierlein, K.A. Porter, J. Stewart, and E. Taciroglu (2006). *An Assessment to Benchmark the Seismic Performance of a Code-Conforming Reinforced-Concrete Moment-Frame Building*, PEER Report 2006, Pacific Earthquake Engineering Research Center, University of California, Berkeley, California, (in preparation).

Ibarra, L.F., Medina, R.A., and Krawinkler, H. (2005). “Hysteretic models that incorporate strength and stiffness deterioration,” *Earthquake Engineering and Structural Dynamics*, Vol. 34, pp. 1489-1511..

Ibarra, L., Krawinkler, H. (2004). *Global Collapse of Deteriorating MDOF Systems*, 13th World Conference on Earthquake Engineering, Vancouver, B.C., Canada, August 1-6, 2004, Paper No. 116.

Ibarra, L. (2003). *Global Collapse of Frame Structures Under Seismic Excitations*, Ph.D. Dissertation, Department of Civil and Environmental Engineering, Stanford University.

Ingham, J.M., Lidell, D., and B.J. Davidson (2001). *Influence of Loading History on the Response of a Reinforced Concrete Beam*, Bulletin of the New Zealand Society for Earthquake Engineering, Vol. 34, No. 2, 2001, pp. 107-124.

Legeron, F., and Paultre, P. (2000). "Behavior of High-Strength Concrete Columns under Cyclic Flexure and Constant Axial Load," *American Concrete Institute Structural Journal*, Vol. 97, No. 4, July-August 2000, pp. 591-601.

Lehman, D.E., and J.P. Moehle (1998). “Seismic Performance of Well-Confined Concrete Bridge Columns,” PEER Report 1998/01, PEER, UC Berkeley, 295 pp.

Mander, J. B., Priestley, M. J. N., Park, R. (1988a). “Theoretical Stress-Strain Model for Confined Concrete,” *Journal of Structural Engineering*, Vol. 114, No. 8, August 1988, pp. 1804-1826.

Mander, J. B., Priestley, M. J. N., Park, R. (1988b). "Observed Stress-Strain Behavior of Confined Concrete," *Journal of Structural Engineering*, Vol. 114, No. 8, August 1988, pp. 1827-1849.

Mathworks, 2005. *Matlab Documentation,* http://www.mathworks.com/access/helpdesk/help/techdoc/matlab.shtml.

Median, R.A. (2002). *Seismic Demands for Nondeteriorating Frame Structures and Their Dependence on Ground Motions*, Ph.D. Dissertation, Department of Civil and Environmental Engineering, Stanford University.

Mehanny, S.S.F. (1999). *Modeling and Assessment of Seismic Performance of Composite Frames with Reinforced Concrete Columns and Steel Beams*, Dissertation, Department of Civil and Environmental Engineering, Stanford University.

Open System for Earthquake Engineering Simulation (Opensees). (2005). Pacific Earthquake Engineering Research Center, University of California, Berkeley, http://opensees.berkeley.edu/ (last accessed May 24, 2005).

Panagiotakos, T. B. and Fardis, M. N. (2001). "Deformations of Reinforced Concrete at Yielding and Ultimate," *ACI Structural Journal*, Vol. 98, No. 2, March-April 2001, pp. 135-147.

Park, R. et al. (1972). "Reinforced Concrete Members with Cyclic Loading," *Journal of the Structural Division*, ST7, July 1972.

Park, R., and T. Paulay, T. (1975). "*Reinforced Concrete Structures*," A Wiley-Interscience Publication, pp. 740-757.

Paulay, T. and Priestley, M. J. N. (1992). *Seismic Deign of Reinforced Concrete and Masonry Buildings*, John Wiley and Sons Inc., New York.

Paultre, P., Legeron, F., and Mongeau, D. (2001), "Influence of Concrete Strength and Transverse Reinforcement Yield Strength on Behavior of High-Strength Concrete Columns", American Concrete Institute, *ACI Structural Journal*, Vol. 98, No. 4, July-August 2001,

PEER (2005). *Pacific Earthquake Engineering Research Center: Structural Performance Database*, University of California, Berkeley, Available at http://nisee.berkeley.edu/spd/ and http://maximus.ce.washington.edu/~peera1/ (March 10, 2005).

Saatcioglu, M and Grira, M. (1999). "Confinement of Reinforced Concrete Columns with Welded Reinforcement Grids," *ACI Structural Journal*, American Concrete Institute, Vol. 96, No. 1, January-February 1999, pp. 29-39.

Soesianawati, M.T., Park, R., and Priestley, M.J.N. (1986). "Limited Ductility Design of Reinforced Concrete Columns," Report 86-10, Department of Civil Engineering, University of Canterbury, Christchurch, New Zealand, March 1986, 208 pages.

Vamvatsikos, D. and C. Allin Cornell (2002). "Incremental Dynamic Analysis," *Earthquake Engineering and Structural Dynamics*, Vol. 31, Issue 3, pp. 491-514.

Vamvatsikos, D. (2002). *Seismic Performance, Capacity and Reliability of Structures as Seem Through Incremental Dynamic Analysis*, Dissertation, Department of Civil and Environmental Engineering, Stanford University.

Xiao, Y. and Martirossyan, A. (1998). "Seismic Performance of High-Strength Concrete Columns," *Journal of Structural Engineering*, March 1998, pp. 241-251.

Appendix A: Test Series Used to Isolate the Effects of Individual Variables

This appendix is composed of a single table that lists the information for each test series which have only a single parameter varied.[26] An example of such a test series is tests #215-217 by Legeron and Paultre (2000); in these tests, all variables were held constant except the axial load ratio was varied. The series listed in this table are used to isolate the effects of each single variable, to judge trends in these data, and then to help determine the proper form of the regression equations. For further discussion of these results see Section 2.2, and Figure 11.

[26] Transverse reinforce ratio (ρ_{sh}) and hoop spacing (s) are often varied together and are considered together in Table 9.

Table 11a. Table of test series with one parameter varied and the others held constant.

Index	Test Numbers from Database	Test Series	Properties Varied	Notes	f'c (MPa)	v ($P/A_g f'_c$)	ρ_{sh}	s (mm)	Stirrup Config. (as in Berry 2004)	$f_{y,sh}$ (MPa)
1	7, 9	Soesianawati et al. 1986	v			0.10, 0.30				
2	8, 9	Soesianawati et al. 1986	ρ_{sh}, s				0.0064, 0.0042	78, 91		
4	13, 16	Watson and Park 1989	v			0.50, 0.70				
5	13, 14	Watson and Park 1989	ρ_{sh}, s	$f_{y,sh}$ varies slightly			0.0062, 0.0029	81, 96		
6	15, 16, 17	Watson and Park 1989	ρ_{sh}, s	$f_{y,sh}$ varies slightly			0.0118, 0.0065, 0.0217	96, 77, 52		
7	19, 20	Tanaka and Park 1990	Stirrup config.						6, 9	
8	22, 23	Tanaka and Park 1990	Stirrup config.						6, 8	
9	24, 25	Tanaka and Park 1990	Stirrup config.						6, 8	
10	56, 62	Muguruma et al. 1989	f'c	Axial load changes, but v is constant	85.7, 115.8					
11	57, 63	Muguruma et al. 1989	f'c	Axial load changes, but v is constant	85.7, 115.8					
12	56, 58	Muguruma et al. 1989	v			0.40, 0.63				
13	57, 59	Muguruma et al. 1989	v			0.40, 0.63				
14	60, 62	Muguruma et al. 1989	v			0.25, 0.42				
15	61, 63	Muguruma et al. 1989	v			0.25, 0.42				
16	66, 67	Sakai et al. 1990	ρ_{sh}, s				0.0052, 0.0079	60, 40		
17	71, 72	Sakai et al. 1990	s	ρ_{sh} is constant				60, 30		
18	66, 68, 69	Sakai et al. 1990	f_{ysh}	Test 68 has 20% larger ρ_{sh}						774, 344, 1126
19	66, 71	Sakai et al. 1990	Stirrup config.	$f_{y,sh}$ changes slightly					4, 2	
20	88, 92, 94	Atalay and Penzien 1975	v			0.10, 0.20, 0.26				
21	90, 92, 96	Atalay and Penzien 1975	v			0.10, 0.20, 0.28				
22	89, 93, 95	Atalay and Penzien 1975	v			0.09, 0.18, 0.27				
23	91, 93, 97	Atalay and Penzien 1975	v			0.10, 0.18, 0.27				
24	88, 89	Atalay and Penzien 1975	ρ_{sh}, s				0.0061, 0.0037			
25	90, 91	Atalay and Penzien 1975	ρ_{sh}, s				0.0061, 0.0037			
26	92, 93	Atalay and Penzien 1975	ρ_{sh}, s				0.0061, 0.0037			
27	94, 95	Atalay and Penzien 1975	ρ_{sh}, s				0.0061, 0.0037			
28	96, 97	Atalay and Penzien 1975	ρ_{sh}, s				0.0061, 0.0037			
29	105, 106	Saatcioglu and Ozcebe 1989	ρ_{sh}, s				0.006, 0.009			
30	109, 114, 118	Galeota et al. 1996	ρ_{sh}, s				0.0054, 0.008, 0.0161			
31	122, 127, 131	Galeota et al. 1996	ρ_{sh}, s				0.0054, 0.008, 0.0161			
32	110, 115, 120	Galeota et al. 1996	ρ_{sh}, s				0.0054, 0.008, 0.0161			

Table 11**b. Table of test series with one parameter varied and the others held constant.**

Index	Test Numbers from Database	Test Series	Properties Varied	Notes	f'c (MPa)	v (P/A_gf'$_c$)	ρ_{sh}	s (mm)	Stirrup Config. (as in Berry 2004)	$f_{y,sh}$ (MPa)
33	123, 128, 132	Galeota et al. 1996	ρ_{sh}, s				0.0054, 0.008, 0.0161			
34	111, 113, 117	Galeota et al. 1996	ρ_{sh}, s				0.0054, 0.008, 0.0161			
35	121, 125, 129	Galeota et al. 1996	ρ_{sh}, s				0.0054, 0.008, 0.0161			
36	112, 116, 119	Galeota et al. 1996	ρ_{sh}, s				0.0054, 0.008, 0.0161			
37	124, 126, 130	Galeota et al. 1996	ρ_{sh}, s				0.0054, 0.008, 0.0161			
38	109, 111	Galeota et al. 1996	v			0.20, 0.30				
39	110, 112	Galeota et al. 1996	v			0.20, 0.30				
40	121, 122	Galeota et al. 1996	v			0.20, 0.30				
41	123, 124	Galeota et al. 1996	v			0.20, 0.30				
42	113, 114	Galeota et al. 1996	v			0.20, 0.30				
43	115, 116	Galeota et al. 1996	v			0.20, 0.30				
44	125, 127	Galeota et al. 1996	v			0.20, 0.30				
45	126, 128	Galeota et al. 1996	v			0.20, 0.30				
46	117, 118	Galeota et al. 1996	v			0.20, 0.30				
47	119, 120	Galeota et al. 1996	v			0.20, 0.30				
48	129, 131	Galeota et al. 1996	v			0.20, 0.30				
49	130, 132	Galeota et al. 1996	v			0.20, 0.30				
50	133, 134	Wehbe et al. 1998	v			0.10, 0.24				
51	135, 136	Wehbe et al. 1998	v			0.09, 0.23				
52	133, 135	Wehbe et al. 1998	ρ_{sh}, s				0.0027, 0.0036	110, 83		
53	134, 136	Wehbe et al. 1998	ρ_{sh}, s				0.0027, 0.0036	110, 83		
54	145, 147	Xiao and Martirossyan 1998	f'c		76.0, 86.0					
55	146, 148	Xiao and Martirossyan 1998	f'c		76.0, 86.0					
56	145, 146	Xiao and Martirossyan 1998	v			0.10, 0.20				
57	147, 148	Xiao and Martirossyan 1998	v			0.10, 0.19				
58	152, 154	Sugano 1996	v			0.30, 0.60				
59	153, 155	Sugano 1996	v			0.30, 0.60				
60	151, 152, 153	Sugano 1996	ρ_{sh}, s				0.0081, 0.0127, 0.0163	45, 45, 35		
61	154, 155	Sugano 1996	ρ_{sh}, s				0.0127, 0.0163	45, 35		
62	159, 163	Bayrak and Sheikh 1996	f'c	ρ_{sh} varies slightly	71.8, 102.0					
63	158, 159	Bayrak and Sheikh 1996	v			0.36, 0.50				
64	157, 159, 160	Bayrak and Sheikh 1996	ρ_{sh}, s				0.0138, 0.0124, 0.0224	95, 90, 100		

Table 11**c. Table of test series with one parameter varied and the others held constant.**

Index	Test Numbers from Database	Test Series	Properties Varied	Notes	f'c (MPa)	v ($P/A_g f'_c$)	ρ_{sh}	s (mm)	Stirrup Config. (as in Berry 2004)	$f_{y,sh}$ (MPa)
65	161, 162, 163, 164	Bayrak and Sheikh 1996	ρ_{sh}, s				0.0248, 0.0294, 0.0119, 0.0187	90, 76, 94, 70		
66	166, 167	Saatcioglu and Grira 1999	v			0.20, 0.43				
67	171, 172	Saatcioglu and Grira 1999	v			0.23, 0.46				
68	166, 169, 171	Saatcioglu and Grira 1999	ρ_{sh}; s constant				0.0080, 0.0107, 0.0051	76		
69	166, 173, 174	Saatcioglu and Grira 1999	ρ_{sh}; s constant				0.0080, 0.0107, 0.0051	76		
70	165, 168	Saatcioglu and Grira 1999	ρ_{sh}; s constant				0.004, 0.0054	152		
71	167, 172	Saatcioglu and Grira 1999	ρ_{sh}; s constant				0.008, 0.0051	76		
72	177, 179	Matamoros et al. 1999	v	f'c changes slightly		0.10, 0.21				
73	178, 180	Matamoros et al. 1999	v	f'c changes slightly		0.10, 0.21				
74	187, 190	Mo and Wang 2000	Stirrup config.	ρ_{sh} and s also change slightly					6, 4	
75	188, 191	Mo and Wang 2000	Stirrup config.	ρ_{sh} and s also change slightly					6, 4	
76	189, 192	Mo and Wang 2000	Stirrup config.	ρ_{sh} and s also change slightly					6, 4	
77	187, 188, 189	Mo and Wang 2000	v			0.11, 0.16, 0.22				
78	190, 191, 192	Mo and Wang 2000	v			0.11, 0.16, 0.21				
79	193, 194, 195	Mo and Wang 2000	v			0.11, 0.15, 0.21				
80	203, 204, 205	Thomsen and Wallace 1994	v	f'c changes slightly		0.00, 0.10, 0.20				
81	209, 211	Thomsen and Wallace 1994	ρ_{sh}, s	s changes slightly			0.0056, 0.004	32, 44		
82	205, 209	Thomsen and Wallace 1994	$f_{y,sh}$	fy changes slightly						793, 1262
83	215, 216, 217	Paultre & Legeron, 2000	v			0.14, 0.28, 0.39				
84	218, 219, 220	Paultre & Legeron, 2000	v			0.14, 0.26, 0.37				
85	215, 218	Paultre & Legeron, 2000	ρ_{sh}, s				0.0187, 0.0086	60, 130		
86	216, 219	Paultre & Legeron, 2000	ρ_{sh}, s				0.0187, 0.0086	60, 130		
87	217, 220	Paultre & Legeron, 2000	ρ_{sh}, s				0.0187, 0.0086	60, 130		
88	221, 222	Paultre et al., 2001	f'c		78.7, 109.2					
89	243, 244	Bechtoula et al., 2002	v			0.30, 0.60				
90	244, 245, 247	Bechtoula et al., 2002	ρ_{sh}, s				0.005, 0.0084, 0.009	40, 100, 100		
91	254, 255	Xaio & Yun 2002	v			0.20, 0.32				
92	256, 257	Xaio & Yun 2002	v			0.22, 0.32				
93	254, 258	Xaio & Yun 2002	ρ_{sh}, s				0.0117, 0.0078			
94	256, 259	Xaio & Yun 2002	ρ_{sh}, s				0.0093, 0.0078			
95	286, 287	Esaki, 1996	s; ρ_{sh} constant				0.0052	50, 75		
96	288, 289	Esaki, 1996	s; ρ_{sh} constant				0.0065	40, 60		

Appendix B: Database of Column Design Information and Calibrated Parameters

This Appendix contains two sets of tables. The first set of tables (Table 12) provides column design information (i.e. dimensions, reinforcement, material strengths, etc.) for each column used for calibration in this study. This first set of tables also includes predictions by Fardis et al. (Fardis 2003, Panagiotakos and Fardis 2001) for flexural strength, yield curvature, yield chord rotation, and ultimate plastic rotation. The Fardis et al. predictions are included here because they are used for comparisons throughout this study.

The second set of tables (Table 13) includes the calibration parameters (strength, stiffness, plastic rotation capacity, energy dissipation capacity, etc.) for each column obtained from calibration of each column test in this study.

Table 12a. Table of column design information.

Test Index	Test Num. from PEER SPD	Test Series	b (mm)	h (mm)	Ls/H	v	P/P_b	f'_c (MPa)	f_y (MPa)	ρ	d_b (mm)	s (mm)	s_n	ρ_{sh}	$\rho_{sh,eff}$	a_{sl}	M_y (Fardis) (kN-m)	φ_y (Fardis) (rad/m)	$\theta_{u,mono}^{pl}$ (Fardis) (rad)	θ_y (Fardis) (rad)
1	1	Gill et al. 1979, No. 1	550	550	2.2	0.26	0.65	23.1	375	0.020	24	80	6.5	0.0071	0.092	0	713.0	0.0069	0.032	0.0055
2	2	Gill et al. 1979, No. 2	550	550	2.2	0.21	0.61	41.4	375	0.020	24	75	6.1	0.0110	0.084	0	882.5	0.00698	0.039	0.0055
3	3	Gill et al. 1979, No. 3	550	550	2.2	0.42	1.05	21.4	375	0.020	24	75	6.1	0.0076	0.106	0	787.2	0.00666	0.025	0.0054
4	4	Gill et al. 1979, No. 4	550	550	2.2	0.60	1.50	23.5	375	0.020	24	62	5.0	0.0133	0.166	0	854.7	0.00551	0.021	0.0050
5	5	Ang et al. 1981, No. 3	400	400	4.0	0.38	1.00	23.6	427	0.017	16	100	12.9	0.0113	0.153	0	331.5	0.01137	0.037	0.0088
6	6	Ang et al. 1981, No. 4	400	400	4.0	0.21	0.55	25	427	0.017	16	90	11.6	0.0087	0.098	0	259.4	0.00992	0.045	0.0080
7	7	Soesianawati et al. 1986, No. 1	400	400	4.0	0.10	0.30	46.5	446	0.016	16	85	11.2	0.0045	0.035	0	266.1	0.00904	0.055	0.0076
8	8	Soesianawati et al. 1986, No. 2	400	400	4.0	0.30	0.89	44	446	0.016	16	78	10.3	0.0064	0.053	0	440.9	0.01118	0.040	0.0087
9	9	Soesianawati et al. 1986, No. 3	400	400	4.0	0.30	0.89	44	446	0.016	16	91	12.0	0.0042	0.035	0	441.4	0.01114	0.039	0.0087
10	10	Soesianawati et al. 1986, No. 4	400	400	4.0	0.30	0.86	40	446	0.016	16	94	12.4	0.0030	0.019	0	416.6	0.01097	0.037	0.0086
11	11	Zahn et al. 1986, No. 7	400	400	4.0	0.22	0.58	28.3	440	0.016	16	117	15.3	0.0067	0.111	0	292.5	0.00999	0.046	0.0081
12	12	Zahn et al. 1986, No. 8	400	400	4.0	0.39	1.12	40.1	440	0.016	16	92	12.1	0.0085	0.099	0	512.8	0.01325	0.037	0.0098
13	13	Watson and Park 1989, No. 5	400	400	4.0	0.50	1.49	41	474	0.016	16	81	11.0	0.0062	0.056	0	536.1	0.01127	0.029	0.0088
14	14	Watson and Park 1989, No. 6	400	400	4.0	0.50	1.46	40	474	0.016	16	96	13.1	0.0029	0.029	0	527.6	0.01113	0.027	0.0087
15	15	Watson and Park 1989, No. 7	400	400	4.0	0.70	2.12	42	474	0.016	16	96	13.1	0.0118	0.086	0	545.9	0.0086	0.022	0.0073
16	16	Watson and Park 1989, No. 8	400	400	4.0	0.70	2.04	39	474	0.016	16	77	10.5	0.0065	0.062	0	514.6	0.00831	0.021	0.0072
17	17	Watson and Park 1989, No. 9	400	400	4.0	0.70	2.08	40	474	0.016	16	52	7.1	0.0217	0.167	0	522.2	0.00841	0.026	0.0072
18	18	Tanaka and Park 1990, No. 1	400	400	4.0	0.20	0.58	25.6	474	0.019	20	80	8.7	0.0106	0.138	0	274.4	0.01178	0.050	0.0090
19	19	Tanaka and Park 1990, No. 2	400	400	4.0	0.20	0.58	25.6	474	0.019	20	80	8.7	0.0106	0.138	0	274.4	0.01178	0.050	0.0090
20	20	Tanaka and Park 1990, No. 3	400	400	4.0	0.20	0.58	25.6	474	0.019	20	80	8.7	0.0106	0.138	0	274.4	0.01178	0.050	0.0090
21	21	Tanaka and Park 1990, No. 4	400	400	4.0	0.20	0.58	25.6	474	0.019	20	80	8.7	0.0106	0.138	0	274.4	0.01178	0.050	0.0090
22	22	Tanaka and Park 1990, No. 5	550	550	3.0	0.10	0.30	32	511	0.014	20	110	12.4	0.0075	0.076	1	565.3	0.00772	0.075	0.0091
23	23	Tanaka and Park 1990, No. 6	550	550	3.0	0.10	0.30	32	511	0.014	20	110	12.4	0.0075	0.076	1	565.3	0.00772	0.075	0.0091
24	24	Tanaka and Park 1990, No. 7	550	550	3.0	0.30	0.89	32.1	511	0.014	20	90	10.2	0.0091	0.093	1	920.3	0.00923	0.057	0.0099
25	25	Tanaka and Park 1990, No. 8	550	550	3.0	0.30	0.89	32.1	511	0.014	20	90	10.2	0.0091	0.093	1	920.3	0.00923	0.057	0.0099
26	26	Park and Paulay 1990, No. 9	400	600	3.0	0.10	0.26	26.9	432	0.020	24	80	6.9	0.0106	0.120	1	585.0	0.00596	0.079	0.0080
27	27	Arakawa et al. 1982, No. 102	250	250	1.5	0.33	0.79	20.6	393	0.007	9.5	32	6.7	0.0089	0.140	1	53.1	0.0144	0.041	0.0059
28	29	Nagasaka 1982, HPRC19-32	200	200	1.5	0.35	0.88	21	371	0.014	12.7	20	3.0	0.0119	0.195	1	35.1	0.01995	0.045	0.0072
29	30	Ohno and Nishioka 1984, L1	400	400	4.0	0.03	0.08	24.8	362	0.016	19	100	10.0	0.0032	0.042	1	121.9	0.00734	0.083	0.0083
30	31	Ohno and Nishioka 1984, L2	400	400	4.0	0.03	0.08	24.8	362	0.016	19	100	10.0	0.0032	0.042	1	121.9	0.00734	0.083	0.0083
31	32	Ohno and Nishioka 1984, L3	400	400	4.0	0.03	0.08	24.8	362	0.016	19	100	10.0	0.0032	0.042	1	121.9	0.00734	0.083	0.0083
32	33	Ohue et al. 1985, 2D16RS	200	200	2.0	0.14	0.37	32	369	0.023	16	50	6.0	0.0048	0.047	1	36.2	0.01758	0.057	0.0076
33	34	Ohue et al. 1985, 4D13RS	200	200	2.0	0.15	0.39	29.9	370	0.030	13	50	7.4	0.0048	0.050	1	35.6	0.01809	0.056	0.0072
34	35	Zhou et al. 1985, No. 806	80	80	1.0	0.60	1.69	32.3	336	0.022	6	80	24.4	0.0039	0.041	1	3.2	0.04389	0.021	0.0064
35	37	Zhou et al. 1985, No. 1309	80	80	1.0	0.90	2.55	32.8	336	0.022	6	80	24.4	0.0039	0.041	1	3.1	0.03082	0.013	0.0061
36	42	Zhou et al. 1987, No. 204-08	160	160	2.0	0.80	1.99	21.1	341	0.026	9.5	40	7.8	0.0061	0.163	1	19.3	0.01458	0.023	0.0063
37	43	Zhou et al. 1987, No. 214-08	160	160	2.0	0.80	1.99	21.1	341	0.026	9.5	40	7.8	0.0061	0.163	1	19.3	0.01458	0.023	0.0063
38	44	Zhou et al. 1987, No. 223-09	160	160	2.0	0.90	2.24	21.1	341	0.026	9.5	40	7.8	0.0105	0.277	1	18.7	0.01313	0.024	0.0062
39	45	Zhou et al. 1987, No. 302-07	160	160	3.0	0.70	1.76	28.8	341	0.026	9.5	40	7.8	0.0061	0.119	1	25.8	0.01869	0.030	0.0075
40	46	Zhou et al. 1987, No. 312-07	160	160	3.0	0.70	1.76	28.8	341	0.026	9.5	40	7.8	0.0061	0.119	1	25.8	0.01869	0.030	0.0075

Table 12b. Table of column design information.

Test Index	Test Num. from PEER SPD	Test Series	b (mm)	h (mm)	Ls/ H	v	P/P_b	f'_c (MPa)	f_y (MPa)	ρ	d_b (mm)	s (mm)	s_n	ρ_{sh}	$\rho_{sh,eff}$	a_{sl}	M_y (Fardis) (kN-m)	φ_y (Fardis) (rad/m)	$\theta_{u,mono}^{pl}$ (Fardis) (rad)	θ_y (Fardis) (rad)
41	47	Zhou et al. 1987, No. 322-07	160	160	3.0	0.70	1.76	28.8	341	0.026	9.5	40	7.8	0.0105	0.203	1	25.8	0.01869	0.036	0.0075
42	48	Kanda et al. 1988, 85STC-1	250	250	3.0	0.11	0.29	27.9	374	0.020	12.7	50	7.6	0.0038	0.069	1	47.0	0.01496	0.072	0.0086
43	49	Kanda et al. 1988, 85STC-2	250	250	3.0	0.11	0.29	27.9	374	0.020	12.7	50	7.6	0.0038	0.069	1	47.0	0.01496	0.072	0.0086
44	50	Kanda et al. 1988, 85STC-3	250	250	3.0	0.11	0.29	27.9	374	0.020	12.7	50	7.6	0.0038	0.069	1	47.0	0.01496	0.072	0.0086
45	51	Kanda et al. 1988, 85PDC-1	250	250	3.0	0.12	0.32	24.8	374	0.020	12.7	50	7.6	0.0038	0.054	1	46.7	0.01515	0.066	0.0087
46	52	Kanda et al. 1988, 85PDC-2	250	250	3.0	0.11	0.29	27.9	374	0.020	12.7	50	7.6	0.0038	0.069	1	47.0	0.01496	0.072	0.0086
47	53	Kanda et al. 1988, 85PDC-3	250	250	3.0	0.11	0.29	27.9	374	0.020	12.7	50	7.6	0.0038	0.069	1	47.0	0.01496	0.072	0.0086
48	56	Muguruma et al. 1989, AL-1	200	200	2.5	0.40	1.33	85.7	400	0.043	12.7	35	5.5	0.0162	0.062	0	156.3	0.03757	0.034	0.0090
49	57	Muguruma et al. 1989, AH-1	200	200	2.5	0.40	1.33	85.7	400	0.043	12.7	35	5.5	0.0162	0.149	0	156.3	0.03757	0.040	0.0090
50	58	Muguruma et al. 1989, AL-2	200	200	2.5	0.63	2.09	85.7	400	0.043	12.7	35	5.5	0.0162	0.062	0	155.1	0.0281	0.024	0.0074
51	59	Muguruma et al. 1989, AH-2	200	200	2.5	0.63	2.09	85.7	400	0.043	12.7	35	5.5	0.0162	0.149	0	155.1	0.0281	0.028	0.0074
52	60	Muguruma et al. 1989, BL-1	200	200	2.5	0.25	0.85	115.8	400	0.043	12.7	35	5.5	0.0162	0.046	0	116.2	0.02407	0.045	0.0068
53	61	Muguruma et al. 1989, BH-1	200	200	2.5	0.25	0.85	115.8	400	0.043	12.7	35	5.5	0.0162	0.111	0	116.2	0.02407	0.051	0.0068
54	62	Muguruma et al. 1989, BL-2	200	200	2.5	0.42	1.41	115.8	400	0.043	12.7	35	5.5	0.0162	0.046	0	200.6	0.04248	0.034	0.0098
55	63	Muguruma et al. 1989, BH-2	200	200	2.5	0.42	1.41	115.8	400	0.043	12.7	35	5.5	0.0162	0.111	0	200.6	0.04248	0.039	0.0098
56	64	Ono et al. 1989, CA025C	200	200	1.5	0.26	0.66	25.8	361	0.025	9.5	70	14.0	0.0081	0.133	1	37.1	0.01989	0.048	0.0064
57	65	Ono et al. 1989, CA060C	200	200	1.5	0.62	1.58	25.8	361	0.025	9.5	70	14.0	0.0081	0.133	1	44.3	0.01568	0.027	0.0060
58	66	Sakai et al. 1990, B1	250	250	2.0	0.35	1.19	99.5	379	0.028	12.7	60	9.2	0.0052	0.041	1	284.2	0.03562	0.052	0.0097
59	67	Sakai et al. 1990, B2	250	250	2.0	0.35	1.19	99.5	379	0.028	12.7	40	6.1	0.0079	0.061	1	284.2	0.03562	0.054	0.0097
60	68	Sakai et al. 1990, B3	250	250	2.0	0.35	1.19	99.5	379	0.028	12.7	60	9.2	0.0063	0.022	1	283.4	0.03562	0.050	0.0097
61	69	Sakai et al. 1990, B4	250	250	2.0	0.35	1.19	99.5	379	0.028	12.7	60	9.2	0.0052	0.059	1	284.2	0.03562	0.054	0.0097
62	70	Sakai et al. 1990, B5	250	250	2.0	0.35	1.19	99.5	379	0.028	12.7	30	4.6	0.0052	0.041	1	284.2	0.03562	0.052	0.0097
63	71	Sakai et al. 1990, B6	250	250	2.0	0.35	1.20	99.5	379	0.029	12.7	60	9.2	0.0051	0.044	1	281.1	0.03562	0.053	0.0097
64	72	Sakai et al. 1990, B7	250	250	2.0	0.35	1.19	99.5	339	0.022	19	30	2.9	0.0052	0.041	1	265.7	0.03618	0.052	0.0101
65	73	Amitsu et al. 1991, CB060C	278	278	1.2	0.74	2.42	46.3	441	0.032	13	52	8.4	0.0078	0.070	1	209.2	0.01307	0.020	0.0060
66	74	Wight and Sozen 1973, No. 40.033a(East)	152	305	2.9	0.12	0.36	34.7	496	0.028	19	127	14.9	0.0032	0.032	0	87.0	0.01487	0.044	0.0071
67	75	Wight and Sozen 1973, No. 40.033a(West)	152	305	2.9	0.12	0.36	34.7	496	0.028	19	127	14.9	0.0032	0.032	0	87.0	0.01487	0.044	0.0071
68	76	Wight and Sozen 1973, No. 40.048(East)	152	305	2.9	0.15	0.42	26.1	496	0.028	19	89	10.4	0.0046	0.061	0	85.3	0.01519	0.041	0.0072
69	77	Wight and Sozen 1973, No. 40.048(West)	152	305	2.9	0.15	0.42	26.1	496	0.028	19	89	10.4	0.0046	0.061	0	85.3	0.01519	0.041	0.0072
70	78	Wight and Sozen 1973, No. 40.033(East)	152	305	2.9	0.11	0.34	33.6	496	0.028	19	127	14.9	0.0032	0.033	0	85.7	0.01482	0.044	0.0071
71	79	Wight and Sozen 1973, No. 40.033(West)	152	305	2.9	0.11	0.34	33.6	496	0.028	19	127	14.9	0.0032	0.033	0	85.7	0.01482	0.044	0.0071
72	81	Wight and Sozen 1973, No. 25.033(West)	152	305	2.9	0.07	0.21	33.6	496	0.028	19	127	14.9	0.0032	0.033	0	78.5	0.01426	0.047	0.0069
73	82	Wight and Sozen 1973, No. 40.067(East)	152	305	2.9	0.11	0.34	33.4	496	0.028	19	64	7.5	0.0064	0.066	0	85.7	0.01483	0.046	0.0071
74	83	Wight and Sozen 1973, No. 40.067(West)	152	305	2.9	0.11	0.34	33.4	496	0.028	19	64	7.5	0.0064	0.066	0	85.7	0.01483	0.046	0.0071
75	84	Wight and Sozen 1973, No. 40.147(East)	152	305	2.9	0.11	0.34	33.5	496	0.028	19	64	7.5	0.0146	0.138	0	85.7	0.01483	0.053	0.0071
76	85	Wight and Sozen 1973, No. 40.147(West)	152	305	2.9	0.11	0.34	33.5	496	0.028	19	64	7.5	0.0146	0.138	0	85.7	0.01483	0.053	0.0071
77	86	Wight and Sozen 1973, No. 40.092(East)	152	305	2.9	0.11	0.34	33.5	496	0.028	19	102	12.0	0.0091	0.087	0	85.7	0.01483	0.048	0.0071
78	87	Wight and Sozen 1973, No. 40.092(West)	152	305	2.9	0.11	0.34	33.5	496	0.028	19	102	12.0	0.0091	0.087	0	85.7	0.01483	0.048	0.0071
79	88	Atalay and Penzien 1975, No. 1S1	305	305	5.5	0.10	0.27	29.1	367	0.020	22	76	6.6	0.0061	0.076	0	91.2	0.01166	0.060	0.0093
80	89	Atalay and Penzien 1975, No. 2S1	305	305	5.5	0.09	0.26	30.7	367	0.020	22	127	11.1	0.0037	0.043	0	91.4	0.0116	0.057	0.0092

Table 12c. Table of column design information.

Test Index	Test Num. from PEER SPD	Test Series	b (mm)	h (mm)	Ls/ H	v	P/P_b	f'_c (MPa)	f_y (MPa)	ρ	d_b (mm)	s (mm)	s_n	ρ_{sh}	$\rho_{sh,eff}$	a_{sl}	M_y (Fardis) (kN-m)	φ_y (Fardis) (rad/m)	$\theta_{u,mono}^{pl}$ (Fardis) (rad)	θ_y (Fardis) (rad)
81	90	Atalay and Penzien 1975, No. 3S1	305	305	5.5	0.10	0.27	29.2	367	0.020	22	76	6.6	0.0061	0.076	0	91.2	0.01166	0.060	0.0093
82	91	Atalay and Penzien 1975, No. 4S1	305	305	5.5	0.10	0.29	27.6	429	0.020	22	127	12.0	0.0037	0.048	0	101.7	0.01346	0.056	0.0103
83	92	Atalay and Penzien 1975, No. 5S1	305	305	5.5	0.20	0.56	29.4	429	0.020	22	76	7.2	0.0061	0.082	0	129.6	0.01474	0.052	0.0110
84	93	Atalay and Penzien 1975, No. 6S1	305	305	5.5	0.18	0.53	31.8	429	0.020	22	127	12.0	0.0037	0.045	0	130.0	0.0146	0.051	0.0109
85	94	Atalay and Penzien 1975, No. 9	305	305	5.5	0.26	0.72	33.3	363	0.020	22	76	6.6	0.0061	0.072	0	144.9	0.01386	0.047	0.0105
86	95	Atalay and Penzien 1975, No. 10	305	305	5.5	0.27	0.73	32.4	363	0.020	22	127	11.0	0.0037	0.044	0	144.8	0.01392	0.044	0.0105
87	96	Atalay and Penzien 1975, No. 11	305	305	5.5	0.28	0.76	31	363	0.020	22	76	6.6	0.0061	0.074	0	144.5	0.01401	0.045	0.0106
88	97	Atalay and Penzien 1975, No. 12	305	305	5.5	0.27	0.74	31.8	363	0.020	22	127	11.0	0.0037	0.043	0	144.6	0.01395	0.043	0.0105
89	102	Azizinamini et al. 1988, NC-2	457	457	3.0	0.21	0.63	39.3	439	0.023	25.4	102	8.4	0.0093	0.107	0	544.0	0.00983	0.046	0.0072
90	103	Azizinamini et al. 1988, NC-4	457	457	3.0	0.31	0.95	39.8	439	0.023	25.4	102	8.4	0.0052	0.080	0	671.9	0.0108	0.037	0.0077
91	104	Saatcioglu and Ozcebe 1989, U1	350	350	2.9	0.00	0.00	43.6	430	0.037	25	150	12.4	0.0030	0.032	1	202.3	0.0103	0.086	0.0088
92	105	Saatcioglu and Ozcebe 1989, U3	350	350	2.9	0.14	0.40	34.8	430	0.037	25	75	6.2	0.0060	0.081	1	271.1	0.012	0.071	0.0097
93	106	Saatcioglu and Ozcebe 1989, U4	350	350	2.9	0.15	0.43	32	438	0.037	25	50	4.2	0.0090	0.132	1	274.1	0.0123	0.076	0.0100
94	107	Saatcioglu and Ozcebe 1989, U6	350	350	2.9	0.13	0.39	37.3	437	0.037	25	65	5.4	0.0085	0.097	1	275.1	0.01208	0.076	0.0097
95	108	Saatcioglu and Ozcebe 1989, U7	350	350	2.9	0.13	0.38	39	437	0.037	25	65	5.4	0.0085	0.092	1	275.5	0.01203	0.077	0.0096
96	109	Galeota et al. 1996, AA1	250	250	4.6	0.30	1.11	80	430	0.018	10	150	31.1	0.0054	0.029	0	196.1	0.03581	0.046	0.0164
97	110	Galeota et al. 1996, AA2	250	250	4.6	0.30	1.11	80	430	0.018	10	150	31.1	0.0054	0.029	0	196.1	0.03581	0.046	0.0164
98	111	Galeota et al. 1996, AA3	250	250	4.6	0.20	0.74	80	430	0.018	10	150	31.1	0.0054	0.029	0	119.3	0.01978	0.054	0.0103
99	112	Galeota et al. 1996, AA4	250	250	4.6	0.20	0.74	80	430	0.018	10	150	31.1	0.0054	0.029	0	119.3	0.01978	0.054	0.0103
100	113	Galeota et al. 1996, BA1	250	250	4.6	0.20	0.74	80	430	0.018	10	100	20.7	0.0080	0.043	0	119.3	0.01978	0.056	0.0103
101	114	Galeota et al. 1996, BA2	250	250	4.6	0.30	1.11	80	430	0.018	10	100	20.7	0.0080	0.043	0	196.1	0.03581	0.048	0.0164
102	115	Galeota et al. 1996, BA3	250	250	4.6	0.30	1.11	80	430	0.018	10	100	20.7	0.0080	0.043	0	196.1	0.03581	0.048	0.0164
103	116	Galeota et al. 1996, BA4	250	250	4.6	0.20	0.74	80	430	0.018	10	100	20.7	0.0080	0.043	0	119.3	0.01978	0.056	0.0103
104	117	Galeota et al. 1996, CA1	250	250	4.6	0.20	0.74	80	430	0.018	10	50	10.4	0.0161	0.086	0	119.3	0.01978	0.061	0.0103
105	118	Galeota et al. 1996, CA2	250	250	4.6	0.30	1.11	80	430	0.018	10	50	10.4	0.0161	0.086	0	196.1	0.03581	0.052	0.0164
106	119	Galeota et al. 1996, CA3	250	250	4.6	0.20	0.74	80	430	0.018	10	50	10.4	0.0161	0.086	0	119.3	0.01978	0.061	0.0103
107	120	Galeota et al. 1996, CA4	250	250	4.6	0.30	1.11	80	430	0.018	10	50	10.4	0.0161	0.086	0	196.1	0.03581	0.052	0.0164
108	121	Galeota et al. 1996, AB1	250	250	4.6	0.20	0.76	80	430	0.075	20	150	15.6	0.0054	0.029	0	195.7	0.02179	0.054	0.0110
109	122	Galeota et al. 1996	250	250	4.6	0.30	1.14	80	430	0.075	20	150	15.6	0.0054	0.029	0	286.4	0.03166	0.046	0.0148
110	123	Galeota et al. 1996, AB3	250	250	4.6	0.30	1.14	80	430	0.075	20	150	15.6	0.0054	0.029	0	286.4	0.03166	0.046	0.0148
111	124	Galeota et al. 1996, AB4	250	250	4.6	0.20	0.76	80	430	0.075	20	150	15.6	0.0054	0.029	0	195.7	0.02179	0.054	0.0110
112	125	Galeota et al. 1996, BB	250	250	4.6	0.20	0.76	80	430	0.075	20	100	10.4	0.0080	0.043	0	195.7	0.02179	0.056	0.0110
113	126	Galeota et al. 1996, BB1	250	250	4.6	0.20	0.76	80	430	0.075	20	100	10.4	0.0080	0.043	0	195.7	0.02179	0.056	0.0110
114	127	Galeota et al. 1996, BB4	250	250	4.6	0.30	1.14	80	430	0.075	20	100	10.4	0.0080	0.043	0	286.4	0.03166	0.048	0.0148
115	128	Galeota et al. 1996, BB4B	250	250	4.6	0.30	1.14	80	430	0.075	20	100	10.4	0.0080	0.043	0	286.4	0.03166	0.048	0.0148
116	129	Galeota et al. 1996, CB1	250	250	4.6	0.20	0.76	80	430	0.075	20	50	5.2	0.0161	0.086	0	195.7	0.02179	0.061	0.0110
117	130	Galeota et al. 1996, CB2	250	250	4.6	0.20	0.76	80	430	0.075	20	50	5.2	0.0161	0.086	0	195.7	0.02179	0.061	0.0110
118	131	Galeota et al. 1996, CB3	250	250	4.6	0.30	1.14	80	430	0.075	20	50	5.2	0.0161	0.086	0	286.4	0.03166	0.052	0.0148
119	132	Galeota et al. 1996, CB4	250	250	4.6	0.30	1.14	80	430	0.075	20	50	5.2	0.0161	0.086	0	286.4	0.03166	0.052	0.0148
120	133	Wehbe et al. 1998, A1	380	610	3.8	0.10	0.25	27.2	448	0.024	19.1	110	12.2	0.0027	0.043	1	667.3	0.00605	0.075	0.0088

Table 12d. Table of column design information.

Test Index	Test Num. from PEER SPD	Test Series	b (mm)	h (mm)	Ls/H	v	P/P_b	f'_c (MPa)	f_y (MPa)	ρ	d_b (mm)	s (mm)	s_n	ρ_{sh}	$\rho_{sh,eff}$	a_{sl}	M_y (Fardis) (kN-m)	φ_y (Fardis) (rad/m)	$\theta_{u,mono}^{pl}$ (Fardis) (rad)	θ_y (Fardis) (rad)
121	134	Wehbe et al. 1998, A2	380	610	3.8	0.24	0.61	27.2	448	0.024	19.1	110	12.2	0.0027	0.043	1	850.0	0.00676	0.060	0.0094
122	135	Wehbe et al. 1998, B1	380	610	3.8	0.09	0.24	28.1	448	0.024	19.1	83	9.2	0.0036	0.055	1	668.9	0.00598	0.078	0.0087
123	136	Wehbe et al. 1998, B2	380	610	3.8	0.23	0.60	28.1	448	0.024	19.1	83	9.2	0.0036	0.055	1	857.0	0.00669	0.062	0.0093
124	137	Lynn et al. 1998, 2CLH18	457.2	457.2	3.2	0.07	0.19	33.1	331	0.022	25.4	457	32.7	0.0007	0.008	1	293.8	0.00651	0.072	0.0073
125	138	Lynn et al. 1998, 2CMH18	457.2	457.2	3.2	0.28	0.69	25.5	331	0.022	25.4	457	32.7	0.0007	0.011	1	438.7	0.00803	0.048	0.0083
126	143	Lynn et al. 1996, 2SLH18	457.2	457.2	3.2	0.07	0.19	33.1	331	0.022	25.4	457	32.7	0.0007	0.008	1	293.8	0.00651	0.072	0.0073
127	144	Lynn et al. 1996, 3SMD12	457.2	457.2	3.2	0.28	0.70	25.5	331	0.035	31.75	305	17.5	0.0017	0.027	1	540.4	0.00827	0.050	0.0088
128	145	Xiao and Martirossyan 1998, HC4-8L19-T10-0.1P	254	254	2.0	0.10	0.38	76	510	0.041	19.1	51	6.0	0.0157	0.106	1	145.6	0.01876	0.083	0.0088
129	146	Xiao and Martirossyan 1998, HC4-8L19-T10-0.2P	254	254	2.0	0.20	0.75	76	510	0.041	19.1	51	6.0	0.0157	0.106	1	185.8	0.02096	0.071	0.0092
130	147	Xiao and Martirossyan 1998, HC4-8L16-T10-0.1P	254	254	2.0	0.10	0.36	86	510	0.028	15.9	51	7.2	0.0157	0.093	1	121.6	0.01807	0.084	0.0080
131	148	Xiao and Martirossyan 1998, HC4-8L16-T10-0.2P	254	254	2.0	0.19	0.72	86	510	0.028	15.9	51	7.2	0.0157	0.093	1	166.0	0.0205	0.072	0.0084
132	149	Xiao and Martirossyan 1998, HC4-8L16-T6-0.1P	254	254	2.0	0.10	0.36	86	510	0.028	15.9	51	7.2	0.0075	0.039	1	122.8	0.01774	0.076	0.0079
133	150	Xiao and Martirossyan 1998, HC4-8L16-T6-0.2P	254	254	2.0	0.19	0.71	86	510	0.028	15.9	51	7.2	0.0075	0.039	1	167.2	0.02012	0.065	0.0083
134	151	Sugano 1996, UC10H	225	225	2.0	0.60	1.96	118	393	0.021	10	45	8.9	0.0081	0.097	1	257.9	0.02896	0.041	0.0078
135	152	Sugano 1996, UC15H	225	225	2.0	0.60	1.97	118	393	0.021	10	45	8.9	0.0127	0.153	1	256.9	0.02896	0.045	0.0079
136	153	Sugano 1996, UC20H	225	225	2.0	0.60	1.97	118	393	0.021	10	35	6.9	0.0163	0.197	1	256.9	0.02896	0.049	0.0079
137	154	Sugano 1996, UC15L	225	225	2.0	0.35	1.15	118	393	0.021	10	45	8.9	0.0127	0.153	1	236.2	0.04392	0.068	0.0101
138	155	Sugano 1996, UC20L	225	225	2.0	0.35	1.15	118	393	0.021	10	35	6.9	0.0163	0.197	1	236.2	0.04392	0.074	0.0101
139	157	Bayrak and Sheikh 1996, ES-1HT	305	305	6.0	0.50	1.78	72.1	454	0.029	19.54	95	10.4	0.0138	0.089	1	425.8	0.01971	0.063	0.0168
140	158	Bayrak and Sheikh 1996, AS-2HT	305	305	6.0	0.36	1.27	71.7	454	0.029	19.54	90	9.8	0.0124	0.094	1	421.5	0.02411	0.080	0.0195
141	159	Bayrak and Sheikh 1996, AS-3HT	305	305	6.0	0.50	1.77	71.8	454	0.029	19.54	90	9.8	0.0124	0.094	1	428.3	0.01967	0.064	0.0168
142	160	Bayrak and Sheikh 1996, AS-4HT	305	305	6.0	0.50	1.78	71.9	454	0.029	19.54	100	10.9	0.0224	0.144	1	424.7	0.01968	0.071	0.0168
143	161	Bayrak and Sheikh 1996, AS-5HT	305	305	6.0	0.45	1.61	101.8	454	0.029	19.54	90	9.8	0.0248	0.113	1	571.6	0.02516	0.078	0.0199
144	162	Bayrak and Sheikh 1996, AS-6HT	305	305	6.0	0.46	1.64	101.9	454	0.029	19.54	76	8.3	0.0294	0.134	1	573.3	0.02479	0.080	0.0196
145	163	Bayrak and Sheikh 1996, AS-7HT	305	305	6.0	0.45	1.59	102	454	0.029	19.54	94	10.3	0.0119	0.063	1	577.9	0.02518	0.071	0.0199
146	164	Bayrak and Sheikh 1996, ES-8HT	305	305	6.0	0.47	1.68	102.2	454	0.029	19.54	70	7.6	0.0187	0.085	1	575.9	0.02445	0.071	0.0194
147	165	Saatcioglu and Grira 1999, BG-1	350	350	4.7	0.43	1.26	34	456	0.023	19.5	152	16.6	0.0040	0.067	1	301.7	0.01307	0.053	0.0126
148	166	Saatcioglu and Grira 1999, BG-2	350	350	4.7	0.43	1.26	34	456	0.023	19.5	76	8.3	0.0080	0.135	1	301.7	0.01307	0.060	0.0126
149	167	Saatcioglu and Grira 1999, BG-3	350	350	4.7	0.20	0.59	34	456	0.023	19.5	76	8.3	0.0080	0.135	1	230.5	0.01301	0.086	0.0125
150	168	Saatcioglu and Grira 1999, BG-4	350	350	4.7	0.46	1.36	34	456	0.034	19.5	152	16.6	0.0054	0.090	1	335.9	0.0125	0.052	0.0122
151	169	Saatcioglu and Grira 1999, BG-5	350	350	4.7	0.46	1.36	34	456	0.034	19.5	76	8.3	0.0107	0.180	1	335.9	0.0125	0.062	0.0122
152	170	Saatcioglu and Grira 1999, BG-6	350	350	4.7	0.46	1.39	34	478	0.027	29.9	76	5.6	0.0107	0.180	1	327.4	0.01257	0.062	0.0143
153	171	Saatcioglu and Grira 1999, BG-7	350	350	4.7	0.46	1.35	34	456	0.034	19.5	76	8.3	0.0051	0.088	1	341.4	0.0125	0.052	0.0122
154	172	Saatcioglu and Grira 1999, BG-8	350	350	4.7	0.23	0.67	34	456	0.034	19.5	76	8.3	0.0051	0.088	1	296.7	0.01347	0.075	0.0127
155	173	Saatcioglu and Grira 1999, BG-9	350	350	4.7	0.46	1.30	34	428	0.037	16	76	9.8	0.0051	0.088	1	351.9	0.01251	0.052	0.0115
156	174	Saatcioglu and Grira 1999, BG-10	350	350	4.7	0.46	1.32	34	428	0.038	16	76	9.8	0.0107	0.180	1	346.1	0.01251	0.062	0.0115
157	175	Matamoros et al. 1999,C10-05N	203	203	3.0	0.05	0.24	69.637	586	0.027	15.9	76	11.6	0.0092	0.054	1	41.6	0.03131	0.093	0.0163
158	176	Matamoros et al. 1999,C10-05S	203	203	3.0	0.05	0.24	69.637	586	0.027	15.9	76	11.6	0.0092	0.054	1	41.7	0.03123	0.093	0.0162
159	177	Matamoros et al. 1999,C10-10N	203	203	3.0	0.10	0.45	67.775	572	0.024	15.9	76	11.5	0.0092	0.069	1	53.3	0.02881	0.088	0.0139
160	178	Matamoros et al. 1999,C10-10S	203	203	3.0	0.10	0.45	67.775	573	0.024	15.9	77	11.6	0.0090	0.069	1	53.8	0.02833	0.088	0.0136

Table 12e. Table of column design information.

Test Index	Test Num. from PEER SPD	Test Series	b (mm)	h (mm)	Ls/ H	v	P/P_b	f'_c (MPa)	f_y (MPa)	ρ	d_b (mm)	s (mm)	s_n	ρ_{sh}	$\rho_{sh,eff}$	a_{sl}	M_y (Fardis) (kN-m)	φ_y (Fardis) (rad/m)	$\theta_{u,mono}^{pl}$ (Fardis) (rad)	θ_y (Fardis) (rad)
161	179	Matamoros et al. 1999,C10-20N	203	203	3.0	0.21	0.91	65.5	572	0.024	15.9	76	11.5	0.0092	0.072	1	73.5	0.03148	0.074	0.0142
162	180	Matamoros et al. 1999,C10-20S	203	203	3.0	0.21	0.87	65.5	573	0.023	15.9	77	11.6	0.0090	0.071	1	75.4	0.02957	0.074	0.0133
163	181	Matamoros et al. 1999,C5-00N	203	203	3.0	0.00	0.00	37.921	572	0.024	15.9	76	11.5	0.0092	0.124	1	32.2	0.02531	0.101	0.0147
164	182	Matamoros et al. 1999,C5-00S	203	203	3.0	0.00	0.00	37.921	573	0.025	15.9	77	11.6	0.0090	0.123	1	31.5	0.02627	0.101	0.0154
165	183	Matamoros et al. 1999,C5-20N	203	203	3.0	0.14	0.64	48.263	586	0.027	15.9	76	11.6	0.0092	0.077	1	51.0	0.03451	0.077	0.0181
166	184	Matamoros et al. 1999,C5-20S	203	203	3.0	0.14	0.65	48.263	587	0.027	15.9	77	11.8	0.0090	0.076	1	51.0	0.03484	0.077	0.0183
167	185	Matamoros et al. 1999,C5-40N	203	203	3.0	0.36	1.30	38.059	572	0.024	15.9	76	11.5	0.0092	0.124	1	61.9	0.02625	0.056	0.0145
168	186	Matamoros et al. 1999,C5-40S	203	203	3.0	0.36	1.31	38.059	573	0.024	15.9	77	11.6	0.0090	0.122	1	61.9	0.02625	0.056	0.0145
169	187	Mo and Wang 2000,C1-1	400	400	3.5	0.11	0.32	24.94	497	0.024	19.05	50	5.9	0.0063	0.117	1	287.8	0.01116	0.080	0.0110
170	188	Mo and Wang 2000,C1-2	400	400	3.5	0.16	0.45	26.67	497	0.024	19.05	50	5.9	0.0063	0.109	1	318.3	0.01156	0.075	0.0111
171	189	Mo and Wang 2000,C1-3	400	400	3.5	0.22	0.61	26.13	497	0.024	19.05	50	5.9	0.0063	0.111	1	347.2	0.01203	0.068	0.0113
172	190	Mo and Wang 2000,C2-1	400	400	3.5	0.11	0.32	25.33	497	0.024	19.05	52	6.1	0.0061	0.110	1	288.0	0.01115	0.080	0.0110
173	191	Mo and Wang 2000,C2-2	400	400	3.5	0.16	0.44	27.12	497	0.024	19.05	52	6.1	0.0061	0.103	1	318.5	0.01154	0.074	0.0110
174	192	Mo and Wang 2000,C2-3	400	400	3.5	0.21	0.60	26.77	497	0.024	19.05	52	6.1	0.0061	0.105	1	347.5	0.012	0.068	0.0113
175	193	Mo and Wang 2000,C3-1	400	400	3.5	0.11	0.30	26.38	497	0.024	19.05	54	6.3	0.0059	0.102	1	288.4	0.01111	0.080	0.0109
176	194	Mo and Wang 2000,C3-2	400	400	3.5	0.15	0.44	27.48	497	0.024	19.05	54	6.3	0.0059	0.098	1	318.7	0.01152	0.074	0.0110
177	195	Mo and Wang 2000,C3-3	400	400	3.5	0.21	0.60	26.9	497	0.024	19.05	54	6.3	0.0059	0.100	1	347.6	0.012	0.068	0.0113
178	201	Thomsen and Wallace 1994, A1	152.4	152.4	3.9	0.00	0.00	102.7	517	0.028	9.525	25	6.1	0.0061	0.047	1	16.1	0.02567	0.121	0.0100
179	202	Thomsen and Wallace 1994, A3	152.4	152.4	3.9	0.20	0.76	86.3	517	0.028	9.525	25	6.1	0.0061	0.056	1	36.7	0.03519	0.085	0.0121
180	203	Thomsen and Wallace 1994, B1	152.4	152.4	3.9	0.00	0.00	87.5	455	0.028	9.525	25	5.7	0.0070	0.063	1	14.1	0.02282	0.120	0.0091
181	204	Thomsen and Wallace 1994, B2	152.4	152.4	3.9	0.10	0.36	83.4	455	0.028	9.525	25	5.7	0.0070	0.066	1	24.4	0.02771	0.102	0.0101
182	205	Thomsen and Wallace 1994, B3	152.4	152.4	3.9	0.20	0.72	90	455	0.028	9.525	25	5.7	0.0070	0.061	1	35.5	0.03208	0.087	0.0109
183	206	Thomsen and Wallace 1994, C1	152.4	152.4	3.9	0.00	0.00	67.5	476	0.028	9.525	25	5.8	0.0070	0.130	1	14.6	0.02427	0.129	0.0098
184	207	Thomsen and Wallace 1994, C2	152.4	152.4	3.9	0.10	0.37	74.6	476	0.028	9.525	25	5.8	0.0070	0.118	1	23.9	0.02863	0.109	0.0106
185	208	Thomsen and Wallace 1994, C3	152.4	152.4	3.9	0.20	0.73	81.8	476	0.028	9.525	25	5.8	0.0070	0.108	1	34.2	0.03283	0.093	0.0113
186	209	Thomsen and Wallace 1994, D1	152.4	152.4	3.9	0.20	0.73	75.8	476	0.028	9.525	32	7.3	0.0056	0.093	1	32.8	0.03258	0.089	0.0113
187	210	Thomsen and Wallace 1994, D2	152.4	152.4	3.9	0.20	0.73	87	476	0.028	9.525	38	8.7	0.0046	0.067	1	35.5	0.03304	0.087	0.0113
188	211	Thomsen and Wallace 1994, D3	152.4	152.4	3.9	0.20	0.73	71.2	476	0.028	9.525	44	10.2	0.0040	0.071	1	31.7	0.03238	0.084	0.0114
189	212	Sezen and Moehle No. 1	457.2	457.2	3.2	0.15	0.44	21.063	434	0.031	28.651	305	22.2	0.0017	0.039	1	417.4	0.01028	0.061	0.0119
190	213	Sezen and Moehle No. 2	457.2	457.2	3.2	0.60	1.77	21.126	434	0.031	28.651	305	22.2	0.0017	0.039	1	437.6	0.00641	0.029	0.0100
191	214	Sezen and Moehle No. 4	457.2	457.2	3.2	0.15	0.43	21.781	434	0.031	28.651	305	22.2	0.0017	0.038	1	418.1	0.01024	0.061	0.0118
192	215	Paultre & Legeron, 2000, No. 1006015	305	305	6.6	0.14	0.50	92.4	451	0.027	19.54	60	6.5	0.0187	0.079	1	237.1	0.01483	0.121	0.0144
193	216	Paultre & Legeron, 2000, No. 1006025	305	305	6.6	0.28	0.98	93.3	430	0.027	19.54	60	6.4	0.0187	0.078	1	344.8	0.01714	0.097	0.0158
194	217	Paultre & Legeron, 2000, No. 1006040	305	305	6.6	0.39	1.42	98.2	451	0.027	19.54	60	6.5	0.0187	0.080	1	535.2	0.02701	0.082	0.0225
195	218	Paultre & Legeron, 2000, No. 10013015	305	305	6.6	0.14	0.49	94.8	451	0.027	19.54	130	14.1	0.0086	0.036	1	237.4	0.01478	0.113	0.0144
196	219	Paultre & Legeron, 2000, No. 10013025	305	305	6.6	0.26	0.93	97.7	430	0.027	19.54	130	13.8	0.0086	0.035	1	345.6	0.01701	0.092	0.0157
197	220	Paultre & Legeron, 2000, No. 10013040	305	305	6.6	0.37	1.33	104.3	451	0.027	19.54	130	14.1	0.0086	0.035	1	560.4	0.02894	0.079	0.0237
198	221	Paultre et al., 2001, No. 806040	305	305	6.6	0.40	1.42	78.7	446	0.027	19.54	60	6.5	0.0187	0.104	1	442.1	0.02403	0.081	0.0207
199	222	Paultre et al., 2001, No. 1206040	305	305	6.6	0.41	1.48	109.2	446	0.027	19.54	60	6.5	0.0187	0.075	1	590.4	0.02764	0.080	0.0228
200	223	Paultre et al., 2001, No. 1005540	305	305	6.6	0.41	1.48	109.5	446	0.027	19.54	55	5.9	0.0204	0.154	1	591.7	0.02773	0.094	0.0228

Table 12f. Table of column design information.

Test Index	Test Num. from PEER SPD	Test Series	b (mm)	h (mm)	Ls/ H	v	P/P_b	f'_c (MPa)	f_y (MPa)	ρ	d_b (mm)	s (mm)	s_n	ρ_{sh}	$\rho_{sh,eff}$	a_{sl}	M_y (Fardis) (kN-m)	φ_y (Fardis) (rad/m)	$\theta_{u,mono}^{pl}$ (Fardis) (rad)	θ_y (Fardis) (rad)
201	224	Paultre et al., 2001, No. 1008040	305	305	6.6	0.37	1.33	104.2	446	0.027	19.54	80	8.6	0.0140	0.111	1	560.0	0.02891	0.091	0.0237
202	225	Paultre et al., 2001, No. 1005552	305	305	6.6	0.53	1.90	104.5	446	0.027	19.54	55	5.9	0.0204	0.145	1	584.0	0.02255	0.076	0.0194
203	226	Paultre et al., 2001, No. 1006052	305	305	6.6	0.51	1.81	109.4	446	0.027	19.54	60	6.5	0.0187	0.084	1	605.8	0.0239	0.071	0.0203
204	227	Pujol 2002, No. 10-2-3N	152.4	304.8	2.3	0.09	0.25	33.715	453	0.028	19.05	76	8.5	0.0055	0.066	1	74.4	0.01354	0.069	0.0088
205	228	Pujol 2002, No. 10-2-3S	152.4	304.8	2.3	0.09	0.25	33.715	453	0.028	19.05	76	8.5	0.0055	0.066	1	74.4	0.01354	0.069	0.0088
206	229	Pujol 2002, No. 10-3-1.5N	152.4	304.8	2.3	0.09	0.26	32.13	453	0.028	19.05	38	4.3	0.0109	0.140	1	74.3	0.0136	0.078	0.0089
207	230	Pujol 2002, No. 10-3-1.5S	152.4	304.8	2.3	0.09	0.26	32.13	453	0.028	19.05	38	4.3	0.0109	0.140	1	74.3	0.0136	0.078	0.0089
208	231	Pujol 2002, No. 10-3-3N	152.4	304.8	2.3	0.10	0.27	29.923	453	0.028	19.05	76	8.5	0.0055	0.075	1	74.2	0.01369	0.067	0.0090
209	232	Pujol 2002, No. 10-3-3S	152.4	304.8	2.3	0.10	0.27	29.923	453	0.028	19.05	76	8.5	0.0055	0.075	1	74.2	0.01369	0.067	0.0090
210	233	Pujol 2002, No. 10-3-2.25N	152.4	304.8	2.3	0.10	0.29	27.372	453	0.028	19.05	57	6.4	0.0073	0.109	1	74.0	0.01381	0.069	0.0092
211	234	Pujol 2002, No. 10-3-2.25S	152.4	304.8	2.3	0.10	0.29	27.372	453	0.028	19.05	57	6.4	0.0073	0.109	1	74.0	0.01381	0.069	0.0092
212	237	Pujol 2002, No. 20-3-3N	152.4	304.8	2.3	0.16	0.47	36.404	453	0.028	19.05	76	8.5	0.0055	0.062	1	88.5	0.01452	0.062	0.0089
213	238	Pujol 2002, No. 20-3-3S	152.4	304.8	2.3	0.16	0.47	36.404	453	0.028	19.05	76	8.5	0.0055	0.062	1	88.5	0.01452	0.062	0.0089
214	239	Pujol 2002, No. 10-2-2.25N	152.4	304.8	2.3	0.08	0.24	34.887	453	0.028	19.05	57	6.4	0.0073	0.086	1	74.4	0.0135	0.072	0.0087
215	240	Pujol 2002, No. 10-2-2.25S	152.4	304.8	2.3	0.08	0.24	34.887	453	0.028	19.05	57	6.4	0.0073	0.086	1	74.4	0.0135	0.072	0.0087
216	241	Pujol 2002, No. 10-1-2.25N	152.4	304.8	2.3	0.08	0.24	36.473	453	0.028	19.05	57	6.4	0.0073	0.082	1	74.5	0.01344	0.073	0.0086
217	242	Pujol 2002, No. 10-1-2.25S	152.4	304.8	2.3	0.08	0.24	36.473	453	0.028	19.05	57	6.4	0.0073	0.082	1	74.5	0.01344	0.073	0.0086
218	243	Bechtoula, Kono, Arai and Watanabe, 2002, D1N30	250	250	2.5	0.30	0.89	37.6	461	0.027	12.7	40	6.8	0.0050	0.065	1	116.9	0.01954	0.052	0.0090
219	244	Bechtoula, Kono, Arai and Watanabe, 2002, D1N60	250	250	2.5	0.60	1.79	37.6	461	0.027	12.7	40	6.8	0.0050	0.065	1	130.3	0.01539	0.032	0.0082
220	245	Bechtoula, Kono, Arai and Watanabe, 2002, 1D60	600	600	2.0	0.57	1.60	39.2	388	0.019	25.4	100	7.8	0.0084	0.113	1	1713.0	0.00669	0.034	0.0067
221	246	Bechtoula, Kono, Arai and Watanabe, 2002, 1.1N60	600	600	2.0	0.57	1.60	39.2	388	0.019	25.4	100	7.8	0.0084	0.113	1	1713.0	0.00669	0.034	0.0067
222	247	Bechtoula, Kono, Arai and Watanabe, 2002, 1.1N6B	560	560	2.1	0.59	1.53	32.2	388	0.021	25.4	100	7.8	0.0090	0.147	1	1248.6	0.00634	0.035	0.0067
223	248	Takemura and Kawashima, 1997, Test 1 (JSCE-4)	400	400	3.1	0.03	0.07	35.9	363	0.018	12.7	70	10.5	0.0020	0.021	1	148.7	0.00702	0.079	0.0065
224	249	Takemura and Kawashima, 1997, Test 2 (JSCE-5)	400	400	3.1	0.03	0.07	35.7	363	0.018	12.7	70	10.5	0.0020	0.021	1	148.7	0.00703	0.079	0.0065
225	250	Takemura and Kawashima, 1997, Test 3 (JSCE-6)	400	400	3.1	0.03	0.07	34.3	363	0.018	12.7	70	10.5	0.0020	0.022	1	148.5	0.00705	0.079	0.0065
226	251	Takemura and Kawashima, 1997, Test 4 (JSCE-7)	400	400	3.1	0.03	0.08	33.2	363	0.018	12.7	70	10.5	0.0020	0.022	1	148.3	0.00707	0.078	0.0066
227	252	Takemura and Kawashima, 1997, Test 5 (JSCE-8)	400	400	3.1	0.03	0.07	36.8	363	0.018	12.7	70	10.5	0.0020	0.020	1	148.8	0.00701	0.080	0.0065
228	253	Takemura and Kawashima, 1997, Test 6 (JSCE-9)	400	400	3.1	0.03	0.07	35.9	363	0.018	12.7	70	10.5	0.0020	0.021	1	148.7	0.00702	0.079	0.0065
229	254	Xiao & Yun 2002, No. FHC1-0.2	510	510	3.5	0.20	0.75	64.1	473	0.033	35.8	100	6.1	0.0117	0.081	1	1195.3	0.00993	0.080	0.0113
230	255	Xiao & Yun 2002, No. FHC2-0.34	510	510	3.5	0.33	1.24	62.1	473	0.033	35.8	100	6.1	0.0117	0.084	1	1737.1	0.01383	0.065	0.0137
231	256	Xiao & Yun 2002, No. FHC3-0.22	510	510	3.5	0.22	0.84	62.1	473	0.033	35.8	125	7.6	0.0093	0.079	1	1241.5	0.01015	0.076	0.0115
232	257	Xiao & Yun 2002, No. FHC4-0.33	510	510	3.5	0.32	1.21	62.1	473	0.033	35.8	125	7.6	0.0093	0.079	1	1736.2	0.01399	0.065	0.0138
233	258	Xiao & Yun 2002, No. FHC5-0.2	510	510	3.5	0.20	0.75	64.1	473	0.033	35.8	150	9.1	0.0078	0.054	1	1195.3	0.00993	0.076	0.0113
234	259	Xiao & Yun 2002, No. FHC6-0.2	510	510	3.5	0.20	0.75	64.1	473	0.033	35.8	150	9.1	0.0078	0.064	1	1195.3	0.00993	0.078	0.0113
235	260	Bayrak & Sheikh, 2002, No. RS-9HT	250	350	5.3	0.34	1.21	71.2	454	0.031	19.54	80	8.7	0.0171	0.130	1	459.1	0.02149	0.084	0.0177
236	261	Bayrak & Sheikh, 2002, No. RS-10HT	250	350	5.3	0.50	1.77	71.1	454	0.031	19.54	80	8.7	0.0171	0.130	1	464.4	0.01708	0.065	0.0150
237	262	Bayrak & Sheikh, 2002, No. RS-11HT	250	350	5.3	0.51	1.82	70.8	454	0.031	19.54	80	8.7	0.0249	0.177	1	458.7	0.01681	0.070	0.0148
238	263	Bayrak & Sheikh, 2002, No. RS-12HT	250	350	5.3	0.34	1.21	70.9	454	0.031	19.54	150	16.4	0.0091	0.070	1	457.5	0.02144	0.075	0.0176
239	264	Bayrak & Sheikh, 2002, No. RS-13HT	250	350	5.3	0.35	1.24	112.1	454	0.031	19.54	70	7.6	0.0195	0.081	1	671.9	0.02692	0.083	0.0206
240	265	Bayrak & Sheikh, 2002, No. RS-14HT	250	350	5.3	0.46	1.63	112.1	454	0.031	19.54	70	7.6	0.0195	0.081	1	687.0	0.02266	0.070	0.0180

Table 12g. Table of column design information.

Test Index	Test Num. from PEER SPD	Test Series	b (mm)	h (mm)	Ls/ H	v	P/P_b	f'_c (MPa)	f_y (MPa)	ρ	d_b (mm)	s (mm)	s_n	ρ_{sh}	$\rho_{sh,eff}$	a_{sl}	M_y (Fardis) (kN-m)	φ_y (Fardis) (rad/m)	$\theta_{u,mono}^{pl}$ (Fardis) (rad)	θ_y (Fardis) (rad)
241	266	Bayrak & Sheikh, 2002, No. RS-15HT	250	350	5.3	0.36	1.28	56.2	454	0.031	19.54	100	10.9	0.0136	0.113	1	378.3	0.01843	0.075	0.0160
242	267	Bayrak & Sheikh, 2002, No. RS-16HT	250	350	5.3	0.37	1.31	56.2	454	0.031	19.54	150	16.4	0.0091	0.075	1	378.3	0.01818	0.068	0.0158
243	268	Bayrak & Sheikh, 2002, No. RS-17HT	250	350	5.3	0.34	1.27	74.1	521	0.031	19.54	75	8.8	0.0091	0.168	1	482.6	0.02195	0.091	0.0184
244	269	Bayrak & Sheikh, 2002, No. RS-18HT	250	350	5.3	0.50	1.87	74.1	521	0.031	19.54	75	8.8	0.0091	0.168	1	487.8	0.01743	0.071	0.0156
245	270	Bayrak & Sheikh, 2002, No. RS-19HT	250	350	5.3	0.53	2.00	74.2	521	0.031	19.54	75	8.8	0.0176	0.333	1	483.3	0.01673	0.093	0.0152
246	271	Bayrak & Sheikh, 2002, No. RS-20HT	250	350	5.3	0.34	1.28	74.2	521	0.031	19.54	140	16.4	0.0094	0.178	1	475.5	0.02196	0.093	0.0185
247	272	Bayrak & Sheikh, 2002, No. WRS-21HT	350	250	7.4	0.47	1.87	91.3	521	0.033	19.54	70	8.2	0.0139	0.071	1	386.2	0.02822	0.073	0.0233
248	273	Bayrak & Sheikh, 2002, No. WRS-22HT	350	250	7.4	0.31	1.23	91.3	521	0.033	19.54	70	8.2	0.0139	0.071	1	370.2	0.03597	0.095	0.0280
249	274	Bayrak & Sheikh, 2002, No. WRS-23HT	350	250	7.4	0.33	1.31	72.2	521	0.033	19.54	80	9.3	0.0122	0.092	1	304.6	0.03076	0.090	0.0252
250	275	Bayrak & Sheikh, 2002, No. WRS-24HT	350	250	7.4	0.50	1.99	72.2	521	0.033	19.54	80	9.3	0.0122	0.092	1	315.1	0.02409	0.069	0.0211
251	285	Saatcioglu and Ozcebe 1989, U2	350	350	2.9	0.16	0.46	30.2	453	0.037	25	150	12.8	0.0030	0.047	1	280.6	0.01275	0.063	0.0105
252	286	Esaki, 1996 H-2-1/5	200	200	2.0	0.20	0.50	23	363	0.029	12.7	50	7.5	0.0052	0.082	1	37.4	0.01837	0.052	0.0075
253	287	Esaki, 1996 HT-2-1/5	200	200	2.0	0.20	0.50	20.2	363	0.029	12.7	75	11.3	0.0052	0.094	1	35.8	0.01828	0.051	0.0076
254	288	Esaki, 1996 H-2-1/3	200	200	2.0	0.33	0.84	23	363	0.029	12.7	40	6.0	0.0065	0.103	1	45.0	0.02022	0.044	0.0077
255	289	Esaki, 1996 HT-2-1/3	200	200	2.0	0.33	0.83	20.2	363	0.029	12.7	60	9.0	0.0065	0.117	1	42.5	0.01998	0.043	0.0078

Table 13a. Table of calibrated model parameters for each column.

Test Index	Test Num. from PEER SPD	Test Series	θ_y (rad)	Ely / EI_g	EI_{stf40} / EI_g	M_y (kN-m)	M_c / M_y	α_s	$\theta_{cap,pl}$ (rad)	isLB	θ_{pc} (rad)	α_c	λ
1	1	Gill et al. 1979, No. 1	0.0076	0.25	0.47	849.6	1.04	0.010	0.028	1	nd	nd	136
2	2	Gill et al. 1979, No. 2	0.0063	0.26	0.56	969.6	1.06	0.020	0.018	1	nd	nd	118
3	3	Gill et al. 1979, No. 3	0.0043	0.42	0.76	771.6	1.20	0.050	0.017	1	nd	nd	83
4	4	Gill et al. 1979, No. 4	0.0035	0.52	0.73	804.0	1.38	0.070	0.019	1	nd	nd	87
5	5	Ang et al. 1981, No. 3	0.0097	0.37	0.91	329.6	1.07	0.020	0.034	1	nd	nd	63
6	6	Ang et al. 1981, No. 4	0.0096	0.31	0.83	279.2	1.15	0.040	0.036	1	nd	nd	64
7	7	Soesianawati et al. 1986, No. 1	0.0089	0.28	0.67	320.0	1.25	0.034	0.065	1	nd	nd	118
8	8	Soesianawati et al. 1986, No. 2	0.0084	0.45	1.10	468.0	1.05	0.010	0.040	0	0.15	-0.060	74
9	9	Soesianawati et al. 1986, No. 3	0.0083	0.45	1.30	472.0	1.03	0.010	0.027	0	0.02	-0.375	37
10	10	Soesianawati et al. 1986, No. 4	0.0091	0.42	1.12	435.2	1.03	0.010	0.024	0	0.02	-0.480	38
11	11	Zahn et al. 1986, No. 7	0.0103	0.34	0.75	332.8	1.49	0.065	0.078	1	nd	nd	74
12	12	Zahn et al. 1986, No. 8	0.0086	0.45	0.77	456.0	1.50	0.075	0.058	1	nd	nd	127
13	13	Watson and Park 1989, No. 5	0.0072	0.58	0.92	502.4	1.15	0.060	0.018	0	0.05	-0.180	55
14	14	Watson and Park 1989, No. 6	0.0069	0.61	1.50	504.0	1.12	0.070	0.012	0	0.01	-0.800	32
15	15	Watson and Park 1989, No. 7	0.0041	1.03	1.27	472.0	1.00	0.001	0.008	0	0.01	-0.280	36
16	16	Watson and Park 1989, No. 8	0.0049	0.88	1.33	460.8	1.06	0.045	0.006	0	0.00	-1.100	25
17	17	Watson and Park 1989, No. 9	0.0075	0.64	1.27	548.0	1.14	0.040	0.026	1	nd	nd	72
18	18	Tanaka and Park 1990, No. 1	0.0099	0.30	0.65	281.6	1.19	0.023	0.083	1	nd	nd	114
19	19	Tanaka and Park 1990, No. 2	0.0091	0.33	0.77	280.0	1.15	0.020	0.069	1	nd	nd	89
20	20	Tanaka and Park 1990, No. 3	dr	dr	dr	291.2	1.14	0.020	0.065	1	nd	nd	41
21	21	Tanaka and Park 1990, No. 4	0.0094	0.32	1.14	286.4	1.08	0.010	0.073	1	nd	nd	159
22	22	Tanaka and Park 1990, No. 5	0.0100	0.18	0.35	655.1	1.11	0.030	0.038	1	nd	nd	132
23	23	Tanaka and Park 1990, No. 6	0.0099	0.19	0.40	680.6	1.21	0.030	0.070	1	nd	nd	145
24	24	Tanaka and Park 1990, No. 7	0.0097	0.28	0.79	1039.5	1.21	0.040	0.050	1	nd	nd	105
25	25	Tanaka and Park 1990, No. 8	0.0109	0.27	0.73	1075.8	1.04	0.010	0.046	1	nd	nd	127
26	26	Park and Paulay 1990, No. 9	0.0084	0.27	0.61	691.3	1.23	0.035	0.055	1	nd	nd	200
27	27	Arakawa et al. 1982, No. 102	0.0093	0.11	0.22	58.5	1.12	0.040	0.028	1	nd	nd	182
28	29	Nagasaka 1982, HPRC19-32	0.0067	0.17	0.39	33.6	1.40	0.030	0.088	1	nd	nd	55
29	30	Ohno and Nishioka 1984, L1	dr	dr	dr	331.5	1.35	0.040	0.034	1	nd	nd	173
30	31	Ohno and Nishioka 1984, L2	dr	dr	dr	340.5	1.56	0.080	0.028	1	nd	nd	309
31	32	Ohno and Nishioka 1984, L3	dr	dr	dr	330.0	1.74	0.120	0.025	1	nd	nd	164
32	33	Ohue et al. 1985, 2D16RS	0.0124	0.12	0.21	38.4	1.10	0.020	0.060	1	nd	nd	20
33	34	Ohue et al. 1985, 4D13RS	0.0115	0.15	0.25	42.0	1.29	0.060	0.055	1	nd	nd	13
34	35	Zhou et al. 1985, No. 806	0.0271	0.03	0.05	2.5	1.00	0.010	0.011	0	0.18	-0.150	59
35	37	Zhou et al. 1985, No. 1309	0.0269	0.03	0.04	2.7	1.01	0.050	0.008	0	0.18	-0.150	4
36	42	Zhou et al. 1987, No. 204-08	0.0042	0.46	1.12	21.5	1.11	0.020	0.023	1	nd	nd	13
37	43	Zhou et al. 1987, No. 214-08	0.0075	0.24	0.53	21.8	1.06	0.010	0.045	0	0.03	-0.250	27
38	44	Zhou et al. 1987, No. 223-09	0.0103	0.18	0.54	20.5	1.03	0.020	0.018	0	0.13	-0.080	33
39	45	Zhou et al. 1987, No. 302-07	0.0052	0.54	0.57	25.7	1.06	0.030	0.010	0	0.01	-0.600	31
40	46	Zhou et al. 1987, No. 312-07	0.0063	0.49	0.65	25.2	1.04	0.020	0.012	0	0.01	-0.600	16

Table 13b. Table of calibrated model parameters for each column.

Test Index	Test Num. from PEER SPD	Test Series	θ_y (rad)	Ely / EI_g	EI_{stf40} / EI_g	M_y (kN-m)	M_c / M_y	α_s	$\theta_{cap,pl}$ (rad)	isLB	θ_{pc} (rad)	α_c	λ
41	47	Zhou et al. 1987, No. 322-07	0.0067	0.42	0.51	24.0	1.08	0.020	0.028	1	nd	nd	30
42	48	Kanda et al. 1988, 85STC-1	0.0092	0.20	0.35	61.1	1.15	0.015	0.090	1	nd	nd	118
43	49	Kanda et al. 1988, 85STC-2	0.0093	0.20	0.58	61.1	1.09	0.010	0.088	1	nd	nd	118
44	50	Kanda et al. 1988, 85STC-3	0.0087	0.21	0.39	60.8	1.20	0.020	0.087	1	nd	nd	132
45	51	Kanda et al. 1988, 85PDC-1	0.0097	0.22	0.51	61.5	1.02	0.010	0.015	1	nd	nd	45
46	52	Kanda et al. 1988, 85PDC-2	0.0080	0.22	0.57	59.3	1.06	0.030	0.017	1	nd	nd	73
47	53	Kanda et al. 1988, 85PDC-3	0.0076	0.23	0.47	57.4	1.08	0.025	0.023	1	nd	nd	109
48	56	Muguruma et al. 1989, AL-1	0.0088	0.42	0.80	130.5	1.16	0.025	0.055	1	nd	nd	136
49	57	Muguruma et al. 1989, AH-1	0.0096	0.37	0.70	125.0	1.66	0.065	0.098	1	nd	nd	209
50	58	Muguruma et al. 1989, AL-2	0.0074	0.52	0.78	133.8	1.07	0.030	0.018	0	0.05	-0.170	25
51	59	Muguruma et al. 1989, AH-2	0.0120	0.34	0.87	138.3	1.45	0.075	0.072	1	nd	nd	109
52	60	Muguruma et al. 1989, BL-1	0.0090	0.35	0.56	132.0	1.21	0.025	0.075	1	nd	nd	191
53	61	Muguruma et al. 1989, BH-1	0.0090	0.35	0.73	132.3	1.32	0.035	0.083	1	nd	nd	300
54	62	Muguruma et al. 1989, BL-2	0.0080	0.49	0.74	160.0	1.08	0.010	0.065	0	0.03	-0.250	50
55	63	Muguruma et al. 1989, BH-2	0.0080	0.47	0.76	154.8	1.41	0.045	0.072	1	nd	nd	177
56	64	Ono et al. 1989, CA025C	0.0073	0.16	0.33	38.3	1.29	0.060	0.035	1	nd	nd	27
57	65	Ono et al. 1989, CA060C	0.0042	0.31	0.42	41.3	1.06	0.020	0.012	0	0.09	-0.050	36
58	66	Sakai et al. 1990, B1	0.0060	0.35	0.46	200.0	1.06	0.020	0.017	0	0.04	-0.150	24
59	67	Sakai et al. 1990, B2	0.0060	0.37	0.62	205.0	1.01	0.001	0.032	0	0.12	-0.050	86
60	68	Sakai et al. 1990, B3	0.0080	0.28	0.39	215.5	1.06	0.015	0.030	0	0.04	-0.200	8
61	69	Sakai et al. 1990, B4	0.0060	0.35	0.58	197.0	1.05	0.010	0.030	0	0.13	-0.050	55
62	70	Sakai et al. 1990, B5	0.0064	0.34	0.43	195.3	1.04	0.030	0.010	0	0.02	-0.350	18
63	71	Sakai et al. 1990, B6	0.0074	0.30	0.46	208.5	1.05	0.030	0.012	0	0.02	-0.330	9
64	72	Sakai et al. 1990, B7	0.0040	0.49	0.80	192.5	1.00	0.001	0.019	0	0.03	-0.160	15
65	73	Amitsu et al. 1991, CB060C	0.0050	0.22	0.39	167.2	1.10	0.060	0.008	0	0.02	-0.300	15
66	74	Wight and Sozen 1973, No. 40.033a(East)	0.0114	0.25	0.65	104.9	1.28	0.140	0.023	1	nd	nd	20
67	75	Wight and Sozen 1973, No. 40.033a(West)	0.0126	0.22	0.44	99.4	1.25	0.200	0.016	0	0.20	-0.080	27
68	76	Wight and Sozen 1973, No. 40.048(East)	0.0137	0.24	0.51	89.8	1.56	0.240	0.032	1	nd	nd	45
69	77	Wight and Sozen 1973, No. 40.048(West)	0.0160	0.21	0.25	100.7	1.52	0.180	0.046	1	nd	nd	36
70	78	Wight and Sozen 1973, No. 40.033(East)	0.0185	0.16	0.25	96.4	1.27	0.250	0.020	0	1.17	-0.020	27
71	79	Wight and Sozen 1973, No. 40.033(West)	0.0183	0.18	0.28	104.9	1.36	0.190	0.035	1	nd	nd	36
72	81	Wight and Sozen 1973, No. 25.033(West)	0.0194	0.14	0.28	88.5	1.31	0.200	0.030	1	nd	nd	22
73	82	Wight and Sozen 1973, No. 40.067(East)	0.0188	0.15	0.23	100.4	1.53	0.250	0.040	1	nd	nd	70
74	83	Wight and Sozen 1973, No. 40.067(West)	0.0200	0.15	0.35	101.2	1.51	0.230	0.044	1	nd	nd	68
75	84	Wight and Sozen 1973, No. 40.147(East)	0.0171	0.19	0.27	112.1	1.49	0.220	0.038	1	nd	nd	95
76	85	Wight and Sozen 1973, No. 40.147(West)	0.0154	0.20	0.28	106.0	1.55	0.200	0.042	1	nd	nd	182
77	86	Wight and Sozen 1973, No. 40.092(East)	0.0148	0.21	0.34	108.6	1.50	0.190	0.039	0	0.15	-0.150	100
78	87	Wight and Sozen 1973, No. 40.092(West)	0.0177	0.19	0.28	113.4	1.46	0.210	0.039	1	nd	nd	77
79	88	Atalay and Penzien 1975, No. 1S1	0.0097	0.34	0.55	104.3	1.07	0.045	0.016	1	nd	nd	123
80	89	Atalay and Penzien 1975, No. 2S1	0.0104	0.30	0.44	100.6	1.13	0.060	0.023	1	nd	nd	123

Table 13c. Table of calibrated model parameters for each column.

Test Index	Test Num. from PEER SPD	Test Series	θ_y (rad)	Ely / EI_g	EI_{stf40} / EI_g	M_y (kN-m)	M_c / M_y	α_s	$\theta_{cap,pl}$ (rad)	isLB	θ_{pc} (rad)	α_c	λ
81	90	Atalay and Penzien 1975, No. 3S1	0.0101	0.30	0.54	101.4	1.13	0.060	0.022	1	nd	nd	127
82	91	Atalay and Penzien 1975, No. 4S1	0.0098	0.28	0.49	107.3	1.04	0.030	0.014	1	nd	nd	77
83	92	Atalay and Penzien 1975, No. 5S1	0.0140	0.30	0.64	141.2	1.02	0.015	0.019	1	nd	nd	82
84	93	Atalay and Penzien 1975, No. 6S1	0.0131	0.31	0.48	131.6	1.08	0.048	0.021	1	nd	nd	89
85	94	Atalay and Penzien 1975, No. 9	0.0116	0.36	0.61	150.0	1.13	0.060	0.026	1	nd	nd	44
86	95	Atalay and Penzien 1975, No. 10	0.0119	0.36	0.63	150.0	1.07	0.035	0.025	1	nd	nd	32
87	96	Atalay and Penzien 1975, No. 11	0.0098	0.43	0.67	148.3	1.03	0.010	0.028	1	nd	nd	45
88	97	Atalay and Penzien 1975, No. 12	0.0137	0.32	0.48	150.8	1.08	0.035	0.030	1	nd	nd	24
89	102	Azizinamini et al. 1988, NC-2	0.0107	0.31	0.43	747.7	1.71	0.200	0.038	1	nd	nd	182
90	103	Azizinamini et al. 1988, NC-4	0.0091	0.41	0.56	878.1	1.40	0.200	0.018	1	nd	nd	68
91	104	Saatcioglu and Ozcebe 1989, U1	0.0200	0.11	0.20	254.5	1.34	0.055	0.125	1	nd	nd	24
92	105	Saatcioglu and Ozcebe 1989, U3	0.0200	0.13	0.28	283.0	1.04	0.010	0.080	0	0.24	-0.085	18
93	106	Saatcioglu and Ozcebe 1989, U4	0.0160	0.20	0.35	315.0	1.47	0.060	0.125	1	nd	nd	91
94	107	Saatcioglu and Ozcebe 1989, U6	0.0205	0.15	0.37	332.5	1.23	0.065	0.072	1	nd	nd	118
95	108	Saatcioglu and Ozcebe 1989, U7	0.0205	0.15	0.35	337.5	1.24	0.070	0.070	1	nd	nd	100
96	109	Galeota et al. 1996, AA1	0.0110	0.42	0.61	179.0	1.00	0.001	0.003	0	0.06	-0.170	4
97	110	Galeota et al. 1996, AA2	0.0110	0.40	0.61	167.6	1.00	0.001	0.003	0	0.05	-0.220	5
98	111	Galeota et al. 1996, AA3	0.0110	0.33	0.55	133.4	1.08	0.020	0.045	1	nd	nd	9
99	112	Galeota et al. 1996, AA4	0.0114	0.43	0.86	180.7	1.01	0.010	0.007	0	0.14	-0.080	13
100	113	Galeota et al. 1996, BA1	0.0110	0.47	0.79	184.1	1.01	0.015	0.004	0	0.12	-0.090	20
101	114	Galeota et al. 1996, BA2	0.0101	0.45	0.61	167.0	1.01	0.010	0.008	0	0.13	-0.080	21
102	115	Galeota et al. 1996, BA3	0.0110	0.40	0.59	166.4	1.03	0.050	0.007	0	0.07	-0.170	18
103	116	Galeota et al. 1996, BA4	0.0118	0.33	0.53	140.2	1.00	0.001	0.006	0	0.26	-0.045	23
104	117	Galeota et al. 1996, CA1	0.0127	0.28	0.55	131.1	1.05	0.010	0.065	1	nd	nd	37
105	118	Galeota et al. 1996, CA2	0.0118	0.40	0.64	168.7	1.09	0.020	0.054	1	nd	nd	41
106	119	Galeota et al. 1996, CA3	0.0110	0.41	0.76	163.0	1.01	0.001	0.093	1	nd	nd	32
107	120	Galeota et al. 1996, CA4	0.0127	0.38	0.64	172.1	1.06	0.010	0.072	1	nd	nd	31
108	121	Galeota et al. 1996, AB1	0.0162	0.38	0.57	212.0	1.00	0.000	0.015	0	0.20	-0.080	91
109	122	Galeota et al. 1996	0.0136	0.45	0.67	221.2	1.02	0.020	0.014	0	0.14	-0.096	30
110	123	Galeota et al. 1996, AB3	0.0154	0.41	0.64	230.3	1.00	0.001	0.015	0	0.15	-0.100	16
111	124	Galeota et al. 1996, AB4	0.0162	0.43	0.76	250.8	1.00	0.001	0.015	0	0.04	-0.450	22
112	125	Galeota et al. 1996, BB	0.0162	0.35	0.54	206.3	1.05	0.015	0.050	0	0.15	-0.110	40
113	126	Galeota et al. 1996, BB1	0.0136	0.49	0.85	239.4	1.03	0.020	0.018	1	nd	nd	40
114	127	Galeota et al. 1996, BB4	0.0149	0.42	0.68	228.0	1.24	0.065	0.056	0	0.09	-0.200	59
115	128	Galeota et al. 1996, BB4B	0.0154	0.41	0.64	234.3	1.07	0.020	0.053	1	nd	nd	67
116	129	Galeota et al. 1996, CB1	0.0180	0.34	0.52	218.3	1.19	0.050	0.068	1	nd	nd	59
117	130	Galeota et al. 1996, CB2	0.0162	0.36	0.61	210.9	1.20	0.045	0.073	1	nd	nd	64
118	131	Galeota et al. 1996, CB3	0.0202	0.32	0.61	230.9	1.20	0.060	0.068	1	nd	nd	66
119	132	Galeota et al. 1996, CB4	0.0254	0.26	0.63	245.7	1.11	0.050	0.058	1	nd	nd	36
120	133	Wehbe et al. 1998, A1	0.0152	0.22	0.39	751.9	1.34	0.070	0.073	1	nd	nd	48

Table 13d. Table of calibrated model parameters for each column.

Test Index	Test Num. from PEER SPD	Test Series	θ_y (rad)	Ely / EI_g	EI_{stf40} / EI_g	M_y (kN-m)	M_c / M_y	α_s	$\theta_{cap,pl}$ (rad)	isLB	θ_{pc} (rad)	α_c	λ
121	134	Wehbe et al. 1998, A2	0.0128	0.30	0.51	879.1	1.29	0.060	0.063	1	nd	nd	37
122	135	Wehbe et al. 1998, B1	0.0152	0.21	0.30	749.5	1.62	0.100	0.094	1	nd	nd	52
123	136	Wehbe et al. 1998, B2	0.0158	0.25	0.36	913.0	1.32	0.079	0.064	1	nd	nd	53
124	137	Lynn et al. 1998, 2CLH18	0.0078	0.22	0.44	337.4	1.19	0.075	0.020	0	0.02	-0.500	105
125	138	Lynn et al. 1998, 2CMH18	0.0058	0.41	0.69	428.7	1.14	0.160	0.005	1	nd	nd	18
126	143	Lynn et al. 1996, 2SLH18	0.0068	0.23	0.45	320.4	1.47	0.100	0.032	0	0.05	-0.220	78
127	144	Lynn et al. 1996, 3SMD12	0.0090	0.34	0.46	553.9	1.24	0.080	0.028	0	0.01	-0.970	9
128	145	Xiao and Martirossyan 1998, HC4-8L19-T10-0.1P	0.0154	0.13	0.28	162.6	1.23	0.040	0.090	0	0.38	-0.050	109
129	146	Xiao and Martirossyan 1998, HC4-8L19-T10-0.2P	0.0138	0.17	0.29	198.1	1.17	0.030	0.080	0	0.32	-0.050	136
130	147	Xiao and Martirossyan 1998, HC4-8L16-T10-0.1P	0.0159	0.10	0.23	137.2	1.13	0.030	0.068	1	nd	nd	89
131	148	Xiao and Martirossyan 1998, HC4-8L16-T10-0.2P	0.0156	0.12	0.23	170.2	1.24	0.040	0.095	1	nd	nd	73
132	149	Xiao and Martirossyan 1998, HC4-8L16-T6-0.1P	0.0157	0.10	0.17	140.7	1.17	0.050	0.053	0	0.06	-0.300	55
133	150	Xiao and Martirossyan 1998, HC4-8L16-T6-0.2P	0.0128	0.15	0.34	171.7	1.05	0.020	0.032	0	0.01	-1.800	83
134	151	Sugano 1996, UC10H	0.0039	0.55	0.68	152.8	1.05	0.030	0.007	1	nd	nd	16
135	152	Sugano 1996, UC15H	0.0056	0.43	0.66	175.5	1.16	0.035	0.025	0	0.03	-0.250	35
136	153	Sugano 1996, UC20H	0.0100	0.26	0.64	198.0	1.08	0.025	0.031	0	0.13	-0.080	54
137	154	Sugano 1996, UC15L	0.0062	0.38	0.57	174.6	1.13	0.009	0.090	1	nd	nd	116
138	155	Sugano 1996, UC20L	0.0062	0.39	0.59	175.5	1.19	0.015	0.082	1	nd	nd	141
139	157	Bayrak and Sheikh 1996, ES-1HT	dr	dr	dr	334.3	1.14	0.070	0.015	1	nd	nd	24
140	158	Bayrak and Sheikh 1996, AS-2HT	dr	dr	dr	322.4	1.37	0.060	0.035	0	0.78	-0.010	132
141	159	Bayrak and Sheikh 1996, AS-3HT	dr	dr	dr	350.0	1.19	0.060	0.022	1	nd	nd	42
142	160	Bayrak and Sheikh 1996, AS-4HT	dr	dr	dr	388.7	1.49	0.090	0.060	1	nd	nd	50
143	161	Bayrak and Sheikh 1996, AS-5HT	dr	dr	dr	386.8	1.05	0.010	0.013	0	0.02	-0.130	65
144	162	Bayrak and Sheikh 1996, AS-6HT	dr	dr	dr	444.8	1.30	0.095	0.025	0	0.15	-0.070	145
145	163	Bayrak and Sheikh 1996, AS-7HT	dr	dr	dr	358.3	1.17	0.070	0.011	0	0.10	-0.054	58
146	164	Bayrak and Sheikh 1996, ES-8HT	dr	dr	dr	368.4	1.23	0.080	0.011	1	nd	nd	49
147	165	Saatcioglu and Grira 1999, BG-1	0.0094	0.54	1.22	324.9	1.02	0.005	0.030	1	nd	nd	24
148	166	Saatcioglu and Grira 1999, BG-2	0.0094	0.51	1.16	308.4	1.15	0.020	0.070	1	nd	nd	68
149	167	Saatcioglu and Grira 1999, BG-3	0.0137	0.31	1.12	259.1	1.10	0.017	0.078	1	nd	nd	127
150	168	Saatcioglu and Grira 1999, BG-4	0.0082	0.65	0.48	341.3	1.01	0.001	0.075	1	nd	nd	80
151	169	Saatcioglu and Grira 1999, BG-5	0.0140	0.37	1.90	357.8	1.18	0.032	0.080	0	0.21	-0.080	84
152	170	Saatcioglu and Grira 1999, BG-6	0.0131	0.43	1.88	346.3	1.21	0.045	0.060	0	0.23	-0.070	81
153	171	Saatcioglu and Grira 1999, BG-7	0.0131	0.41	1.37	345.5	1.16	0.030	0.068	0	0.20	-0.075	82
154	172	Saatcioglu and Grira 1999, BG-8	0.0173	0.30	0.83	327.4	1.12	0.025	0.080	1	nd	nd	83
155	173	Saatcioglu and Grira 1999, BG-9	0.0149	0.38	0.77	351.2	1.10	0.020	0.075	1	nd	nd	100
156	174	Saatcioglu and Grira 1999, BG-10	0.0125	0.43	0.98	361.9	1.22	0.035	0.078	1	nd	nd	127
157	175	Matamoros et al. 1999,C10-05N	0.0189	0.08	0.16	43.5	1.08	0.015	0.105	1	nd	nd	55
158	176	Matamoros et al. 1999,C10-05S	0.0172	0.09	0.17	42.4	1.11	0.025	0.075	1	nd	nd	64
159	177	Matamoros et al. 1999,C10-10N	0.0172	0.13	0.24	61.0	1.10	0.025	0.066	1	nd	nd	81
160	178	Matamoros et al. 1999,C10-10S	0.0164	0.14	0.24	60.7	1.11	0.025	0.070	1	nd	nd	87

Table 13e. Table of calibrated model parameters for each column.

Test Index	Test Num. from PEER SPD	Test Series	θ_y (rad)	Ely / EI_g	EI_{stf40} / EI_g	M_y (kN-m)	M_c / M_y	α_s	$\theta_{cap,pl}$ (rad)	isLB	θ_{pc} (rad)	α_c	λ
161	179	Matamoros et al. 1999,C10-20N	0.0189	0.15	0.29	72.6	1.07	0.025	0.053	1	nd	nd	57
162	180	Matamoros et al. 1999,C10-20S	0.0205	0.13	0.29	72.6	1.06	0.025	0.052	1	nd	nd	45
163	181	Matamoros et al. 1999,C5-00N	0.0172	0.10	0.13	33.9	1.36	0.065	0.095	1	nd	nd	60
164	182	Matamoros et al. 1999,C5-00S	0.0180	0.09	0.13	33.6	1.34	0.065	0.095	1	nd	nd	55
165	183	Matamoros et al. 1999,C5-20N	0.0180	0.11	0.23	47.3	1.08	0.025	0.060	0	0.65	-0.030	44
166	184	Matamoros et al. 1999,C5-20S	0.0159	0.13	0.26	46.7	1.08	0.015	0.082	0	0.57	-0.030	52
167	185	Matamoros et al. 1999,C5-40N	0.0161	0.18	0.33	58.3	1.05	0.025	0.033	1	nd	nd	32
168	186	Matamoros et al. 1999,C5-40S	0.0156	0.18	0.33	55.2	1.13	0.065	0.031	1	nd	nd	32
169	187	Mo and Wang 2000,C1-1	0.0182	0.17	0.37	340.9	1.34	0.070	0.088	1	nd	nd	67
170	188	Mo and Wang 2000,C1-2	0.0168	0.19	0.42	364.0	1.40	0.070	0.095	1	nd	nd	79
171	189	Mo and Wang 2000,C1-3	0.0146	0.25	0.42	406.0	1.23	0.040	0.083	1	nd	nd	135
172	190	Mo and Wang 2000,C2-1	0.0204	0.15	0.36	322.0	1.24	0.070	0.070	0	0.36	-0.070	78
173	191	Mo and Wang 2000,C2-2	0.0125	0.24	0.41	365.4	1.53	0.060	0.110	0	0.14	-0.140	160
174	192	Mo and Wang 2000,C2-3	0.0161	0.21	0.43	388.5	1.24	0.070	0.055	0	0.28	-0.070	115
175	193	Mo and Wang 2000,C3-1	0.0161	0.17	0.33	322.0	1.32	0.060	0.085	1	nd	nd	117
176	194	Mo and Wang 2000,C3-2	0.0193	0.16	0.28	364.0	1.25	0.060	0.080	0	0.48	-0.050	91
177	195	Mo and Wang 2000,C3-3	0.0168	0.21	0.37	394.8	1.21	0.060	0.060	0	0.25	-0.080	141
178	201	Thomsen and Wallace 1994, A1	0.0142	0.15	0.20	24.8	1.19	0.070	0.038	1	nd	nd	141
179	202	Thomsen and Wallace 1994, A3	0.0101	0.42	dr	37.6	1.01	0.001	0.055	0	0.07	-0.150	55
180	203	Thomsen and Wallace 1994, B1	dr	dr	dr	18.5	1.18	0.085	0.023	0	0.06	-0.220	345
181	204	Thomsen and Wallace 1994, B2	0.0101	0.29	0.53	30.4	1.07	0.070	0.010	0	0.22	-0.050	78
182	205	Thomsen and Wallace 1994, B3	dr	dr	dr	37.0	1.00	0.001	0.025	0	0.12	-0.065	87
183	206	Thomsen and Wallace 1994, C1	dr	dr	0.19	18.4	1.41	0.100	0.048	1	nd	nd	133
184	207	Thomsen and Wallace 1994, C2	0.0092	0.32	0.83	28.4	1.20	0.040	0.046	0	0.55	-0.020	82
185	208	Thomsen and Wallace 1994, C3	0.0092	0.37	dr	33.1	1.01	0.001	0.060	0	0.13	-0.073	42
186	209	Thomsen and Wallace 1994, D1	dr	dr	dr	33.1	1.00	0.001	0.020	0	0.13	-0.067	89
187	210	Thomsen and Wallace 1994, D2	0.0092	0.38	1.15	35.8	1.00	0.001	0.010	0	0.13	-0.073	61
188	211	Thomsen and Wallace 1994, D3	dr	dr	dr	30.4	1.00	0.001	0.020	0	0.14	-0.065	58
189	212	Sezen and Moehle No. 1	0.0204	0.14	0.24	484.7	1.10	0.020	0.100	1	nd	nd	16
190	213	Sezen and Moehle No. 2	0.0068	0.43	0.74	524.5	1.09	0.060	0.010	0	0.01	-0.700	15
191	214	Sezen and Moehle No. 4	0.0110	0.23	0.37	381.6	1.12	0.120	0.011	0	0.04	-0.350	45
192	215	Paultre & Legeron, 2000, No. 1006015	0.0133	0.35	0.70	234.0	1.00	0.001	0.020	0	0.66	-0.020	127
193	216	Paultre & Legeron, 2000, No. 1006025	0.0128	0.51	0.74	310.0	1.00	0.001	0.034	1	nd	nd	86
194	217	Paultre & Legeron, 2000, No. 1006040	0.0128	0.49	0.65	360.0	1.00	0.001	0.033	0	0.18	-0.070	39
195	218	Paultre & Legeron, 2000, No. 10013015	0.0118	0.36	0.69	215.0	1.01	0.001	0.077	0	0.12	-0.100	48
196	219	Paultre & Legeron, 2000, No. 10013025	0.0113	0.58	0.93	315.0	1.00	0.001	0.015	0	0.14	-0.080	30
197	220	Paultre & Legeron, 2000, No. 10013040	0.0098	0.72	1.05	353.0	1.04	0.040	0.009	0	0.02	-0.650	75
198	221	Paultre et al., 2001, No. 806040	0.0105	0.70	1.31	335.0	1.12	0.012	0.109	0	0.24	-0.050	182
199	222	Paultre et al., 2001, No. 1206040	0.0113	0.70	0.98	390.0	1.22	0.025	0.098	1	nd	nd	56
200	223	Paultre et al., 2001, No. 1005540	0.0120	0.59	0.79	380.0	1.08	0.010	0.100	1	nd	nd	82

Table 13f. Table of calibrated model parameters for each column

Test Index	Test Num. from PEER SPD	Test Series	θ_y (rad)	Ely / EI_g	EI_{stf40} / EI_g	M_y (kN-m)	M_c / M_y	α_s	$\theta_{cap,pl}$ (rad)	isLB	θ_{pc} (rad)	α_c	λ
201	224	Paultre et al., 2001, No. 1008040	0.0133	0.54	0.70	387.0	1.01	0.001	0.085	1	nd	nd	24
202	225	Paultre et al., 2001, No. 1005552	0.0082	0.85	0.96	374.0	1.04	0.005	0.060	1	nd	nd	40
203	226	Paultre et al., 2001, No. 1006052	0.0113	0.70	0.83	420.0	1.00	0.000	0.060	1	nd	nd	41
204	227	Pujol 2002, No. 10-2-3N	0.0109	0.16	0.32	76.1	1.18	0.065	0.030	1	nd	nd	42
205	228	Pujol 2002, No. 10-2-3S	0.0080	0.22	0.36	78.5	1.05	0.015	0.026	1	nd	nd	118
206	229	Pujol 2002, No. 10-3-1.5N	0.0095	0.19	0.31	75.4	1.23	0.065	0.033	1	nd	nd	127
207	230	Pujol 2002, No. 10-3-1.5S	0.0109	0.16	0.41	76.1	1.14	0.045	0.035	1	nd	nd	114
208	231	Pujol 2002, No. 10-3-3N	0.0117	0.16	0.36	77.8	1.07	0.020	0.040	1	nd	nd	35
209	232	Pujol 2002, No. 10-3-3S	0.0096	0.19	0.41	73.4	1.12	0.040	0.030	1	nd	nd	62
210	233	Pujol 2002, No. 10-3-2.25N	0.0098	0.19	0.35	73.2	1.18	0.040	0.045	1	nd	nd	105
211	234	Pujol 2002, No. 10-3-2.25S	0.0102	0.19	0.37	74.1	1.15	0.045	0.035	1	nd	nd	109
212	237	Pujol 2002, No. 20-3-3N	0.0099	0.20	0.51	88.5	1.13	0.043	0.030	1	nd	nd	80
213	238	Pujol 2002, No. 20-3-3S	0.0105	0.19	0.65	92.2	1.11	0.040	0.030	1	nd	nd	45
214	239	Pujol 2002, No. 10-2-2.25N	0.0098	0.18	0.37	76.1	1.22	0.040	0.055	1	nd	nd	91
215	240	Pujol 2002, No. 10-2-2.25S	0.0099	0.17	0.46	76.1	1.17	0.050	0.034	1	nd	nd	123
216	241	Pujol 2002, No. 10-1-2.25N	0.0093	0.18	0.36	74.8	1.23	0.060	0.035	1	nd	nd	127
217	242	Pujol 2002, No. 10-1-2.25S	0.0099	0.17	0.43	74.8	1.27	0.060	0.045	1	nd	nd	105
218	243	Bechtoula, Kono, Arai and Watanabe, 2002, D1N30	0.0117	0.24	0.84	125.9	1.00	0.001	0.043	1	nd	nd	43
219	244	Bechtoula, Kono, Arai and Watanabe, 2002, D1N60	0.0069	0.40	0.70	124.4	1.03	0.020	0.010	0	0.08	-0.090	68
220	245	Bechtoula, Kono, Arai and Watanabe, 2002, L1D60	0.0050	0.36	0.41	1440.0	1.01	0.001	0.034	1	nd	nd	23
221	246	Bechtoula, Kono, Arai and Watanabe, 2002, L1N60	0.0046	0.44	0.77	1506.0	1.23	0.040	0.026	0	0.03	-0.200	50
222	247	Bechtoula, Kono, Arai and Watanabe, 2002, L1N6B	0.0066	0.40	0.83	1302.0	1.15	0.040	0.025	1	nd	nd	54
223	248	Takemura and Kawashima, 1997, Test 1 (JSCE-4)	0.0080	0.16	0.32	178.7	1.84	0.052	0.130	1	nd	nd	164
224	249	Takemura and Kawashima, 1997, Test 2 (JSCE-5)	dr	dr	dr	176.2	1.78	0.060	0.130	1	nd	nd	38
225	250	Takemura and Kawashima, 1997, Test 3 (JSCE-6)	0.0076	0.16	0.27	174.3	1.37	0.040	0.070	1	nd	nd	55
226	251	Takemura and Kawashima, 1997, Test 4 (JSCE-7)	0.0068	0.20	0.32	186.4	1.02	0.001	0.115	1	nd	nd	48
227	252	Takemura and Kawashima, 1997, Test 5 (JSCE-8)	0.0068	0.19	0.36	187.4	1.10	0.010	0.070	1	nd	nd	77
228	253	Takemura and Kawashima, 1997, Test 6 (JSCE-9)	0.0068	0.19	0.23	188.0	1.12	0.010	0.080	1	nd	nd	45
229	254	Xaio & Yun 2002, No. FHC1-0.2	0.0132	0.28	0.46	666.8	1.00	0.001	dr	0	0.13	-0.100	dr
230	255	Xaio & Yun 2002, No. FHC2-0.34	0.0101	0.43	0.58	766.3	1.00	0.001	0.021	0	0.07	-0.150	45
231	256	Xaio & Yun 2002, No. FHC3-0.22	0.0118	0.31	0.47	659.6	1.00	0.001	0.045	1	nd	nd	45
232	257	Xaio & Yun 2002, No. FHC4-0.33	0.0101	0.40	0.58	711.2	1.00	0.001	0.011	0	0.17	-0.061	45
233	258	Xaio & Yun 2002, No. FHC5-0.2	0.0121	0.29	0.56	640.1	1.01	0.010	0.013	0	0.20	-0.060	45
234	259	Xaio & Yun 2002, No. FHC6-0.2	0.0124	0.29	0.45	644.5	1.00	0.001	dr	1	nd	nd	dr
235	260	Bayrak & Sheikh, 2002, No. RS-9HT	0.0098	0.75	0.83	211.8	1.30	0.070	dr	1	nd	nd	dr
236	261	Bayrak & Sheikh, 2002, No. RS-10HT	0.0075	1.00	1.41	216.4	1.15	0.040	0.028	1	nd	nd	111
237	262	Bayrak & Sheikh, 2002, No. RS-11HT	0.0100	0.79	1.03	230.3	1.23	0.065	0.036	1	nd	nd	45
238	263	Bayrak & Sheikh, 2002, No. RS-12HT	0.0073	0.87	1.56	184.2	1.09	0.030	dr	1	nd	nd	dr
239	264	Bayrak & Sheikh, 2002, No. RS-13HT	0.0073	0.90	1.38	239.5	1.21	0.040	dr	1	nd	nd	dr
240	265	Bayrak & Sheikh, 2002, No. RS-14HT	0.0111	0.61	0.68	246.8	1.06	0.050	dr	1	nd	nd	dr

Table 13g. Table of calibrated model parameters for each column

Test Index	Test Num. from PEER SPD	Test Series	θ_y (rad)	Ely / EI_g	EI_{stf40} / EI_g	M_y (kN-m)	M_c / M_y	α_s	$\theta_{cap,pl}$ (rad)	isLB	θ_{pc} (rad)	α_c	λ
241	266	Bayrak & Sheikh, 2002, No. RS-15HT	0.0141	0.52	0.72	188.8	1.09	0.040	dr	1	nd	nd	dr
242	267	Bayrak & Sheikh, 2002, No. RS-16HT	0.0098	0.66	0.72	167.6	1.08	0.040	dr	1	nd	nd	dr
243	268	Bayrak & Sheikh, 2002, No. RS-17HT	0.0141	0.56	0.65	235.8	1.10	0.040	0.034	1	nd	nd	45
244	269	Bayrak & Sheikh, 2002, No. RS-18HT	0.0065	1.00	1.07	193.4	1.12	0.040	dr	1	nd	nd	dr
245	270	Bayrak & Sheikh, 2002, No. RS-19HT	0.0073	1.01	1.14	219.2	1.20	0.040	dr	1	nd	nd	dr
246	271	Bayrak & Sheikh, 2002, No. RS-20HT	0.0095	0.80	0.82	225.6	1.00	0.001	0.016	1	nd	nd	45
247	272	Bayrak & Sheikh, 2002, No. WRS-21HT	0.0117	0.85	0.89	167.2	1.10	0.072	0.016	1	nd	nd	45
248	273	Bayrak & Sheikh, 2002, No. WRS-22HT	0.0152	0.65	0.75	165.8	1.38	0.160	dr	1	nd	nd	dr
249	274	Bayrak & Sheikh, 2002, No. WRS-23HT	0.0125	0.76	0.84	142.8	1.32	0.120	0.033	1	nd	nd	45
250	275	Bayrak & Sheikh, 2002, No. WRS-24HT	0.0106	0.96	0.99	151.0	1.05	0.025	0.021	1	nd	nd	45
251	285	Saatcioglu and Ozcebe 1989, U2	0.0170	0.17	0.26	286.0	1.08	0.040	dr	1	nd	nd	dr
252	286	Esaki, 1996 H-2-1/5	0.0083	0.21	0.42	40.8	1.02	0.010	dr	1	nd	nd	dr
253	287	Esaki, 1996 HT-2-1/5	0.0083	0.22	0.43	41.3	1.03	0.010	dr	1	nd	nd	dr
254	288	Esaki, 1996 H-2-1/3	0.0075	0.27	0.66	43.8	1.03	0.010	dr	1	nd	nd	dr
255	289	Esaki, 1996 HT-2-1/3	0.0075	0.26	0.62	44.0	1.05	0.020	dr	1	nd	nd	dr

dr – data removed due to questionable reliability

nd – no data available for this value, typically for post-capping slope

Appendix C: Calibration Diagrams for each Column Included in Study

This Appendix includes one figure for each of the 255 calibrations completed in this study. Each figure included the test data (red solid), the calibration to the experimental data (blue dashed) and the calibrated monotonic backbone curve (black solid). For clarity in terminology, the monotonic backbone curve represents the element response if the element were pushed monotonically in one direction. P-Δ effects have been removed from all figures in this Appendix.

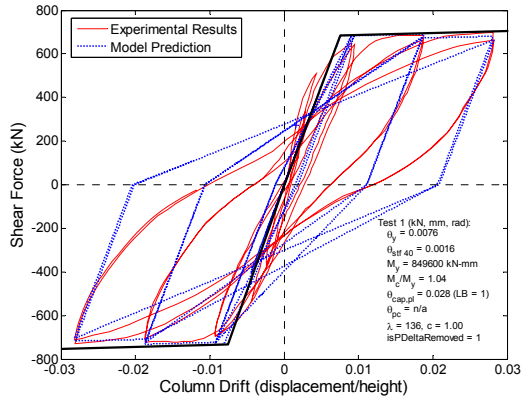

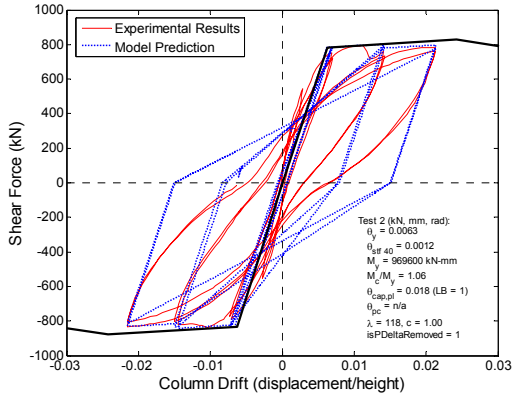

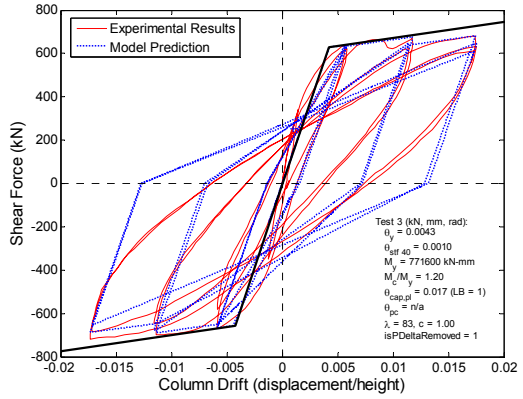

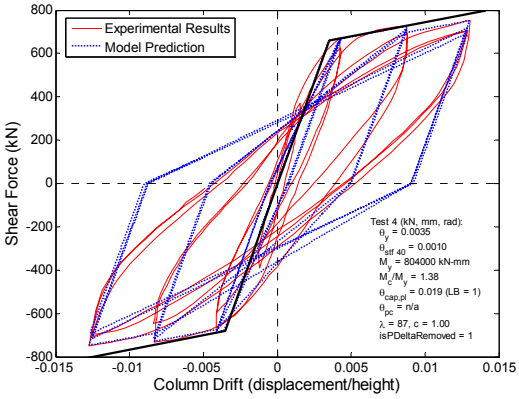

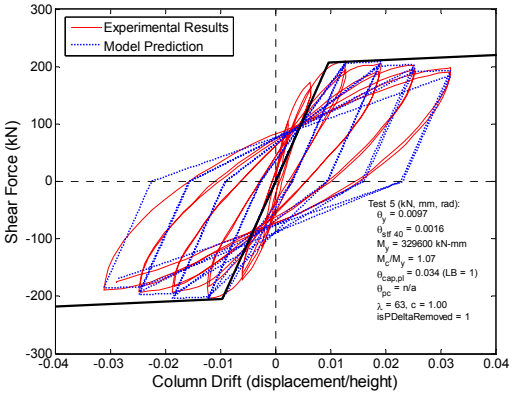
Experimental Results
Model Prediction
Shear Force (kN)
Column Drift (displacement/height)
Test 5 (kN, mm, rad):
θy = 0.0097
θstf 40 = 0.0016
My = 329600 kN-mm
Mc/My = 1.07
θcap,pl = 0.034 (LB = 1)
θpc = n/a
λ = 63, c = 1.00
isPDeltaRemoved = 1

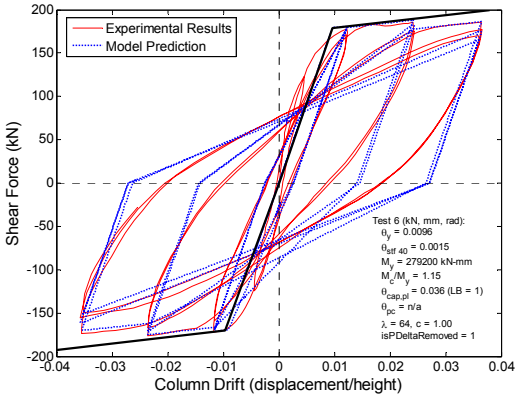
Experimental Results
Model Prediction
Shear Force (kN)
Column Drift (displacement/height)
Test 6 (kN, mm, rad):
θy = 0.0096
θstf 40 = 0.0015
My = 279200 kN-mm
Mc/My = 1.15
θcap,pl = 0.036 (LB = 1)
θpc = n/a
λ = 64, c = 1.00
isPDeltaRemoved = 1

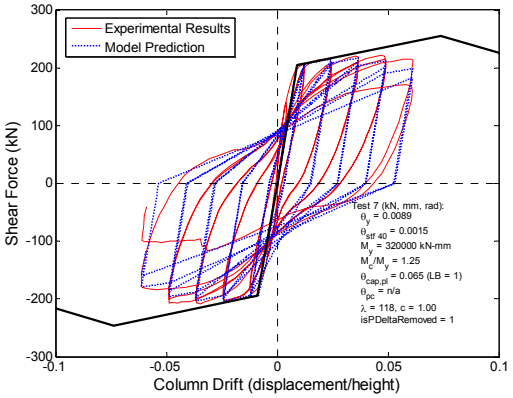
Experimental Results
Model Prediction
Shear Force (kN)
Column Drift (displacement/height)
Test 7 (kN, mm, rad):
θy = 0.0089
θstf 40 = 0.0015
My = 320000 kN-mm
Mc/My = 1.25
θcap,pl = 0.065 (LB = 1)
θpc = n/a
λ = 118, c = 1.00
isPDeltaRemoved = 1

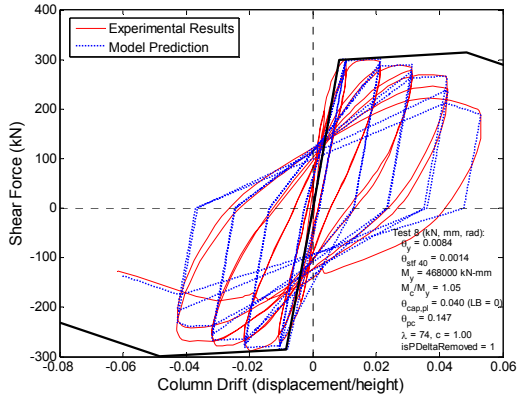
Experimental Results
Model Prediction
Shear Force (kN)
Column Drift (displacement/height)
Test 8 (kN, mm, rad):
θy = 0.0084
θstf 40 = 0.0014
My = 468000 kN-mm
Mc/My = 1.05
θcap,pl = 0.040 (LB = 0)
θpc = 0.147
λ = 74, c = 1.00
isPDeltaRemoved = 1

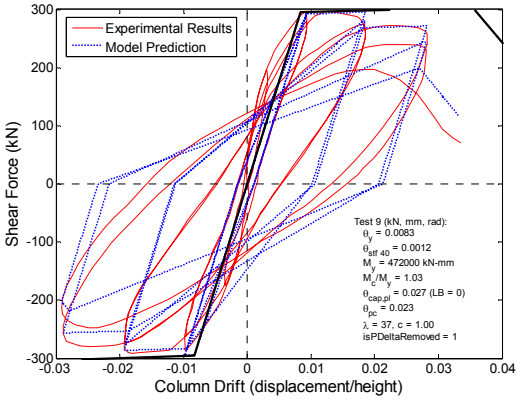
Experimental Results
Model Prediction
Shear Force (kN)
Column Drift (displacement/height)
Test 9 (kN, mm, rad):
θy = 0.0083
θstf 40 = 0.0012
My = 472000 kN-mm
Mc/My = 1.03
θcap,pl = 0.027 (LB = 0)
θpc = 0.023
λ = 37, c = 1.00
isPDeltaRemoved = 1

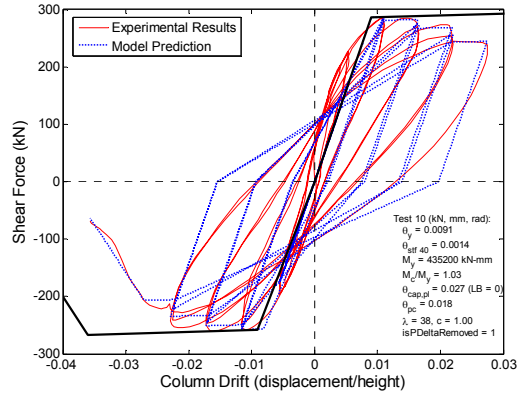
Experimental Results
Model Prediction
Shear Force (kN)
Column Drift (displacement/height)
Test 10 (kN, mm, rad):
θy = 0.0091
θstf 40 = 0.0014
My = 435200 kN-mm
Mc/My = 1.03
θcap,pl = 0.027 (LB = 0)
θpc = 0.018
λ = 38, c = 1.00
isPDeltaRemoved = 1

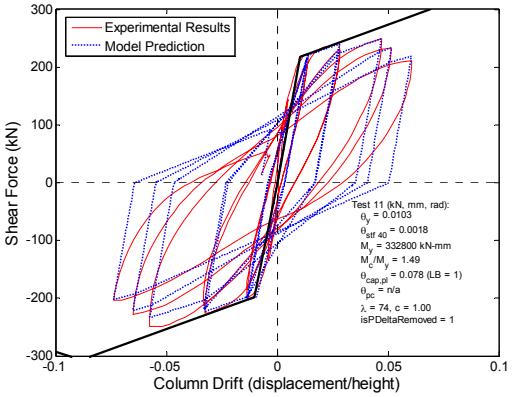
Experimental Results
Model Prediction
Shear Force (kN)
Column Drift (displacement/height)
Test 11 (kN, mm, rad):
θy = 0.0103
θstf 40 = 0.0018
My = 332800 kN-mm
Mc/My = 1.49
θcap,pl = 0.078 (LB = 1)
θpc = n/a
λ = 74, c = 1.00
isPDeltaRemoved = 1

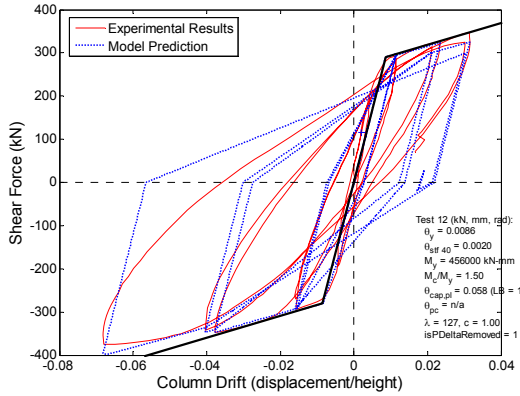
Experimental Results
Model Prediction
Shear Force (kN)
Column Drift (displacement/height)
Test 12 (kN, mm, rad):
θy = 0.0086
θstf 40 = 0.0020
My = 456000 kN-mm
Mc/My = 1.50
θcap,pl = 0.058 (LB = 1)
θpc = n/a
λ = 127, c = 1.00
isPDeltaRemoved = 1

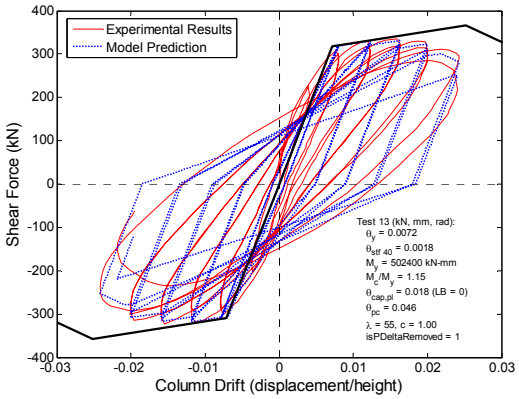
Experimental Results
Model Prediction
Shear Force (kN)
Column Drift (displacement/height)
Test 13 (kN, mm, rad):
θy = 0.0072
θstf 40 = 0.0018
My = 502400 kN-mm
Mc/My = 1.15
θcap,pl = 0.018 (LB = 0)
θpc = 0.046
λ = 55, c = 1.00
isPDeltaRemoved = 1

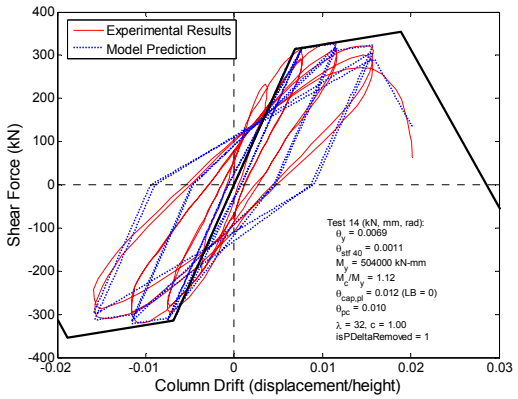
Experimental Results
Model Prediction
Shear Force (kN)
Column Drift (displacement/height)
Test 14 (kN, mm, rad):
θy = 0.0069
θstf 40 = 0.0011
My = 504000 kN-mm
Mc/My = 1.12
θcap,pl = 0.012 (LB = 0)
θpc = 0.010
λ = 32, c = 1.00
isPDeltaRemoved = 1

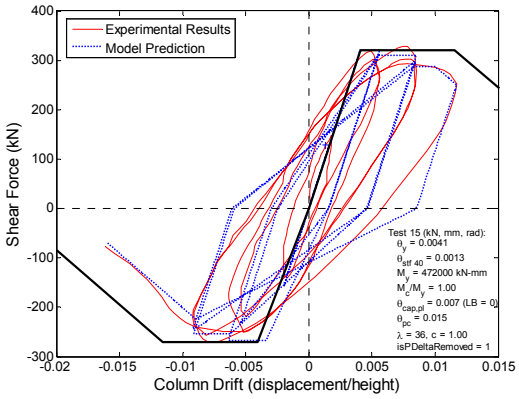
Experimental Results
Model Prediction
Shear Force (kN)
Column Drift (displacement/height)
Test 15 (kN, mm, rad):
θy = 0.0041
θstf 40 = 0.0013
My = 472000 kN-mm
Mc/My = 1.00
θcap,pl = 0.007 (LB = 0)
θpc = 0.015
λ = 36, c = 1.00
isPDeltaRemoved = 1

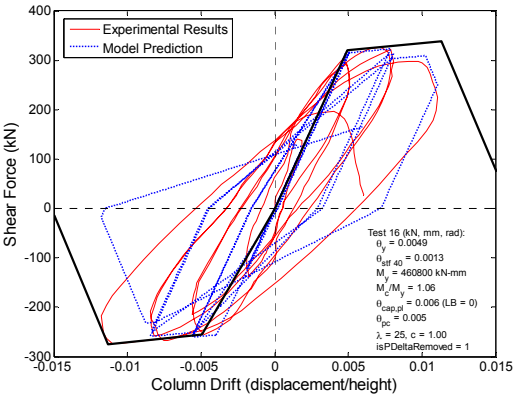
Experimental Results
Model Prediction
Shear Force (kN)
Column Drift (displacement/height)
Test 16 (kN, mm, rad):
θy = 0.0049
θstf 40 = 0.0013
My = 460800 kN-mm
Mc/My = 1.06
θcap,pl = 0.006 (LB = 0)
θpc = 0.005
λ = 25, c = 1.00
isPDeltaRemoved = 1

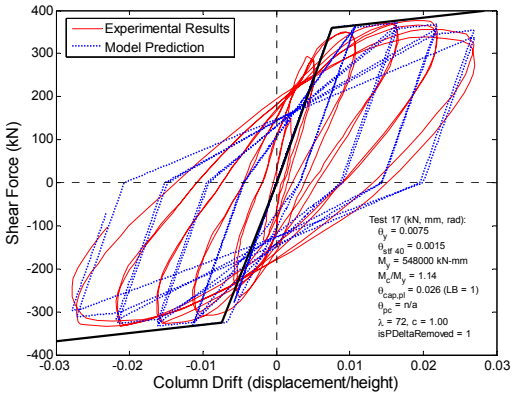
Experimental Results
Model Prediction
Shear Force (kN)
Column Drift (displacement/height)
Test 17 (kN, mm, rad):
θy = 0.0075
θstf 40 = 0.0015
My = 548000 kN-mm
Mc/My = 1.14
θcap,pl = 0.026 (LB = 1)
θpc = n/a
λ = 72, c = 1.00
isPDeltaRemoved = 1

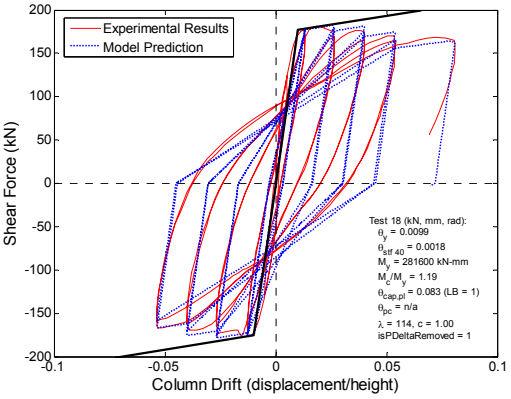
Experimental Results
Model Prediction
Shear Force (kN)
Column Drift (displacement/height)
Test 18 (kN, mm, rad):
θy = 0.0099
θstf 40 = 0.0018
My = 281600 kN-mm
Mc/My = 1.19
θcap,pl = 0.083 (LB = 1)
θpc = n/a
λ = 114, c = 1.00
isPDeltaRemoved = 1

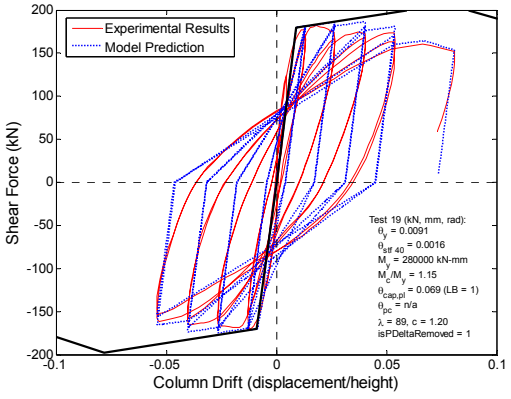
Experimental Results
Model Prediction
Shear Force (kN)
Column Drift (displacement/height)
Test 19 (kN, mm, rad):
θy = 0.0091
θstf 40 = 0.0016
My = 280000 kN-mm
Mc/My = 1.15
θcap,pl = 0.069 (LB = 1)
θpc = n/a
λ = 89, c = 1.20
isPDeltaRemoved = 1

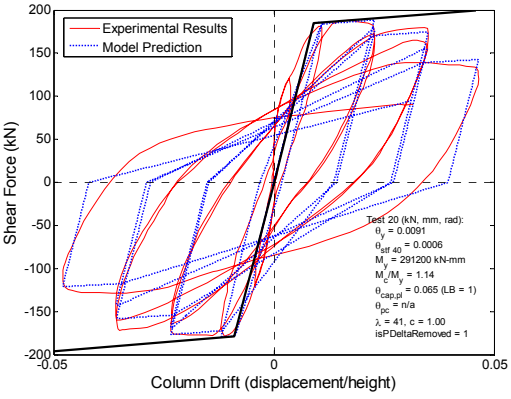
Experimental Results
Model Prediction
Shear Force (kN)
Column Drift (displacement/height)
Test 20 (kN, mm, rad):
θy = 0.0091
θstf 40 = 0.0006
My = 291200 kN-mm
Mc/My = 1.14
θcap,pl = 0.065 (LB = 1)
θpc = n/a
λ = 41, c = 1.00
isPDeltaRemoved = 1

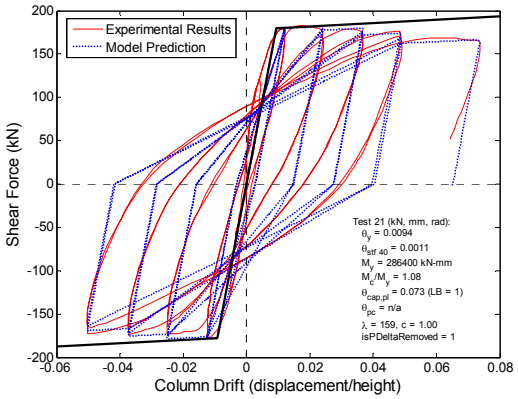
Experimental Results
Model Prediction
Shear Force (kN)
Column Drift (displacement/height)
Test 21 (kN, mm, rad):
θy = 0.0094
θstf 40 = 0.0011
My = 286400 kN-mm
Mc/My = 1.08
θcap,pl = 0.073 (LB = 1)
θpc = n/a
λ = 159, c = 1.00
isPDeltaRemoved = 1

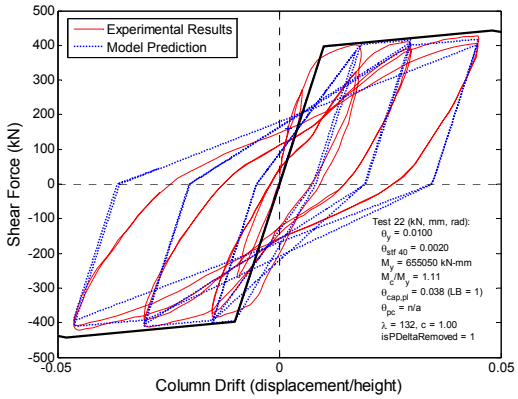
Experimental Results
Model Prediction
Shear Force (kN)
Column Drift (displacement/height)
Test 22 (kN, mm, rad):
θy = 0.0100
θstf 40 = 0.0020
My = 655050 kN-mm
Mc/My = 1.11
θcap,pl = 0.038 (LB = 1)
θpc = n/a
λ = 132, c = 1.00
isPDeltaRemoved = 1

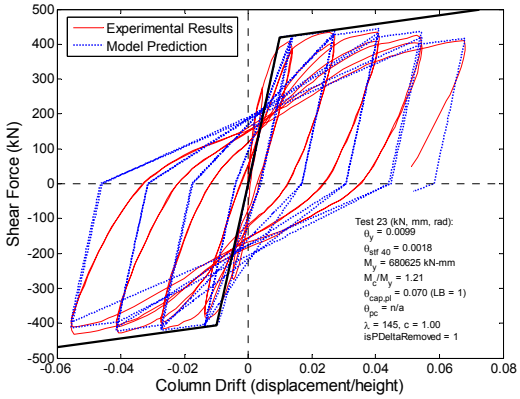
Experimental Results
Model Prediction
Shear Force (kN)
Column Drift (displacement/height)
Test 23 (kN, mm, rad):
θy = 0.0099
θstf 40 = 0.0018
My = 680625 kN-mm
Mc/My = 1.21
θcap,pl = 0.070 (LB = 1)
θpc = n/a
λ = 145, c = 1.00
isPDeltaRemoved = 1

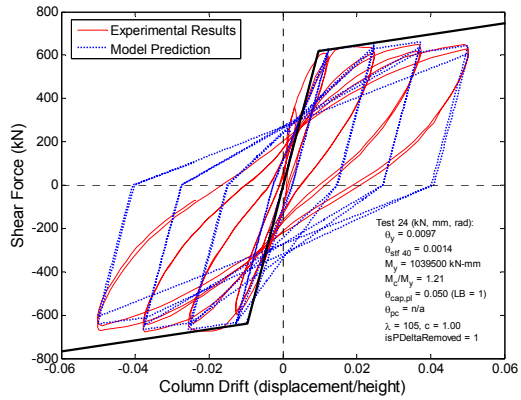
Experimental Results
Model Prediction
Shear Force (kN)
Column Drift (displacement/height)
Test 24 (kN, mm, rad):
θy = 0.0097
θstf 40 = 0.0014
My = 1039500 kN-mm
Mc/My = 1.21
θcap,pl = 0.050 (LB = 1)
θpc = n/a
λ = 105, c = 1.00
isPDeltaRemoved = 1

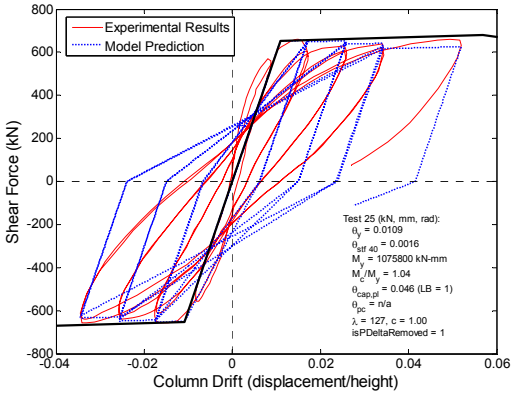
Experimental Results
Model Prediction
Shear Force (kN)
Column Drift (displacement/height)
Test 25 (kN, mm, rad):
θy = 0.0109
θstf 40 = 0.0016
My = 1075800 kN-mm
Mc/My = 1.04
θcap,pl = 0.046 (LB = 1)
θpc = n/a
λ = 127, c = 1.00
isPDeltaRemoved = 1

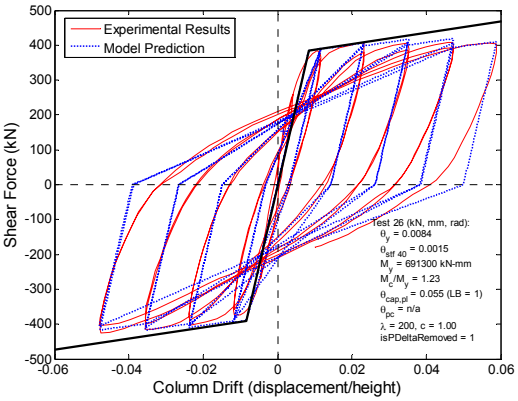
Experimental Results
Model Prediction
Shear Force (kN)
Column Drift (displacement/height)
Test 26 (kN, mm, rad):
θy = 0.0084
θstf 40 = 0.0015
My = 691300 kN-mm
Mc/My = 1.23
θcap,pl = 0.055 (LB = 1)
θpc = n/a
λ = 200, c = 1.00
isPDeltaRemoved = 1

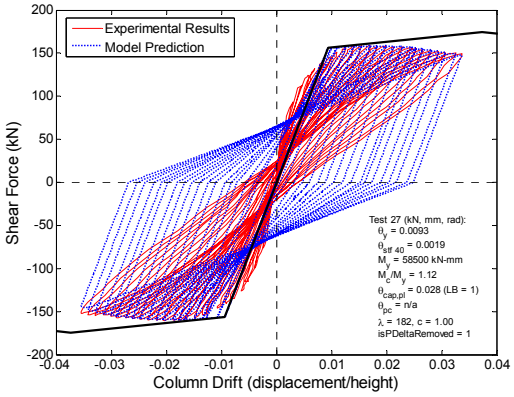
Experimental Results
Model Prediction
Shear Force (kN)
Column Drift (displacement/height)
Test 27 (kN, mm, rad):
θy = 0.0093
θstf 40 = 0.0019
My = 58500 kN-mm
Mc/My = 1.12
θcap,pl = 0.028 (LB = 1)
θpc = n/a
λ = 182, c = 1.00
isPDeltaRemoved = 1

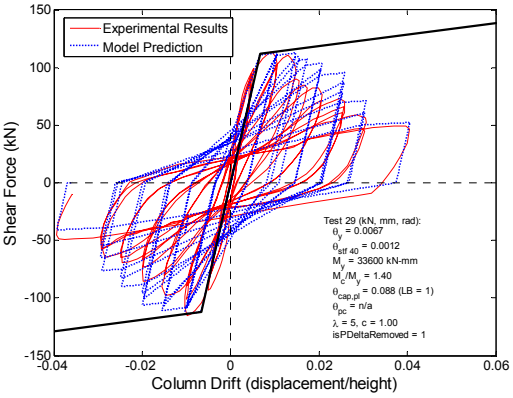
Experimental Results
Model Prediction
Shear Force (kN)
Column Drift (displacement/height)
Test 29 (kN, mm, rad):
θy = 0.0067
θstf 40 = 0.0012
My = 33600 kN-mm
Mc/My = 1.40
θcap,pl = 0.088 (LB = 1)
θpc = n/a
λ = 5, c = 1.00
isPDeltaRemoved = 1

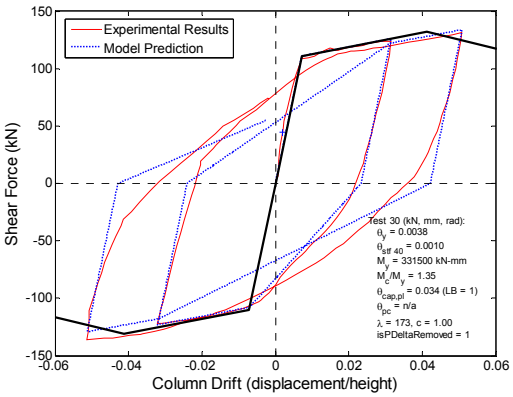
Experimental Results
Model Prediction
Shear Force (kN)
Column Drift (displacement/height)
Test 30 (kN, mm, rad):
θy = 0.0038
θstf 40 = 0.0010
My = 331500 kN-mm
Mc/My = 1.35
θcap,pl = 0.034 (LB = 1)
θpc = n/a
λ = 173, c = 1.00
isPDeltaRemoved = 1

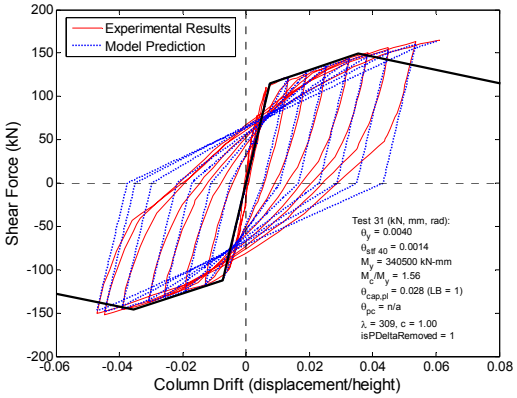
Experimental Results
Model Prediction
Shear Force (kN)
Column Drift (displacement/height)
Test 31 (kN, mm, rad):
θy = 0.0040
θstf 40 = 0.0014
My = 340500 kN-mm
Mc/My = 1.56
θcap,pl = 0.028 (LB = 1)
θpc = n/a
λ = 309, c = 1.00
isPDeltaRemoved = 1

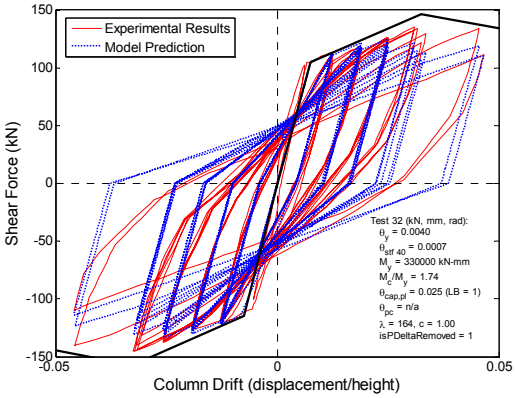
Experimental Results
Model Prediction
Shear Force (kN)
Column Drift (displacement/height)
Test 32 (kN, mm, rad):
θy = 0.0040
θstf 40 = 0.0007
My = 330000 kN-mm
Mc/My = 1.74
θcap,pl = 0.025 (LB = 1)
θpc = n/a
λ = 164, c = 1.00
isPDeltaRemoved = 1

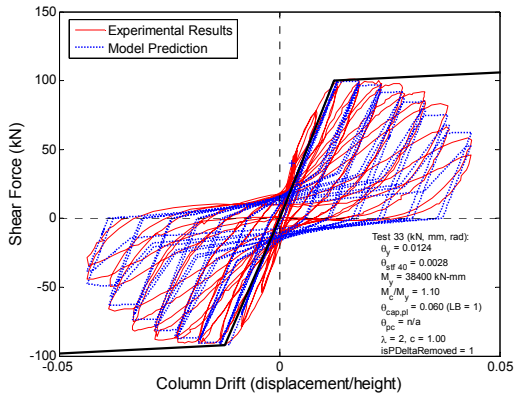
Experimental Results
Model Prediction
Shear Force (kN)
Column Drift (displacement/height)
Test 33 (kN, mm, rad):
θy = 0.0124
θstf 40 = 0.0028
My = 38400 kN-mm
Mc/My = 1.10
θcap,pl = 0.060 (LB = 1)
θpc = n/a
λ = 2, c = 1.00
isPDeltaRemoved = 1

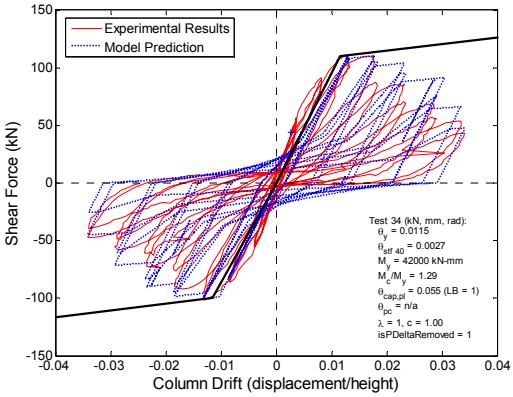
Experimental Results
Model Prediction
Shear Force (kN)
Column Drift (displacement/height)
Test 34 (kN, mm, rad):
θy = 0.0115
θstf 40 = 0.0027
My = 42000 kN-mm
Mc/My = 1.29
θcap,pl = 0.055 (LB = 1)
θpc = n/a
λ = 1, c = 1.00
isPDeltaRemoved = 1

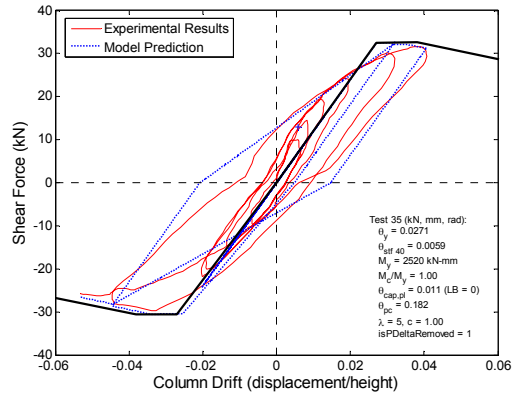
Experimental Results
Model Prediction
Shear Force (kN)
Column Drift (displacement/height)
Test 35 (kN, mm, rad):
θy = 0.0271
θstf 40 = 0.0059
My = 2520 kN-mm
Mc/My = 1.00
θcap,pl = 0.011 (LB = 0)
θpc = 0.182
λ = 5, c = 1.00
isPDeltaRemoved = 1

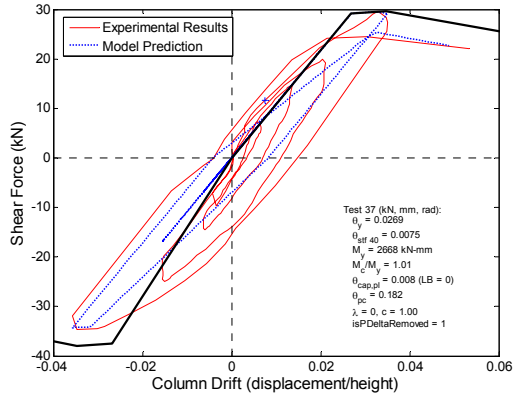
Experimental Results
Model Prediction
Shear Force (kN)
Column Drift (displacement/height)
Test 37 (kN, mm, rad):
θy = 0.0269
θstf 40 = 0.0075
My = 2668 kN-mm
Mc/My = 1.01
θcap,pl = 0.008 (LB = 0)
θpc = 0.182
λ = 0, c = 1.00
isPDeltaRemoved = 1

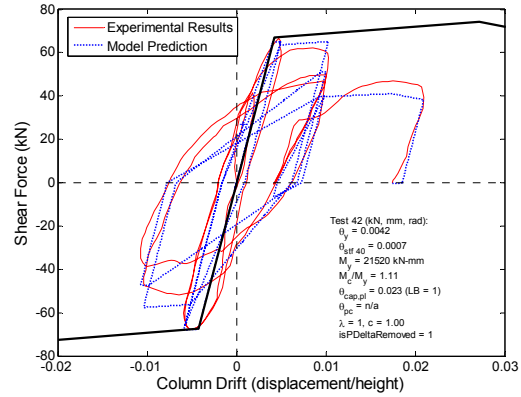
Experimental Results
Model Prediction
Shear Force (kN)
Column Drift (displacement/height)
Test 42 (kN, mm, rad):
θy = 0.0042
θstf 40 = 0.0007
My = 21520 kN-mm
Mc/My = 1.11
θcap,pl = 0.023 (LB = 1)
θpc = n/a
λ = 1, c = 1.00
isPDeltaRemoved = 1

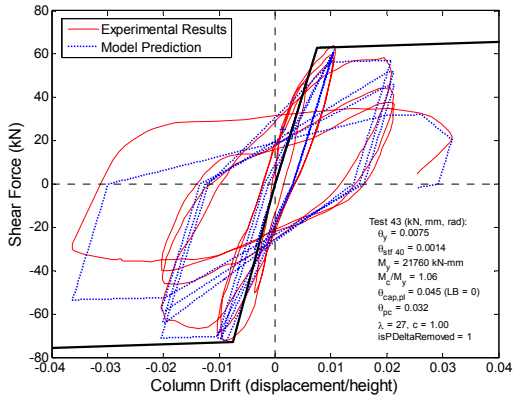
Experimental Results
Model Prediction
Shear Force (kN)
Column Drift (displacement/height)
Test 43 (kN, mm, rad):
θy = 0.0075
θstf 40 = 0.0014
My = 21760 kN-mm
Mc/My = 1.06
θcap,pl = 0.045 (LB = 0)
θpc = 0.032
λ = 27, c = 1.00
isPDeltaRemoved = 1

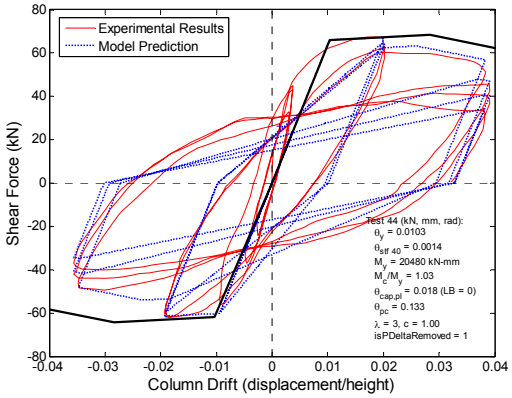
Experimental Results
Model Prediction
Shear Force (kN)
Column Drift (displacement/height)
Test 44 (kN, mm, rad):
θy = 0.0103
θstf 40 = 0.0014
My = 20480 kN-mm
Mc/My = 1.03
θcap,pl = 0.018 (LB = 0)
θpc = 0.133
λ = 3, c = 1.00
isPDeltaRemoved = 1

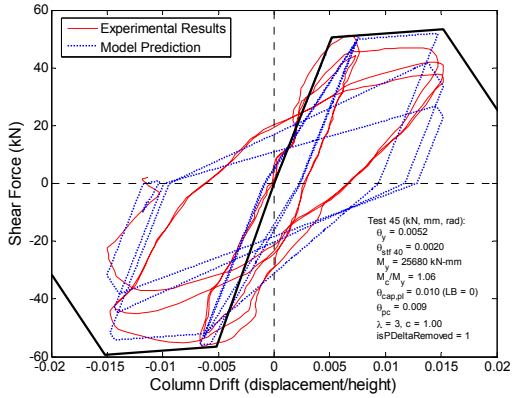
Experimental Results
Model Prediction
Shear Force (kN)
Column Drift (displacement/height)
Test 45 (kN, mm, rad):
θy = 0.0052
θstf 40 = 0.0020
My = 25680 kN-mm
Mc/My = 1.06
θcap,pl = 0.010 (LB = 0)
θpc = 0.009
λ = 3, c = 1.00
isPDeltaRemoved = 1

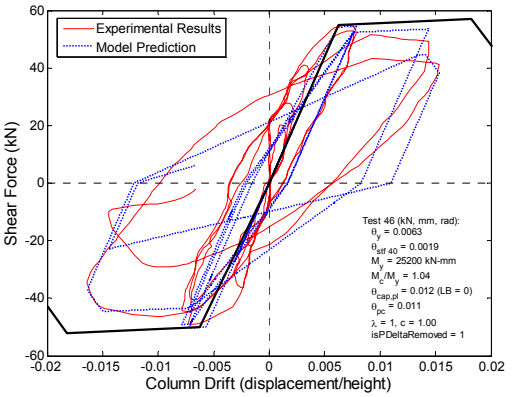
Experimental Results
Model Prediction
Shear Force (kN)
Column Drift (displacement/height)
Test 46 (kN, mm, rad):
θy = 0.0063
θstf 40 = 0.0019
My = 25200 kN-mm
Mc/My = 1.04
θcap,pl = 0.012 (LB = 0)
θpc = 0.011
λ = 1, c = 1.00
isPDeltaRemoved = 1

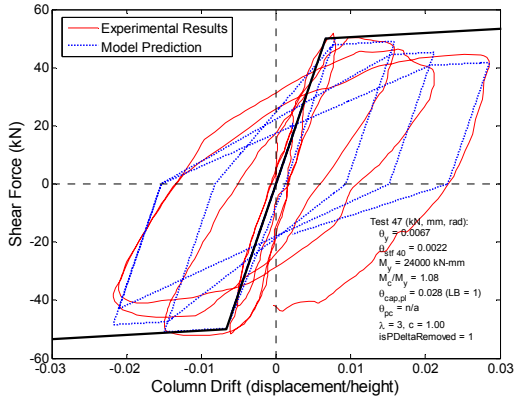
Experimental Results
Model Prediction
Shear Force (kN)
Column Drift (displacement/height)
Test 47 (kN, mm, rad):
θy = 0.0067
θstf 40 = 0.0022
My = 24000 kN-mm
Mc/My = 1.08
θcap,pl = 0.028 (LB = 1)
θpc = n/a
λ = 3, c = 1.00
isPDeltaRemoved = 1

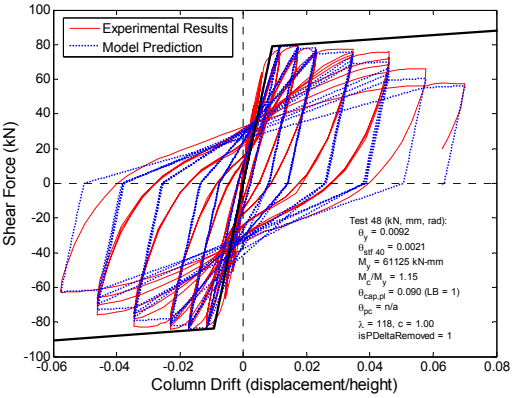
Experimental Results
Model Prediction
Shear Force (kN)
Column Drift (displacement/height)
Test 48 (kN, mm, rad):
θy = 0.0092
θstf 40 = 0.0021
My = 61125 kN-mm
Mc/My = 1.15
θcap,pl = 0.090 (LB = 1)
θpc = n/a
λ = 118, c = 1.00
isPDeltaRemoved = 1

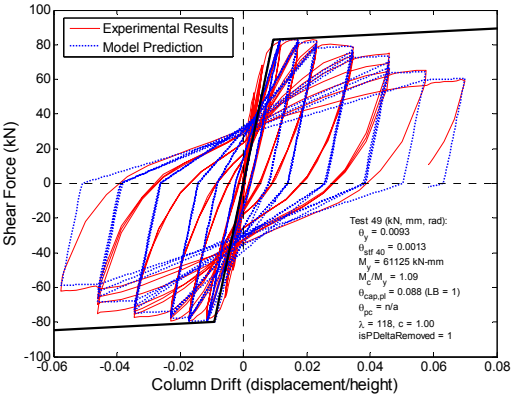
Experimental Results
Model Prediction
Shear Force (kN)
Column Drift (displacement/height)
Test 49 (kN, mm, rad):
θy = 0.0093
θstf 40 = 0.0013
My = 61125 kN-mm
Mc/My = 1.09
θcap,pl = 0.088 (LB = 1)
θpc = n/a
λ = 118, c = 1.00
isPDeltaRemoved = 1

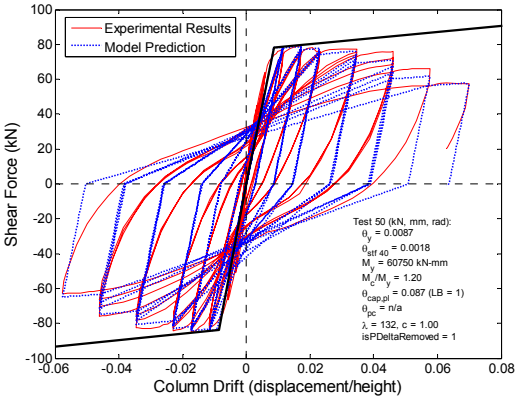
Experimental Results
Model Prediction
Shear Force (kN)
Column Drift (displacement/height)
Test 50 (kN, mm, rad):
θy = 0.0087
θstf 40 = 0.0018
My = 60750 kN-mm
Mc/My = 1.20
θcap,pl = 0.087 (LB = 1)
θpc = n/a
λ = 132, c = 1.00
isPDeltaRemoved = 1

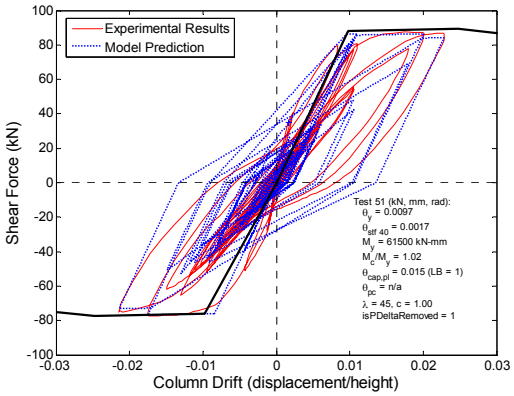
Experimental Results
Model Prediction
Shear Force (kN)
Column Drift (displacement/height)
Test 51 (kN, mm, rad):
θy = 0.0097
θstf 40 = 0.0017
My = 61500 kN-mm
Mc/My = 1.02
θcap,pl = 0.015 (LB = 1)
θpc = n/a
λ = 45, c = 1.00
isPDeltaRemoved = 1

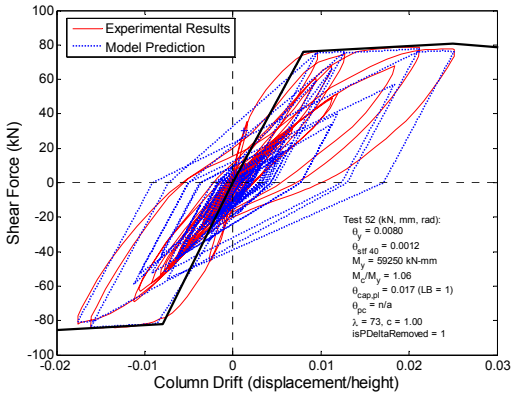
Experimental Results
Model Prediction
Shear Force (kN)
Column Drift (displacement/height)
Test 52 (kN, mm, rad):
θy = 0.0080
θstf 40 = 0.0012
My = 59250 kN-mm
Mc/My = 1.06
θcap,pl = 0.017 (LB = 1)
θpc = n/a
λ = 73, c = 1.00
isPDeltaRemoved = 1

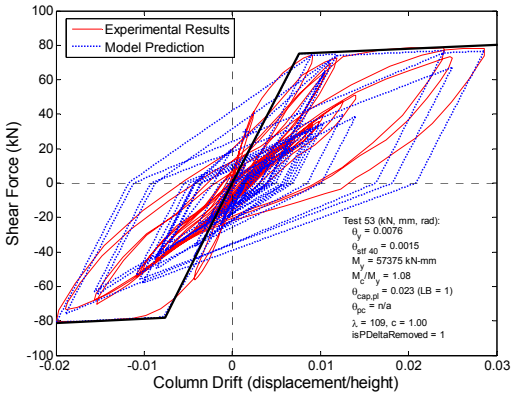
Experimental Results
Model Prediction
Shear Force (kN)
Column Drift (displacement/height)
Test 53 (kN, mm, rad):
θy = 0.0076
θstf 40 = 0.0015
My = 57375 kN-mm
Mc/My = 1.08
θcap,pl = 0.023 (LB = 1)
θpc = n/a
λ = 109, c = 1.00
isPDeltaRemoved = 1

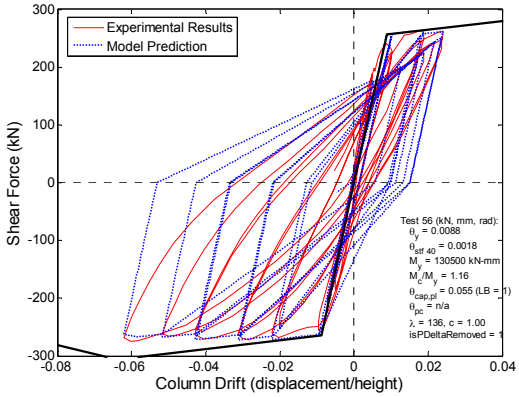
Experimental Results
Model Prediction
Shear Force (kN)
Column Drift (displacement/height)
Test 56 (kN, mm, rad):
θy = 0.0088
θstf 40 = 0.0018
My = 130500 kN-mm
Mc/My = 1.16
θcap,pl = 0.055 (LB = 1)
θpc = n/a
λ = 136, c = 1.00
isPDeltaRemoved = 1

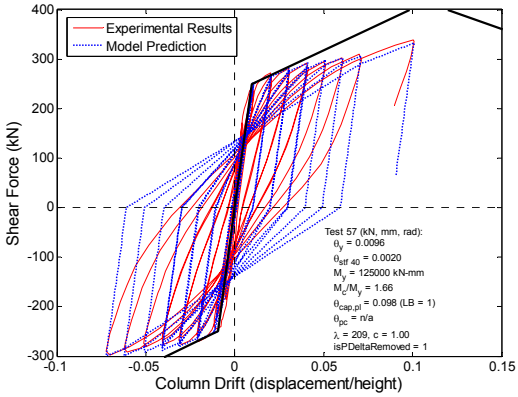
Experimental Results
Model Prediction
Shear Force (kN)
Column Drift (displacement/height)
Test 57 (kN, mm, rad):
θy = 0.0096
θstf 40 = 0.0020
My = 125000 kN-mm
Mc/My = 1.66
θcap,pl = 0.098 (LB = 1)
θpc = n/a
λ = 209, c = 1.00
isPDeltaRemoved = 1

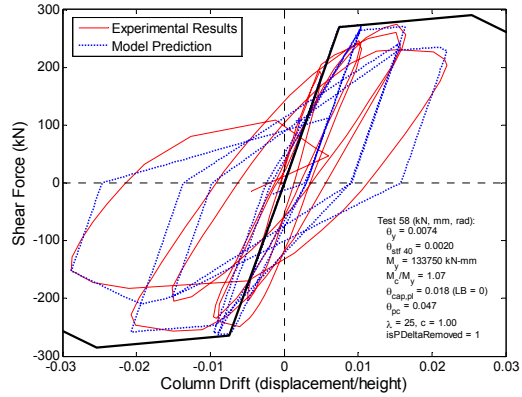
Experimental Results
Model Prediction
Shear Force (kN)
Column Drift (displacement/height)
Test 58 (kN, mm, rad):
θy = 0.0074
θstf 40 = 0.0020
My = 133750 kN-mm
Mc/My = 1.07
θcap,pl = 0.018 (LB = 0)
θpc = 0.047
λ = 25, c = 1.00
isPDeltaRemoved = 1

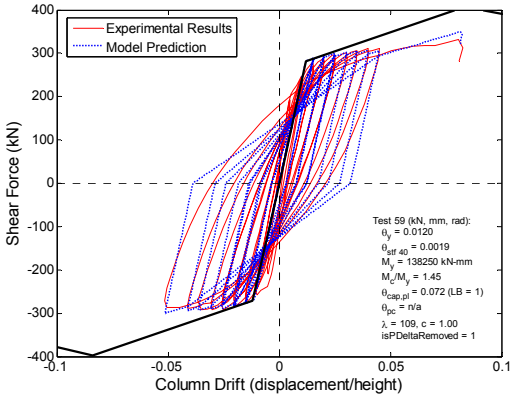
Experimental Results
Model Prediction
Shear Force (kN)
Column Drift (displacement/height)
Test 59 (kN, mm, rad):
θy = 0.0120
θstf 40 = 0.0019
My = 138250 kN-mm
Mc/My = 1.45
θcap,pl = 0.072 (LB = 1)
θpc = n/a
λ = 109, c = 1.00
isPDeltaRemoved = 1

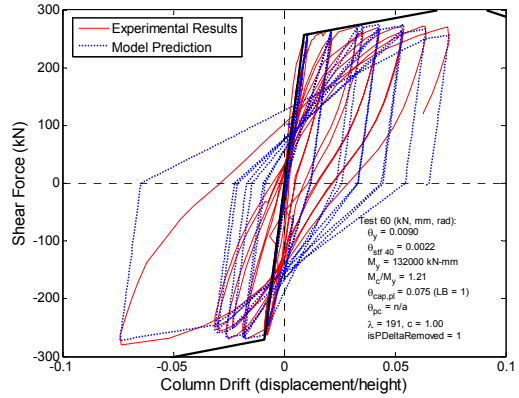
Experimental Results
Model Prediction
Shear Force (kN)
Column Drift (displacement/height)
Test 60 (kN, mm, rad):
θy = 0.0090
θstf 40 = 0.0022
My = 132000 kN-mm
Mc/My = 1.21
θcap,pl = 0.075 (LB = 1)
θpc = n/a
λ = 191, c = 1.00
isPDeltaRemoved = 1

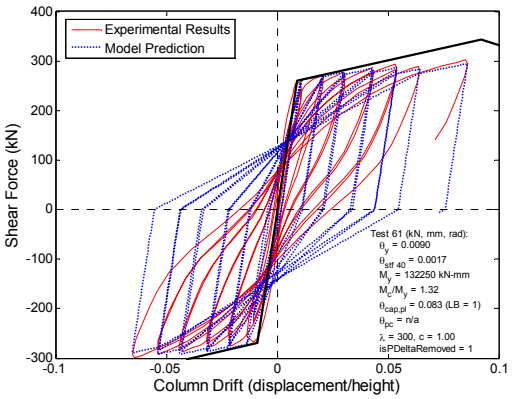
Experimental Results
Model Prediction
Shear Force (kN)
Column Drift (displacement/height)
Test 61 (kN, mm, rad):
θy = 0.0090
θstf 40 = 0.0017
My = 132250 kN-mm
Mc/My = 1.32
θcap,pl = 0.083 (LB = 1)
θpc = n/a
λ = 300, c = 1.00
isPDeltaRemoved = 1

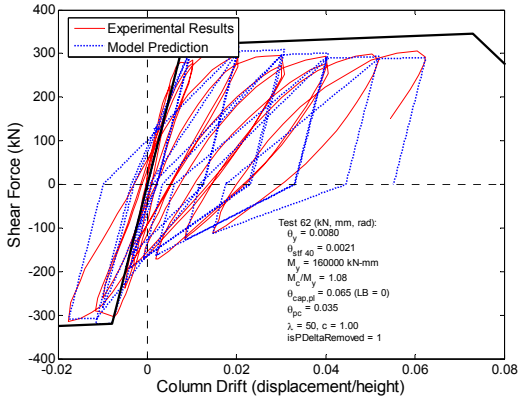
Experimental Results
Model Prediction
Shear Force (kN)
Column Drift (displacement/height)
Test 62 (kN, mm, rad):
θy = 0.0080
θstf 40 = 0.0021
My = 160000 kN-mm
Mc/My = 1.08
θcap,pl = 0.065 (LB = 0)
θpc = 0.035
λ = 50, c = 1.00
isPDeltaRemoved = 1

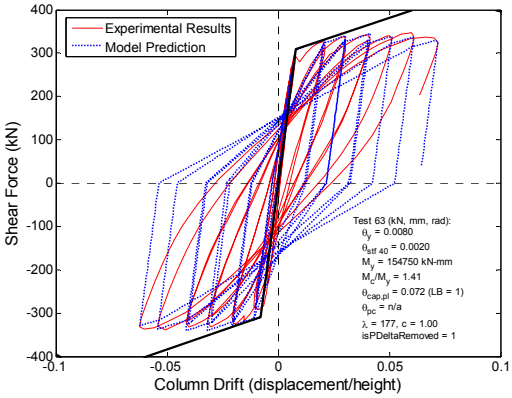
Experimental Results
Model Prediction
Shear Force (kN)
Column Drift (displacement/height)
Test 63 (kN, mm, rad):
θy = 0.0080
θstf 40 = 0.0020
My = 154750 kN-mm
Mc/My = 1.41
θcap,pl = 0.072 (LB = 1)
θpc = n/a
λ = 177, c = 1.00
isPDeltaRemoved = 1

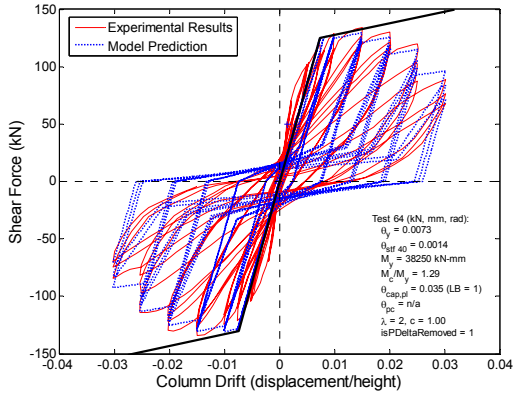
Experimental Results
Model Prediction
Shear Force (kN)
Column Drift (displacement/height)
Test 64 (kN, mm, rad):
θy = 0.0073
θstf 40 = 0.0014
My = 38250 kN-mm
Mc/My = 1.29
θcap,pl = 0.035 (LB = 1)
θpc = n/a
λ = 2, c = 1.00
isPDeltaRemoved = 1

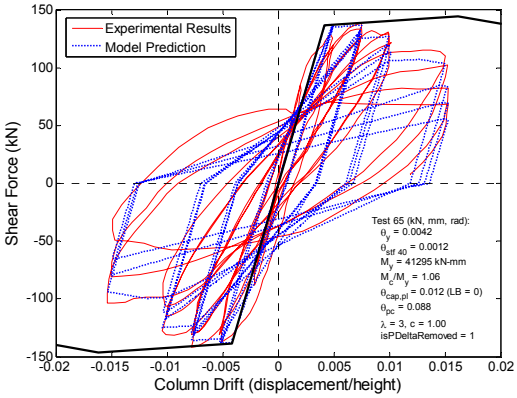
Experimental Results
Model Prediction
Shear Force (kN)
Column Drift (displacement/height)
Test 65 (kN, mm, rad):
θy = 0.0042
θstf 40 = 0.0012
My = 41295 kN-mm
Mc/My = 1.06
θcap,pl = 0.012 (LB = 0)
θpc = 0.088
λ = 3, c = 1.00
isPDeltaRemoved = 1

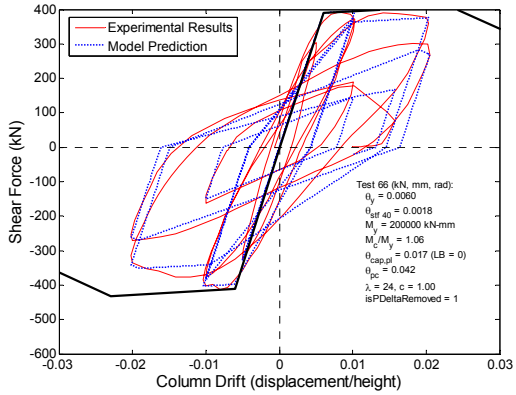
Experimental Results
Model Prediction
Shear Force (kN)
Column Drift (displacement/height)
Test 66 (kN, mm, rad):
θy = 0.0060
θstf 40 = 0.0018
My = 200000 kN-mm
Mc/My = 1.06
θcap,pl = 0.017 (LB = 0)
θpc = 0.042
λ = 24, c = 1.00
isPDeltaRemoved = 1

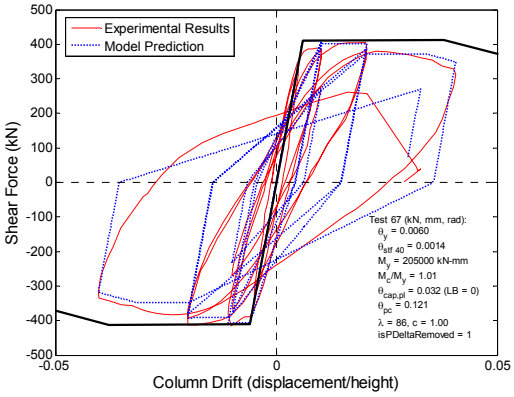
Experimental Results
Model Prediction
Shear Force (kN)
Column Drift (displacement/height)
Test 67 (kN, mm, rad):
θy = 0.0060
θstf 40 = 0.0014
My = 205000 kN-mm
Mc/My = 1.01
θcap,pl = 0.032 (LB = 0)
θpc = 0.121
λ = 86, c = 1.00
isPDeltaRemoved = 1

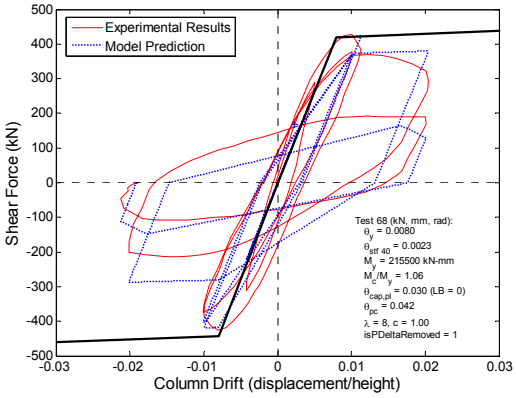
Experimental Results
Model Prediction
Shear Force (kN)
Column Drift (displacement/height)
Test 68 (kN, mm, rad):
θy = 0.0080
θstf 40 = 0.0023
My = 215500 kN-mm
Mc/My = 1.06
θcap,pl = 0.030 (LB = 0)
θpc = 0.042
λ = 8, c = 1.00
isPDeltaRemoved = 1

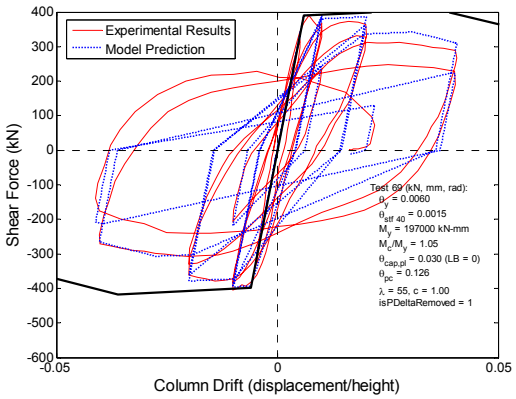
Experimental Results
Model Prediction
Test 69 (kN, mm, rad):
θy = 0.0060
θstf 40 = 0.0015
My = 197000 kN-mm
Mc/My = 1.05
θcap,pl = 0.030 (LB = 0)
θpc = 0.126
λ = 55, c = 1.00
isPDeltaRemoved = 1
Shear Force (kN)
Column Drift (displacement/height)

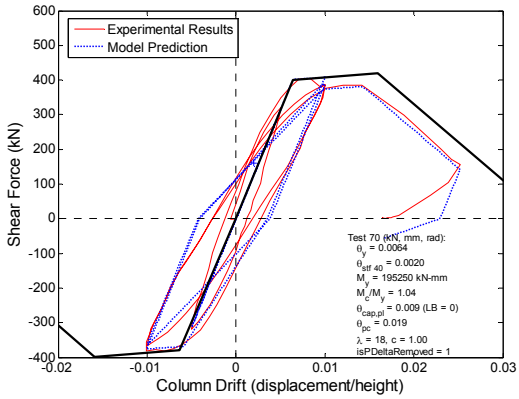
Experimental Results
Model Prediction
Test 70 (kN, mm, rad):
θy = 0.0064
θstf 40 = 0.0020
My = 195250 kN-mm
Mc/My = 1.04
θcap,pl = 0.009 (LB = 0)
θpc = 0.019
λ = 18, c = 1.00
isPDeltaRemoved = 1
Shear Force (kN)
Column Drift (displacement/height)

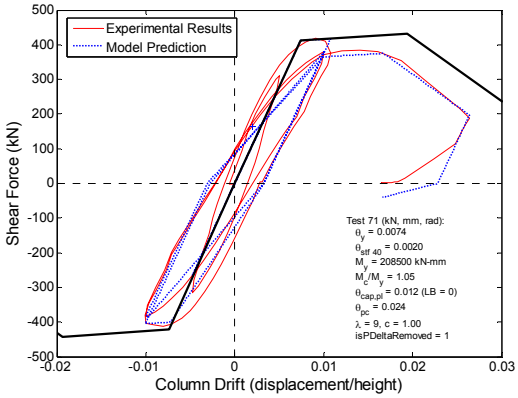
Experimental Results
Model Prediction
Test 71 (kN, mm, rad):
θy = 0.0074
θstf 40 = 0.0020
My = 208500 kN-mm
Mc/My = 1.05
θcap,pl = 0.012 (LB = 0)
θpc = 0.024
λ = 9, c = 1.00
isPDeltaRemoved = 1
Shear Force (kN)
Column Drift (displacement/height)

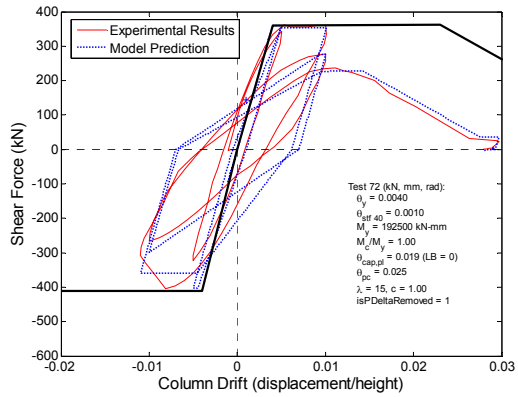
Experimental Results
Model Prediction
Test 72 (kN, mm, rad):
θy = 0.0040
θstf 40 = 0.0010
My = 192500 kN-mm
Mc/My = 1.00
θcap,pl = 0.019 (LB = 0)
θpc = 0.025
λ = 15, c = 1.00
isPDeltaRemoved = 1
Shear Force (kN)
Column Drift (displacement/height)

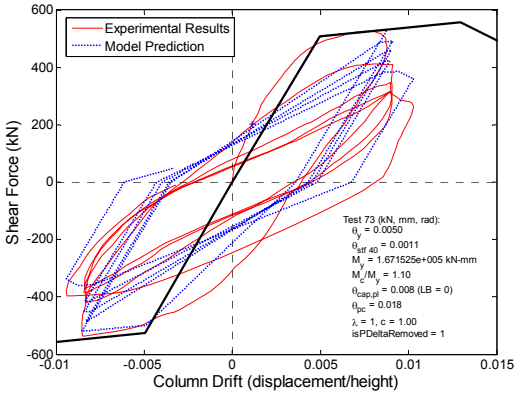
Experimental Results
Model Prediction
Test 73 (kN, mm, rad):
θy = 0.0050
θstf 40 = 0.0011
My = 1.671525e+005 kN-mm
Mc/My = 1.10
θcap,pl = 0.008 (LB = 0)
θpc = 0.018
λ = 1, c = 1.00
isPDeltaRemoved = 1
Shear Force (kN)
Column Drift (displacement/height)

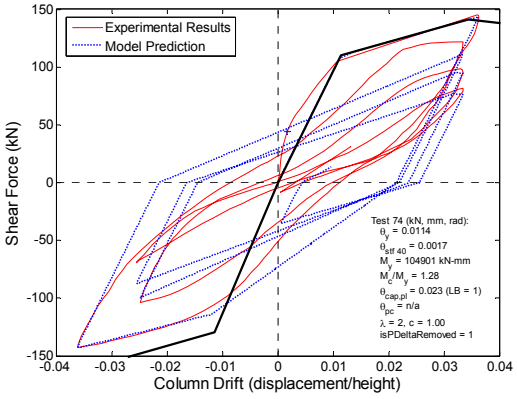
Experimental Results
Model Prediction
Test 74 (kN, mm, rad):
θy = 0.0114
θstf 40 = 0.0017
My = 104901 kN-mm
Mc/My = 1.28
θcap,pl = 0.023 (LB = 1)
θpc = n/a
λ = 2, c = 1.00
isPDeltaRemoved = 1
Shear Force (kN)
Column Drift (displacement/height)

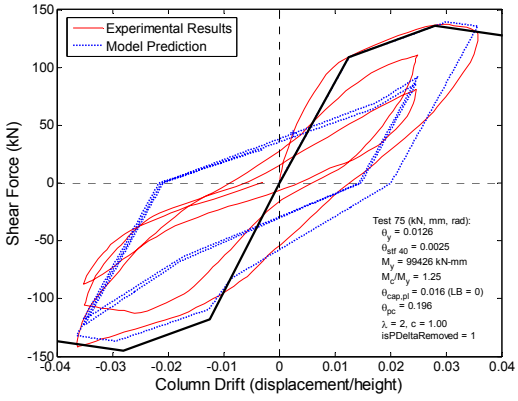
Experimental Results
Model Prediction
Test 75 (kN, mm, rad):
θy = 0.0126
θstf 40 = 0.0025
My = 99426 kN-mm
Mc/My = 1.25
θcap,pl = 0.016 (LB = 0)
θpc = 0.196
λ = 2, c = 1.00
isPDeltaRemoved = 1
Shear Force (kN)
Column Drift (displacement/height)

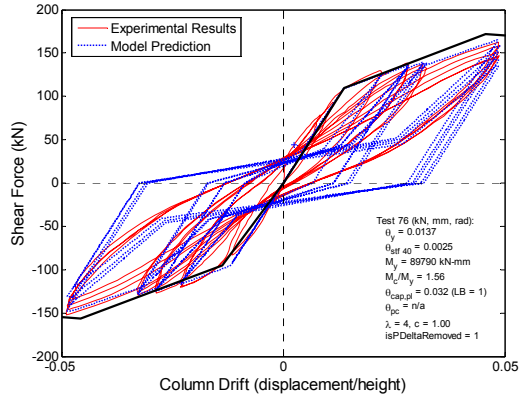
Experimental Results
Model Prediction
Test 76 (kN, mm, rad):
θy = 0.0137
θstf 40 = 0.0025
My = 89790 kN-mm
Mc/My = 1.56
θcap,pl = 0.032 (LB = 1)
θpc = n/a
λ = 4, c = 1.00
isPDeltaRemoved = 1
Shear Force (kN)
Column Drift (displacement/height)

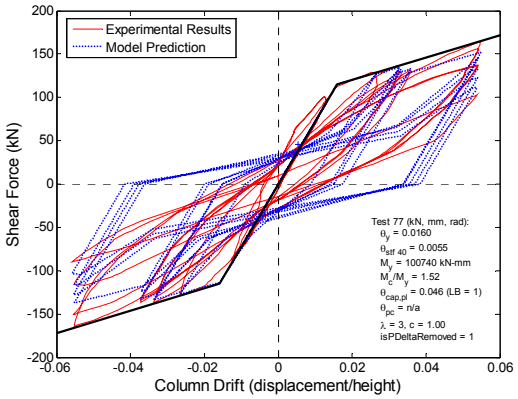
Experimental Results
Model Prediction
Shear Force (kN)
Column Drift (displacement/height)
Test 77 (kN, mm, rad):
θy = 0.0160
θstf 40 = 0.0055
My = 100740 kN-mm
Mc/My = 1.52
θcap,pl = 0.046 (LB = 1)
θpc = n/a
λ = 3, c = 1.00
isPDeltaRemoved = 1

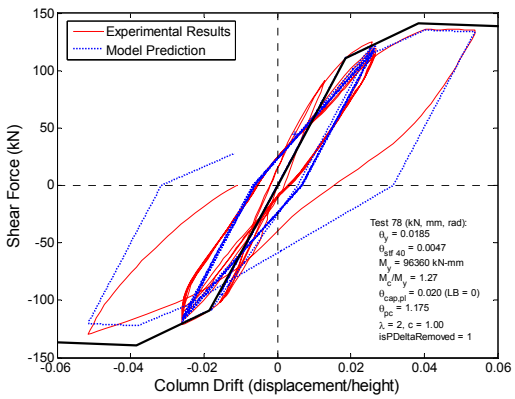
Experimental Results
Model Prediction
Shear Force (kN)
Column Drift (displacement/height)
Test 78 (kN, mm, rad):
θy = 0.0185
θstf 40 = 0.0047
My = 96360 kN-mm
Mc/My = 1.27
θcap,pl = 0.020 (LB = 0)
θpc = 1.175
λ = 2, c = 1.00
isPDeltaRemoved = 1

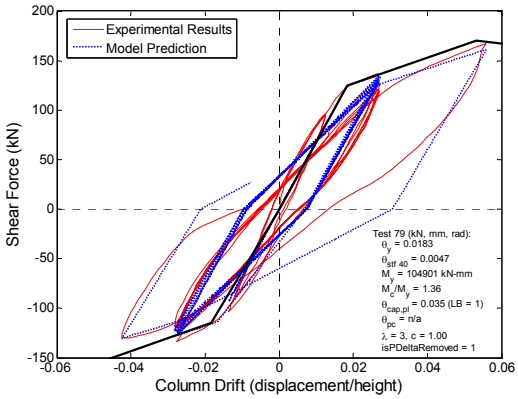
Experimental Results
Model Prediction
Shear Force (kN)
Column Drift (displacement/height)
Test 79 (kN, mm, rad):
θy = 0.0183
θstf 40 = 0.0047
My = 104901 kN-mm
Mc/My = 1.36
θcap,pl = 0.035 (LB = 1)
θpc = n/a
λ = 3, c = 1.00
isPDeltaRemoved = 1

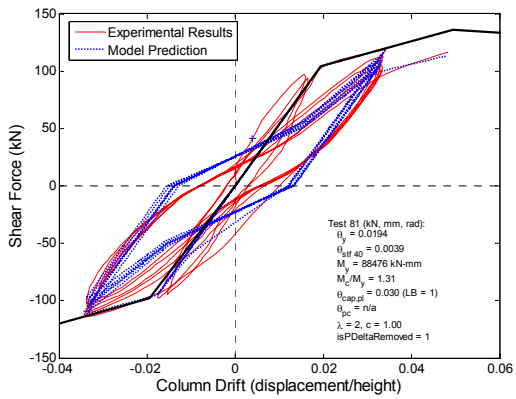
Experimental Results
Model Prediction
Shear Force (kN)
Column Drift (displacement/height)
Test 81 (kN, mm, rad):
θy = 0.0194
θstf 40 = 0.0039
My = 88476 kN-mm
Mc/My = 1.31
θcap,pl = 0.030 (LB = 1)
θpc = n/a
λ = 2, c = 1.00
isPDeltaRemoved = 1

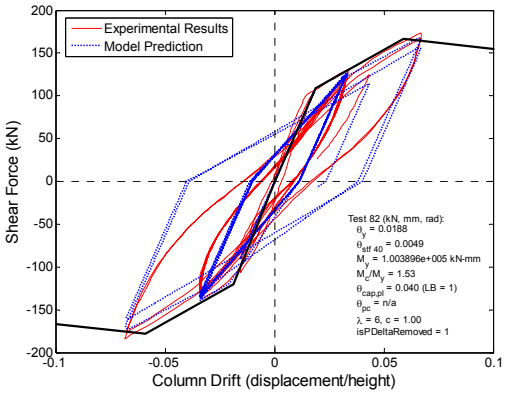
Experimental Results
Model Prediction
Shear Force (kN)
Column Drift (displacement/height)
Test 82 (kN, mm, rad):
θy = 0.0188
θstf 40 = 0.0049
My = 1.003896e+005 kN-mm
Mc/My = 1.53
θcap,pl = 0.040 (LB = 1)
θpc = n/a
λ = 6, c = 1.00
isPDeltaRemoved = 1

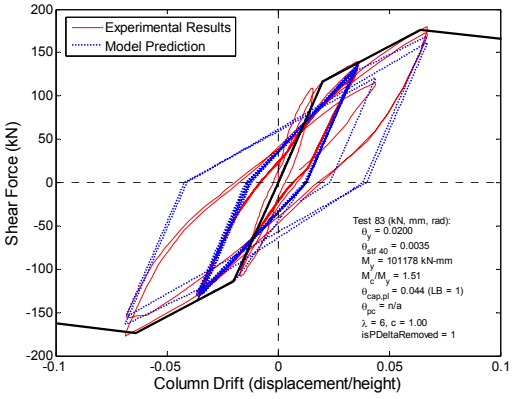
Experimental Results
Model Prediction
Shear Force (kN)
Column Drift (displacement/height)
Test 83 (kN, mm, rad):
θy = 0.0200
θstf 40 = 0.0035
My = 101178 kN-mm
Mc/My = 1.51
θcap,pl = 0.044 (LB = 1)
θpc = n/a
λ = 6, c = 1.00
isPDeltaRemoved = 1

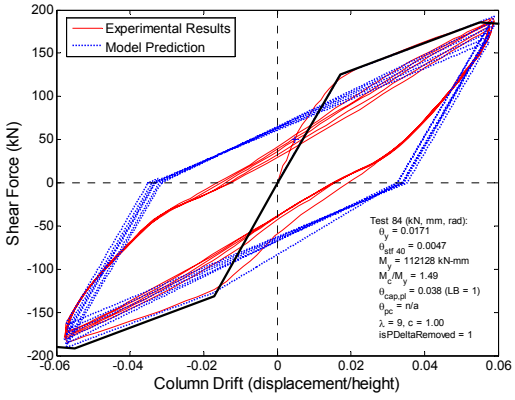
Experimental Results
Model Prediction
Shear Force (kN)
Column Drift (displacement/height)
Test 84 (kN, mm, rad):
θy = 0.0171
θstf 40 = 0.0047
My = 112128 kN-mm
Mc/My = 1.49
θcap,pl = 0.038 (LB = 1)
θpc = n/a
λ = 9, c = 1.00
isPDeltaRemoved = 1

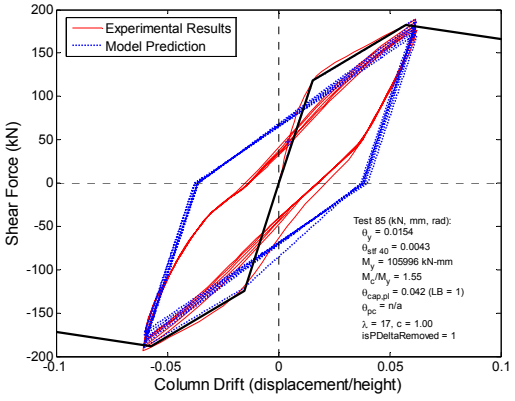
Experimental Results
Model Prediction
Shear Force (kN)
Column Drift (displacement/height)
Test 85 (kN, mm, rad):
θy = 0.0154
θstf 40 = 0.0043
My = 105996 kN-mm
Mc/My = 1.55
θcap,pl = 0.042 (LB = 1)
θpc = n/a
λ = 17, c = 1.00
isPDeltaRemoved = 1

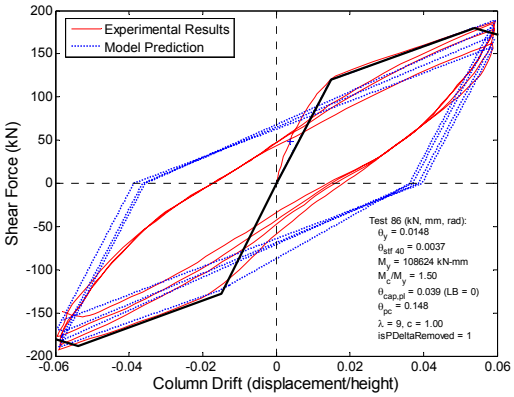
Experimental Results
Model Prediction
Shear Force (kN)
Column Drift (displacement/height)
Test 86 (kN, mm, rad):
θy = 0.0148
θstf 40 = 0.0037
My = 108624 kN-mm
Mc/My = 1.50
θcap,pl = 0.039 (LB = 0)
θpc = 0.148
λ = 9, c = 1.00
isPDeltaRemoved = 1

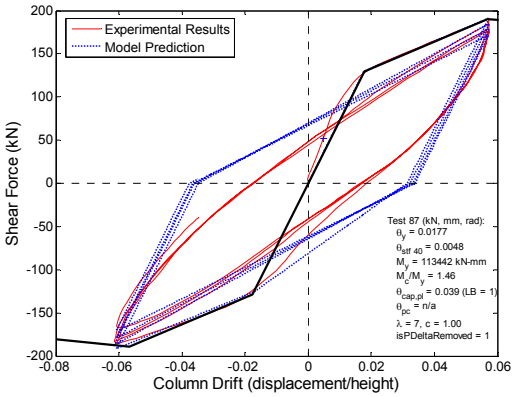
Experimental Results
Model Prediction
Shear Force (kN)
Column Drift (displacement/height)
Test 87 (kN, mm, rad):
θy = 0.0177
θstf 40 = 0.0048
My = 113442 kN-mm
Mc/My = 1.46
θcap,pl = 0.039 (LB = 1)
θpc = n/a
λ = 7, c = 1.00
isPDeltaRemoved = 1

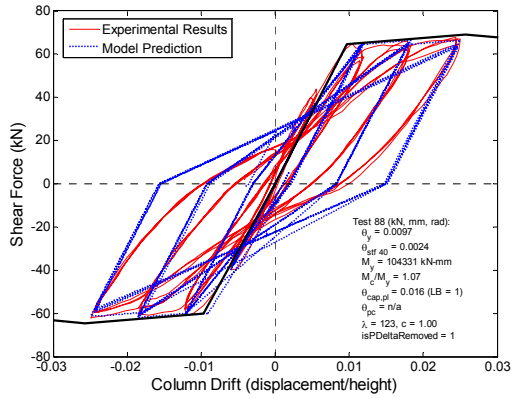
Experimental Results
Model Prediction
Shear Force (kN)
Column Drift (displacement/height)
Test 88 (kN, mm, rad):
θy = 0.0097
θstf 40 = 0.0024
My = 104331 kN-mm
Mc/My = 1.07
θcap,pl = 0.016 (LB = 1)
θpc = n/a
λ = 123, c = 1.00
isPDeltaRemoved = 1

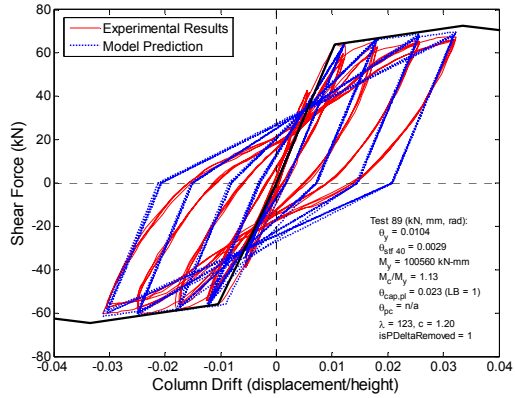
Experimental Results
Model Prediction
Shear Force (kN)
Column Drift (displacement/height)
Test 89 (kN, mm, rad):
θy = 0.0104
θstf 40 = 0.0029
My = 100560 kN-mm
Mc/My = 1.13
θcap,pl = 0.023 (LB = 1)
θpc = n/a
λ = 123, c = 1.20
isPDeltaRemoved = 1

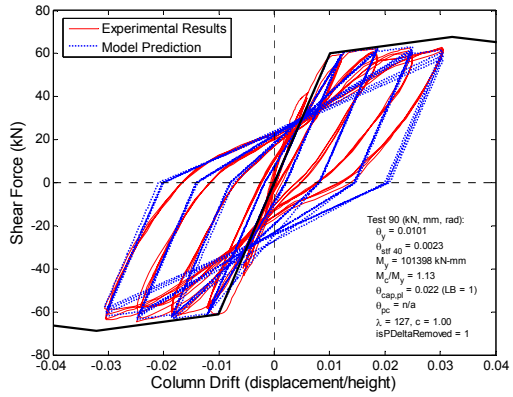
Experimental Results
Model Prediction
Shear Force (kN)
Column Drift (displacement/height)
Test 90 (kN, mm, rad):
θy = 0.0101
θstf 40 = 0.0023
My = 101398 kN-mm
Mc/My = 1.13
θcap,pl = 0.022 (LB = 1)
θpc = n/a
λ = 127, c = 1.00
isPDeltaRemoved = 1

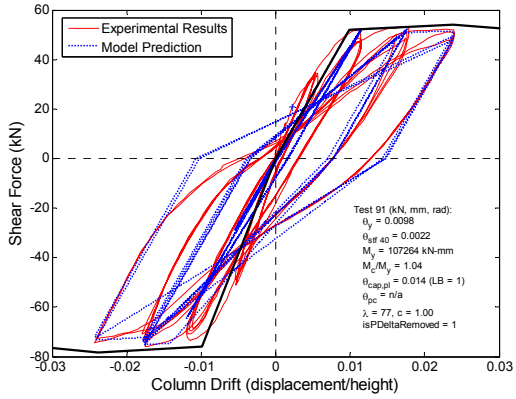
Experimental Results
Model Prediction
Shear Force (kN)
Column Drift (displacement/height)
Test 91 (kN, mm, rad):
θy = 0.0098
θstf 40 = 0.0022
My = 107264 kN-mm
Mc/My = 1.04
θcap,pl = 0.014 (LB = 1)
θpc = n/a
λ = 77, c = 1.00
isPDeltaRemoved = 1

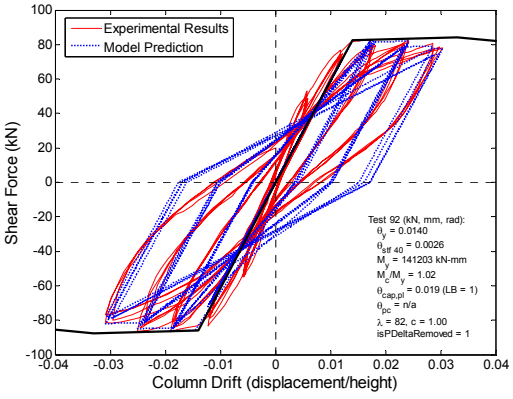
Experimental Results
Model Prediction
Shear Force (kN)
Column Drift (displacement/height)
Test 92 (kN, mm, rad):
θy = 0.0140
θstf 40 = 0.0026
My = 141203 kN-mm
Mc/My = 1.02
θcap,pl = 0.019 (LB = 1)
θpc = n/a
λ = 82, c = 1.00
isPDeltaRemoved = 1

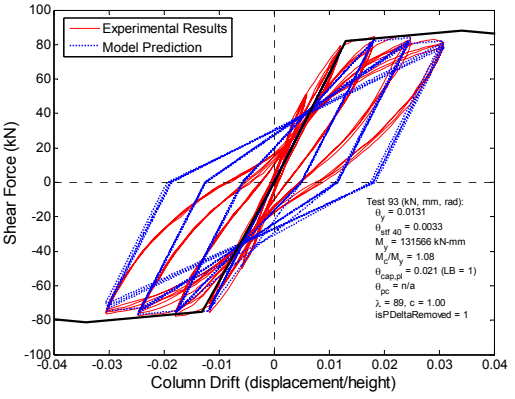
Experimental Results
Model Prediction
Shear Force (kN)
Column Drift (displacement/height)
Test 93 (kN, mm, rad):
θy = 0.0131
θstf 40 = 0.0033
My = 131566 kN-mm
Mc/My = 1.08
θcap,pl = 0.021 (LB = 1)
θpc = n/a
λ = 89, c = 1.00
isPDeltaRemoved = 1

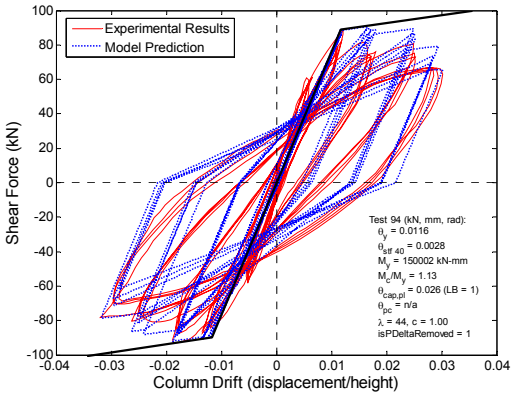
Experimental Results
Model Prediction
Shear Force (kN)
Column Drift (displacement/height)
Test 94 (kN, mm, rad):
θy = 0.0116
θstf 40 = 0.0028
My = 150002 kN-mm
Mc/My = 1.13
θcap,pl = 0.026 (LB = 1)
θpc = n/a
λ = 44, c = 1.00
isPDeltaRemoved = 1

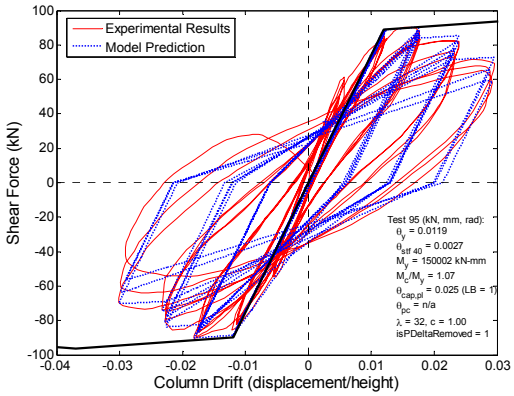
Experimental Results
Model Prediction
Shear Force (kN)
Column Drift (displacement/height)
Test 95 (kN, mm, rad):
θy = 0.0119
θstf 40 = 0.0027
My = 150002 kN-mm
Mc/My = 1.07
θcap,pl = 0.025 (LB = 1)
θpc = n/a
λ = 32, c = 1.00
isPDeltaRemoved = 1

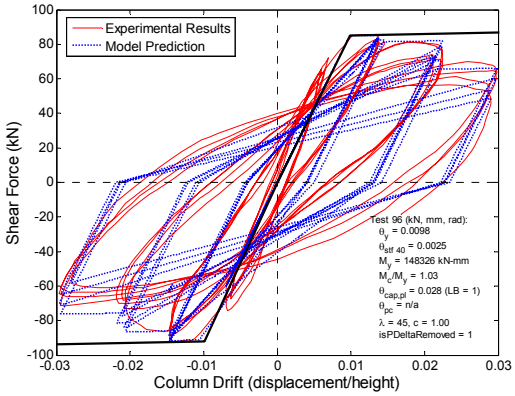
Experimental Results
Model Prediction
Shear Force (kN)
Column Drift (displacement/height)
Test 96 (kN, mm, rad):
θy = 0.0098
θstf 40 = 0.0025
My = 148326 kN-mm
Mc/My = 1.03
θcap,pl = 0.028 (LB = 1)
θpc = n/a
λ = 45, c = 1.00
isPDeltaRemoved = 1

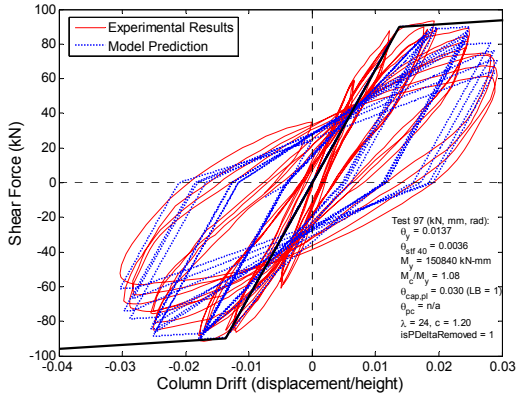
Experimental Results
Model Prediction
Shear Force (kN)
Column Drift (displacement/height)
Test 97 (kN, mm, rad):
θy = 0.0137
θstf 40 = 0.0036
My = 150840 kN-mm
Mc/My = 1.08
θcap,pl = 0.030 (LB = 1)
θpc = n/a
λ = 24, c = 1.20
isPDeltaRemoved = 1

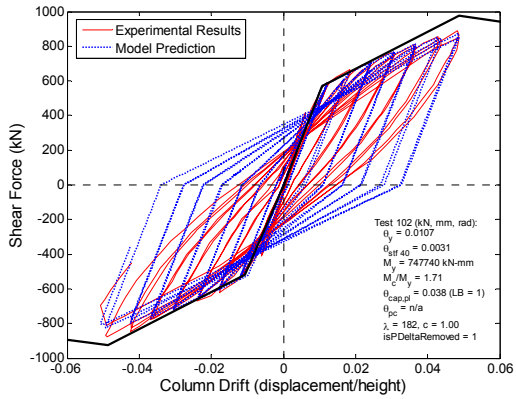
Experimental Results
Model Prediction
Shear Force (kN)
Column Drift (displacement/height)
Test 102 (kN, mm, rad):
θy = 0.0107
θstf 40 = 0.0031
My = 747740 kN-mm
Mc/My = 1.71
θcap,pl = 0.038 (LB = 1)
θpc = n/a
λ = 182, c = 1.00
isPDeltaRemoved = 1

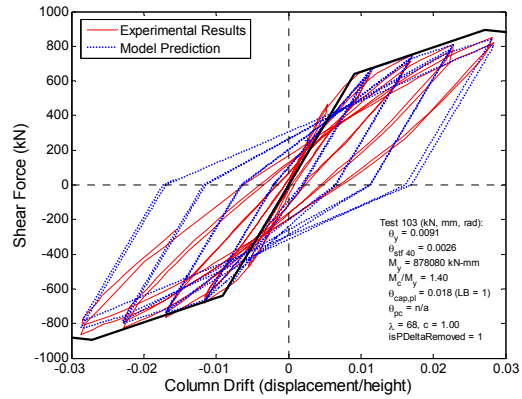
Experimental Results
Model Prediction
Shear Force (kN)
Column Drift (displacement/height)
Test 103 (kN, mm, rad):
θy = 0.0091
θstf 40 = 0.0026
My = 878080 kN-mm
Mc/My = 1.40
θcap,pl = 0.018 (LB = 1)
θpc = n/a
λ = 68, c = 1.00
isPDeltaRemoved = 1

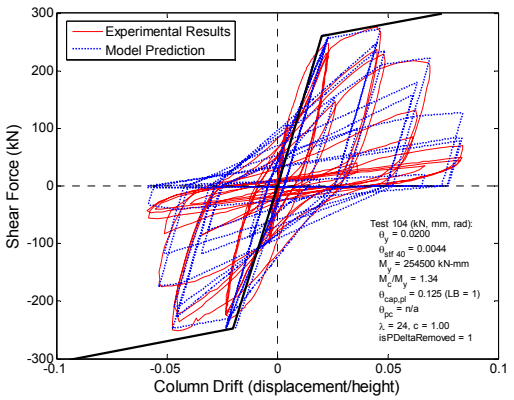
Experimental Results
Model Prediction
Shear Force (kN)
Column Drift (displacement/height)
Test 104 (kN, mm, rad):
θy = 0.0200
θstf 40 = 0.0044
My = 254500 kN-mm
Mc/My = 1.34
θcap,pl = 0.125 (LB = 1)
θpc = n/a
λ = 24, c = 1.00
isPDeltaRemoved = 1

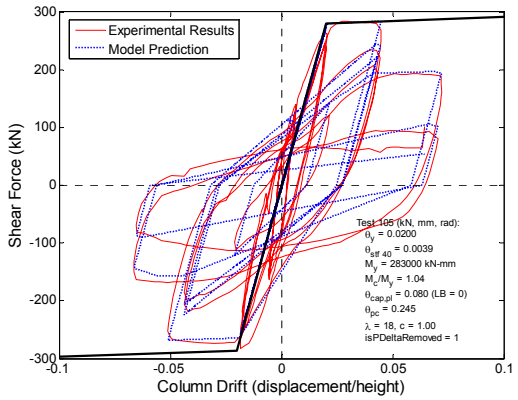
Experimental Results
Model Prediction
Shear Force (kN)
Column Drift (displacement/height)
Test 105 (kN, mm, rad):
θy = 0.0200
θstf 40 = 0.0039
My = 283000 kN-mm
Mc/My = 1.04
θcap,pl = 0.080 (LB = 0)
θpc = 0.245
λ = 18, c = 1.00
isPDeltaRemoved = 1

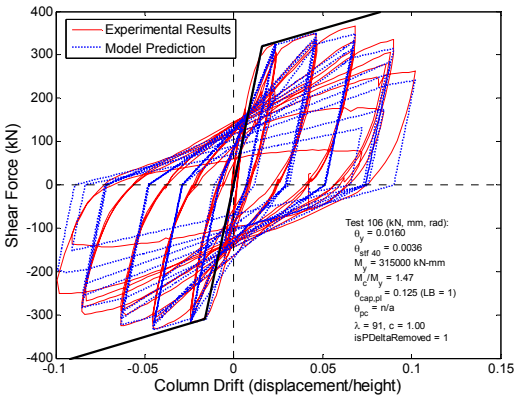
Experimental Results
Model Prediction
Shear Force (kN)
Column Drift (displacement/height)
Test 106 (kN, mm, rad):
θy = 0.0160
θstf 40 = 0.0036
My = 315000 kN-mm
Mc/My = 1.47
θcap,pl = 0.125 (LB = 1)
θpc = n/a
λ = 91, c = 1.00
isPDeltaRemoved = 1

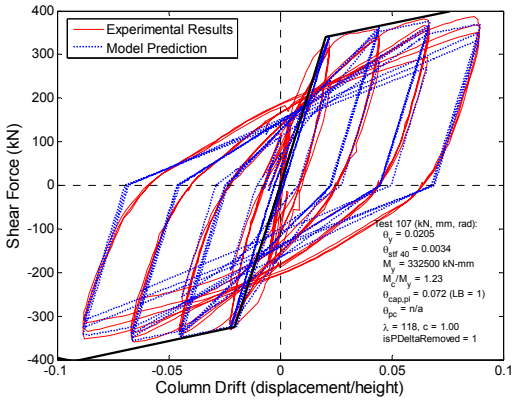
Experimental Results
Model Prediction
Shear Force (kN)
Column Drift (displacement/height)
Test 107 (kN, mm, rad):
θy = 0.0205
θstf 40 = 0.0034
My = 332500 kN-mm
Mc/My = 1.23
θcap,pl = 0.072 (LB = 1)
θpc = n/a
λ = 118, c = 1.00
isPDeltaRemoved = 1

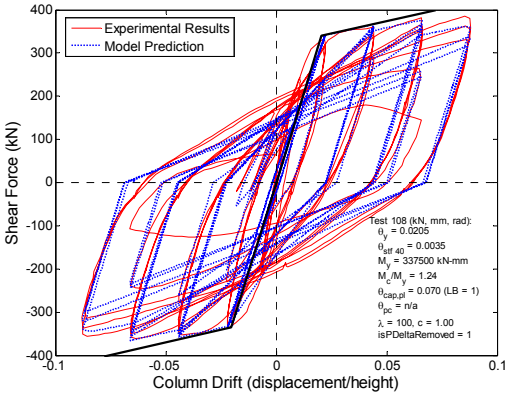
Experimental Results
Model Prediction
Shear Force (kN)
Column Drift (displacement/height)
Test 108 (kN, mm, rad):
θy = 0.0205
θstf 40 = 0.0035
My = 337500 kN-mm
Mc/My = 1.24
θcap,pl = 0.070 (LB = 1)
θpc = n/a
λ = 100, c = 1.00
isPDeltaRemoved = 1

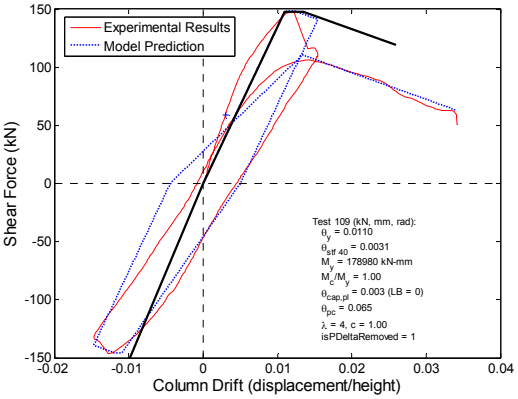
Experimental Results
Model Prediction
Shear Force (kN)
Column Drift (displacement/height)
Test 109 (kN, mm, rad):
θy = 0.0110
θstf 40 = 0.0031
My = 178980 kN-mm
Mc/My = 1.00
θcap,pl = 0.003 (LB = 0)
θpc = 0.065
λ = 4, c = 1.00
isPDeltaRemoved = 1

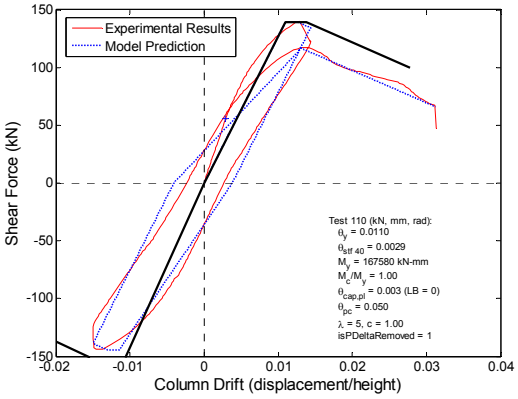
Experimental Results
Model Prediction
Shear Force (kN)
Column Drift (displacement/height)
Test 110 (kN, mm, rad):
θy = 0.0110
θstf 40 = 0.0029
My = 167580 kN-mm
Mc/My = 1.00
θcap,pl = 0.003 (LB = 0)
θpc = 0.050
λ = 5, c = 1.00
isPDeltaRemoved = 1

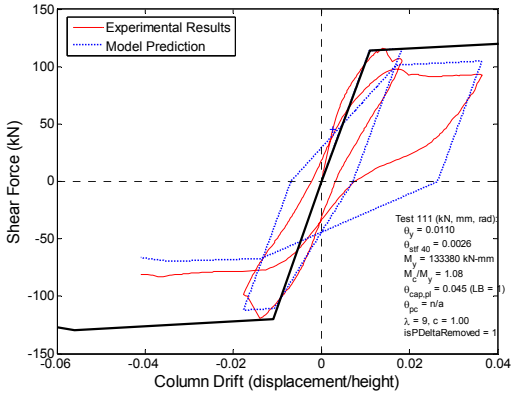
Experimental Results
Model Prediction
Shear Force (kN)
Column Drift (displacement/height)
Test 111 (kN, mm, rad):
θy = 0.0110
θstf 40 = 0.0026
My = 133380 kN-mm
Mc/My = 1.08
θcap,pl = 0.045 (LB = 0)
θpc = n/a
λ = 9, c = 1.00
isPDeltaRemoved = 1

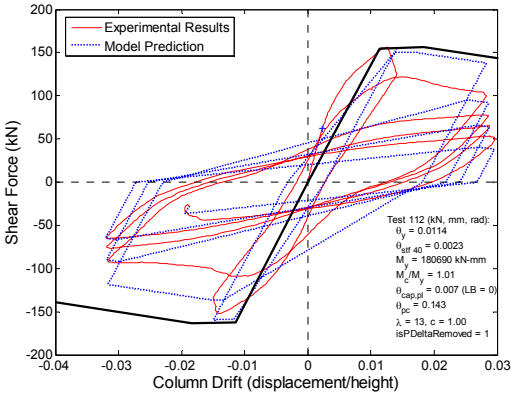
Experimental Results
Model Prediction
Shear Force (kN)
Column Drift (displacement/height)
Test 112 (kN, mm, rad):
θy = 0.0114
θstf 40 = 0.0023
My = 180690 kN-mm
Mc/My = 1.01
θcap,pl = 0.007 (LB = 0)
θpc = 0.143
λ = 13, c = 1.00
isPDeltaRemoved = 1

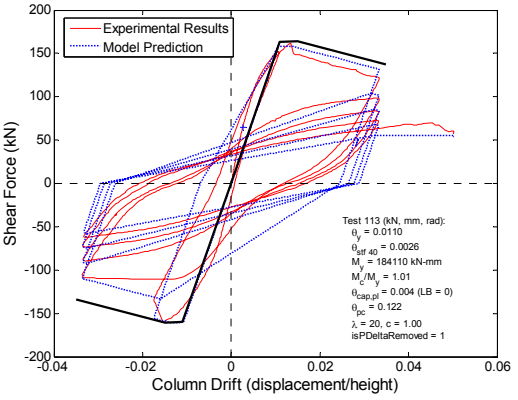
Experimental Results
Model Prediction
Shear Force (kN)
Column Drift (displacement/height)
Test 113 (kN, mm, rad):
θy = 0.0110
θstf 40 = 0.0026
My = 184110 kN-mm
Mc/My = 1.01
θcap,pl = 0.004 (LB = 0)
θpc = 0.122
λ = 20, c = 1.00
isPDeltaRemoved = 1

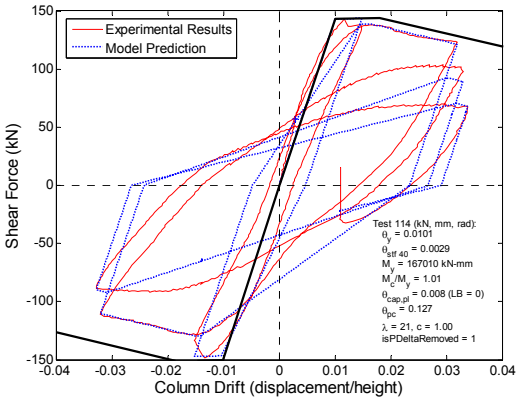
Experimental Results
Model Prediction
Shear Force (kN)
Column Drift (displacement/height)
Test 114 (kN, mm, rad):
θ_y = 0.0101
$\theta_{stf\ 40}$ = 0.0029
M_y = 167010 kN-mm
M_c/M_y = 1.01
$\theta_{cap,pl}$ = 0.008 (LB = 0)
θ_{pc} = 0.127
λ = 21, c = 1.00
isPDeltaRemoved = 1

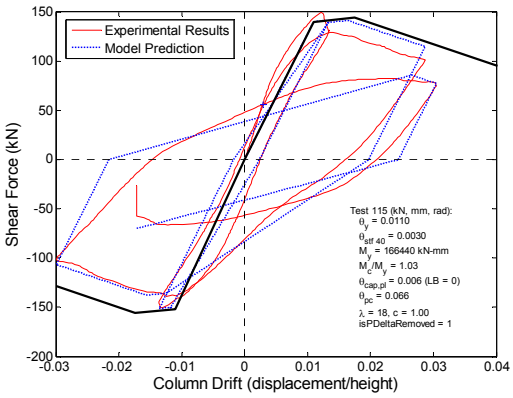
Experimental Results
Model Prediction
Shear Force (kN)
Column Drift (displacement/height)
Test 115 (kN, mm, rad):
θ_y = 0.0110
$\theta_{stf\ 40}$ = 0.0030
M_y = 166440 kN-mm
M_c/M_y = 1.03
$\theta_{cap,pl}$ = 0.006 (LB = 0)
θ_{pc} = 0.066
λ = 18, c = 1.00
isPDeltaRemoved = 1

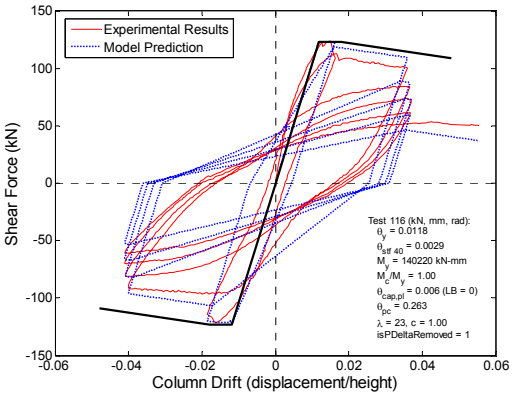
Experimental Results
Model Prediction
Shear Force (kN)
Column Drift (displacement/height)
Test 116 (kN, mm, rad):
θ_y = 0.0118
$\theta_{stf\ 40}$ = 0.0029
M_y = 140220 kN-mm
M_c/M_y = 1.00
$\theta_{cap,pl}$ = 0.006 (LB = 0)
θ_{pc} = 0.263
λ = 23, c = 1.00
isPDeltaRemoved = 1

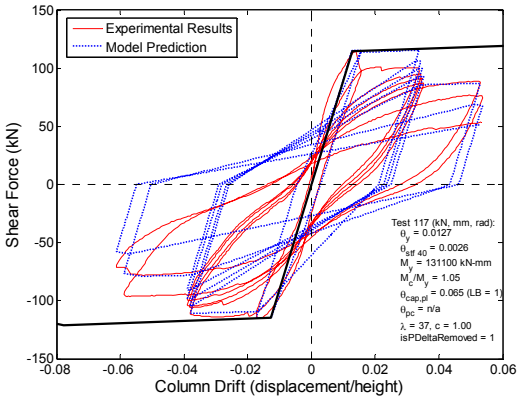
Experimental Results
Model Prediction
Shear Force (kN)
Column Drift (displacement/height)
Test 117 (kN, mm, rad):
θ_y = 0.0127
$\theta_{stf\ 40}$ = 0.0026
M_y = 131100 kN-mm
M_c/M_y = 1.05
$\theta_{cap,pl}$ = 0.065 (LB = 1)
θ_{pc} = n/a
λ = 37, c = 1.00
isPDeltaRemoved = 1

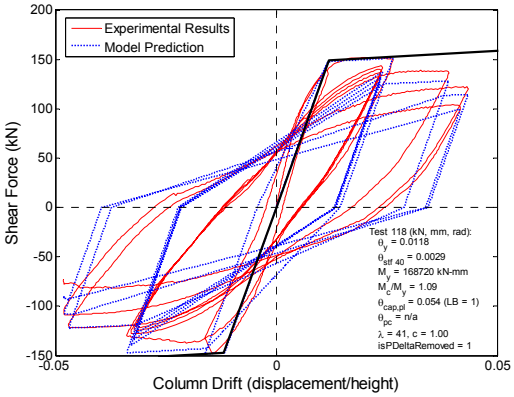
Experimental Results
Model Prediction
Shear Force (kN)
Column Drift (displacement/height)
Test 118 (kN, mm, rad):
θ_y = 0.0118
$\theta_{stf\ 40}$ = 0.0029
M_y = 168720 kN-mm
M_c/M_y = 1.09
$\theta_{cap,pl}$ = 0.054 (LB = 1)
θ_{pc} = n/a
λ = 41, c = 1.00
isPDeltaRemoved = 1

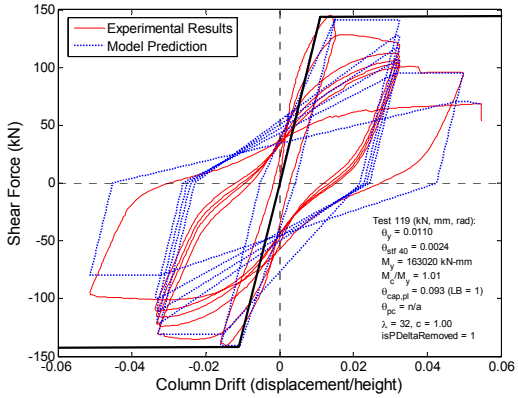
Experimental Results
Model Prediction
Shear Force (kN)
Column Drift (displacement/height)
Test 119 (kN, mm, rad):
θ_y = 0.0110
$\theta_{stf\ 40}$ = 0.0024
M_y = 163020 kN-mm
M_c/M_y = 1.01
$\theta_{cap,pl}$ = 0.093 (LB = 1)
θ_{pc} = n/a
λ = 32, c = 1.00
isPDeltaRemoved = 1

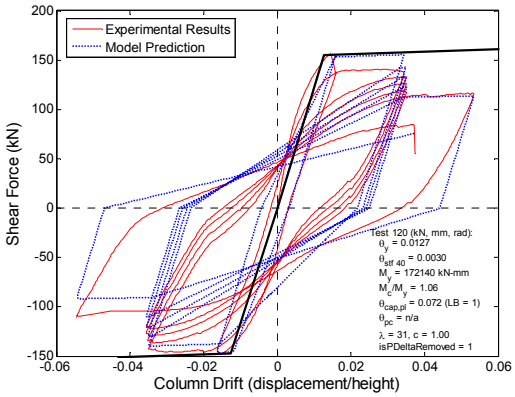
Experimental Results
Model Prediction
Shear Force (kN)
Column Drift (displacement/height)
Test 120 (kN, mm, rad):
θy = 0.0127
θstf 40 = 0.0030
My = 172140 kN-mm
Mc/My = 1.06
θcap,pl = 0.072 (LB = 1)
θpc = n/a
λ = 31, c = 1.00
isPDeltaRemoved = 1

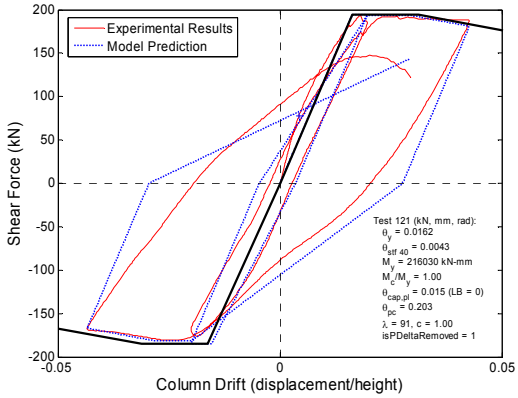
Experimental Results
Model Prediction
Shear Force (kN)
Column Drift (displacement/height)
Test 121 (kN, mm, rad):
θy = 0.0162
θstf 40 = 0.0043
My = 216030 kN-mm
Mc/My = 1.00
θcap,pl = 0.015 (LB = 0)
θpc = 0.203
λ = 91, c = 1.00
isPDeltaRemoved = 1

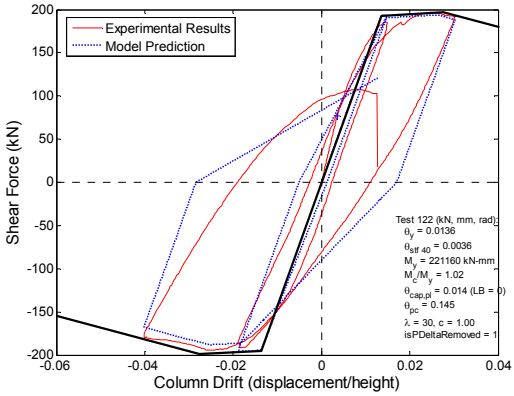
Experimental Results
Model Prediction
Shear Force (kN)
Column Drift (displacement/height)
Test 122 (kN, mm, rad):
θy = 0.0136
θstf 40 = 0.0036
My = 221160 kN-mm
Mc/My = 1.02
θcap,pl = 0.014 (LB = 0)
θpc = 0.145
λ = 30, c = 1.00
isPDeltaRemoved = 1

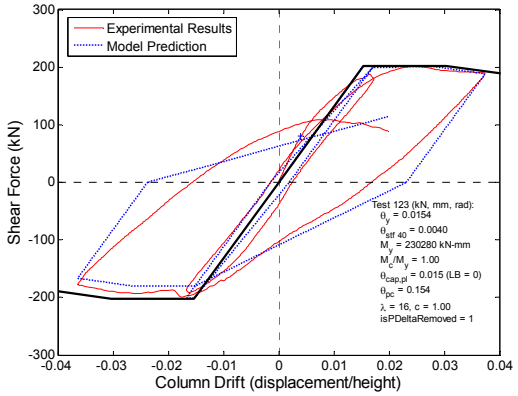
Experimental Results
Model Prediction
Shear Force (kN)
Column Drift (displacement/height)
Test 123 (kN, mm, rad):
θy = 0.0154
θstf 40 = 0.0040
My = 230280 kN-mm
Mc/My = 1.00
θcap,pl = 0.015 (LB = 0)
θpc = 0.154
λ = 16, c = 1.00
isPDeltaRemoved = 1

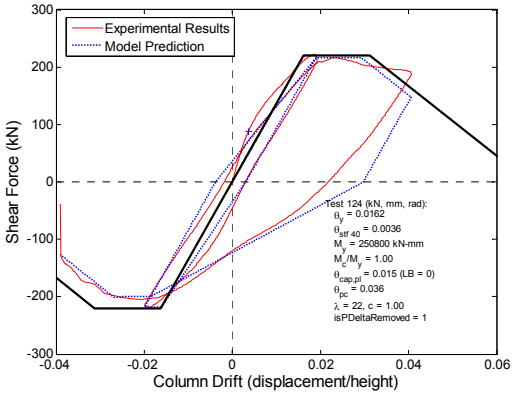
Experimental Results
Model Prediction
Shear Force (kN)
Column Drift (displacement/height)
Test 124 (kN, mm, rad):
θy = 0.0162
θstf 40 = 0.0036
My = 250800 kN-mm
Mc/My = 1.00
θcap,pl = 0.015 (LB = 0)
θpc = 0.036
λ = 22, c = 1.00
isPDeltaRemoved = 1

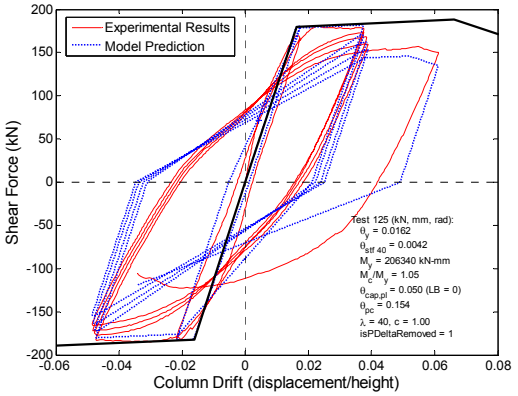
Experimental Results
Model Prediction
Shear Force (kN)
Column Drift (displacement/height)
Test 125 (kN, mm, rad):
θy = 0.0162
θstf 40 = 0.0042
My = 206340 kN-mm
Mc/My = 1.05
θcap,pl = 0.050 (LB = 0)
θpc = 0.154
λ = 40, c = 1.00
isPDeltaRemoved = 1

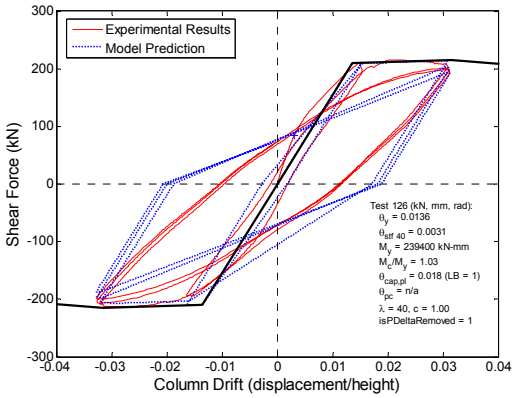
Experimental Results
Model Prediction
Shear Force (kN)
Column Drift (displacement/height)
Test 126 (kN, mm, rad):
θy = 0.0136
θstf 40 = 0.0031
My = 239400 kN-mm
Mc/My = 1.03
θcap,pl = 0.018 (LB = 1)
θpc = n/a
λ = 40, c = 1.00
isPDeltaRemoved = 1

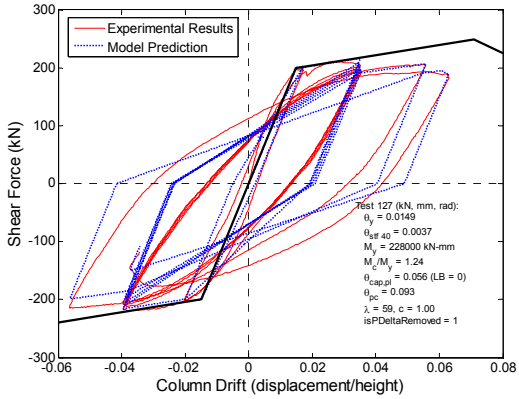
Experimental Results
Model Prediction
Shear Force (kN)
Column Drift (displacement/height)
Test 127 (kN, mm, rad):
θy = 0.0149
θstf 40 = 0.0037
My = 228000 kN-mm
Mc/My = 1.24
θcap,pl = 0.056 (LB = 0)
θpc = 0.093
λ = 59, c = 1.00
isPDeltaRemoved = 1

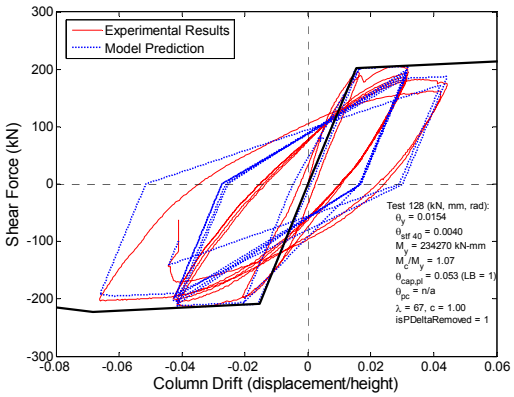
Experimental Results
Model Prediction
Shear Force (kN)
Column Drift (displacement/height)
Test 128 (kN, mm, rad):
θy = 0.0154
θstf 40 = 0.0040
My = 234270 kN-mm
Mc/My = 1.07
θcap,pl = 0.053 (LB = 1)
θpc = n/a
λ = 67, c = 1.00
isPDeltaRemoved = 1

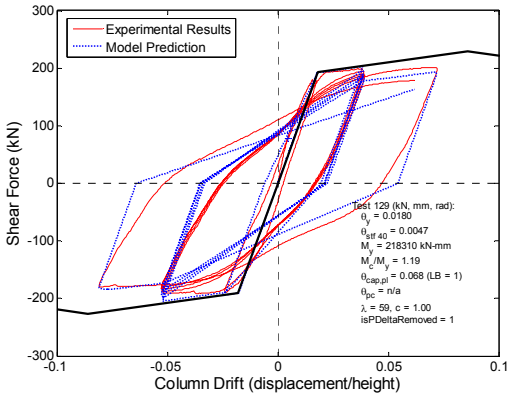
Experimental Results
Model Prediction
Shear Force (kN)
Column Drift (displacement/height)
Test 129 (kN, mm, rad):
θy = 0.0180
θstf 40 = 0.0047
My = 218310 kN-mm
Mc/My = 1.19
θcap,pl = 0.068 (LB = 1)
θpc = n/a
λ = 59, c = 1.00
isPDeltaRemoved = 1

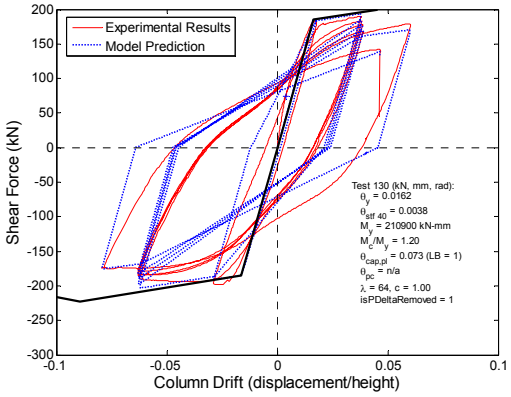
Experimental Results
Model Prediction
Shear Force (kN)
Column Drift (displacement/height)
Test 130 (kN, mm, rad):
θy = 0.0162
θstf 40 = 0.0038
My = 210900 kN-mm
Mc/My = 1.20
θcap,pl = 0.073 (LB = 1)
θpc = n/a
λ = 64, c = 1.00
isPDeltaRemoved = 1

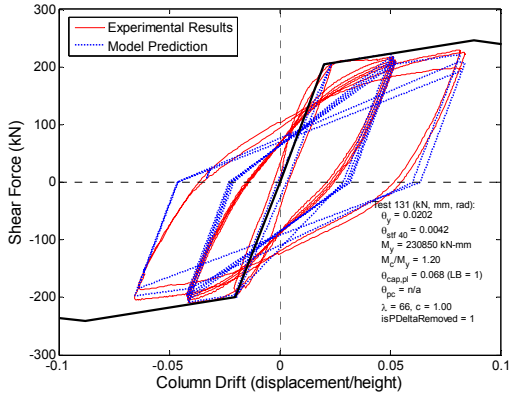
Experimental Results
Model Prediction
Shear Force (kN)
Column Drift (displacement/height)
Test 131 (kN, mm, rad):
θy = 0.0202
θstf 40 = 0.0042
My = 230850 kN-mm
Mc/My = 1.20
θcap,pl = 0.068 (LB = 1)
θpc = n/a
λ = 66, c = 1.00
isPDeltaRemoved = 1

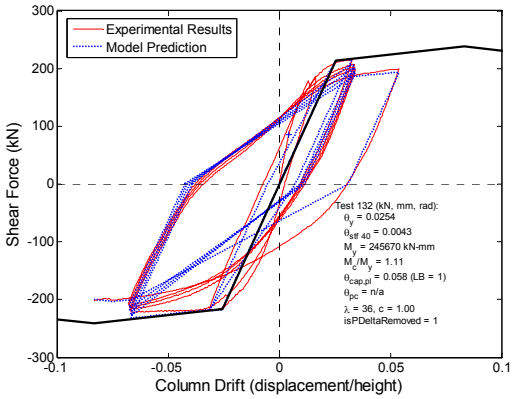
Experimental Results
Model Prediction
Shear Force (kN)
Column Drift (displacement/height)
Test 132 (kN, mm, rad):
θy = 0.0254
θstf 40 = 0.0043
My = 245670 kN-mm
Mc/My = 1.11
θcap,pl = 0.058 (LB = 1)
θpc = n/a
λ = 36, c = 1.00
isPDeltaRemoved = 1

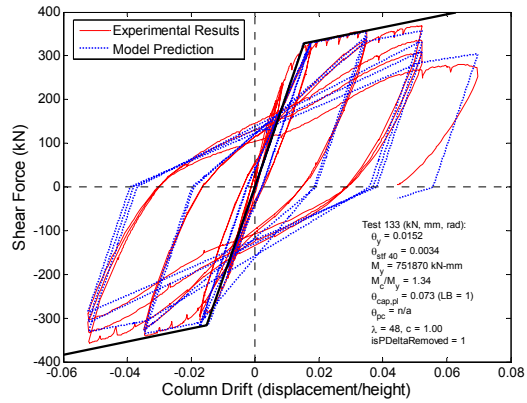
Experimental Results
Model Prediction
Shear Force (kN)
Column Drift (displacement/height)
Test 133 (kN, mm, rad):
θy = 0.0152
θstf 40 = 0.0034
My = 751870 kN-mm
Mc/My = 1.34
θcap,pl = 0.073 (LB = 1)
θpc = n/a
λ = 48, c = 1.00
isPDeltaRemoved = 1

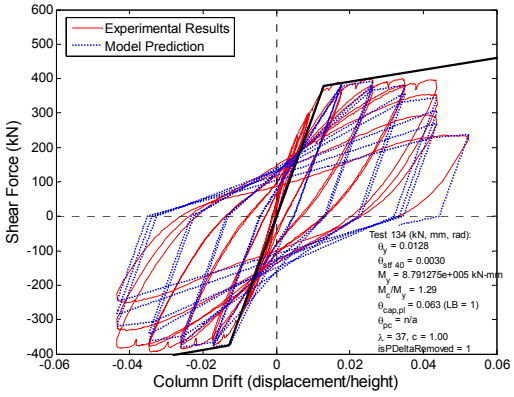
Experimental Results
Model Prediction
Shear Force (kN)
Column Drift (displacement/height)
Test 134 (kN, mm, rad):
θy = 0.0128
θstf 40 = 0.0030
My = 8.791275e+005 kN-mm
Mc/My = 1.29
θcap,pl = 0.063 (LB = 1)
θpc = n/a
λ = 37, c = 1.00
isPDeltaRemoved = 1

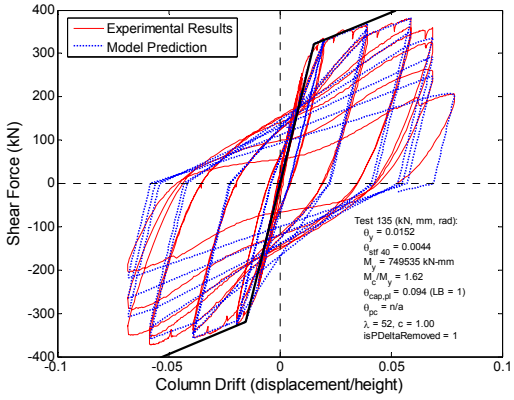
Experimental Results
Model Prediction
Shear Force (kN)
Column Drift (displacement/height)
Test 135 (kN, mm, rad):
θy = 0.0152
θstf 40 = 0.0044
My = 749535 kN-mm
Mc/My = 1.62
θcap,pl = 0.094 (LB = 1)
θpc = n/a
λ = 52, c = 1.00
isPDeltaRemoved = 1

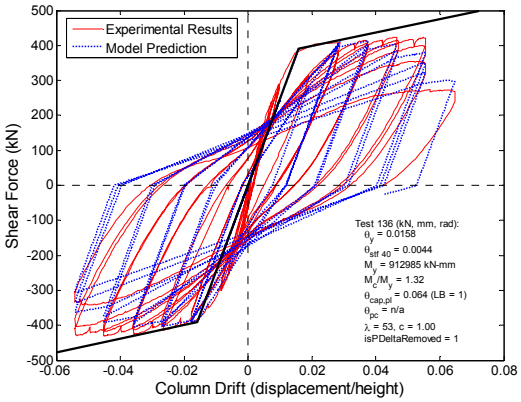
Experimental Results
Model Prediction
Shear Force (kN)
Column Drift (displacement/height)
Test 136 (kN, mm, rad):
θy = 0.0158
θstf 40 = 0.0044
My = 912985 kN-mm
Mc/My = 1.32
θcap,pl = 0.064 (LB = 1)
θpc = n/a
λ = 53, c = 1.00
isPDeltaRemoved = 1

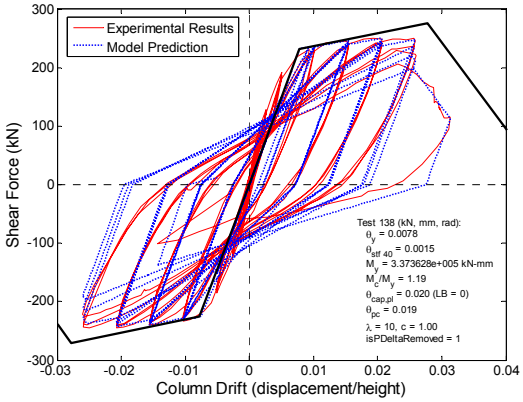
Experimental Results
Model Prediction
Shear Force (kN)
Column Drift (displacement/height)
Test 138 (kN, mm, rad):
θy = 0.0078
θstf 40 = 0.0015
My = 3.373628e+005 kN-mm
Mc/My = 1.19
θcap,pl = 0.020 (LB = 0)
θpc = 0.019
λ = 10, c = 1.00
isPDeltaRemoved = 1

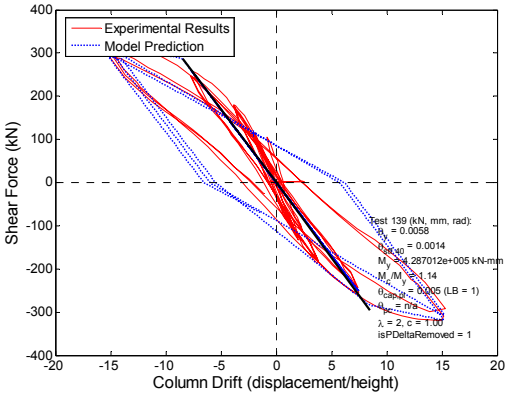
Experimental Results
Model Prediction
Shear Force (kN)
Column Drift (displacement/height)
Test 139 (kN, mm, rad):
θy = 0.0058
θstf 40 = 0.0014
My = 4.287012e+005 kN-mm
Mc/My = 1.14
θcap,pl = 0.005 (LB = 1)
θpc = n/a
λ = 2, c = 1.00
isPDeltaRemoved = 1

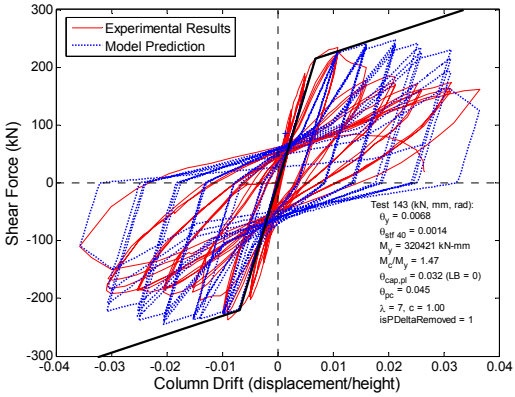
Experimental Results
Model Prediction
Shear Force (kN)
Column Drift (displacement/height)
Test 143 (kN, mm, rad):
θy = 0.0068
θstf 40 = 0.0014
My = 320421 kN-mm
Mc/My = 1.47
θcap,pl = 0.032 (LB = 0)
θpc = 0.045
λ = 7, c = 1.00
isPDeltaRemoved = 1

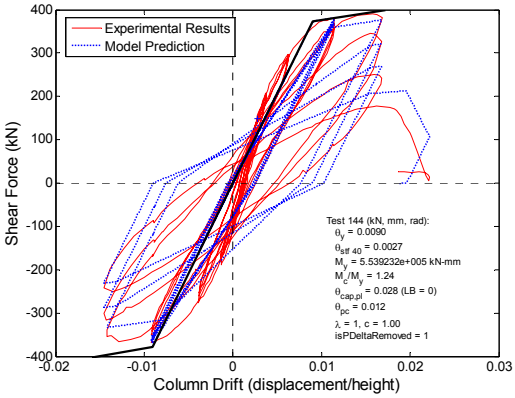
Experimental Results
Model Prediction
Shear Force (kN)
Column Drift (displacement/height)
Test 144 (kN, mm, rad):
θy = 0.0090
θstf 40 = 0.0027
My = 5.539232e+005 kN-mm
Mc/My = 1.24
θcap,pl = 0.028 (LB = 0)
θpc = 0.012
λ = 1, c = 1.00
isPDeltaRemoved = 1

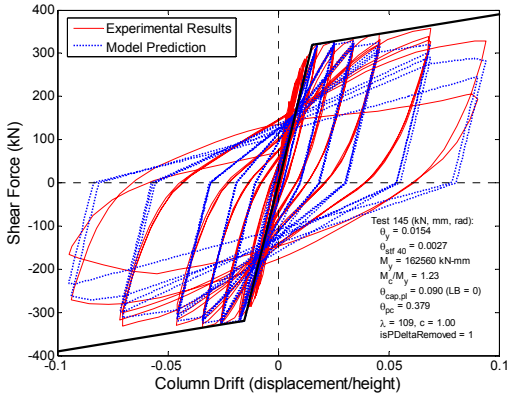
Experimental Results
Model Prediction
Shear Force (kN)
Column Drift (displacement/height)
Test 145 (kN, mm, rad):
θy = 0.0154
θstf 40 = 0.0027
My = 162560 kN-mm
Mc/My = 1.23
θcap,pl = 0.090 (LB = 0)
θpc = 0.379
λ = 109, c = 1.00
isPDeltaRemoved = 1

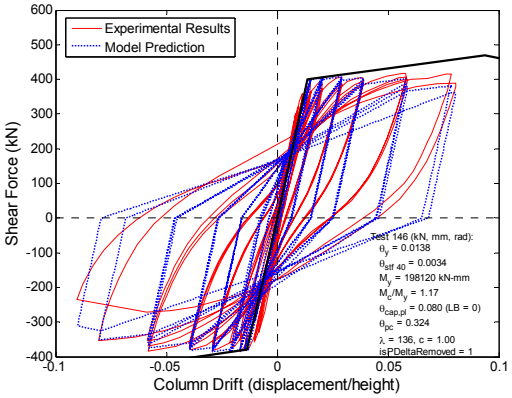
Experimental Results
Model Prediction
Shear Force (kN)
Column Drift (displacement/height)
Test 146 (kN, mm, rad):
θy = 0.0138
θstf 40 = 0.0034
My = 198120 kN-mm
Mc/My = 1.17
θcap,pl = 0.080 (LB = 0)
θpc = 0.324
λ = 136, c = 1.00
isPDeltaRemoved = 1

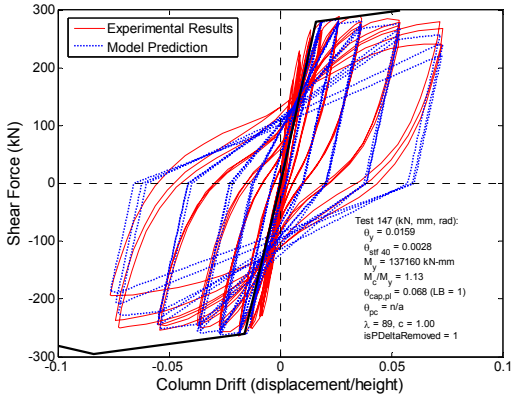
Experimental Results
Model Prediction
Shear Force (kN)
Column Drift (displacement/height)
Test 147 (kN, mm, rad):
θy = 0.0159
θstf 40 = 0.0028
My = 137160 kN-mm
Mc/My = 1.13
θcap,pl = 0.068 (LB = 1)
θpc = n/a
λ = 89, c = 1.00
isPDeltaRemoved = 1

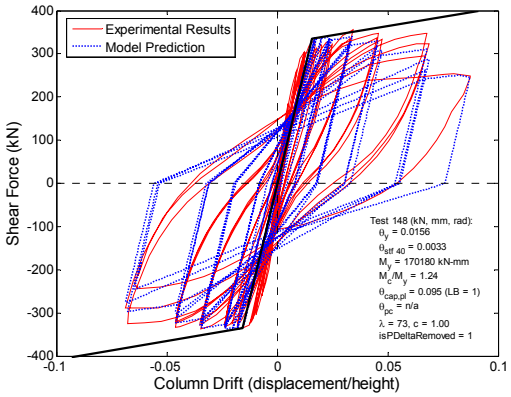
Experimental Results
Model Prediction
Shear Force (kN)
Column Drift (displacement/height)
Test 148 (kN, mm, rad):
θy = 0.0156
θstf 40 = 0.0033
My = 170180 kN-mm
Mc/My = 1.24
θcap,pl = 0.095 (LB = 1)
θpc = n/a
λ = 73, c = 1.00
isPDeltaRemoved = 1

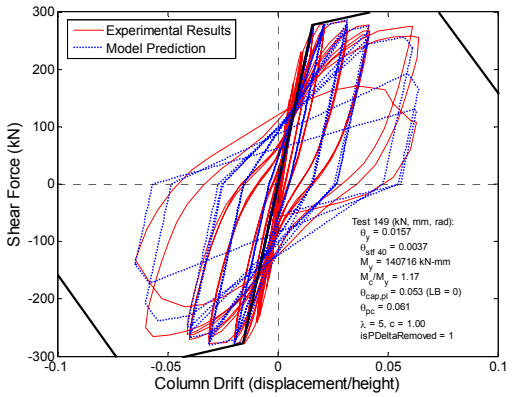
Experimental Results
Model Prediction
Shear Force (kN)
Column Drift (displacement/height)
Test 149 (kN, mm, rad):
θy = 0.0157
θstf 40 = 0.0037
My = 140716 kN-mm
Mc/My = 1.17
θcap,pl = 0.053 (LB = 0)
θpc = 0.061
λ = 5, c = 1.00
isPDeltaRemoved = 1

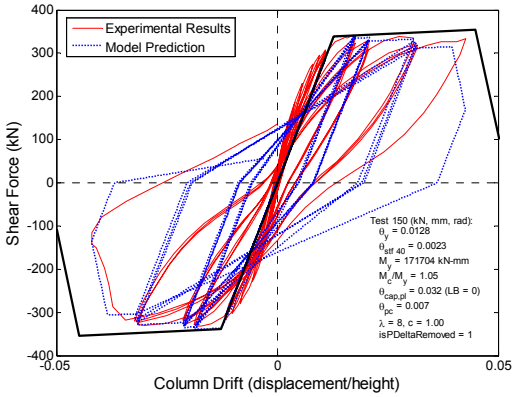
Experimental Results
Model Prediction
Shear Force (kN)
Column Drift (displacement/height)
Test 150 (kN, mm, rad):
θy = 0.0128
θstf 40 = 0.0023
My = 171704 kN-mm
Mc/My = 1.05
θcap,pl = 0.032 (LB = 0)
θpc = 0.007
λ = 8, c = 1.00
isPDeltaRemoved = 1

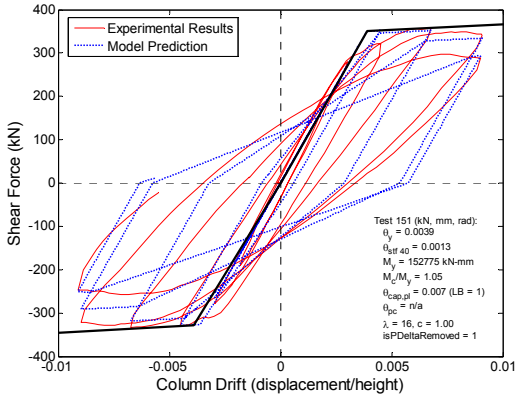
Experimental Results
Model Prediction
Shear Force (kN)
Column Drift (displacement/height)
Test 151 (kN, mm, rad):
θy = 0.0039
θstf 40 = 0.0013
My = 152775 kN-mm
Mc/My = 1.05
θcap,pl = 0.007 (LB = 1)
θpc = n/a
λ = 16, c = 1.00
isPDeltaRemoved = 1

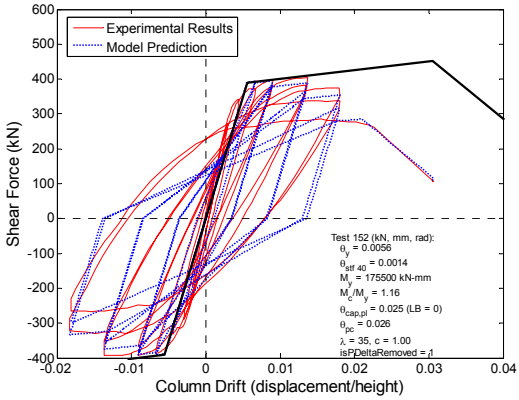
Experimental Results
Model Prediction
Shear Force (kN)
Column Drift (displacement/height)
Test 152 (kN, mm, rad):
θy = 0.0056
θstf 40 = 0.0014
My = 175500 kN-mm
Mc/My = 1.16
θcap,pl = 0.025 (LB = 0)
θpc = 0.026
λ = 35, c = 1.00
isPDeltaRemoved = 1

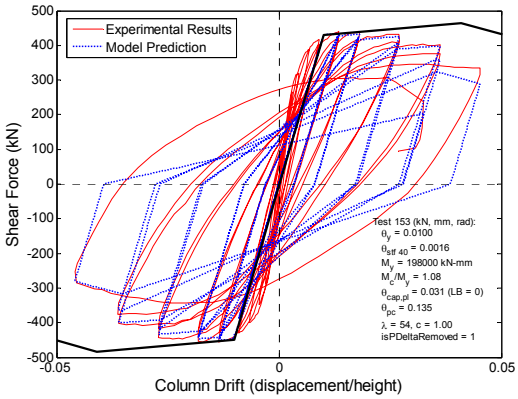
Experimental Results
Model Prediction
Shear Force (kN)
Column Drift (displacement/height)
Test 153 (kN, mm, rad):
θy = 0.0100
θstf 40 = 0.0016
My = 198000 kN-mm
Mc/My = 1.08
θcap,pl = 0.031 (LB = 0)
θpc = 0.135
λ = 54, c = 1.00
isPDeltaRemoved = 1

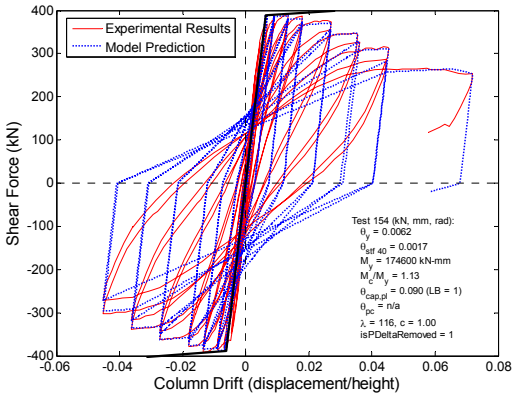
Experimental Results
Model Prediction
Shear Force (kN)
Column Drift (displacement/height)
Test 154 (kN, mm, rad):
θy = 0.0062
θstf 40 = 0.0017
My = 174600 kN-mm
Mc/My = 1.13
θcap,pl = 0.090 (LB = 1)
θpc = n/a
λ = 116, c = 1.00
isPDeltaRemoved = 1

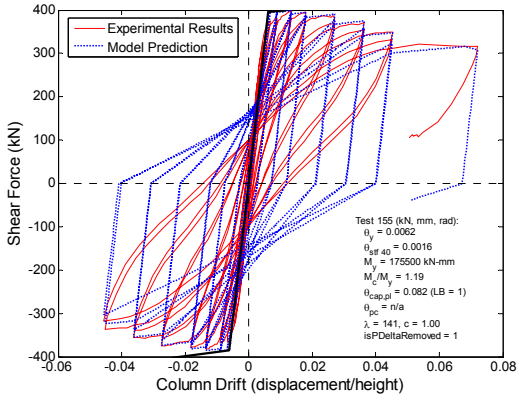
Experimental Results
Model Prediction
Shear Force (kN)
Column Drift (displacement/height)
Test 155 (kN, mm, rad):
θy = 0.0062
θstf 40 = 0.0016
My = 175500 kN-mm
Mc/My = 1.19
θcap,pl = 0.082 (LB = 1)
θpc = n/a
λ = 141, c = 1.00
isPDeltaRemoved = 1

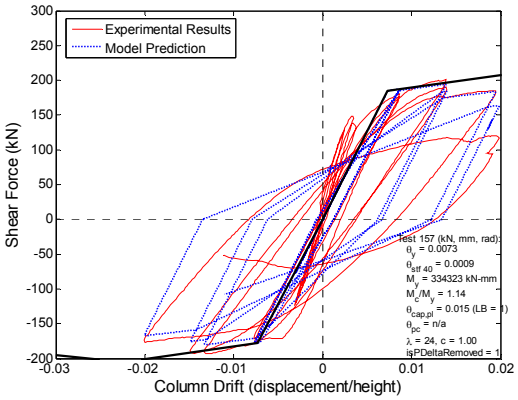
Experimental Results
Model Prediction
Shear Force (kN)
Column Drift (displacement/height)
Test 157 (kN, mm, rad):
θy = 0.0073
θstf 40 = 0.0009
My = 334323 kN-mm
Mc/My = 1.14
θcap,pl = 0.015 (LB = 0)
θpc = n/a
λ = 24, c = 1.00
isPDeltaRemoved = 1

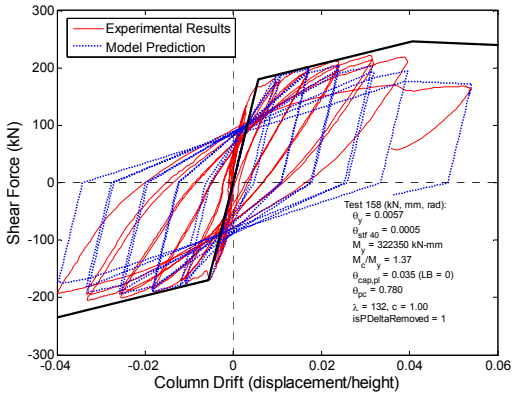
Experimental Results
Model Prediction
Shear Force (kN)
Column Drift (displacement/height)
Test 158 (kN, mm, rad):
θy = 0.0057
θstf 40 = 0.0005
My = 322350 kN-mm
Mc/My = 1.37
θcap,pl = 0.035 (LB = 0)
θpc = 0.780
λ = 132, c = 1.00
isPDeltaRemoved = 1

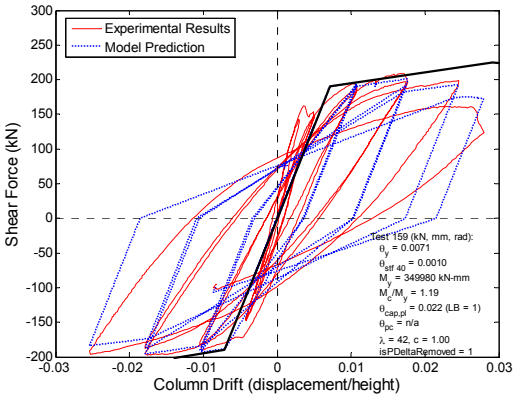
Experimental Results
Model Prediction
Shear Force (kN)
Column Drift (displacement/height)
Test 159 (kN, mm, rad):
θy = 0.0071
θstf 40 = 0.0010
My = 349980 kN-mm
Mc/My = 1.19
θcap,pl = 0.022 (LB = 1)
θpc = n/a
λ = 42, c = 1.00
isPDeltaRemoved = 1

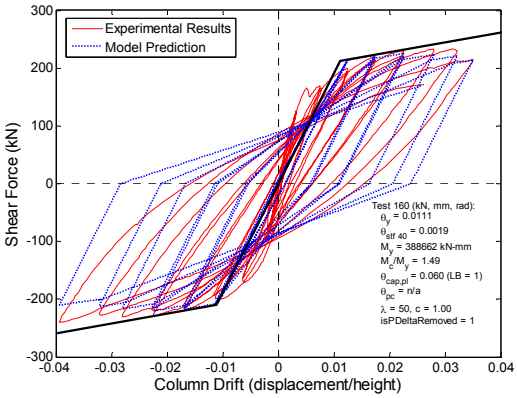
Experimental Results
Model Prediction
Shear Force (kN)
Column Drift (displacement/height)
Test 160 (kN, mm, rad):
θy = 0.0111
θstf 40 = 0.0019
My = 388662 kN-mm
Mc/My = 1.49
θcap,pl = 0.060 (LB = 1)
θpc = n/a
λ = 50, c = 1.00
isPDeltaRemoved = 1

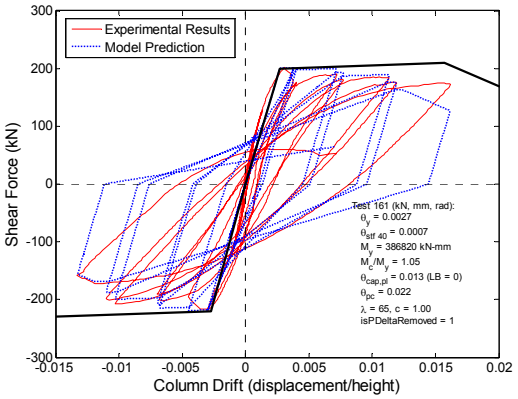
Experimental Results
Model Prediction
Shear Force (kN)
Column Drift (displacement/height)
Test 161 (kN, mm, rad):
θy = 0.0027
θstf 40 = 0.0007
My = 386820 kN-mm
Mc/My = 1.05
θcap,pl = 0.013 (LB = 0)
θpc = 0.022
λ = 65, c = 1.00
isPDeltaRemoved = 1

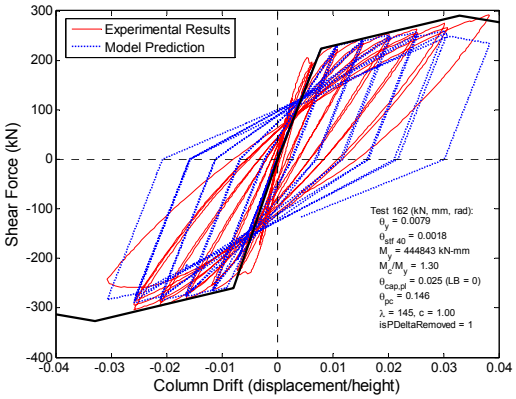
Experimental Results
Model Prediction
Shear Force (kN)
Column Drift (displacement/height)
Test 162 (kN, mm, rad):
θy = 0.0079
θstf 40 = 0.0018
My = 444843 kN-mm
Mc/My = 1.30
θcap,pl = 0.025 (LB = 0)
θpc = 0.146
λ = 145, c = 1.00
isPDeltaRemoved = 1

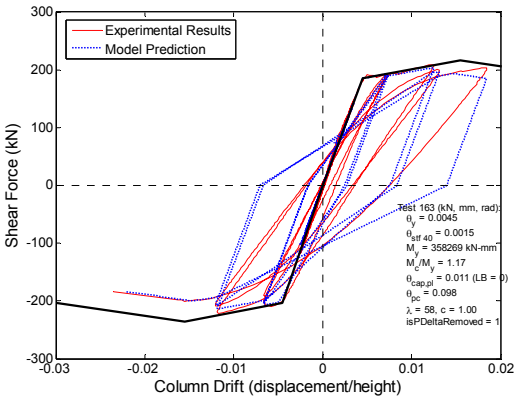
Experimental Results
Model Prediction
Shear Force (kN)
Column Drift (displacement/height)
Test 163 (kN, mm, rad):
θy = 0.0045
θstf 40 = 0.0015
My = 358269 kN-mm
Mc/My = 1.17
θcap,pl = 0.011 (LB = 0)
θpc = 0.098
λ = 58, c = 1.00
isPDeltaRemoved = 1

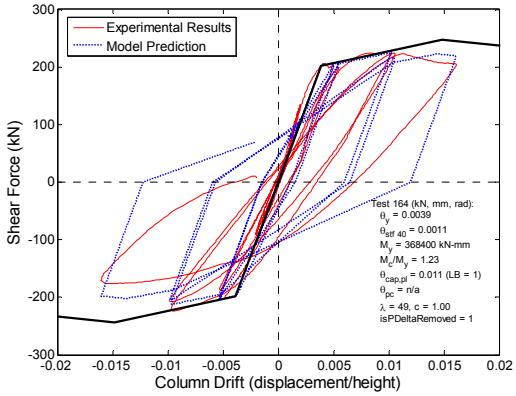
Experimental Results
Model Prediction
Shear Force (kN)
Column Drift (displacement/height)
Test 164 (kN, mm, rad):
θy = 0.0039
θstf 40 = 0.0011
My = 368400 kN-mm
Mc/My = 1.23
θcap,pl = 0.011 (LB = 1)
θpc = n/a
λ = 49, c = 1.00
isPDeltaRemoved = 1

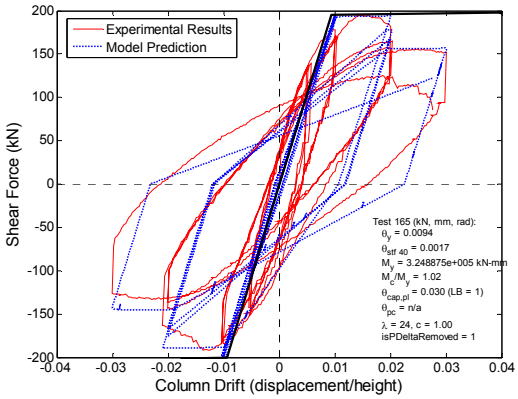
Experimental Results
Model Prediction
Test 165 (kN, mm, rad):
θy = 0.0094
θstf 40 = 0.0017
My = 3.248875e+005 kN-mm
Mc/My = 1.02
θcap,pl = 0.030 (LB = 1)
θpc = n/a
λ = 24, c = 1.00
isPDeltaRemoved = 1
Shear Force (kN)
Column Drift (displacement/height)

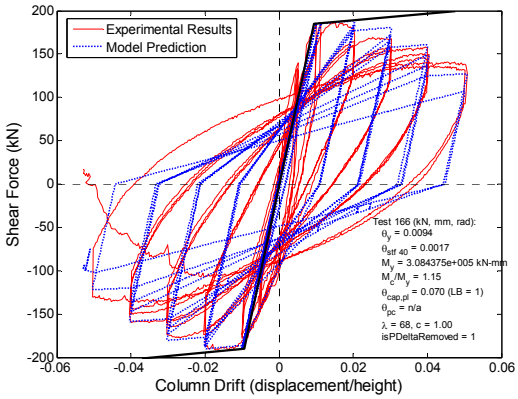
Experimental Results
Model Prediction
Test 166 (kN, mm, rad):
θy = 0.0094
θstf 40 = 0.0017
My = 3.084375e+005 kN-mm
Mc/My = 1.15
θcap,pl = 0.070 (LB = 1)
θpc = n/a
λ = 68, c = 1.00
isPDeltaRemoved = 1
Shear Force (kN)
Column Drift (displacement/height)

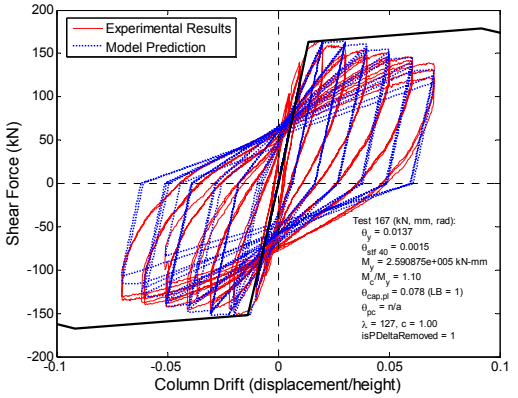
Experimental Results
Model Prediction
Test 167 (kN, mm, rad):
θy = 0.0137
θstf 40 = 0.0015
My = 2.590875e+005 kN-mm
Mc/My = 1.10
θcap,pl = 0.078 (LB = 1)
θpc = n/a
λ = 127, c = 1.00
isPDeltaRemoved = 1
Shear Force (kN)
Column Drift (displacement/height)

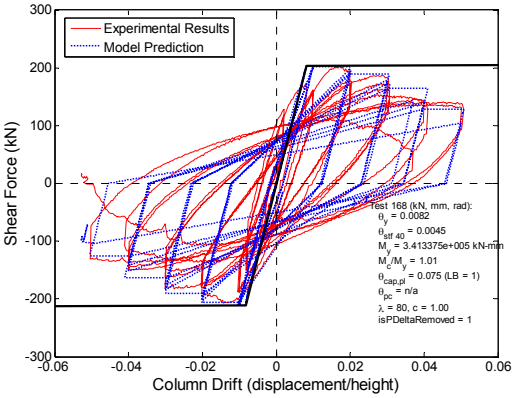
Experimental Results
Model Prediction
Test 168 (kN, mm, rad):
θy = 0.0082
θstf 40 = 0.0045
My = 3.413375e+005 kN-mm
Mc/My = 1.01
θcap,pl = 0.075 (LB = 1)
θpc = n/a
λ = 80, c = 1.00
isPDeltaRemoved = 1
Shear Force (kN)
Column Drift (displacement/height)

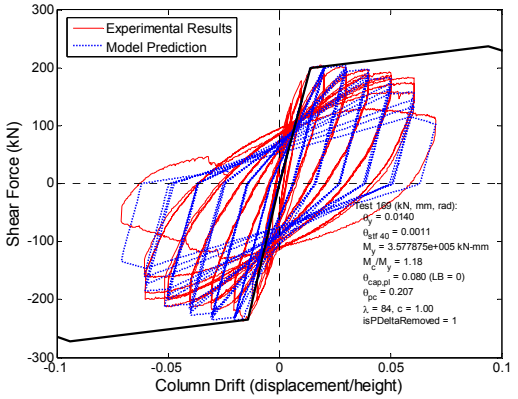
Experimental Results
Model Prediction
Test 169 (kN, mm, rad):
θy = 0.0140
θstf 40 = 0.0011
My = 3.577875e+005 kN-mm
Mc/My = 1.18
θcap,pl = 0.080 (LB = 0)
θpc = 0.207
λ = 84, c = 1.00
isPDeltaRemoved = 1
Shear Force (kN)
Column Drift (displacement/height)

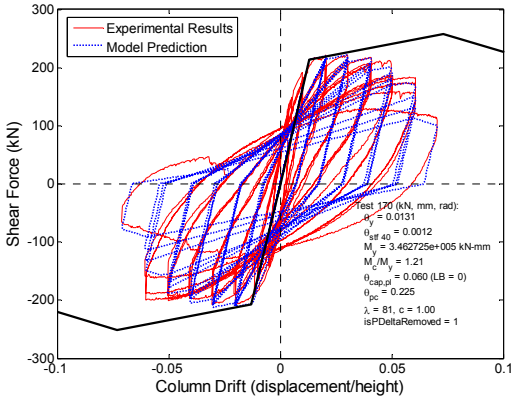
Experimental Results
Model Prediction
Test 170 (kN, mm, rad):
θy = 0.0131
θstf 40 = 0.0012
My = 3.462725e+005 kN-mm
Mc/My = 1.21
θcap,pl = 0.060 (LB = 0)
θpc = 0.225
λ = 81, c = 1.00
isPDeltaRemoved = 1
Shear Force (kN)
Column Drift (displacement/height)

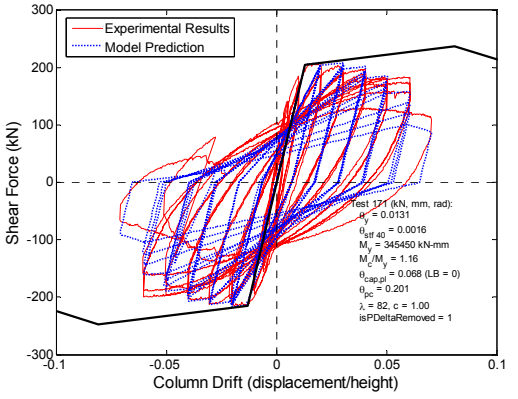
Experimental Results
Model Prediction
Test 171 (kN, mm, rad):
θy = 0.0131
θstf 40 = 0.0016
My = 345450 kN-mm
Mc/My = 1.16
θcap,pl = 0.068 (LB = 0)
θpc = 0.201
λ = 82, c = 1.00
isPDeltaRemoved = 1
Shear Force (kN)
Column Drift (displacement/height)

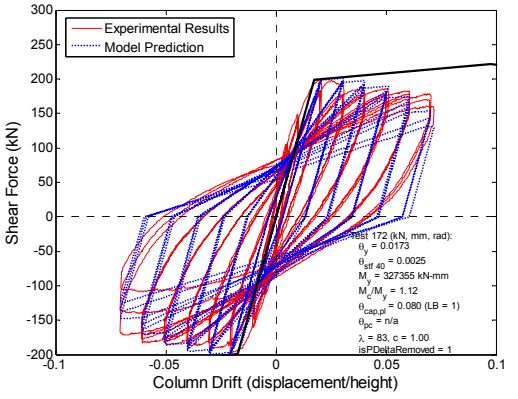
Experimental Results
Model Prediction
Test 172 (kN, mm, rad):
θy = 0.0173
θstf 40 = 0.0025
My = 327355 kN-mm
Mc/My = 1.12
θcap,pl = 0.080 (LB = 1)
θpc = n/a
λ = 83, c = 1.00
isPDeltaRemoved = 1
Shear Force (kN)
Column Drift (displacement/height)

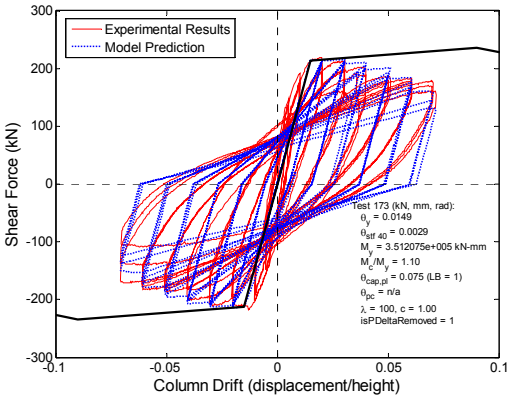
Experimental Results
Model Prediction
Shear Force (kN)
Column Drift (displacement/height)
Test 173 (kN, mm, rad):
θy = 0.0149
θstf 40 = 0.0029
My = 3.512075e+005 kN-mm
Mc/My = 1.10
θcap,pl = 0.075 (LB = 1)
θpc = n/a
λ = 100, c = 1.00
isPDeltaRemoved = 1

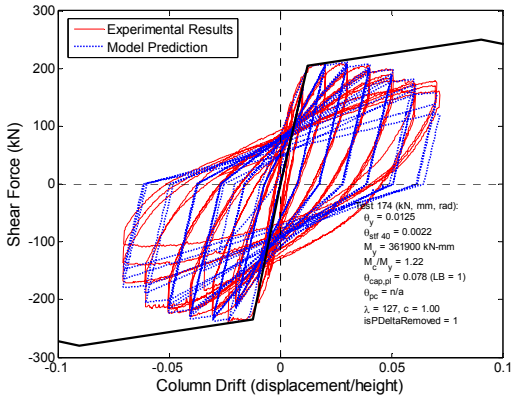
Experimental Results
Model Prediction
Shear Force (kN)
Column Drift (displacement/height)
Test 174 (kN, mm, rad):
θy = 0.0125
θstf 40 = 0.0022
My = 361900 kN-mm
Mc/My = 1.22
θcap,pl = 0.078 (LB = 1)
θpc = n/a
λ = 127, c = 1.00
isPDeltaRemoved = 1

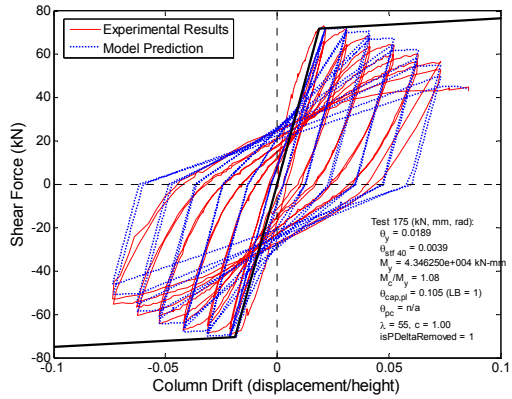
Experimental Results
Model Prediction
Shear Force (kN)
Column Drift (displacement/height)
Test 175 (kN, mm, rad):
θy = 0.0189
θstf 40 = 0.0039
My = 4.346250e+004 kN-mm
Mc/My = 1.08
θcap,pl = 0.105 (LB = 1)
θpc = n/a
λ = 55, c = 1.00
isPDeltaRemoved = 1

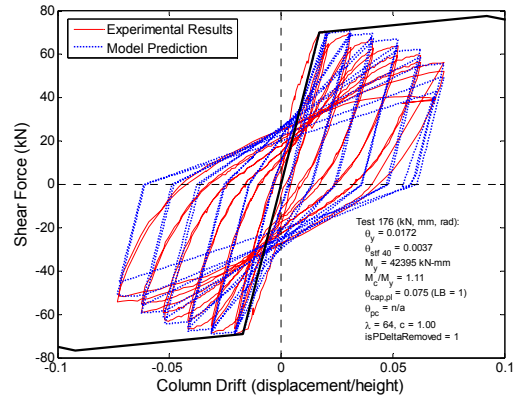
Experimental Results
Model Prediction
Shear Force (kN)
Column Drift (displacement/height)
Test 176 (kN, mm, rad):
θy = 0.0172
θstf 40 = 0.0037
My = 42395 kN-mm
Mc/My = 1.11
θcap,pl = 0.075 (LB = 1)
θpc = n/a
λ = 64, c = 1.00
isPDeltaRemoved = 1

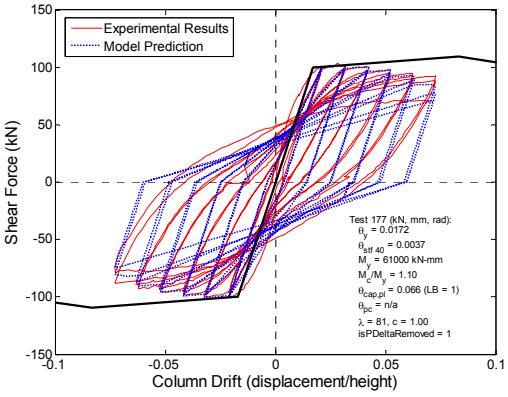
Experimental Results
Model Prediction
Shear Force (kN)
Column Drift (displacement/height)
Test 177 (kN, mm, rad):
θy = 0.0172
θstf 40 = 0.0037
My = 61000 kN-mm
Mc/My = 1.10
θcap,pl = 0.066 (LB = 1)
θpc = n/a
λ = 81, c = 1.00
isPDeltaRemoved = 1

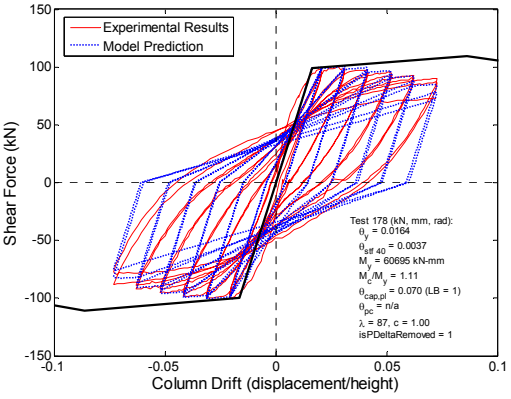
Experimental Results
Model Prediction
Shear Force (kN)
Column Drift (displacement/height)
Test 178 (kN, mm, rad):
θy = 0.0164
θstf 40 = 0.0037
My = 60695 kN-mm
Mc/My = 1.11
θcap,pl = 0.070 (LB = 1)
θpc = n/a
λ = 87, c = 1.00
isPDeltaRemoved = 1

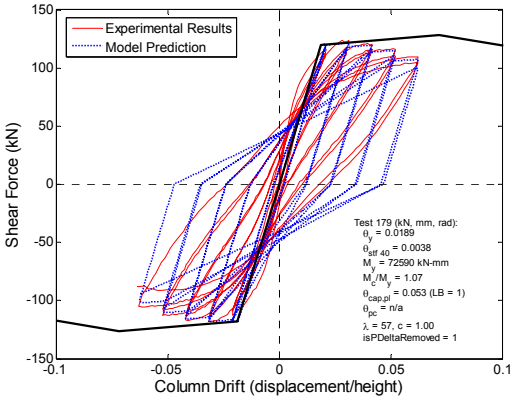
Experimental Results
Model Prediction
Shear Force (kN)
Column Drift (displacement/height)
Test 179 (kN, mm, rad):
θy = 0.0189
θstf 40 = 0.0038
My = 72590 kN-mm
Mc/My = 1.07
θcap,pl = 0.053 (LB = 1)
θpc = n/a
λ = 57, c = 1.00
isPDeltaRemoved = 1

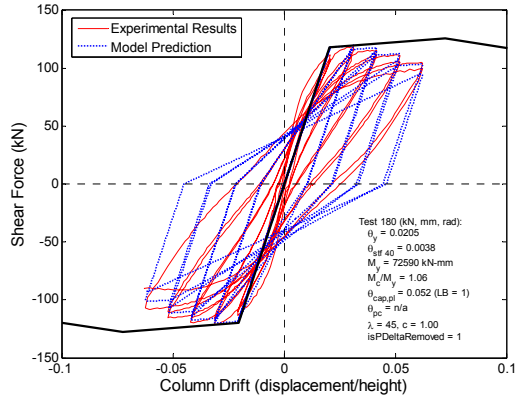
Experimental Results
Model Prediction
Shear Force (kN)
Column Drift (displacement/height)
Test 180 (kN, mm, rad):
θy = 0.0205
θstf 40 = 0.0038
My = 72590 kN-mm
Mc/My = 1.06
θcap,pl = 0.052 (LB = 1)
θpc = n/a
λ = 45, c = 1.00
isPDeltaRemoved = 1

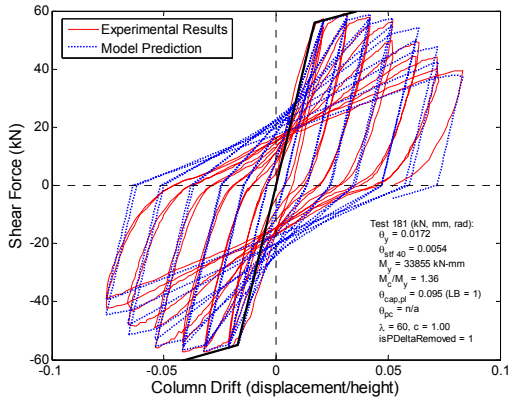
Experimental Results
Model Prediction
Shear Force (kN)
Column Drift (displacement/height)
Test 181 (kN, mm, rad):
θy = 0.0172
θstf 40 = 0.0054
My = 33855 kN-mm
Mc/My = 1.36
θcap,pl = 0.095 (LB = 1)
θpc = n/a
λ = 60, c = 1.00
isPDeltaRemoved = 1

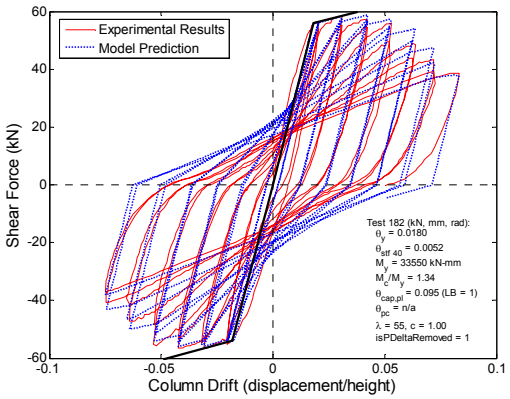
Experimental Results
Model Prediction
Shear Force (kN)
Column Drift (displacement/height)
Test 182 (kN, mm, rad):
θy = 0.0180
θstf 40 = 0.0052
My = 33550 kN-mm
Mc/My = 1.34
θcap,pl = 0.095 (LB = 1)
θpc = n/a
λ = 55, c = 1.00
isPDeltaRemoved = 1

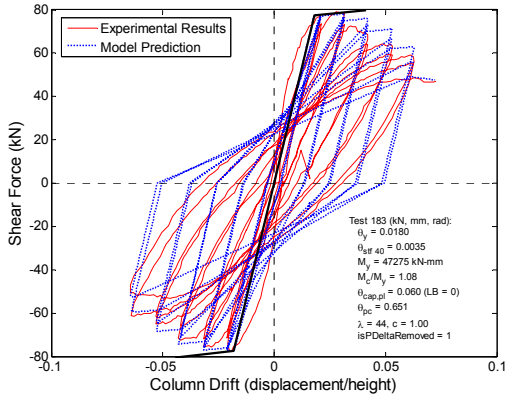
Experimental Results
Model Prediction
Shear Force (kN)
Column Drift (displacement/height)
Test 183 (kN, mm, rad):
θy = 0.0180
θstf 40 = 0.0035
My = 47275 kN-mm
Mc/My = 1.08
θcap,pl = 0.060 (LB = 0)
θpc = 0.651
λ = 44, c = 1.00
isPDeltaRemoved = 1

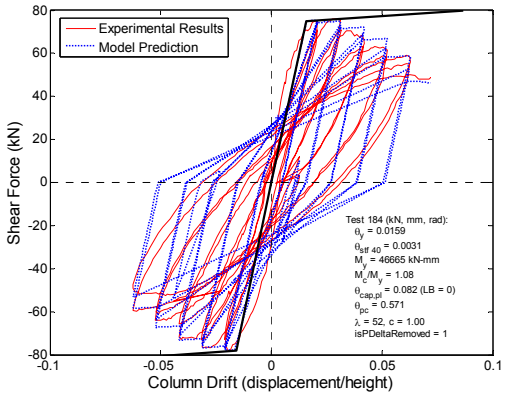
Experimental Results
Model Prediction
Shear Force (kN)
Column Drift (displacement/height)
Test 184 (kN, mm, rad):
θy = 0.0159
θstf 40 = 0.0031
My = 46665 kN-mm
Mc/My = 1.08
θcap,pl = 0.082 (LB = 0)
θpc = 0.571
λ = 52, c = 1.00
isPDeltaRemoved = 1

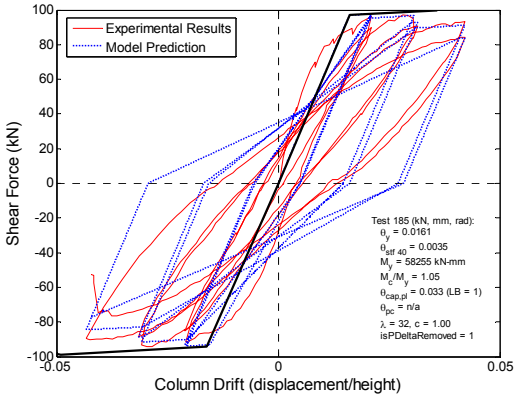
Experimental Results
Model Prediction
Shear Force (kN)
Column Drift (displacement/height)
Test 185 (kN, mm, rad):
θy = 0.0161
θstf 40 = 0.0035
My = 58255 kN-mm
Mc/My = 1.05
θcap,pl = 0.033 (LB = 1)
θpc = n/a
λ = 32, c = 1.00
isPDeltaRemoved = 1

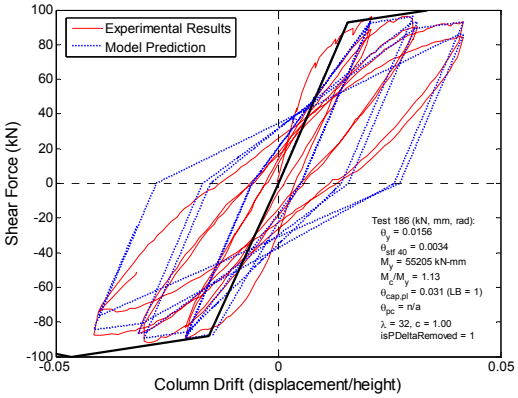
Experimental Results
Model Prediction
Shear Force (kN)
Column Drift (displacement/height)
Test 186 (kN, mm, rad):
θy = 0.0156
θstf 40 = 0.0034
My = 55205 kN-mm
Mc/My = 1.13
θcap,pl = 0.031 (LB = 1)
θpc = n/a
λ = 32, c = 1.00
isPDeltaRemoved = 1

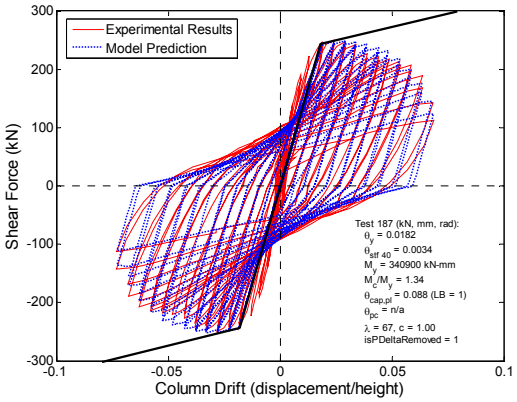
Experimental Results
Model Prediction
Shear Force (kN)
Column Drift (displacement/height)
Test 187 (kN, mm, rad):
θy = 0.0182
θstf 40 = 0.0034
My = 340900 kN-mm
Mc/My = 1.34
θcap,pl = 0.088 (LB = 1)
θpc = n/a
λ = 67, c = 1.00
isPDeltaRemoved = 1

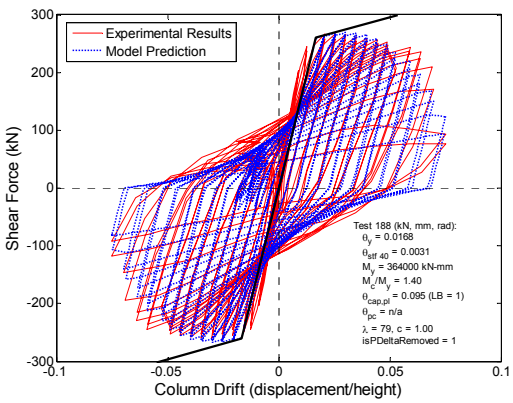
Experimental Results
Model Prediction
Shear Force (kN)
Column Drift (displacement/height)
Test 188 (kN, mm, rad):
θy = 0.0168
θstf 40 = 0.0031
My = 364000 kN-mm
Mc/My = 1.40
θcap,pl = 0.095 (LB = 1)
θpc = n/a
λ = 79, c = 1.00
isPDeltaRemoved = 1

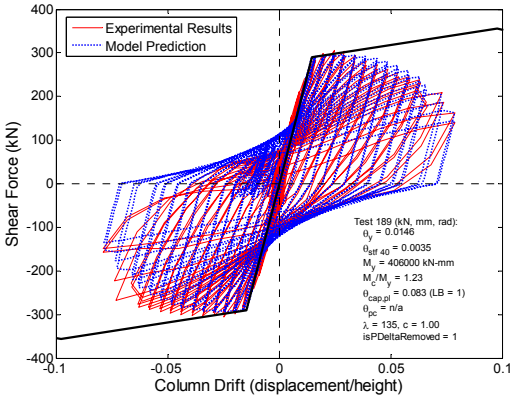
Experimental Results
Model Prediction
Shear Force (kN)
Column Drift (displacement/height)
Test 189 (kN, mm, rad):
θy = 0.0146
θstf 40 = 0.0035
My = 406000 kN-mm
Mc/My = 1.23
θcap,pl = 0.083 (LB = 1)
θpc = n/a
λ = 135, c = 1.00
isPDeltaRemoved = 1

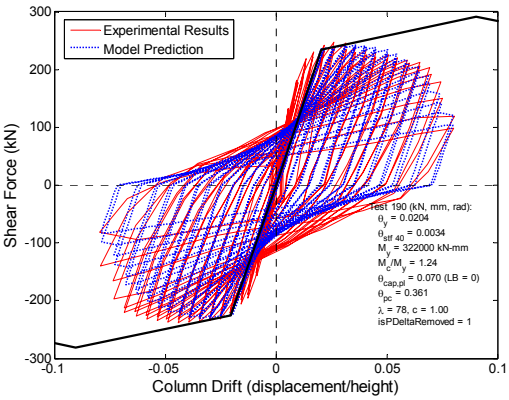
Experimental Results
Model Prediction
Shear Force (kN)
Column Drift (displacement/height)
Test 190 (kN, mm, rad):
θy = 0.0204
θstf 40 = 0.0034
My = 322000 kN-mm
Mc/My = 1.24
θcap,pl = 0.070 (LB = 0)
θpc = 0.361
λ = 78, c = 1.00
isPDeltaRemoved = 1

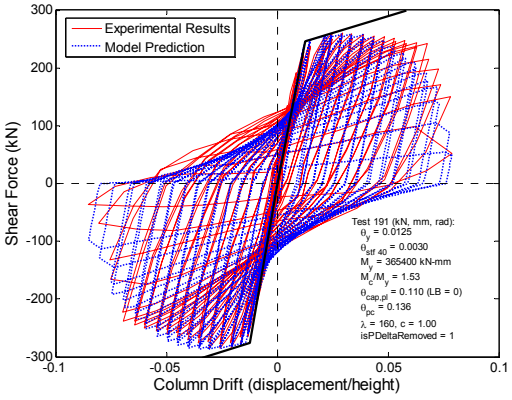
Experimental Results
Model Prediction
Shear Force (kN)
Column Drift (displacement/height)
Test 191 (kN, mm, rad):
θy = 0.0125
θstf 40 = 0.0030
My = 365400 kN-mm
Mc/My = 1.53
θcap,pl = 0.110 (LB = 0)
θpc = 0.136
λ = 160, c = 1.00
isPDeltaRemoved = 1

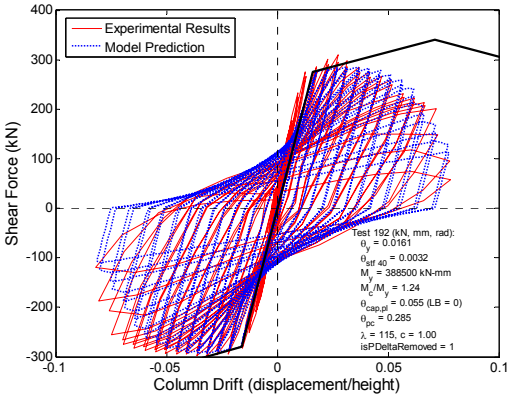
Experimental Results
Model Prediction
Shear Force (kN)
Column Drift (displacement/height)
Test 192 (kN, mm, rad):
θy = 0.0161
θstf 40 = 0.0032
My = 388500 kN-mm
Mc/My = 1.24
θcap,pl = 0.055 (LB = 0)
θpc = 0.285
λ = 115, c = 1.00
isPDeltaRemoved = 1

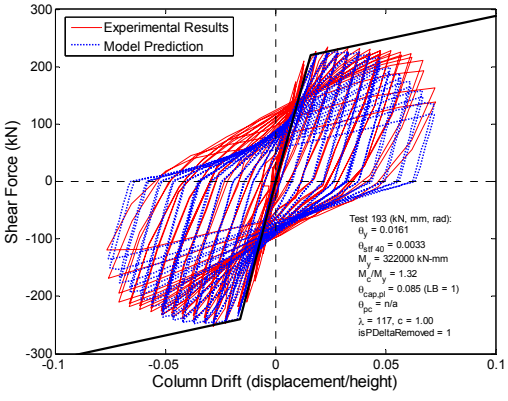
Experimental Results
Model Prediction
Shear Force (kN)
Column Drift (displacement/height)
Test 193 (kN, mm, rad):
θy = 0.0161
θstf 40 = 0.0033
My = 322000 kN-mm
Mc/My = 1.32
θcap,pl = 0.085 (LB = 1)
θpc = n/a
λ = 117, c = 1.00
isPDeltaRemoved = 1

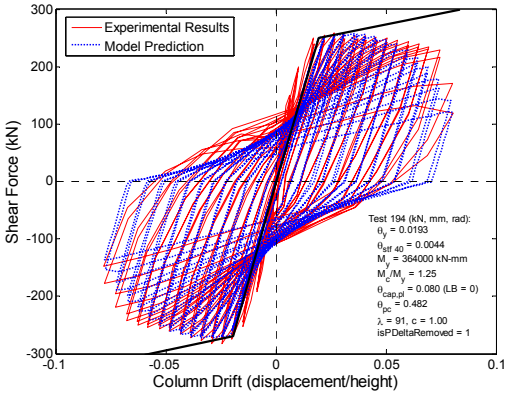
Experimental Results
Model Prediction
Shear Force (kN)
Column Drift (displacement/height)
Test 194 (kN, mm, rad):
θy = 0.0193
θstf 40 = 0.0044
My = 364000 kN-mm
Mc/My = 1.25
θcap,pl = 0.080 (LB = 0)
θpc = 0.482
λ = 91, c = 1.00
isPDeltaRemoved = 1

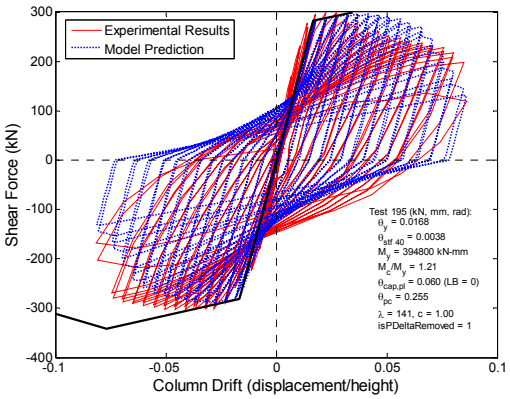
Experimental Results
Model Prediction
Shear Force (kN)
Column Drift (displacement/height)
Test 195 (kN, mm, rad):
θy = 0.0168
θstf 40 = 0.0038
My = 394800 kN-mm
Mc/My = 1.21
θcap,pl = 0.060 (LB = 0)
θpc = 0.255
λ = 141, c = 1.00
isPDeltaRemoved = 1

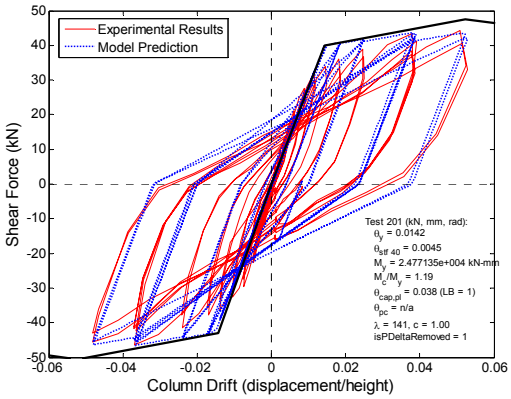
Experimental Results
Model Prediction
Shear Force (kN)
Column Drift (displacement/height)
Test 201 (kN, mm, rad):
θy = 0.0142
θstf 40 = 0.0045
My = 2.477135e+004 kN-mm
Mc/My = 1.19
θcap,pl = 0.038 (LB = 1)
θpc = n/a
λ = 141, c = 1.00
isPDeltaRemoved = 1

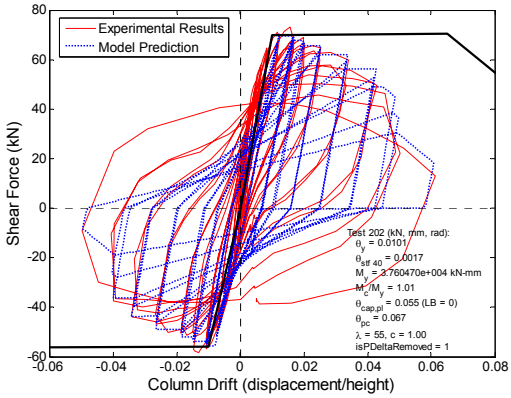
Experimental Results
Model Prediction
Shear Force (kN)
Column Drift (displacement/height)
Test 202 (kN, mm, rad):
θy = 0.0101
θstf 40 = 0.0017
My = 3.760470e+004 kN-mm
Mc/My = 1.01
θcap,pl = 0.055 (LB = 0)
θpc = 0.067
λ = 55, c = 1.00
isPDeltaRemoved = 1

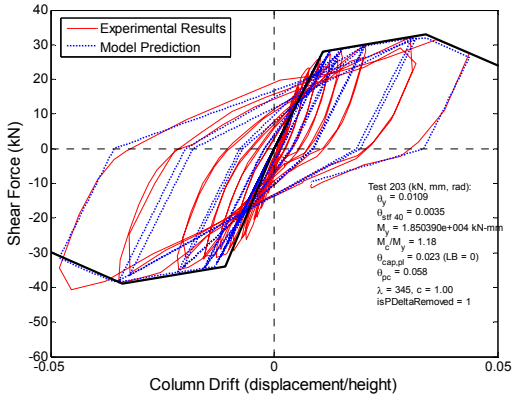
Experimental Results
Model Prediction
Shear Force (kN)
Column Drift (displacement/height)
Test 203 (kN, mm, rad):
θy = 0.0109
θstf 40 = 0.0035
My = 1.850390e+004 kN-mm
Mc/My = 1.18
θcap,pl = 0.023 (LB = 0)
θpc = 0.058
λ = 345, c = 1.00
isPDeltaRemoved = 1

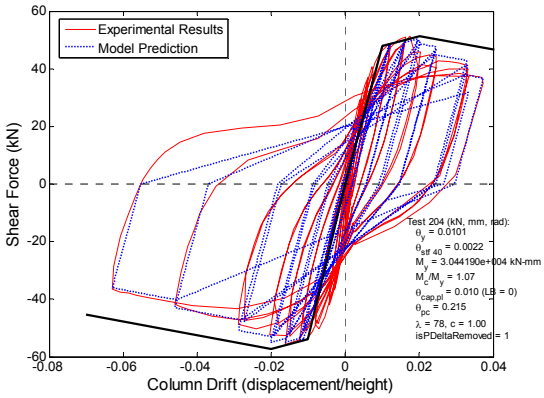
Experimental Results
Model Prediction
Shear Force (kN)
Column Drift (displacement/height)
Test 204 (kN, mm, rad):
θy = 0.0101
θstf 40 = 0.0022
My = 3.044190e+004 kN-mm
Mc/My = 1.07
θcap,pl = 0.010 (LB = 0)
θpc = 0.215
λ = 78, c = 1.00
isPDeltaRemoved = 1

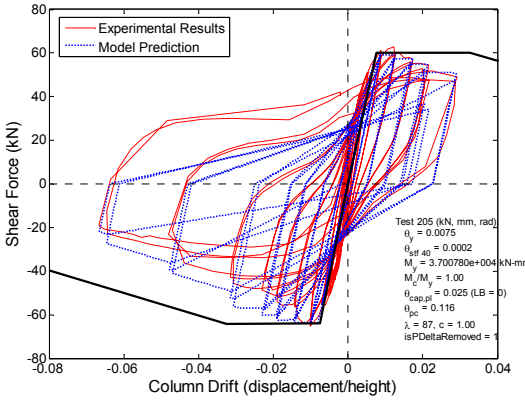
Experimental Results
Model Prediction
Shear Force (kN)
Column Drift (displacement/height)
Test 205 (kN, mm, rad):
θy = 0.0075
θstf 40 = 0.0002
My = 3.700780e+004 kN-mm
Mc/My = 1.00
θcap,pl = 0.025 (LB = 0)
θpc = 0.116
λ = 87, c = 1.00
isPDeltaRemoved = 1

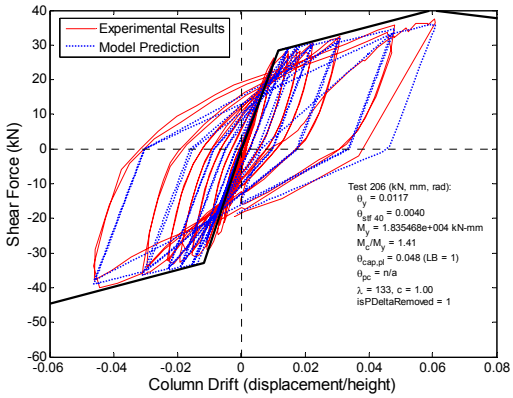
Experimental Results
Model Prediction
Shear Force (kN)
Column Drift (displacement/height)
Test 206 (kN, mm, rad):
θy = 0.0117
θstf 40 = 0.0040
My = 1.835468e+004 kN-mm
Mc/My = 1.41
θcap,pl = 0.048 (LB = 1)
θpc = n/a
λ = 133, c = 1.00
isPDeltaRemoved = 1

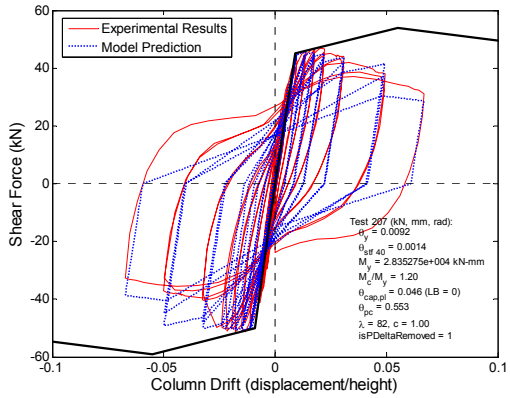
Experimental Results
Model Prediction
Shear Force (kN)
Column Drift (displacement/height)
Test 207 (kN, mm, rad):
θy = 0.0092
θstf 40 = 0.0014
My = 2.835275e+004 kN-mm
Mc/My = 1.20
θcap,pl = 0.046 (LB = 0)
θpc = 0.553
λ = 82, c = 1.00
isPDeltaRemoved = 1

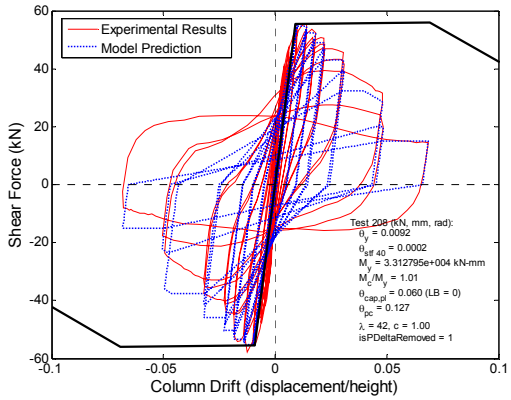
Experimental Results
Model Prediction
Shear Force (kN)
Column Drift (displacement/height)
Test 208 (kN, mm, rad):
θy = 0.0092
θstf 40 = 0.0002
My = 3.312795e+004 kN-mm
Mc/My = 1.01
θcap,pl = 0.060 (LB = 0)
θpc = 0.127
λ = 42, c = 1.00
isPDeltaRemoved = 1

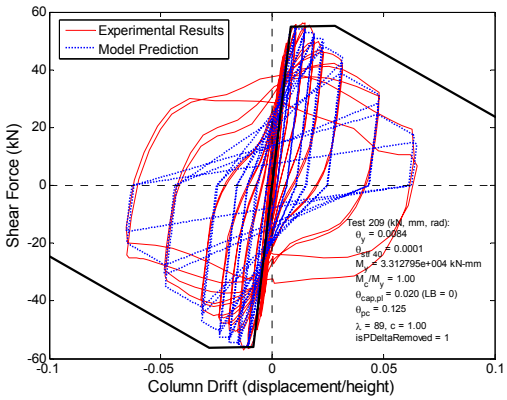
Experimental Results
Model Prediction
Shear Force (kN)
Column Drift (displacement/height)
Test 209 (kN, mm, rad):
θy = 0.0084
θstf 40 = 0.0001
My = 3.312795e+004 kN-mm
Mc/My = 1.00
θcap,pl = 0.020 (LB = 0)
θpc = 0.125
λ = 89, c = 1.00
isPDeltaRemoved = 1

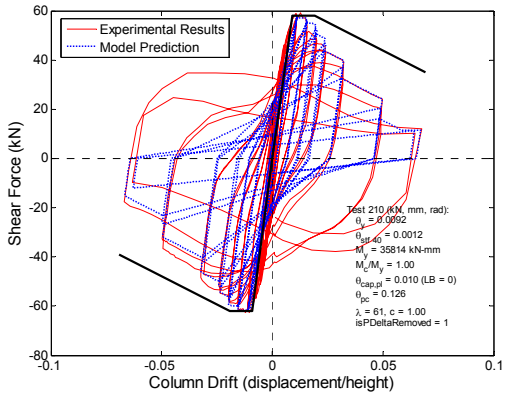
Experimental Results
Model Prediction
Shear Force (kN)
Column Drift (displacement/height)
Test 210 (kN, mm, rad):
θy = 0.0092
θstf 40 = 0.0012
My = 35814 kN-mm
Mc/My = 1.00
θcap,pl = 0.010 (LB = 0)
θpc = 0.126
λ = 61, c = 1.00
isPDeltaRemoved = 1

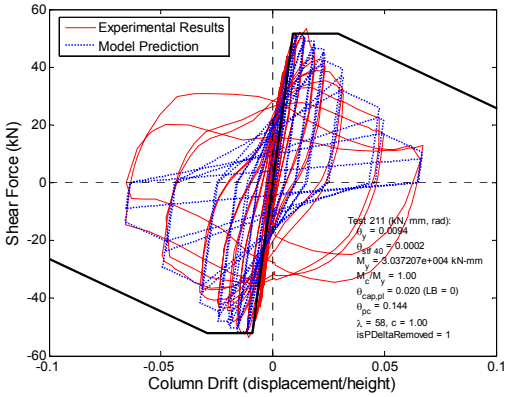
Experimental Results
Model Prediction
Shear Force (kN)
Column Drift (displacement/height)
Test 211 (kN, mm, rad):
θy = 0.0094
θstf 40 = 0.0002
My = 5.037207e+004 kN-mm
Mc/My = 1.00
θcap,pl = 0.020 (LB = 0)
θpc = 0.144
λ = 58, c = 1.00
isPDeltaRemoved = 1

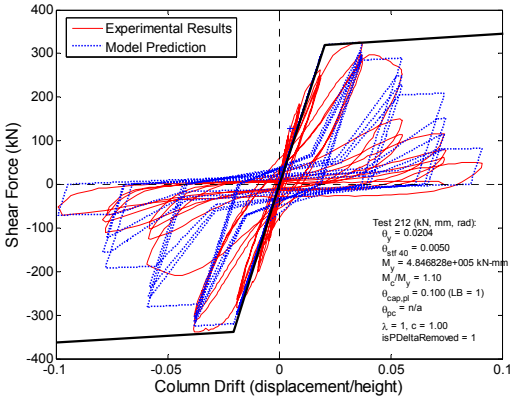
Experimental Results
Model Prediction
Shear Force (kN)
Column Drift (displacement/height)
Test 212 (kN, mm, rad):
θy = 0.0204
θstf 40 = 0.0050
My = 4.846828e+005 kN-mm
Mc/My = 1.10
θcap,pl = 0.100 (LB = 1)
θpc = n/a
λ = 1, c = 1.00
isPDeltaRemoved = 1

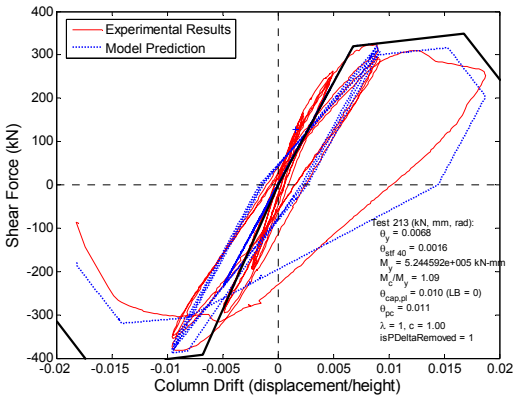
Experimental Results
Model Prediction
Shear Force (kN)
Column Drift (displacement/height)
Test 213 (kN, mm, rad):
θy = 0.0068
θstf 40 = 0.0016
My = 5.244592e+005 kN-mm
Mc/My = 1.09
θcap,pl = 0.010 (LB = 0)
θpc = 0.011
λ = 1, c = 1.00
isPDeltaRemoved = 1

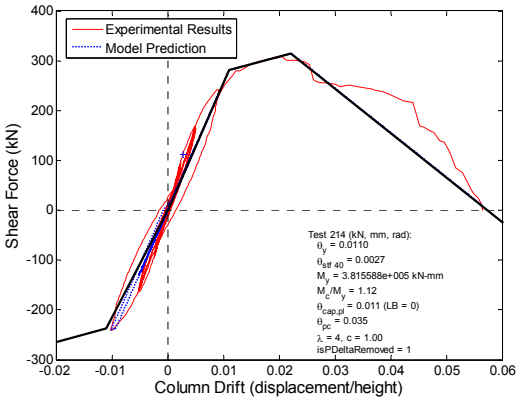
Experimental Results
Model Prediction
Shear Force (kN)
Column Drift (displacement/height)
Test 214 (kN, mm, rad):
θy = 0.0110
θstf 40 = 0.0027
My = 3.815588e+005 kN-mm
Mc/My = 1.12
θcap,pl = 0.011 (LB = 0)
θpc = 0.035
λ = 4, c = 1.00
isPDeltaRemoved = 1

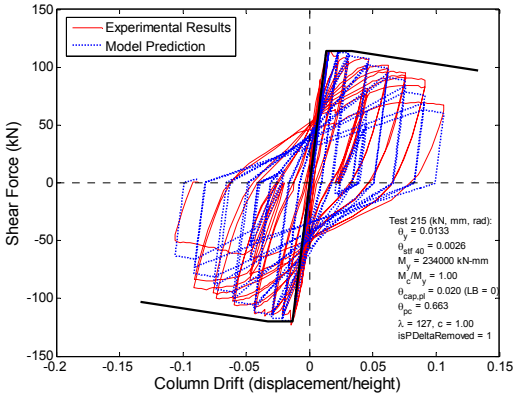
Experimental Results
Model Prediction
Shear Force (kN)
Column Drift (displacement/height)
Test 215 (kN, mm, rad):
θy = 0.0133
θstf 40 = 0.0026
My = 234000 kN-mm
Mc/My = 1.00
θcap,pl = 0.020 (LB = 0)
θpc = 0.663
λ = 127, c = 1.00
isPDeltaRemoved = 1

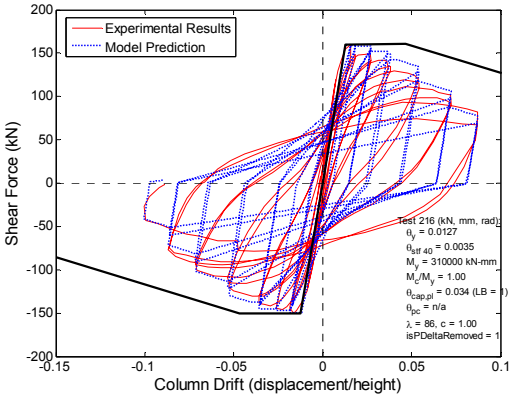
Experimental Results
Model Prediction
Shear Force (kN)
Column Drift (displacement/height)
Test 216 (kN, mm, rad):
θy = 0.0127
θstf 40 = 0.0035
My = 310000 kN-mm
Mc/My = 1.00
θcap,pl = 0.034 (LB = 0)
θpc = n/a
λ = 86, c = 1.00
isPDeltaRemoved = 1

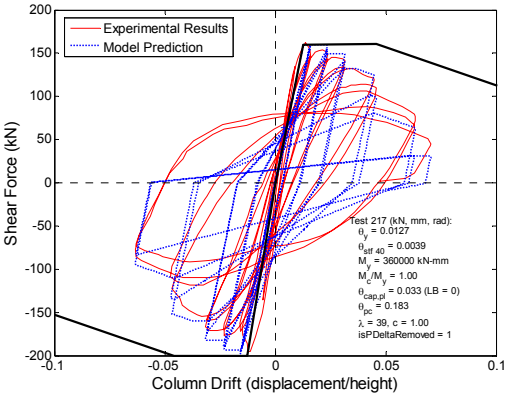
Experimental Results
Model Prediction
Shear Force (kN)
Column Drift (displacement/height)
Test 217 (kN, mm, rad):
θy = 0.0127
θstf 40 = 0.0039
My = 360000 kN-mm
Mc/My = 1.00
θcap,pl = 0.033 (LB = 0)
θpc = 0.183
λ = 39, c = 1.00
isPDeltaRemoved = 1

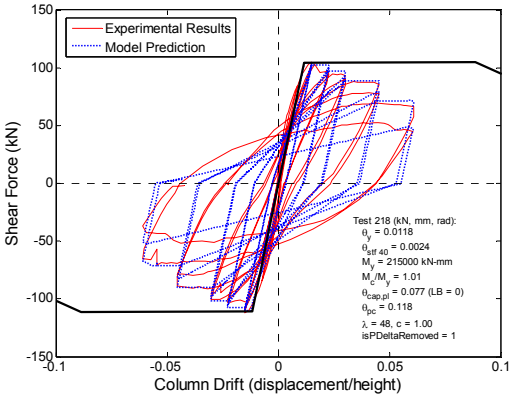
Experimental Results
Model Prediction
Shear Force (kN)
Column Drift (displacement/height)
Test 218 (kN, mm, rad):
θy = 0.0118
θstf 40 = 0.0024
My = 215000 kN-mm
Mc/My = 1.01
θcap,pl = 0.077 (LB = 0)
θpc = 0.118
λ = 48, c = 1.00
isPDeltaRemoved = 1

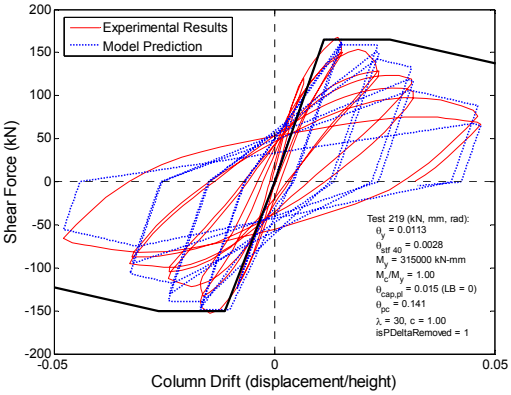
Experimental Results
Model Prediction
Shear Force (kN)
Column Drift (displacement/height)
Test 219 (kN, mm, rad):
θy = 0.0113
θstf 40 = 0.0028
My = 315000 kN-mm
Mc/My = 1.00
θcap,pl = 0.015 (LB = 0)
θpc = 0.141
λ = 30, c = 1.00
isPDeltaRemoved = 1

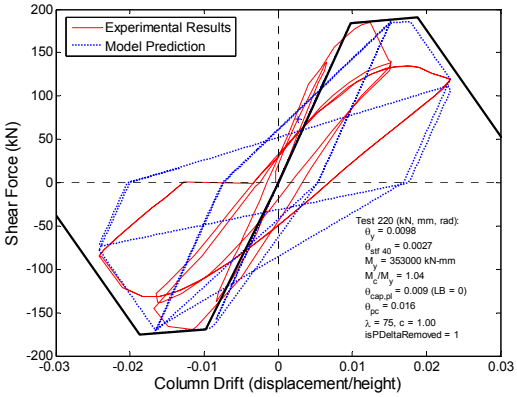
Experimental Results
Model Prediction
Shear Force (kN)
Column Drift (displacement/height)
Test 220 (kN, mm, rad):
θy = 0.0098
θstf 40 = 0.0027
My = 353000 kN-mm
Mc/My = 1.04
θcap,pl = 0.009 (LB = 0)
θpc = 0.016
λ = 75, c = 1.00
isPDeltaRemoved = 1

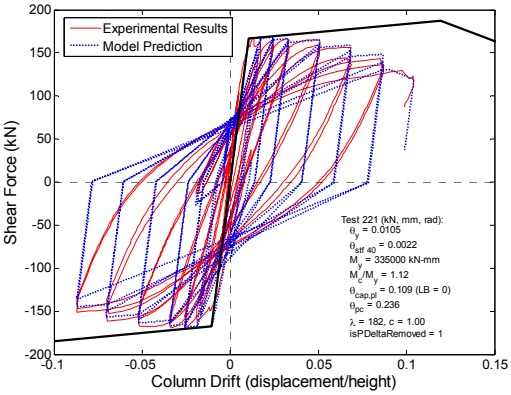
Experimental Results
Model Prediction
Shear Force (kN)
Column Drift (displacement/height)
Test 221 (kN, mm, rad):
θy = 0.0105
θstf 40 = 0.0022
My = 335000 kN-mm
Mc/My = 1.12
θcap,pl = 0.109 (LB = 0)
θpc = 0.236
λ = 182, c = 1.00
isPDeltaRemoved = 1

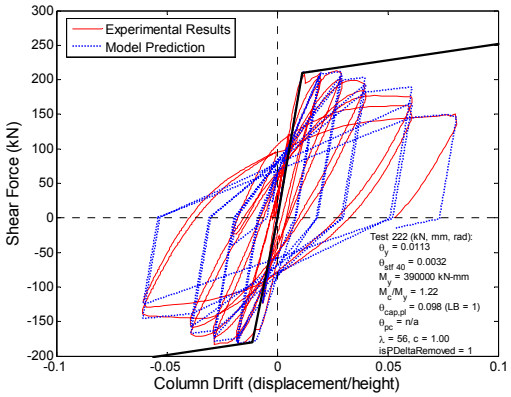
Experimental Results
Model Prediction
Shear Force (kN)
Column Drift (displacement/height)
Test 222 (kN, mm, rad):
θy = 0.0113
θstf 40 = 0.0032
My = 390000 kN-mm
Mc/My = 1.22
θcap,pl = 0.098 (LB = 1)
θpc = n/a
λ = 56, c = 1.00
isPDeltaRemoved = 1

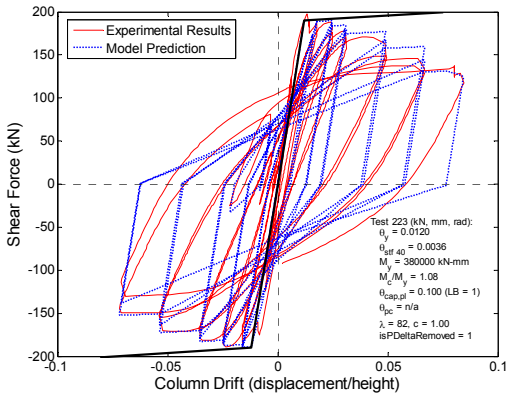
Experimental Results
Model Prediction
Shear Force (kN)
Column Drift (displacement/height)
Test 223 (kN, mm, rad):
θy = 0.0120
θstf 40 = 0.0036
My = 380000 kN-mm
Mc/My = 1.08
θcap,pl = 0.100 (LB = 1)
θpc = n/a
λ = 82, c = 1.00
isPDeltaRemoved = 1

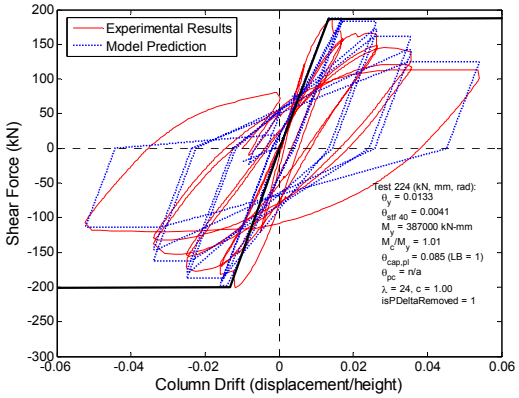
Experimental Results
Model Prediction
Shear Force (kN)
Column Drift (displacement/height)
Test 224 (kN, mm, rad):
θy = 0.0133
θstf 40 = 0.0041
My = 387000 kN-mm
Mc/My = 1.01
θcap,pl = 0.085 (LB = 1)
θpc = n/a
λ = 24, c = 1.00
isPDeltaRemoved = 1

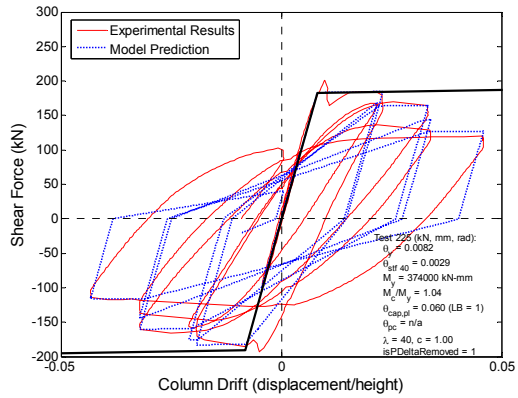
Experimental Results
Model Prediction
Shear Force (kN)
Column Drift (displacement/height)
Test 225 (kN, mm, rad):
θy = 0.0082
θstf 40 = 0.0029
My = 374000 kN-mm
Mc/My = 1.04
θcap,pl = 0.060 (LB = 1)
θpc = n/a
λ = 40, c = 1.00
isPDeltaRemoved = 1

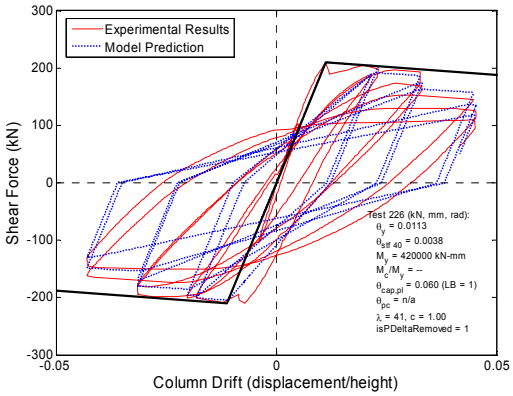
Experimental Results
Model Prediction
Shear Force (kN)
Column Drift (displacement/height)
Test 226 (kN, mm, rad):
θy = 0.0113
θstf 40 = 0.0038
My = 420000 kN-mm
Mc/My = --
θcap,pl = 0.060 (LB = 1)
θpc = n/a
λ = 41, c = 1.00
isPDeltaRemoved = 1

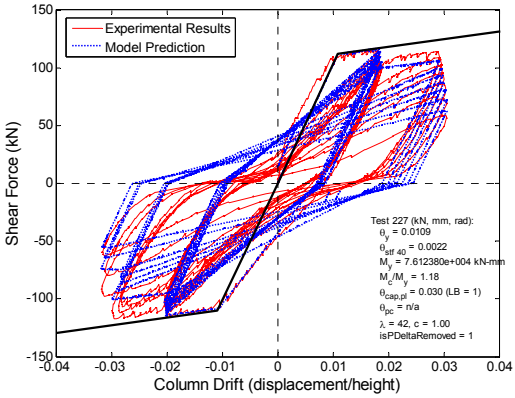
Experimental Results
Model Prediction
Shear Force (kN)
Column Drift (displacement/height)
Test 227 (kN, mm, rad):
θy = 0.0109
θstf 40 = 0.0022
My = 7.612380e+004 kN-mm
Mc/My = 1.18
θcap,pl = 0.030 (LB = 1)
θpc = n/a
λ = 42, c = 1.00
isPDeltaRemoved = 1

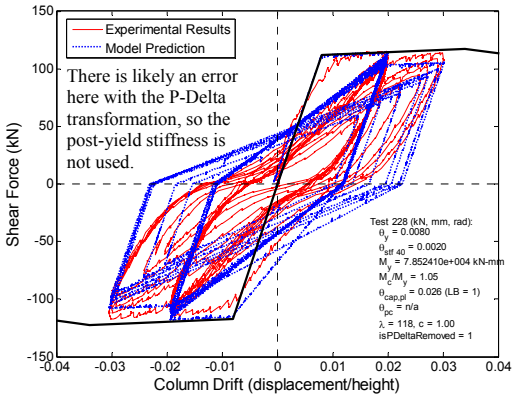
Experimental Results
Model Prediction
There is likely an error here with the P-Delta transformation, so the post-yield stiffness is not used.
Shear Force (kN)
Column Drift (displacement/height)
Test 228 (kN, mm, rad):
θy = 0.0080
θstf 40 = 0.0020
My = 7.852410e+004 kN-mm
Mc/My = 1.05
θcap,pl = 0.026 (LB = 1)
θpc = n/a
λ = 118, c = 1.00
isPDeltaRemoved = 1

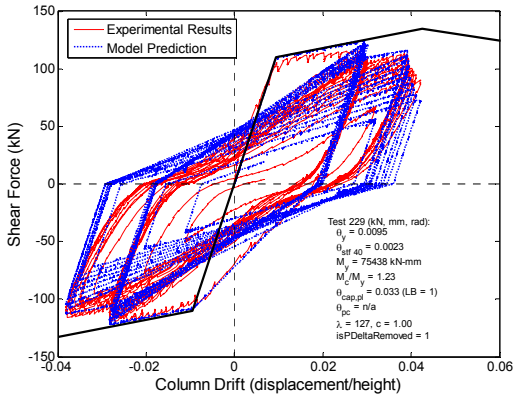
Experimental Results
Model Prediction
Shear Force (kN)
Column Drift (displacement/height)
Test 229 (kN, mm, rad):
θy = 0.0095
θstf 40 = 0.0023
My = 75438 kN-mm
Mc/My = 1.23
θcap,pl = 0.033 (LB = 1)
θpc = n/a
λ = 127, c = 1.00
isPDeltaRemoved = 1

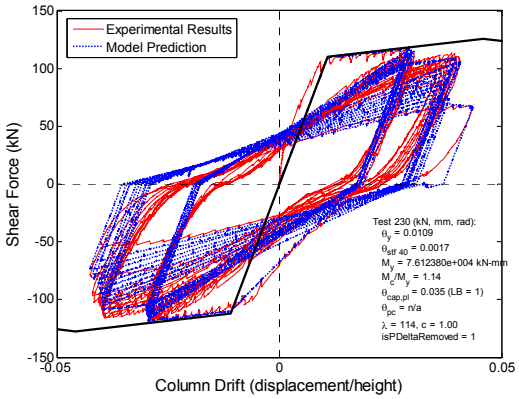
Experimental Results
Model Prediction
Shear Force (kN)
Column Drift (displacement/height)
Test 230 (kN, mm, rad):
θy = 0.0109
θstf 40 = 0.0017
My = 7.612380e+004 kN-mm
Mc/My = 1.14
θcap,pl = 0.035 (LB = 1)
θpc = n/a
λ = 114, c = 1.00
isPDeltaRemoved = 1

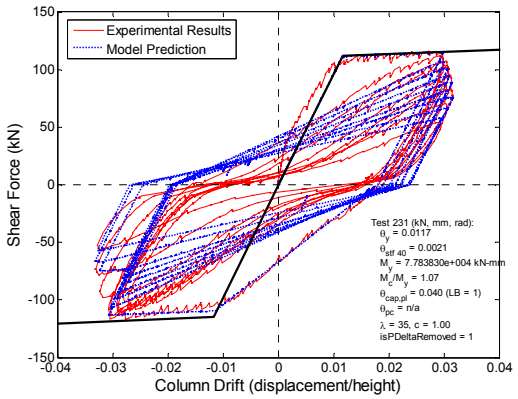
Experimental Results
Model Prediction
Shear Force (kN)
Column Drift (displacement/height)
Test 231 (kN, mm, rad):
θy = 0.0117
θstf 40 = 0.0021
My = 7.783830e+004 kN-mm
Mc/My = 1.07
θcap,pl = 0.040 (LB = 1)
θpc = n/a
λ = 35, c = 1.00
isPDeltaRemoved = 1

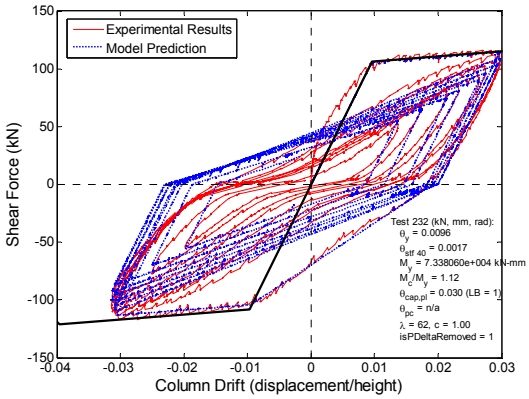
Experimental Results
Model Prediction
Shear Force (kN)
Column Drift (displacement/height)
Test 232 (kN, mm, rad):
θy = 0.0096
θstf 40 = 0.0017
My = 7.338060e+004 kN-mm
Mc/My = 1.12
θcap,pl = 0.030 (LB = 1)
θpc = n/a
λ = 62, c = 1.00
isPDeltaRemoved = 1

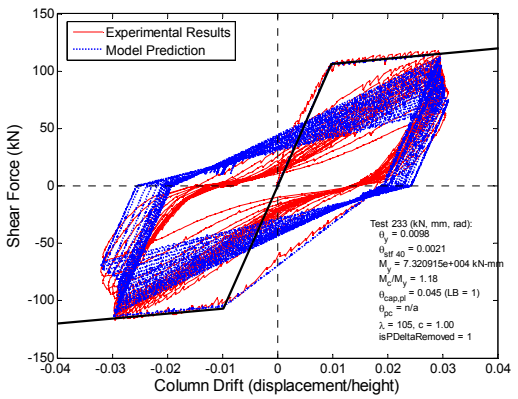
Experimental Results
Model Prediction
Shear Force (kN)
Column Drift (displacement/height)
Test 233 (kN, mm, rad):
θy = 0.0098
θstf 40 = 0.0021
My = 7.320915e+004 kN-mm
Mc/My = 1.18
θcap,pl = 0.045 (LB = 1)
θpc = n/a
λ = 105, c = 1.00
isPDeltaRemoved = 1

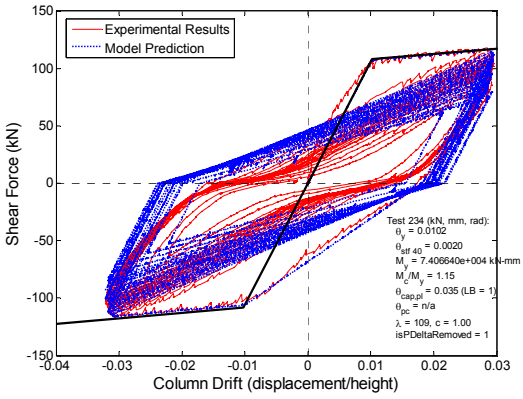
Experimental Results
Model Prediction
Shear Force (kN)
Column Drift (displacement/height)
Test 234 (kN, mm, rad):
θy = 0.0102
θstf 40 = 0.0020
My = 7.406640e+004 kN-mm
Mc/My = 1.15
θcap,pl = 0.035 (LB = 1)
θpc = n/a
λ = 109, c = 1.00
isPDeltaRemoved = 1

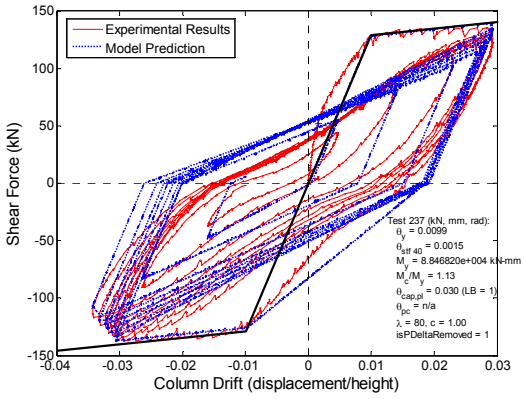
Experimental Results
Model Prediction
Shear Force (kN)
Column Drift (displacement/height)
Test 237 (kN, mm, rad):
θy = 0.0099
θstf 40 = 0.0015
My = 8.846820e+004 kN-mm
Mc/My = 1.13
θcap,pl = 0.030 (LB = 1)
θpc = n/a
λ = 80, c = 1.00
isPDeltaRemoved = 1

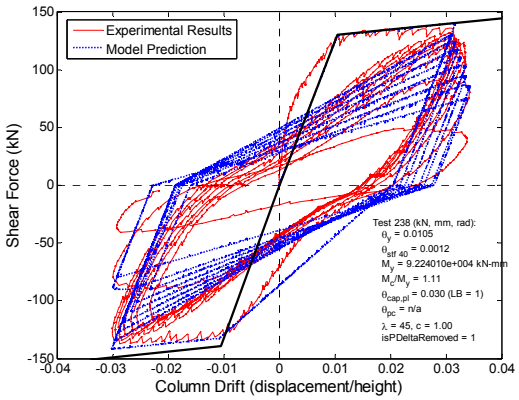
Experimental Results
Model Prediction
Shear Force (kN)
Column Drift (displacement/height)
Test 238 (kN, mm, rad):
θy = 0.0105
θstf 40 = 0.0012
My = 9.224010e+004 kN-mm
Mc/My = 1.11
θcap,pl = 0.030 (LB = 1)
θpc = n/a
λ = 45, c = 1.00
isPDeltaRemoved = 1

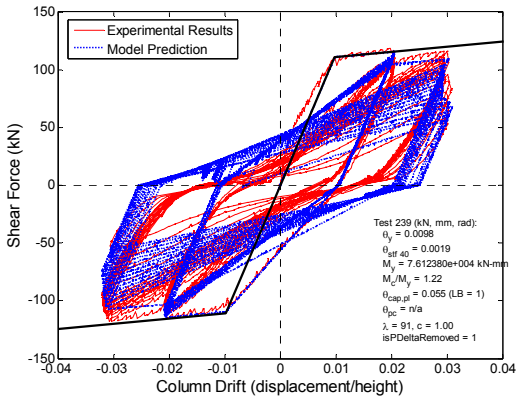
Experimental Results
Model Prediction
Shear Force (kN)
Column Drift (displacement/height)
Test 239 (kN, mm, rad):
θy = 0.0098
θstf 40 = 0.0019
My = 7.612380e+004 kN-mm
Mc/My = 1.22
θcap,pl = 0.055 (LB = 1)
θpc = n/a
λ = 91, c = 1.00
isPDeltaRemoved = 1

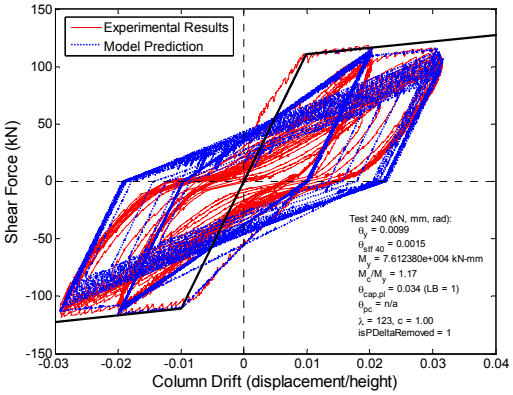
Experimental Results
Model Prediction
Test 240 (kN, mm, rad):
θy = 0.0099
θstf 40 = 0.0015
My = 7.612380e+004 kN-mm
Mc/My = 1.17
θcap,pl = 0.034 (LB = 1)
θpc = n/a
λ = 123, c = 1.00
isPDeltaRemoved = 1
Shear Force (kN)
Column Drift (displacement/height)

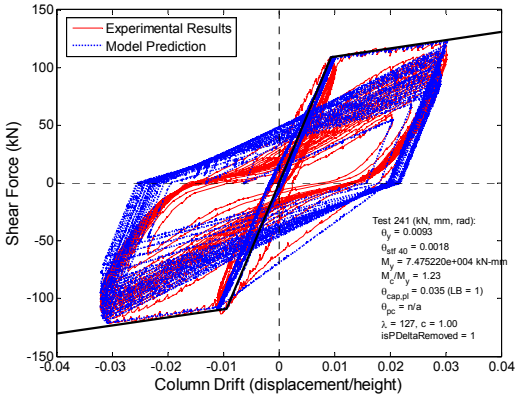
Experimental Results
Model Prediction
Test 241 (kN, mm, rad):
θy = 0.0093
θstf 40 = 0.0018
My = 7.475220e+004 kN-mm
Mc/My = 1.23
θcap,pl = 0.035 (LB = 1)
θpc = n/a
λ = 127, c = 1.00
isPDeltaRemoved = 1
Shear Force (kN)
Column Drift (displacement/height)

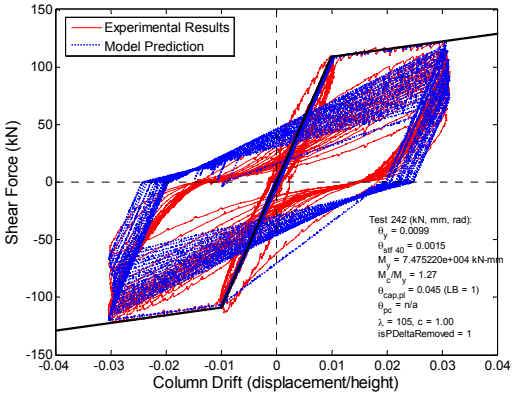
Experimental Results
Model Prediction
Test 242 (kN, mm, rad):
θy = 0.0099
θstf 40 = 0.0015
My = 7.475220e+004 kN-mm
Mc/My = 1.27
θcap,pl = 0.045 (LB = 1)
θpc = n/a
λ = 105, c = 1.00
isPDeltaRemoved = 1
Shear Force (kN)
Column Drift (displacement/height)

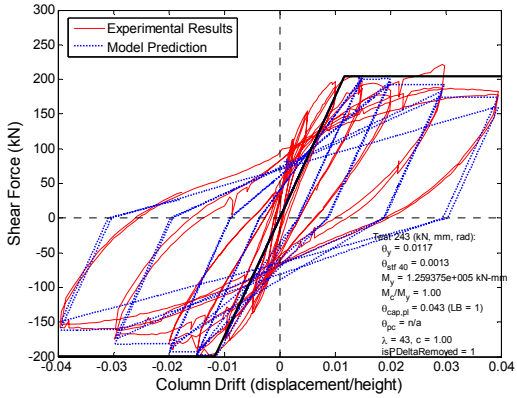
Experimental Results
Model Prediction
Test 243 (kN, mm, rad):
θy = 0.0117
θstf 40 = 0.0013
My = 1.259375e+005 kN-mm
Mc/My = 1.00
θcap,pl = 0.043 (LB = 1)
θpc = n/a
λ = 43, c = 1.00
isPDeltaRemoved = 1
Shear Force (kN)
Column Drift (displacement/height)

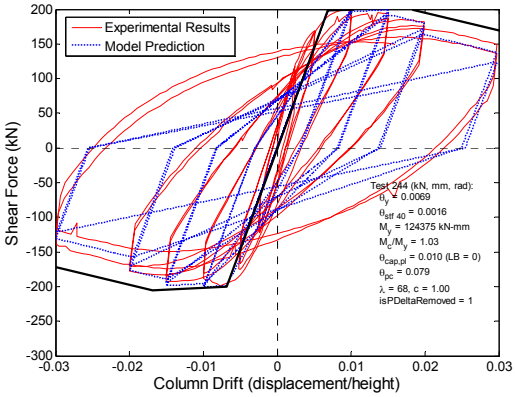
Experimental Results
Model Prediction
Test 244 (kN, mm, rad):
θy = 0.0069
θstf 40 = 0.0016
My = 124375 kN-mm
Mc/My = 1.03
θcap,pl = 0.010 (LB = 0)
θpc = 0.079
λ = 68, c = 1.00
isPDeltaRemoved = 1
Shear Force (kN)
Column Drift (displacement/height)

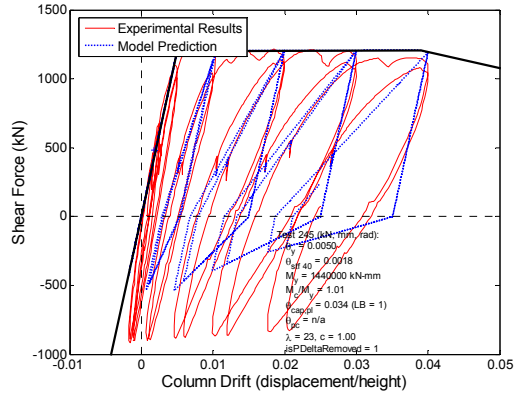
Experimental Results
Model Prediction
Test 245 (kN, mm, rad):
θy = 0.0050
θstf 40 = 0.0018
My = 1440000 kN-mm
Mc/My = 1.01
θcap,pl = 0.034 (LB = 1)
θpc = n/a
λ = 23, c = 1.00
isPDeltaRemoved = 1
Shear Force (kN)
Column Drift (displacement/height)

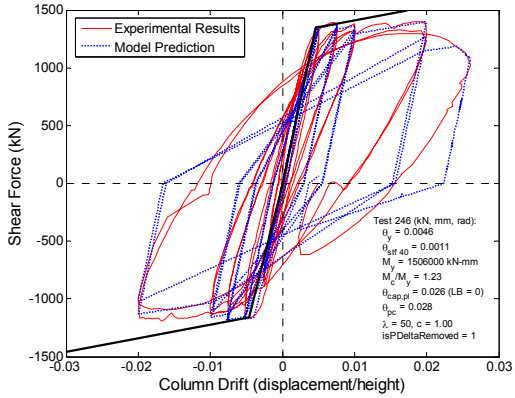
Experimental Results
Model Prediction
Test 246 (kN, mm, rad):
θy = 0.0046
θstf 40 = 0.0011
My = 1506000 kN-mm
Mc/My = 1.23
θcap,pl = 0.026 (LB = 0)
θpc = 0.028
λ = 50, c = 1.00
isPDeltaRemoved = 1
Shear Force (kN)
Column Drift (displacement/height)

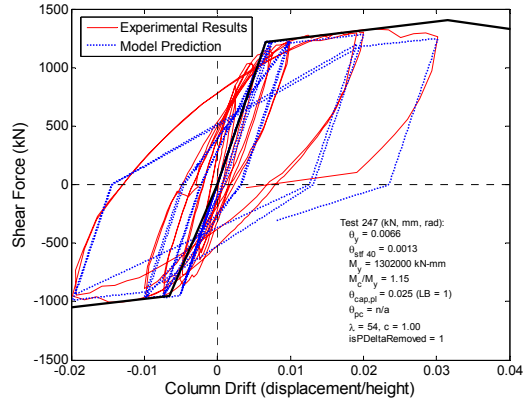
Experimental Results
Model Prediction
Test 247 (kN, mm, rad):
θy = 0.0066
θstf 40 = 0.0013
My = 1302000 kN-mm
Mc/My = 1.15
θcap,pl = 0.025 (LB = 1)
θpc = n/a
λ = 54, c = 1.00
isPDeltaRemoved = 1
Shear Force (kN)
Column Drift (displacement/height)

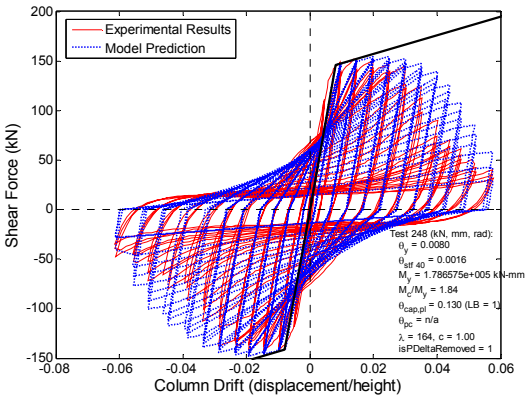
Experimental Results
Model Prediction
Shear Force (kN)
Column Drift (displacement/height)
Test 248 (kN, mm, rad):
θy = 0.0080
θstf 40 = 0.0016
My = 1.786575e+005 kN-mm
Mc/My = 1.84
θcap,pl = 0.130 (LB = 1)
θpc = n/a
λ = 164, c = 1.00
isPDeltaRemoved = 1

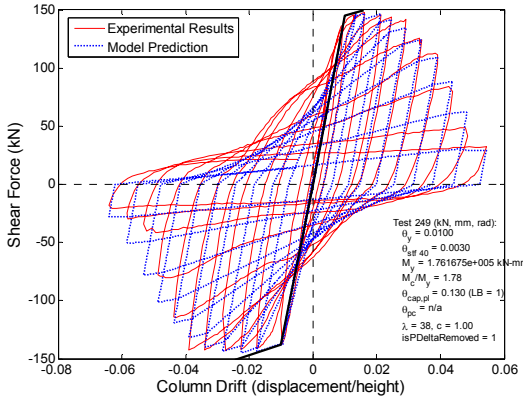
Experimental Results
Model Prediction
Shear Force (kN)
Column Drift (displacement/height)
Test 249 (kN, mm, rad):
θy = 0.0100
θstf 40 = 0.0030
My = 1.761675e+005 kN-mm
Mc/My = 1.78
θcap,pl = 0.130 (LB = 1)
θpc = n/a
λ = 38, c = 1.00
isPDeltaRemoved = 1

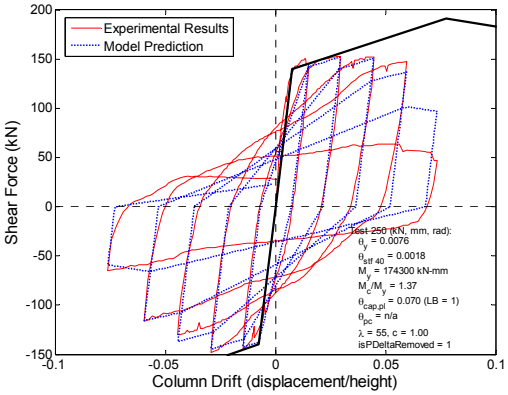
Experimental Results
Model Prediction
Shear Force (kN)
Column Drift (displacement/height)
Test 250 (kN, mm, rad):
θy = 0.0076
θstf 40 = 0.0018
My = 174300 kN-mm
Mc/My = 1.37
θcap,pl = 0.070 (LB = 1)
θpc = n/a
λ = 55, c = 1.00
isPDeltaRemoved = 1

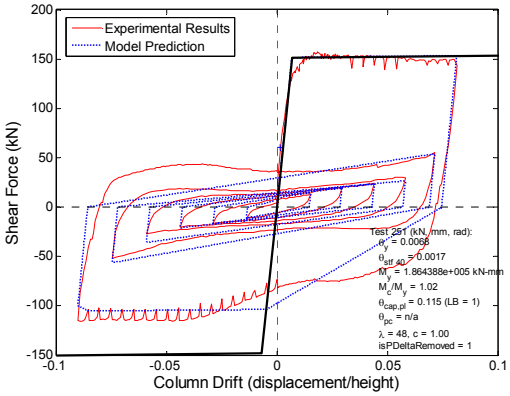
Experimental Results
Model Prediction
Shear Force (kN)
Column Drift (displacement/height)
Test 251 (kN, mm, rad):
θy = 0.0068
θstf 40 = 0.0017
My = 1.864388e+005 kN-mm
Mc/My = 1.02
θcap,pl = 0.115 (LB = 1)
θpc = n/a
λ = 48, c = 1.00
isPDeltaRemoved = 1

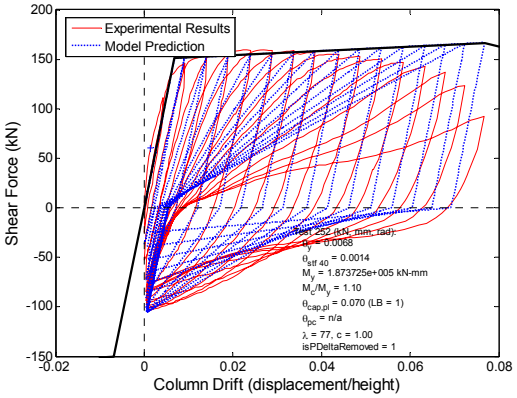
Experimental Results
Model Prediction
Shear Force (kN)
Column Drift (displacement/height)
Test 252 (kN, mm, rad):
θy = 0.0068
θstf 40 = 0.0014
My = 1.873725e+005 kN-mm
Mc/My = 1.10
θcap,pl = 0.070 (LB = 1)
θpc = n/a
λ = 77, c = 1.00
isPDeltaRemoved = 1

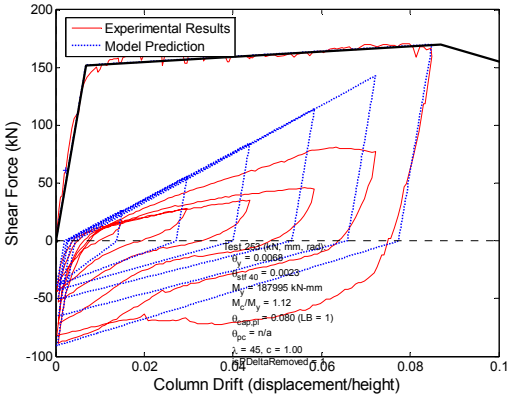
Experimental Results
Model Prediction
Shear Force (kN)
Column Drift (displacement/height)
Test 253 (kN, mm, rad):
θy = 0.0068
θstf 40 = 0.0023
My = 187995 kN-mm
Mc/My = 1.12
θcap,pl = 0.080 (LB = 1)
θpc = n/a
λ = 45, c = 1.00
isPDeltaRemoved = 1

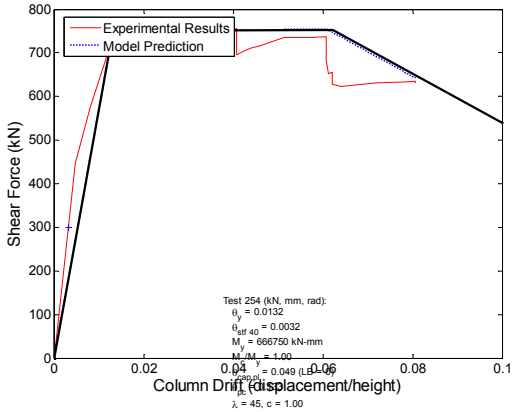
Experimental Results
Model Prediction
Shear Force (kN)
Column Drift (displacement/height)
Test 254 (kN, mm, rad):
θy = 0.0132
θstf 40 = 0.0032
My = 666750 kN-mm
Mc/My = 1.00
θcap,pl = 0.049 (LB = 0)
θpc = n/a
λ = 45, c = 1.00

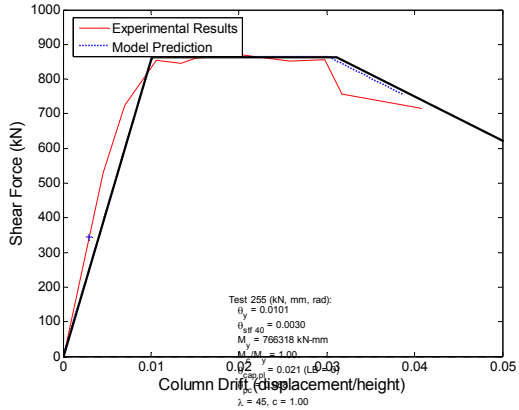
Experimental Results
Model Prediction
Shear Force (kN)
Column Drift (displacement/height)
Test 255 (kN, mm, rad):
θy = 0.0101
θstf 40 = 0.0030
My = 766318 kN-mm
Mc/My = 1.00
θcap,pl = 0.021 (LB = 0)
θpc = n/a
λ = 45, c = 1.00

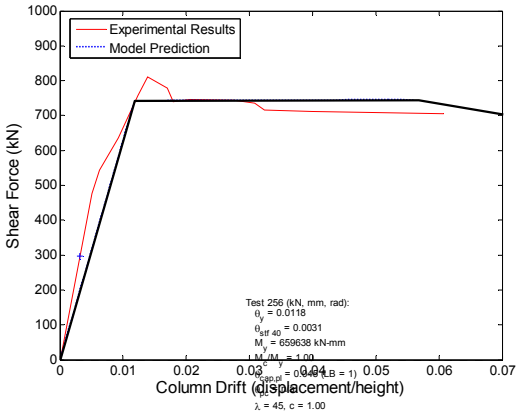
Experimental Results
Model Prediction
Shear Force (kN)
Column Drift (displacement/height)
Test 256 (kN, mm, rad):
θy = 0.0118
θstf 40 = 0.0031
My = 659638 kN-mm
Mc/My = 1.00
θcap,pl = 0.040 (LB = 1)
λ = 45, c = 1.00

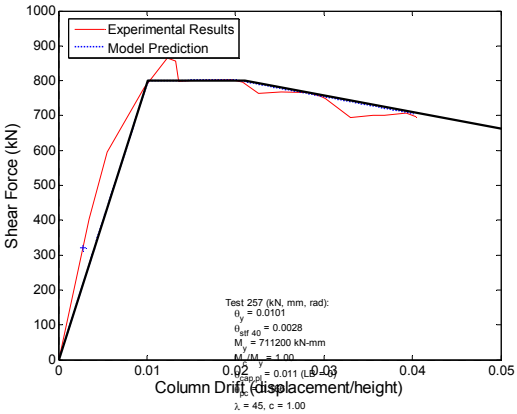
Experimental Results
Model Prediction
Shear Force (kN)
Column Drift (displacement/height)
Test 257 (kN, mm, rad):
θy = 0.0101
θstf 40 = 0.0028
My = 711200 kN-mm
Mc/My = 1.00
θcap,pl = 0.011 (LB = 1)
λ = 45, c = 1.00

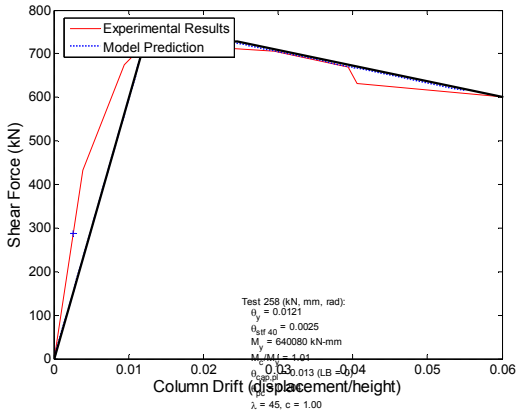
Experimental Results
Model Prediction
Shear Force (kN)
Column Drift (displacement/height)
Test 258 (kN, mm, rad):
θy = 0.0121
θstf 40 = 0.0025
My = 640080 kN-mm
Mc/My = 1.01
θcap,pl = 0.013 (LB = 1)
λ = 45, c = 1.00

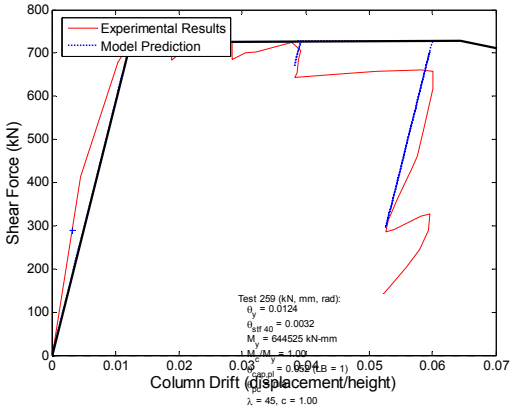
Experimental Results
Model Prediction
Shear Force (kN)
Column Drift (displacement/height)
Test 259 (kN, mm, rad):
θy = 0.0124
θstf 40 = 0.0032
My = 644525 kN-mm
Mc/My = 1.00
θcap,pl = 0.038 (LB = 1)
λ = 45, c = 1.00

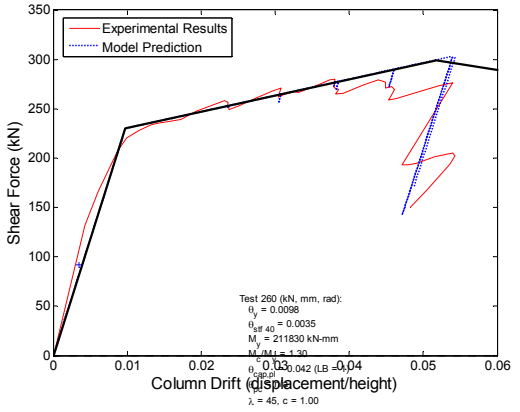
Experimental Results
Model Prediction
Shear Force (kN)
Column Drift (displacement/height)
Test 260 (kN, mm, rad):
θy = 0.0098
θstf 40 = 0.0035
My = 211830 kN-mm
Mc/My = 1.30
θcap,pl = 0.042 (LB = 1)
λ = 45, c = 1.00

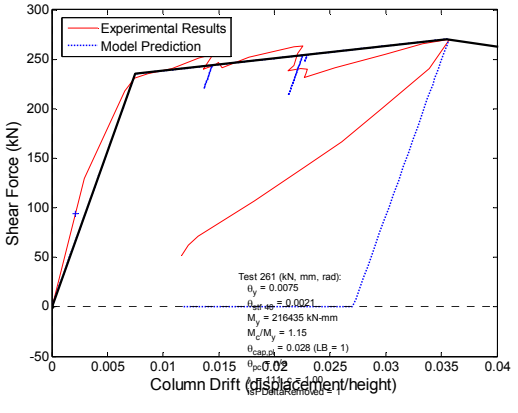
Experimental Results
Model Prediction
Shear Force (kN)
Column Drift (displacement/height)
Test 261 (kN, mm, rad):
θy = 0.0075
θstf 40 = 0.0021
My = 216435 kN-mm
Mc/My = 1.15
θcap,pl = 0.028 (LB = 1)
λ = 45, c = 1.00

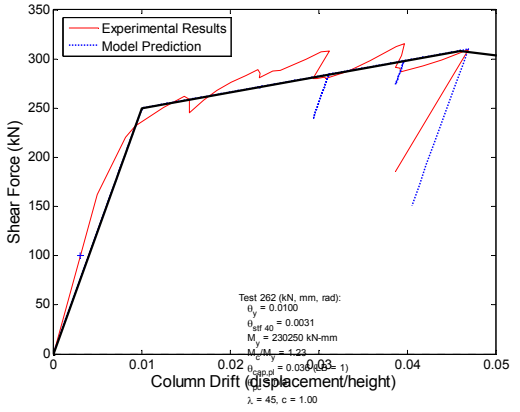
Experimental Results
Model Prediction
Shear Force (kN)
Column Drift (displacement/height)
Test 262 (kN, mm, rad):
θy = 0.0100
θstf 40 = 0.0031
My = 230250 kN-mm
Mc/My = 1.23
θcap,pl = 0.030 (LB = 1)
λ = 45, c = 1.00

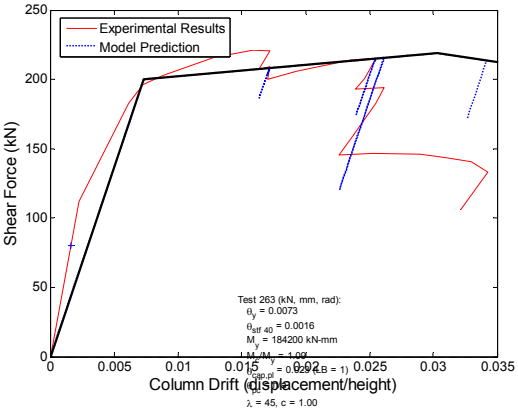
Experimental Results
Model Prediction
Shear Force (kN)
Column Drift (displacement/height)
Test 263 (kN, mm, rad):
θy = 0.0073
θstf 40 = 0.0016
My = 184200 kN-mm
Mc/My = 1.09
θcap,pl = 0.026 (LB = 1)
λ = 45, c = 1.00

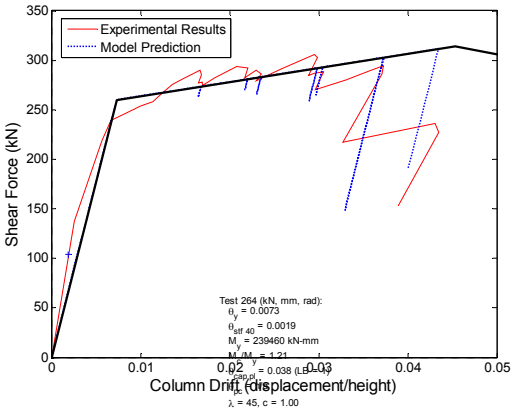
Experimental Results
Model Prediction
Shear Force (kN)
Column Drift (displacement/height)
Test 264 (kN, mm, rad):
θy = 0.0073
θstf 40 = 0.0019
My = 239460 kN-mm
Mc/My = 1.21
θcap,pl = 0.038 (LB = 1)
λ = 45, c = 1.00

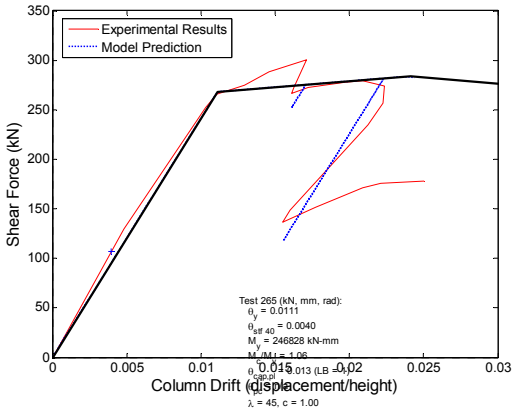
Experimental Results
Model Prediction
Shear Force (kN)
Column Drift (displacement/height)
Test 265 (kN, mm, rad):
θy = 0.0111
θstf 40 = 0.0040
My = 246828 kN-mm
Mc/My = 1.06
θcap,pl = 0.013 (LB = 1)
λ = 45, c = 1.00

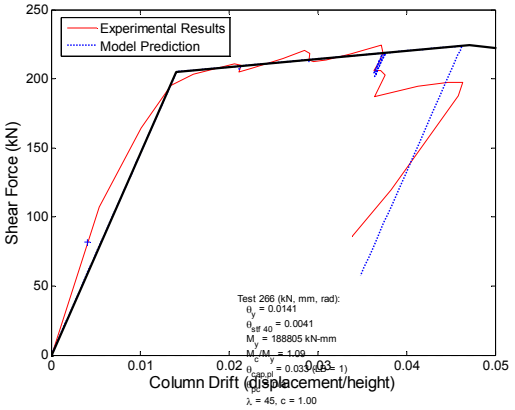
Experimental Results
Model Prediction
Shear Force (kN)
Column Drift (displacement/height)
Test 266 (kN, mm, rad):
θy = 0.0141
θstf 40 = 0.0041
My = 188805 kN-mm
Mc/My = 1.09
θcap,pl = 0.030 (LB = 1)
λ = 45, c = 1.00

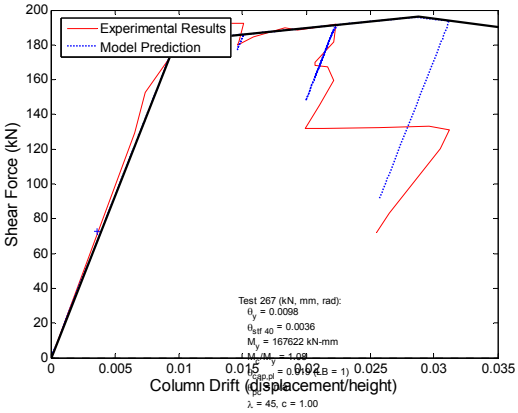
Experimental Results
Model Prediction
Shear Force (kN)
Column Drift (displacement/height)
Test 267 (kN, mm, rad):
θy = 0.0098
θstf 40 = 0.0036
My = 167622 kN-mm
Mc/My = 1.08
θcap,pl = 0.019 (LB = 1)
λ = 45, c = 1.00

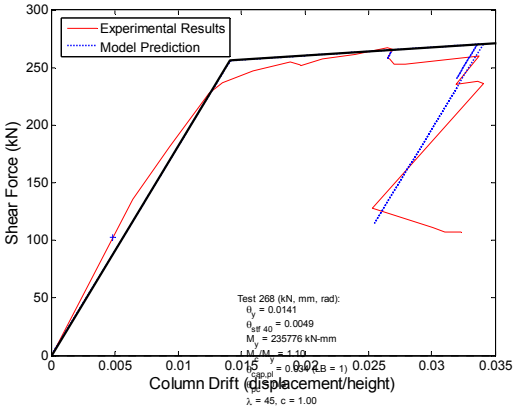
Experimental Results
Model Prediction
Shear Force (kN)
Column Drift (displacement/height)
Test 268 (kN, mm, rad):
θy = 0.0141
θstf 40 = 0.0049
My = 235776 kN-mm
Mc/My = 1.10
θcap,pl = 0.030 (LB = 1)
λ = 45, c = 1.00

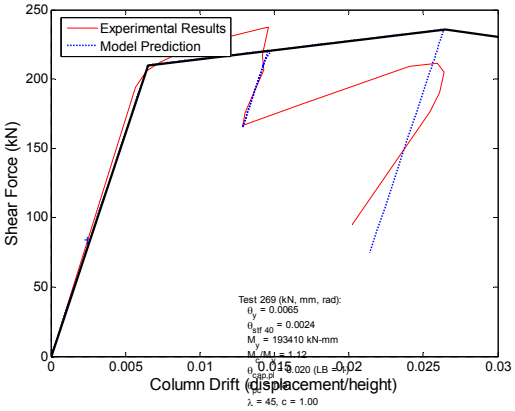
Experimental Results
Model Prediction
Shear Force (kN)
Column Drift (displacement/height)
Test 269 (kN, mm, rad):
θy = 0.0065
θstf 40 = 0.0024
My = 193410 kN-mm
Mc/My = 1.12
θcap,pl = 0.020 (LB = 1)
λ = 45, c = 1.00

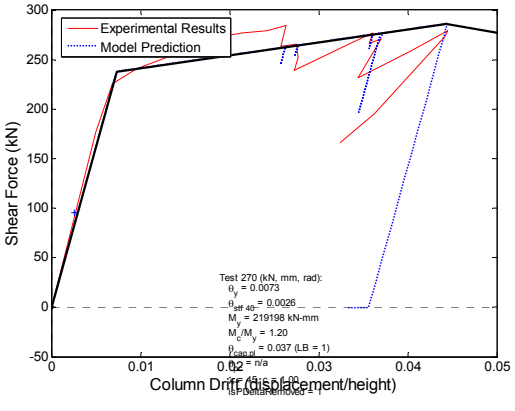
Experimental Results
Model Prediction
Shear Force (kN)
Column Drift (displacement/height)
Test 270 (kN, mm, rad):
θy = 0.0073
θstf 40 = 0.0026
My = 219198 kN-mm
Mc/My = 1.20
θcap,pl = 0.037 (LB = 1)
λ = 45, c = 1.00

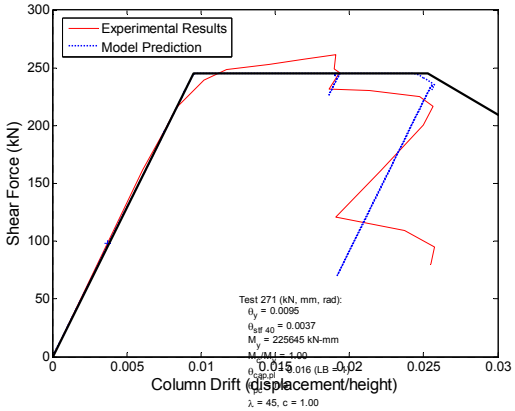
Experimental Results
Model Prediction
Shear Force (kN)
Column Drift (displacement/height)
Test 271 (kN, mm, rad):
θy = 0.0095
θstf 40 = 0.0037
My = 225645 kN-mm
Mc/My = 1.00
θcap,pl = 0.016 (LB = 1)
λ = 45, c = 1.00

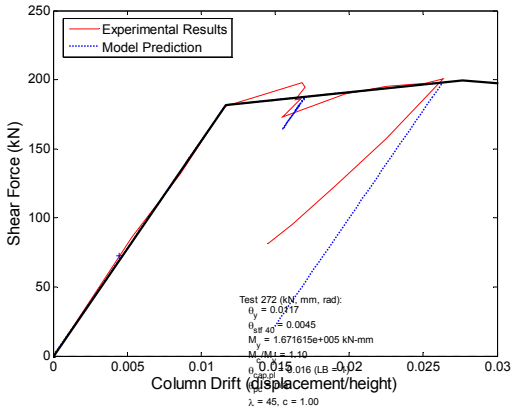
Experimental Results
Model Prediction
Shear Force (kN)
Column Drift (displacement/height)
Test 272 (kN, mm, rad):
θ_y = 0.0117
$\theta_{stf\ 40}$ = 0.0045
M_y = 1.671615e+005 kN-mm
M_c/M_y = 1.10
$\theta_{cap,pl}$ = 0.016 (LB = 1)
θ_{pc} = n/a
λ = 45, c = 1.00

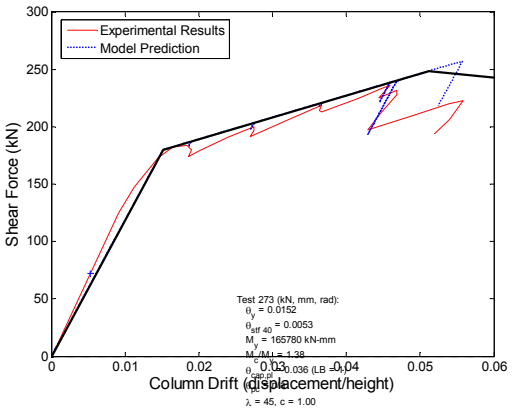
Experimental Results
Model Prediction
Shear Force (kN)
Column Drift (displacement/height)
Test 273 (kN, mm, rad):
θ_y = 0.0152
$\theta_{stf\ 40}$ = 0.0053
M_y = 165780 kN-mm
M_c/M_y = 1.38
$\theta_{cap,pl}$ = 0.036 (LB = 1)
θ_{pc} = n/a
λ = 45, c = 1.00

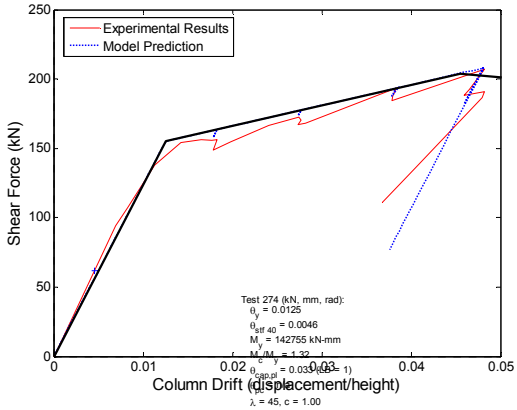
Experimental Results
Model Prediction
Shear Force (kN)
Column Drift (displacement/height)
Test 274 (kN, mm, rad):
θ_y = 0.0125
$\theta_{stf\ 40}$ = 0.0046
M_y = 142755 kN-mm
M_c/M_y = 1.32
$\theta_{cap,pl}$ = 0.032 (LB = 1)
θ_{pc} = n/a
λ = 45, c = 1.00

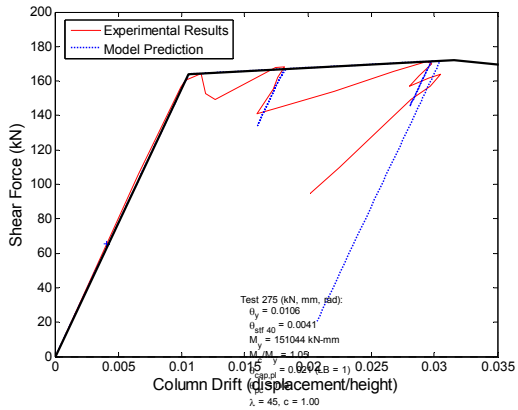
Experimental Results
Model Prediction
Shear Force (kN)
Column Drift (displacement/height)
Test 275 (kN, mm, rad):
θ_y = 0.0106
$\theta_{stf\ 40}$ = 0.0041
M_y = 151044 kN-mm
M_c/M_y = 1.09
$\theta_{cap,pl}$ = 0.027 (LB = 1)
θ_{pc} = n/a
λ = 45, c = 1.00

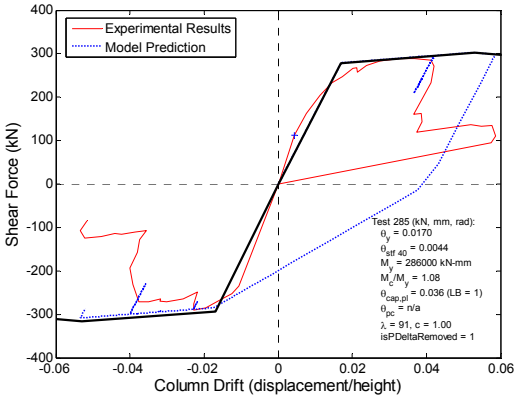
Experimental Results
Model Prediction
Shear Force (kN)
Column Drift (displacement/height)
Test 285 (kN, mm, rad):
θ_y = 0.0170
$\theta_{stf\ 40}$ = 0.0044
M_y = 286000 kN-mm
M_c/M_y = 1.08
$\theta_{cap,pl}$ = 0.036 (LB = 1)
θ_{pc} = n/a
λ = 91, c = 1.00
isPDeltaRemoved = 1

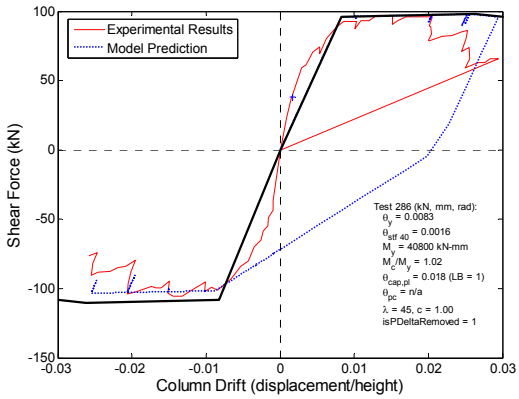
Experimental Results
Model Prediction
Shear Force (kN)
Column Drift (displacement/height)
Test 286 (kN, mm, rad):
θ_y = 0.0083
$\theta_{stf\ 40}$ = 0.0016
M_y = 40800 kN-mm
M_c/M_y = 1.02
$\theta_{cap,pl}$ = 0.018 (LB = 1)
θ_{pc} = n/a
λ = 45, c = 1.00
isPDeltaRemoved = 1

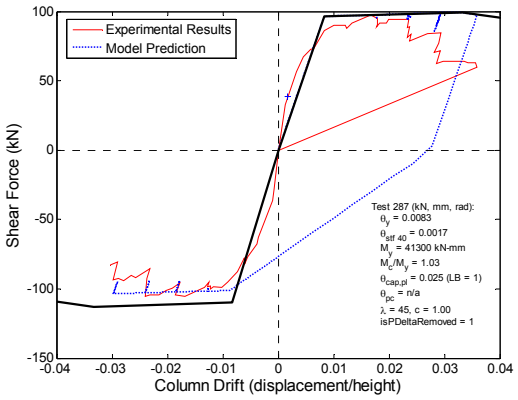
Experimental Results
Model Prediction
Shear Force (kN)
Column Drift (displacement/height)
Test 287 (kN, mm, rad):
θy = 0.0083
θstf 40 = 0.0017
My = 41300 kN-mm
Mc/My = 1.03
θcap,pl = 0.025 (LB = 1)
θpc = n/a
λ = 45, c = 1.00
isPDeltaRemoved = 1

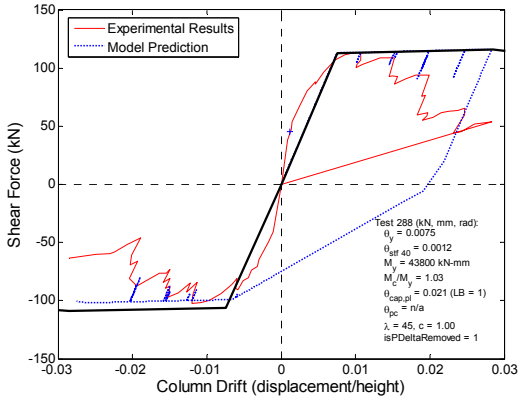
Experimental Results
Model Prediction
Shear Force (kN)
Column Drift (displacement/height)
Test 288 (kN, mm, rad):
θy = 0.0075
θstf 40 = 0.0012
My = 43800 kN-mm
Mc/My = 1.03
θcap,pl = 0.021 (LB = 1)
θpc = n/a
λ = 45, c = 1.00
isPDeltaRemoved = 1

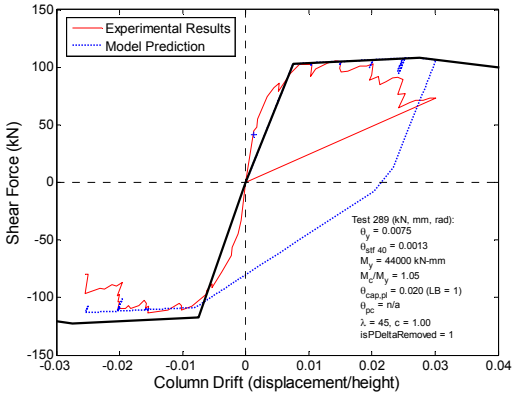
Experimental Results
Model Prediction
Shear Force (kN)
Column Drift (displacement/height)
Test 289 (kN, mm, rad):
θy = 0.0075
θstf 40 = 0.0013
My = 44000 kN-mm
Mc/My = 1.05
θcap,pl = 0.020 (LB = 1)
θpc = n/a
λ = 45, c = 1.00
isPDeltaRemoved = 1